NASA TECHNICAL TRANSLATION

NASA TT F-600

NASA TT F-600
2.1

TECH LIBRARY KAFB, NM
0068946

LOAN COPY: RETURN
AFWL (DOGL)
KIRTLAND AFB, N.

FLIGHT DYNAMICS IN MOVING AIR

by Yu. P. Dobrolenskiy

"Mashinostroyeniye" Press
Moscow, 1969

NATIONAL AERONAUTICS AND SPACE ADMINISTRATION • WASHINGTON, D. C. • JULY 1971

TECH LIBRARY KAFB, NM
0068946

NASA TT F-600

FLIGHT DYNAMICS IN MOVING AIR

By Yu. P. Dobrolenskiy

Translation of "Dinamika Poleta
v Nespokoynoy Atmosfere,"
"Mashinostroyeniye" Press, Moscow, 1969

NATIONAL AERONAUTICS AND SPACE ADMINISTRATION

For sale by the National Technical Information Service, Springfield, Virginia 22151 – Price $3.00

ANNOTATION

This book reviews the characteristics of flight dynamics, the result of air motion with respect to the ground. Particular attention is given to the influence of turbulent air motion on airplane flight. An analytical evaluation of the action of a discrete rectangular wind gust is provided simultaneously in many of the cases considered. The results of the analytical investigation of the motion of an airplane in turbulent air are compared with data obtained from in-flight experiments.

Information on the kinematics of turbulent air motion is systematized, and methods used to describe this motion analytically are reviewed. A method for obtaining equations for the longitudinal and lateral motions of the airplane with the wind taken into consideration is described in detail. Transfer functions for parameters characterizing the movement of the center of gravity, as well as the angular motions of the airplane acted on by gusts, are derived. These transfer functions are then used to evaluate steady-state motion of the airplane acted on by discrete rectangular gusts.

The analysis of the dynamics of an airplane in turbulent air is made by modeling the motion equations on analog computers. The result is the obtaining of root-mean-squares and spectral densities of the airplane motion parameters when the airplane is flying with fixed controls and when the autopilot is used. The effect of turbulence, and of airplane characteristics, on airplane motion are evaluated. It is shown that use of the autopilot results in some reduction in the flight parameter disturbances under these conditions.

Various methods for countering the loads on the airplane attributable to wind gust action are reviewed, and the feasibilities of these methods are evaluated.

Equations describing take-off and landing processes in a wind are introduced, and a number of examples explaining the use of these equations are reviewed.

The appendices contain certain airplane characteristics and brief information on the methodology for obtaining and processing data on wind gusts, and on the parameters of airplane motion in turbulent air.

The book is recommended to aviation industry engineers. It will also be useful to students in the senior courses in the aviation institutes.

The book contains 20 tables, 159 illustrations, and a bibliography of 52 citations.

FOREWORD

There are two basic trends in current research on airplane dynamics. The first of these includes determination of speed ranges, takeoff and landing data, the lift to be derived from speed, ceiling, range and other airplane flight characteristics. The second trend is that associated with research on airplane stability and performance, and it is because of this that consideration must be given to the effect of the airplane's structural resilience.

Of the great many problems of flight dynamics already pointed out, this book will deal only with those upon which the motion of the air relative to the earth's surface (the wind) plays a significant role. Even with this limitation, the problems remaining for consideration are many. It is for this reason that the author makes no pretense at an exhaustive discussion of all the problems associated with the flight of an airplane in turbulent air. The book gives its primary attention to flight dynamics under turbulent air conditions, that is, under so-called "rough air" conditions.

The first chapter systematizes the materials that deal with the characteristics of the constant and variable components of the wind. The cited results of experimental research on the wind velocity field in a turbulent atmosphere confirm the fact that the apparatus of stationary random functions can be used to describe this field.

The second chapter is devoted to obtaining equations for aircraft dynamics in turbulent air, and to methods for modeling the motion of an airplane under turbulent air conditions. Structural diagrams are recommended for the shaping filters needed to obtain spectral densities and dispersions of wind and parameters of the disturbed motion of the airplane in turbulent air.

The third and fourth chapters consider in great detail the longitudinal and lateral motion of the aircraft in turbulent air. The effect of the degree of turbulence on spectral density and on the dispersion of motion parameters under these conditions is brought out. The effect of certain characteristics of automatic pilots on flight dynamics in gusts is reviewed.

A methodology that takes into consideration the effect of such factors as the nonstationary aspect of flows over bodies, wing span, the tail and structural resilience is cited for longitudinal motion. The value of the nonuniformity in the distribution of the velocity of a vertical gust with respect to the wing span is estimated for lateral motion.

The fifth chapter contains a brief description of passive and active systems for reducing loads on an aircraft that occur as a result of gusts. An estimate is made of the probability that permissible accelerations will result in flight. Established is the fact that the use of a pitch stabilization automatic pilot will result in a reduction in the probability that the aircraft will arrive at the limit of permissible angles of attack.

The sixth chapter reviews some of the problems involved in the dynamics of airplane takeoff and landing in turbulent air.

The author thanks I. S. Zakharov and A. P. Kalugin for their help in describing the characteristics of the constant wind component.

The author feels it his duty to express his appreciation to V. I. Funikov and G. D. Petrov for modeling airplane dynamics in turbulent air (the results are cited in chapters 3 - 5).

The author requests that all critical comments and suggestions concerning the book's contents be sent to Moscow, I-51, Petrovka, 24, "Mashinostroyeniye" Press.

TABLE OF CONTENTS

ANNOTATION iii
FOREWORD v

CHAPTER I. Motion of the Air Relative to the Earth's Surface 1
1.1. General Information 1
1.2. Characteristics of the Constant Wind Component 3
1.3. General Characteristics of Atmospheric Turbulence 8
1.4. Analytical Description of the Kinematics of Turbulent Air Motion in the Atmosphere 16
1.5. Results of Some Experimental Investigations of Air Turbulence 33

CHAPTER II. Motion Equations for an Airplane in Moving Air 49
2.1. Statement of the Problem 49
2.2. Equations for Longitudinal Motion in Moving Air 51
2.3. Equations for Lateral Motion in Moving Air 62
2.4. General Characteristics of Dynamic Systems 72
2.5. Modeling the Motion of an Airplane in Turbulent Air 76

CHAPTER III. Longitudinal Motion of an Airplane in Moving Air .. 83
3.1. Transfer and Response Functions for the Parameters of Wind-caused Longitudinal Motion 83
3.2. Longitudinal Motion of an Airplane in Turbulent Air 98
3.3. Effect of the Characteristics of a Real Autopilot on Flight Dynamics in Turbulent Air 108
3.4. The Effect of the Nonstationary Nature of Flow on the Dynamics of Flight in Turbulent Air 114
3.5. Effect of Airplane Size on Dynamics of Flight in Turbulent Air 119
3.6. The Effect of Airplane Structure Elasticity on Flight Dynamics in Turbulent Air 131
3.7. Deviation of an Airplane From its Assigned Flight Path When Flying in Turbulent Atmosphere 145
3.8. An Approximate Method for Computing the Vertical Acceleration when Flying in a Turbulent Atmosphere 146
3.9. Some Experimental Data with Respect to the Longitudinal Motion of an Airplane in a Turbulent Atmosphere 151

CHAPTER IV. Lateral Motion of an Airplane in Moving Air 155
4.1. Transfer and Response Functions for the Parameters of Lateral Motion Resulting from Wing Action 155
4.2. Forces and Moments Determining the Lateral Motion of an Airplane in Turbulent Air 164
4.3. Lateral Motion of an Airplane in Turbulent Air 170

CHAPTER V. Countering Wind Loads on an Airplane 186
5.1. General Information 186
5.2. Permissible Acceleration and Vertical Wind Gust Velocities 187
5.3. Passive Methods for Reducing Vertical Wind Gust Loads ... 190
5.4. Active Systems for Reducing Vertical Wind Gust Loads 192
5.5. Evaluation of the Probability of Achieving Permissible In-flight Accelerations 208

CHAPTER VI. Airplane Takeoff and Landing in Moving Air 215
6.1. General Information 215
6.2. Takeoff in Moving Air 216
6.3. Landing in Moving Air 227

Appendix A 243
Appendix B 249
Appendix C 254
Appendix D 262

References 274

CHAPTER I

MOTION OF THE AIR RELATIVE TO THE EARTH'S SURFACE

1.1. General Information

Airplane motion in the general case is effected by the following forces: /5*
engine thrust, gravity, and the aerodynamic forces attributable to the interaction between the airplane and the air. The points at which these forces are applied, their magnitudes, and directions, determine the path of the airplane's center of gravity, as well as its angular motions relative to the center of gravity. The distribution of such meteorological factors as wind, temperature, pressure, density, and humidity along the airplane's flight path has a significant effect on engine thrust and on the aerodynamic forces. Weather stations make periodic measurements of meteorological factors, as well as of a number of other parameters (cloud cover, precipitation, visibility), knowledge of which is necessary in order to support flights, in order to forecast weather conditions along flight routes.

Of all meteorological factors, the one with the greatest effect on flight dynamics is the wind. Wind, in the broad sense of the term, is any motion of the air relative to the earth's surface. Air motion is caused by the difference between the real distribution of pressure in the atmosphere and the hypothetical distribution corresponding to a stationary atmosphere. The source of the upset in the equilibrium condition of the atmosphere is the nonuniform heating of the various parts of the atmosphere by direct and reflected solar radiation. Consequently, it is the energy of solar radiation that sustains the motion of the atmosphere. This motion has a turbulent, that is, a chaotic, random, character. However, certain components of this motion are characterized by such large scales that from the point of view of flight dynamics they can be considered as a motion with constant velocity. There is no question that the global movement of air masses in

---

* Numbers in the margin indicate pagination in the foreign text.

which the average value of the wind velocity is constant, or very nearly constant, while an airplane is flying hundreds of kilometers, can be included in these motions. Jet streams, too, belong to motions such as these. /6 Jet streams are horizontal air flows in the upper troposphere, or in the stratosphere, with a sharply defined velocity maximum at a definite altitude. Jet streams are thousands of kilometers in length, and hundreds of kilometers in width. Jet streams are not very deep, usually 2 to 5 kilometers.

Very large-scale movements of air occur over the earth's surface limiting such movements, so the mean direction of wind in the vertical plane practically coincides with the horizontal direction at any given point. These horizontal and constant velocities at which the air moves (from the point of view of the effect on the airplane) have a significant effect on the solution of navigation problems.[1] Moreover, a strong wind complicates airplane takeoff and landing, and sometimes even makes doing so impossible.

Much smaller scale air movements, called turbulence, always accompany the large-scale movements of the atmosphere described. So far as airplane flight practice is concerned, atmospheric turbulence is understood to mean an atmospheric condition in which wind gusts, random with respect to magnitude, as well as direction, occur in some definite region covering several kilometers, or less. Various types of air turbulence will be reviewed in what follows, but for now we will limit ourselves to a brief capitulation of the problems, solutions of which must take into consideration airplane dynamics in a turbulent zone.

Flight in turbulent air has associated with it the onset of accelerations, linear oscillations in the aircraft's center of gravity, and angular oscillations relative to the center of gravity ("rough air"). When turbulence becomes very intense the accelerations can become so great that the airplane can no longer be controlled, and will be destroyed in exceptional cases. Consequently, flight dynamics methods that result in reasonably precise determinations of the accelerations acting at the center of gravity, and at other points on the fuselage when the airplane is flying through turbulent air, are of unquestioned interest.

---

1. These problems will not be considered in this book.

The linear and angular oscillations that occur in an airplane when flying through "rough air" have a significant effect on the quality of the work performed by the equipment installed in some modern airplanes, such as cameras, radars, and precision instruments. Analytical computations of these oscillations are extremely difficult to make when the airplane is being flown by the pilot, the result of the random nature of his interaction with the controls when flying in rough air, so experimental data usually are used for this purpose. Today, because of the widespread use of the automatic pilot to fly the airplane, it is possible to make an analytical /7 determination of the linear and angular oscillations that occur in the airplane flying through turbulent air during most stages of the flight.

Some of the experimental data characterizing the manner in which air moves relative to the earth's surface, and analytical equations obtained by an approximation of these experimental data, are cited in what follows.

1.2. Characteristics of the Constant Wind Component

The airplane's crew, and the flight supervisor, have data on the force and direction of the constant wind component at takeoff and landing fields for every flight. These data are used by the crew in planning and executing the takeoff and landing. The weather service also advises the crew of the wind to be expected along the track, and this information is refined by the crew during the flight from the navigator's computations.

However, it is often necessary to estimate the effect of the wind on dynamics for all flights that will be made by a particular type of airplane while it is in service, rather than while on a specific flight. This problem has become a particularly current one, because automatic control of airplanes is being used on an ever-increaseing scale, and here the wind is one of the principal disturbing forces.

The total solution of this problem requires the ordering of some of the general characteristics of the distribution of wind velocity and direction at any moment in time for every point in the area under consideration, from ground level to the airplane's ceiling. Since, as has already been pointed out in Section 1.1, air motion is a turbulent process, wind velocity

and direction at every point, and at every moment in time, are random. There are no current, complete characteristics of the wind velocity field, so what will be presented in what follows will be some of the characteristics of the mean wind velocity that can be used to analyze airplane dynamics.

An increase in wind velocity with increase in altitude is axiomatic for the troposphere. The maximum wind velocity in the troposphere usually is observed near the tropopause. Maximum wind velocity is very sharply defined when there is a jet stream over the site at which the vertical profile of the wind velocity is being measured. Figure 1.1 shows a typical relationship between the velocity of the constant wind component, W_e, and the altitude[2], y_g, in the case of a strong jet stream [1]. Since this profile consists of segments of straight lines, a magnitude for the vertical gradient of the wind velocity can be shown for each of these segments. These magnitudes are shown on the right in Figure 1.1. Let us emphasize the fact that the real vertical profile of the wind velocity will vary greatly with the geographic position of the particular point, as well as with the time of year and day. Maximum values of the wind velocity along the axis of the jet stream can vary from 30 to 200 meters/second. The low limit (30 m/sec) is the conventional minimum value for jet streams. The upper limit (200 m/sec) is close to the maximum value recorded by jet stream observations. The mean velocity of tropospheric jet streams is 40 to 50 m/sec, based on data

/8

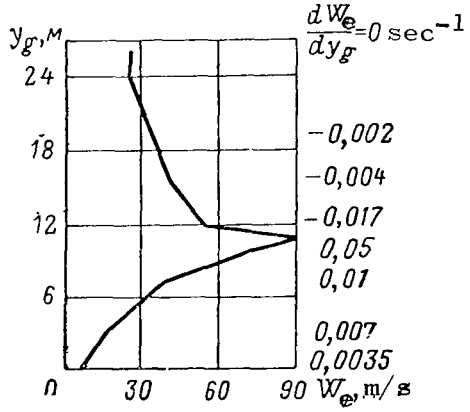

Figure 1.1. A typical profile of the wind velocity in a strong jet stream region. The y_g values are in kilometers.

2. In flight dynamics it is accepted that the coordinates of the airplane's center of gravity are measured in a geographic system of coordinates, x_g, y_g, z_g, with x_g axis coinciding with flight direction, and y_g with the vertical.

cited in [2]. The altitude of the jet stream, that is, the altitude at which the wind velocity is maximum, also varies greatly. Over Moscow, for example, the altitude of jet streams varies from 5 to 17 km [2]. Higher wind velocities are observed in the winter time in the troposphere in the temperate latitudes than in the summer time.

The wind velocity decreases in the lower region of the stratosphere, and drops to zero in the summer time in the temperate zones at altitudes of about 25 kilometers. The latter is associated with the change in the prevailing wind direction from west to east (the wind reversal). Wind velocity increases with increase in altitude, beginning at an altitude of about 25 kilometers, and reaches a maximum at altitudes of from 50 to 60 kilometers. The mean value of the wind velocity at this altitude is 80 to 100 meters/second in the winter, and 60 to 80 meters/second in the summer [2].

There are jet streams in the stratosphere as well, but little study has been made of them.

The available data on wind velocity in the lowest atmospheric layer must be taken up in more detail in order to analyze airplane takeoff and landing dynamics. Wind velocity drops off sharply with decrease in altitude at low altitudes (beginning at 100 to 200 meters), because of friction as the air flows over the ground and over local objects. This is illustrated in Figure 1.2, which shows wind profiles at low altitudes in the Leningrad [3] area, averaged over the years. These curves show that at very low altitudes the day wind is stronger than the night wind. The night wind gets stronger /9 than the day wind above a point which, for this particular locality, is at an altitude of some 50 meters. Although the low altitude wind profiles shown are typical, so far as shape is concerned, it must be remembered that all the characteristics of these profiles are very greatly dependent on meteorological conditions in the lowest atmospheric layer. There are a great many different formulas for making an analytical computation of this profile [4], but all require a knowledge of various parameters that depend on meteorological conditions, so it is obvious that formulas such as these are not suitable for making a general estimate of the effect the wind will have on the dynamics of an airplane that is constantly flying through regions with changing meteoro-

logical conditions. The solution of this problem requires the averaging of the statistical characteristics of the wind at low altitudes, obtained by processing experimental data.

Many papers on the subject have pointed out that the vertical profile of the constant component of the wind velocity at low altitudes can be described, approximately, by a power law

$$\frac{W_0}{W_{01}} = \left(\frac{y_g}{y_{g1}}\right)^n, \qquad (1.1)$$

where W_e is the mathematical expectation for the constant wind component;
y_g is altitude above the earth's surface;
n is an exponent, the magnitude of which depends on meteorological conditions.

The subscript "1" denotes the supporting values for altitude and wind velocity used as a basis for constructing the profile.

The highest altitude for which Equation (1.1) can be used is limited by the values y_g=300 to 500 meters.

The magnitudes of n, according to the data in [5], are between 0.145 and 0.77, and between 0.1 and 0.4, according to the data in [6]. Processing many experimental data established the mean value of n as between 0.15 and 0.2. It is recommended that the mathematical expectation for the mean wind be taken as W_{e1} =3 to 4 m/s for a supporting altitude y_{g1}=10 m. The profile of the mean wind at low altitudes, obtained through Equation (1.1) for n=0.2 and W_{e1}=4 m/s (y_{g1}=10 m) is shown in Figure 1.3.

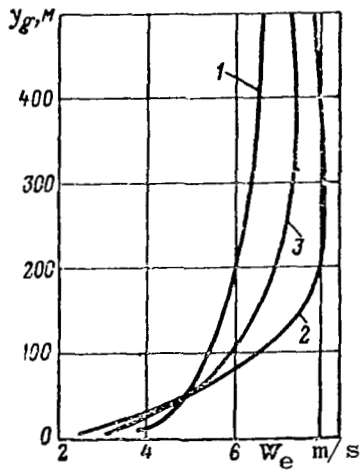

Figure 1.2. Wind profiles at low altitudes. 1 - day (from 1000 to 1700 hours); 2 - night (from 2200 to 0500 hours); 3 - 24 hour curve.

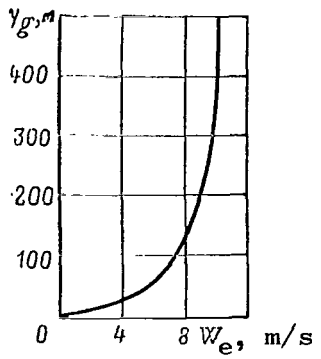

Figure 1.3. Profile of mean wind value at low altitudes.

/10

As has already been pointed out, the constant component of the wind velocity is a random magnitude, so in order to analyze the effect of this component in airplane flight, one must know the probability of the airplane encountering a wind of some particular velocity. Experimental data on the distribution of the probability that there will be a constant component of the wind velocity modulus for a definite altitude above the ground are in good concordance with the Rayleigh distribution. The density of the Rayleigh distribution for this case can be established through the expression

$$f(W)=\frac{\pi}{2}\frac{W}{W_e}e^{-\frac{\pi}{4}\left(\frac{W}{W_e}\right)^2}, \tag{1.2}$$

where

W is the value of the constant component of the wind velocity modulus, the probability of the encountering of which in flight at altitude y_g can be established;

W_e is the mean value of the wind velocity for flight at altitude y_g, obtained through Equation (1.1).

A function of the distribution showing the probability that an airplane flying at altitude y_g will encounter a wind, the constant component of the velocity of which exceeds a specified level, can be obtained through the density of distribution at Equation (1.2). This function can be described by the expression

$$F(W)=e^{-\frac{\pi}{4}\left(\frac{W}{W_e}\right)^2}. \tag{1.3}$$

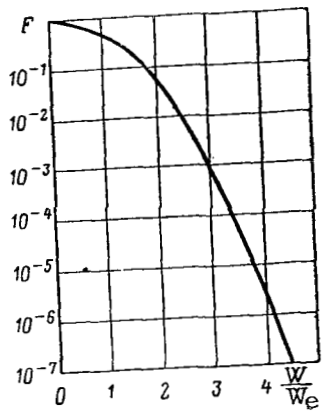

Figure 1.4. Function of the distribution of the probability of a wind with a velocity higher than some W value being encountered.

Figure 1.4 shows the curve for the function of the probability distribution constructed using Equation (1.3) as a basis. The curve can be used to estimate the conditions for a great (within the limits of infinitely great) number of flights. The F(W) values can be interpreted in the same manner as the ratio of the total length of those sections of flights for which the wind velocity exceeds a specified level to the total time of the flights, if this time is very long. /11

The use of the Rayleigh distribution applies with equal force to the assumption of an equal probability for wind direction, something that cannot be contradicted with any degree of authority if one bears in mind that the averaged characteristics of wind direction over a large territory are what are being considered. But it must be stipulated that if these averaged lowest atmosphere layer wind characteristics are used to estimate takeoff and landing dynamics, their use with a Rayleigh distribution will result in significant errors. This is because runways are oriented with respect to the prevailing direction of the strongest winds in the airfield area.

1.3. General Characteristic of Atmospheric Turbulence

As was pointed out in Section 1.1, it is conventional to consider the effect wind velocity has on airplane flight in the form of a sum of two components, one constant, the other variable. The variable component of the wind velocity also characterizes the turbulence in the atmosphere. Turbulence is understood to mean the disordered, chaotic motion of air in the atmosphere. This book will consider that turbulent air motion for which the velocities at any point considered in the region where this motion is taking

place are random functions of the coordinates of that point and time, and functions that can be described by theory of probability methods [7].

The vertical and horizontal gradients of temperature and wind velocity are the proximate cause of turbulence in the atmosphere. Reference [8] lists the following phenomena contributing to the turbulent nature of air motion in the atmosphere:

(1) friction of the air flow over the ground and local objects causing the onset of vertical and horizontal wind velocity gradients;

(2) vertical air currents, the result of uneven heating of the different parts of the ground, giving rise to so-called thermal, or convection, turbulence;

(3) cloud formation processes associated with the appearance of significant temperature and wind velocity gradients;

(4) the interaction of air masses with different thermal conditions, /12 forming fronts with strong horizontal temperature and wind velocity gradients;

(5) strong wind gradients on the boundaries of the jet streams;

(6) deformations of air currents by mountains and plateaus.

The entire range of air motion in the atmosphere can be broken down into three intervals in terms of occurrence, character, and energy processes:

(1) an interval of large-scale air motions;

(2) an inertia interval;

(3) a viscous interval.

Most of the solar energy supporting the turbulent motion is introduced into the atmosphere by the motions during the large-scale interval. These motions are attributable to the upsetting of the equilibrium state of the atmosphere during uneven heating that results from direct and reflected solar radiation. Although these large-scale horizontal air motions are also turbulent in nature, as pointed out above, they can be considered as constant velocity winds in the study of flight dynamics.

It is obvious that there is a sharply defined anisotropy in this large-scale interval of air motion, the result of the limiting effect of the ground, and by the dependence of the characteristics of the atmosphere on the alti-

tude of a particular point above the ground.

The energy of large-scale motions is transmitted by smaller scale wind gusts that usually can be equated to the inertia interval of the turbulence. It is in this interval that the vortex motion of the air loses its direct association with the large-scale air motion that causes it.

The vortex gusts in the inertia range do not have a preferred direction, so can be considered as isotropic in a statistical sense. Naturally, the sizes of the largest vortices in the inertia interval depend on the altitude of the point in the atmosphere under consideration, and on the meteorological conditions causing the turbulence. There is a boundary layer adjacent to the ground, the altitude of which depends on meteorological conditions and varies within limits of several hundred meters [9]. Assumed above was so-called free air, for which the limits of the size of vortices in the inertia interval vary from several hundred meters [10] to several kilometers [48].

The smallest vortices in the inertia interval are limited by the viscous interval, encompassing the region of the highest frequencies for air particle motion. The conversion of most of the mechanical energy into thermal energy, the result of the viscous friction force, takes place in the viscous interval. Reference [9] cites data on the limiting sizes of vortices of the /13
viscous interval. These vortices measure several centimeters for free air. Accordingly, the inertia interval of turbulent motion in the atmosphere encompasses a range of vortices from several hundred meters (or a few kilometers) to several centimeters, and is of great interest so far as its effect on the dynamics of modern airplanes is concerned. Widespread gusts beyond the limits of the inertia range take on greater importance for flight dynamics as airplane flight speeds increase.

If the molecules of the gases in the air deliver more energy than is lost in the process of converting the mechanical energy of the large-scale air motions into thermal energy, the surplus energy goes toward increasing the intensity of the turbulent motion. But if more energy is converted into heat than is supplied from the large-scale air motions, the turbulence degenerates. However, the processes involved in the development and degeneration of turbulence are quite lengthy ones, so from the point of view of effect on a rapidly flying airplane, turbulence is usually considered to be steady-

state, that is, a balanced process from the point of view of energy. This is why this book will not consider questions that concern themselves with the dynamics of turbulence.

Let us now introduce some data on concrete types of turbulence in the atmosphere.

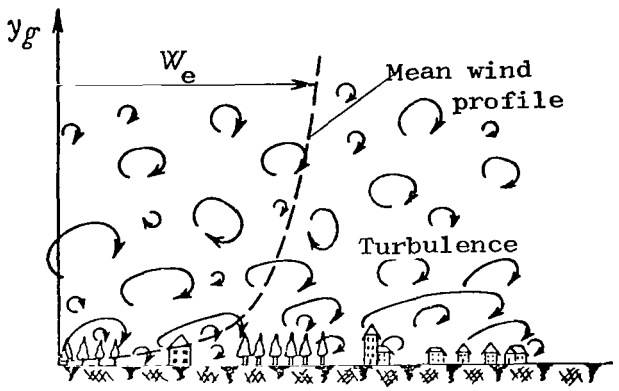

Figure 1.5. Diagram of a turbulent flow of air in the lowest atmospheric layer.

Turbulence in the ground boundary layer occurs as a result of the interaction between the air flow and the ground, as a result of the effect of convective air currents, and as a result of the influence of the vertical and horizontal air velocity and temperature gradients. Figure 1.5 shows a diagram of a turbulent flow in the lowest atmospheric layer. At altitudes /14 near those of obstacles, and below, the turbulence reflects, to some degree, the geometric form of such obstacles. The turbulent motion of the air becomes random with increase in altitude.

The characteristics of the flow in the lowest atmospheric layer [9], given indifferent stratification of the atmosphere[3], should not differ significantly from the very well researched characteristics in the turbulent

3. By stratification of the atmosphere is meant the distribution of temperature in the atmosphere in terms of altitude on which the intensity of the convection processes depends.

boundary layer on a flat plate developed in a wind tunnel. But there is quite a significant change in the characteristics of air motion in the boundary layer when there is a change in stratification to stable, or unstable. Although study of these characteristics is quite intensive, it is still far from complete. A quite complete survey of available data on turbulence in the lowest atmospheric layer is contained in [9].

The causes giving rise to turbulence in a free atmosphere were listed at the beginning of this paragraph. Turbulent zones in a free atmosphere are in the form of comparatively thin layers covering vast areas with quite clear-cut boundaries.

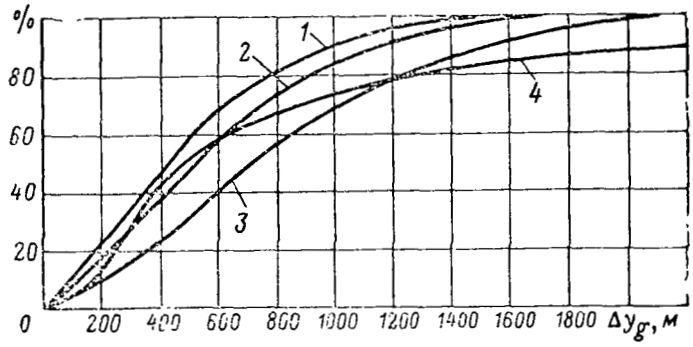

Figure 1.6. Frequency of thicknesses of turbulent zones.
1 - data for the northern latitudes of the USSR;
2 - data for the temperate latitudes of the USSR;
3 - data for the southern latitudes of the USSR;
4 - Canadian data.

Figure 1.6 shows curves characterizing the frequency of the thicknesses of zones such as these, in %, for Canada (curve 4), and for different latitudes in the Soviet Union (curves 1-3) [8]. The graphics show the frequency of thicknesses less than the values plotted on the axis of the abscissa. The curves of Figure 1.6 show, for example, that zones less than 1000 meters thick are found in the northern latitudes of the Soviet Union in approximately 90% of the cases, in the temperate zones in 85% of the cases, in Canada in approximately 75% of the cases, and in the southern latitudes in 70% of the cases. The maximum thickness of turbulent zones is virtually never in excess of 2000 meters. What follows, then, is that in order to get out of /15 a zone of "rough air," when this is permissible under prevailing flight

conditions, one must change altitude.

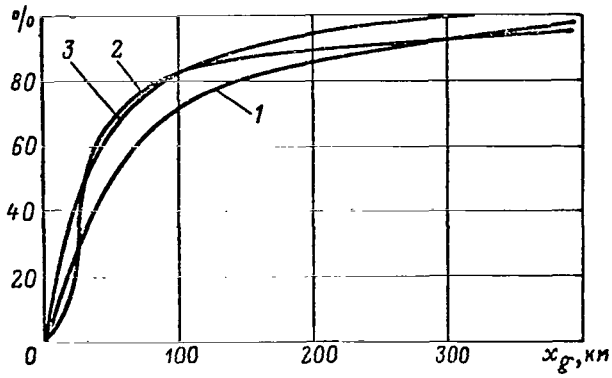

Figure 1.7. Frequency of the horizontal dimensions of turbulence zones. 1 - data for temperate latitudes in the USSR; 2 - Canadian data; 3 - United States data.

Figure 1.7 contains curves [8] for frequency of horizontal dimensions of turbulent zones. The sense of these curves is that of the curves in Figure 1.6. The curves in Figure 1.7 show, for example, that for the USSR, the extent of a turbulent zone less than 20 km is encountered in approximately 20% of the cases, and one less than 100 km in extent is encountered in 70% of the cases.

Consequently, flight time in turbulent zones is quite lengthy, and can be measured in minutes in the case of modern airplanes.

Zones of turbulence usually contain clouds, or are near heavy cumulus clouds. These signs are a warning to the crew that their airplane could be entering a turbulent zone. Yet turbulent zones can be encountered even in cloudless weather. They occur in the boundary of a jet stream, as well as during local wind velocity gradients resulting from the air flowing over mountain ranges. Airplanes have no equipment on board at this time for forecasting clear air turbulence, so that flying into such a zone usually comes as a surprise to the crew.

The greatest danger to an airplane in flight is the turbulence in thunderstorms. Flight instructions for all types of airplanes forbid taking an airplane into thunderstorm areas. The locations of these areas are established by meteorological service ground installations, as well as by the main types of thunderstorm locators installed in the aircraft. Nonetheless, despite /16 all these precautions, there are cases of airplanes entering thunderstorm

areas. This is why thunderstorm turbulence research is quite intensive.

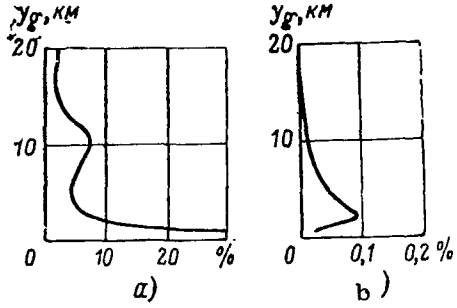

Figure 1.8. Relative flight distance in turbulence in terms of altitude. a - general data; b - flight under thunderstorm conditions.

Figure 1.8 shows relative flight distance under turbulent conditions in terms of altitude [1]. Turbulence is conventionally broken down into thunderstorm, and nonthunderstorm turbulence. What must be borne in mind is that the curves in Figure 1.8 were obtained by processing a great amount of statistical material, and therefore are valid only for estimating average conditions during a great many flights. These curves are an objective reflection of the probability of encountering turbulence at altitude with the measures that can be taken to go around, or fly out of turbulent areas, taken into consideration. One author [1] is of the opinion that the actual extent of thunderstorm areas is greater by an order of magnitude than that indicated by Figure 1.8-b, or the curve which was constructed with the steps utilized in flight to go around thunderstorms taken into consideration.

As the curve in Figure 1.8-a indicates, turbulence is most often encountered at low altitudes; that is, the turbulence encountered is thermal, or convection turbulence. The probability that a flight will encounter turbulent conditions decreases with increase in altitude. It is only somewhat below the tropopause that some increase in this probability is noted, and this is because of the jet streams present at this altitude. The probability of encountering an area of turbulence continues to decrease above the tropopause, and in the lower stratosphere.

In concluding this section, we include Table 1.1, showing how the effect of turbulent air on an aircraft is estimated. The result of this effect ("rough air") is established by the amplitude of the normal acceleration experienced in flight.

TABLE 1.1

Airplane "rough air" characteristic	"Rough air" intensity, scale number	Range of increase in acceleration
Light	σ^1	$\lvert \Delta n_y \rvert \leq 0.20$
Moderate	σ^2	$\lvert \Delta n_y \rvert \leq 0.50$
Severe	σ^3	$\lvert \Delta n_y \rvert \leq 1.0$
Storm	σ^4	$\lvert \Delta n_y \rvert > 1.0$

Data on turbulence intensity estimates made by pilots, and the root-mean-squares of the vertical acceleration corresponding to these estimates, also are of interest. These data were obtained experimentally as a result of flights made in high-speed fighter planes [49]. They are very approximate, and can be used only for a tentative estimate of turbulence intensity. /17

The results of the investigations are listed in Table 1.2.

TABLE 1.2

Estimate of turbulence intensity by pilot	Root-mean-squares of acceleration
Negligibly light	0.05
Light	0.1
Moderate	0.1-0.15
Severe	0.2-0.3
Very severe	0.3

1.4. Analytical Description of the Kinematics of Turbulent Air Motion in the Atmosphere

An analytical method of describing the wind velocity field must be available in order to investigate flight dynamics in turbulent air. Two methods are currently in use to describe moving air in order to determine how it acts on the airplane: the discrete gusts method, and the continuous random gusts method. The former appeared much earlier than did the latter, and as of this time is widely used to compute loads on newly designated airplanes caused by vertical gusts. The discrete gusts method is based on the following assumptions:

(1) the shape of the discrete gust is taken as fixed;

(2) the airplane can be displaced in the vertical direction only, the angle of pitch remaining unchanged;

(3) the dynamic properties of all airplanes are identical.

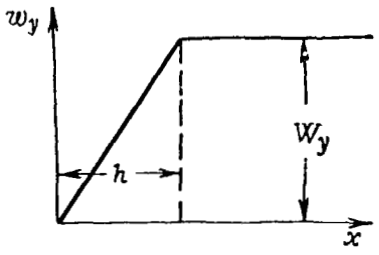

Figure 1.9. Standard shape of a discrete gust.

Figure 1.9 shows the standard shape of a discrete gust used to compute loads. The linear section of the increase in speed (of the length h) is called the "gradient section." Distance x, covered by the airplane in time t at constant speed V, is taken as an independent variable.

Given the assumptions indicated above, the increases in the vertical acceleration, Δn_y, measured in flight, can be converted into the velocity of the vertical gusts through the formula /18

$$W_y = \frac{2G/S}{k\rho V C_y^{\alpha}} \Delta n_y, \qquad (1.4)$$

where G is aircraft weight;

ρ is the air mass density;

V is the flight speed;

S is the wing area;

C_y^{α} is the angle of attack derivative from the lift coefficient;

k is the acceleration attenuation constant attributable to the "gradient section" of the gust.

This constant is computed through the formula

$$k = \frac{1 - e^{-\nu}}{\nu},$$

where

$$\nu = \frac{C_y^{\alpha} g \rho h}{2G/S}$$

and g is the acceleration of gravity.

Used for Δn_y to compute W_y through Equation (1.4) are the amplitude values of the increase in the acceleration as recorded by accelerometers installed in the aircraft when the aircraft is in normal operation, or during flights to investigate turbulent air.

It must be pointed out that the gust velocity computed through Equation (1.4) is not true air speed because the assumptions made in order to obtain this formula are very rough. However, it can be supposed that the use of these gust velocities for computing wind accelerations for another airplane will yield approximately correct results. What follows from the very nature of the assumptions made above is that the discrete gusts method has virtually no connection with the real nature of gusts in the atmosphere, and that its use can provide satisfactory results only when the airplanes are dynamically similar.

This book will use the second method, wherein a statistical description of the wind velocity field is used. This method is now widely used in work on flight dynamics in moving air. The statistical method results in a much more precise description of the real processes involved in air motion in the atmosphere than does the discrete gusts method, but it too requires the introduction of certain assumptions. These reduce to the following:

(1) the wind velocity field in defined sections of turbulent air is homogeneous and isotropic; /19

(2) the wind velocity field is "frozen" for a flying airplane; that is,

it does not change with time (the Taylor hypothesis).

A more detailed meaning, and the significance, of these assumptions will be found in what follows.

Let us now proceed to an analytical description of the wind velocity field. Since it has already been stipulated that the random component of wind velocity under consideration is a random function, we must obtain a correlation function, or spectral density, as well as a law for distribution of instantaneous values of wind velocity, to describe that function fully.

We have seen several times that the complete wind vector, $\overline{W}$, can be represented conventionally as the sum of a constant, $\overline{W}_e$, and a variable, $\overline{w}$, component:

$$\overline{W} = \overline{W}_e + \overline{w}. \tag{1.5}$$

In what follows in this chapter, only the variable wind component, $\overline{w}$, will be considered, and will be taken as a random function of time and of the coordinates of a definite point in the field. Let us consider two points in a velocity field at a given moment in time. Given this condition, $\overline{w}$ will be a random function of the space coordinates only. Let one point in the field be defined by the radius vector $\overline{x}$, and any other point be defined by the vector $\overline{r}$, drawn from the tip of the $\overline{x}$ vector. We will suppose that the air turbulence under consideration is homogeneous and isotropic. "Homogeneous turbulence" is understood to mean turbulent motion, the probability characteristics of which are identical for the entire wind velocity field under consideration. "Isotropic turbulence" is understood to mean turbulent motion, the probability characteristics of which do not depend on the direction $\overline{r}$ along which the correlation between the velocities at two points in the field is being considered. What follows from the general theory of homogeneous and isotropic turbulence is that all that need be known to describe the velocity field in this case is the two correlation functions for the projections of the velocity factor on the rectangular coordinate axis [11]. The functions taken for the experimental investigation of turbulence are the correlation functions for the projections of the velocity vector, $\overline{w}$, in a direction coinciding with the $\overline{r}$ vector direction (longitudinal), and in a direction perpendicular to it (lateral). The geometric sense of these projections is explained in Figure 1.10-a. Figure 1.10-a is the basis for the obtaining

of the expressions for the longitudinal and lateral correlation functions (see Appendix D):

$$R_t(r) = \overline{w_t(\bar{x})\, w_t(\bar{x}+\bar{r})}, \tag{1.6}$$

/20

$$R_n(r) = \overline{w_n(\bar{x})\, w_n(\bar{x}+\bar{r})}. \tag{1.7}$$

The bar over the product of the instantaneous values of the velocities in Equations (1.6) and (1.7) signifies averaging. The sign of the vector in the argument of the correlation functions is omitted because in isotropic turbulence these functions are invariant to rotation of the vector $\bar{r}$. The functions $R_t(r)$ and $R_n(r)$ are not independent functions. According to [11], the association between these functions for isotropic and homogeneous turbulence can be established by the relationship

$$R_n(r) = R_t(r) + \frac{1}{2} r \frac{\partial R_t(r)}{\partial r}. \tag{1.8}$$

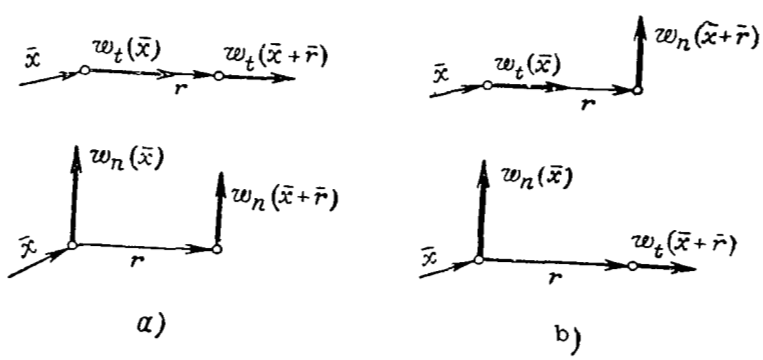

Figure 1.10. Wind velocity components.
a - longitudinal and lateral with respect to the direction of $\bar{r}$, and with respect to which the correlation can be considered; b - cross.

The general theory of turbulence [11] is the basis for saying that all cross correlation functions of a kind (Figure 1.10-b) are identically equal to zero:

$$\left.\begin{aligned} R_{tn}(r) &= \overline{w_t(\bar{x})\, w_n(\bar{x}+\bar{r})} = 0, \\ R_{nt}(r) &= \overline{w_n(\bar{x})\, w_t(\bar{x}+\bar{r})} = 0. \end{aligned}\right\} \tag{1.9}$$

Let us find the kind of correlation functions for the projections of the wind vector $\overline{w}$ on a Cartesian coordinate axis. Let the wind velocity vector, $\overline{w}$, have the components $w_x(x, y, z)$, $w_y(x, y, z)$, and $w_z(x, y, z)$ at a point with coordinates x, y, and z (Figure 1.11). The wind velocity vector will then have the projections $w_x(x+\Delta x, y, z)$, $w_y(x+\Delta x, y, z)$, and $w_z(x+\Delta x, y, z)$ at point 1 with coordinates $x+\Delta x$, y, z. Correspondingly, at point 2, with coordinates x, $y+\Delta y$, z, the projections will have the form $w_x(x, y+\Delta y, z)$, $w_y(x, y+\Delta y, z)$, and $w_z(x, y+\Delta y, z)$, and at point 3, with coordinates x, y, $z+\Delta z$, they will be $w_x(x, y, z+\Delta z)$, $w_y(x, y, z+\Delta z)$, and $w_z(x, y, z+\Delta z)$.[4] /21

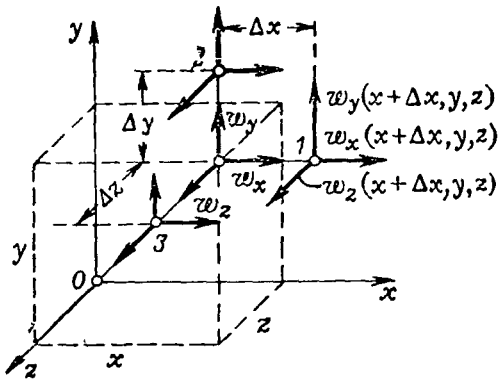

Figure 1.11. Cartesian wind components at four points in a wind velocity field.

The following obvious relationships derive from a comparison of the disposition of the projections of the velocity vectors in Figures 1.11 and 1.10 based on Equations (1.6), (1.7) and (1.9).

Based on Equation (1.6)

$$\overline{w_x(x, y, z)\,w_x(x+\Delta x, y, z)} = \overline{w_y(x, y, z)\,w_y(x, y+\Delta y, z)} = \overline{w_z(x, y, z)\,w_z(x, y, z+\Delta z)} = R_t(r). \tag{1.10}$$

And we understand r to mean that coordinate at which correlation is being considered.

Based on Equation (1.7)

4. Figure 1.11 does not contain the inscriptions for the projections of the w vector at points 2 and 3 in order to avoid cluttering up the drawing.

$$\begin{aligned} w_y(x, y, z)\,\overline{w_y(x+\Delta x, y, z)} &= w_z(x, y, z)\,\overline{w_z(x+\Delta x, y, z)} = \\ = w_x(x, y, z)\,\overline{w_x(x, y+\Delta y, z)} &= w_z(x, y, z)\,\overline{w_z(x, y+\Delta y, z)} = \\ = w_x(x, y, z)\,\overline{w_x(x, y, z+\Delta z)} &= w_y(x, y, z)\,\overline{w_y(x, y, z+\Delta z)} = \\ &= R_n(r) \end{aligned} \tag{1.11}$$

Based on Equation (1.9), the remaining 18 correlation functions of the $\overline{w_x w_y}$, $\overline{w_y w_z}$ and $\overline{w_z w_x}$ kind are identically equal to zero.

Since only one argument changes in each of the correlation functions cited in Equation (1.10) and Equation (1.11), the computation of any of these functions is made using the general formula (see Appendix D): /22

$$R(x) = \lim_{X\to\infty} \frac{1}{2X} \int_{-X}^{X} f(x) f(x+x)\, dx.$$

The nature of correlation functions $R_t(r)$ and $R_n(r)$ was established by experiments in wind tunnels in which practically homogeneous and isotropic turbulence was created. Approximating analytical expressions of the following type [14] were obtained by processing the experiments indicated for longitudinal and lateral correlation functions

$$R_t(r) = \sigma_w^2 e^{-|r|/L}, \tag{1.12}$$

$$R_n(r) = \sigma_w^2 (1 - |r|/2L)\, e^{-|r|/L}, \tag{1.13}$$

where

$\sigma_w^2 = \overline{w}_t^2 = \overline{w}_n^2$ is the mean value of the square (variance) of any component of the velocity of turbulent air motion;

L is the so-called turbulence scale.

Direct substitution will be persuasive that the approximating formulas at (1.12) and (1.13) satisfy Equation (1.8).

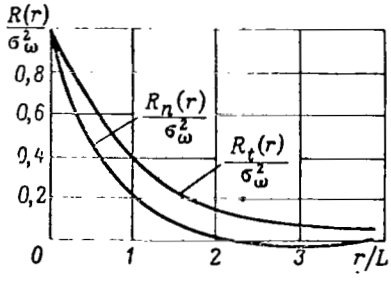

Figure 1.12. Curves of standardized functions of longitudinal and lateral wind velocity components.

Curves of the functions $R_t(r)$ and $R_n(r)$ in standardized form are shown in Figure 1.12. These curves show that the turbulence scale, L, is a convenient characteristic to use for the linear dimensions of an area in which the corresponding components of the velocity are correlated in the manner indicated. It must be pointed out that the turbulence scale, L, in Equations (1.12) and (1.13) is the same and is purely formal. As will be seen from the curves in Figure 1.12, the function $R_n(r)$ drops to the axis of abscissa more sharply than does the function $R_t(r)$. If the turbulence scale is defined as the integral of a normalized correlation function, we obtain the following values for the scales for the longitudinal and lateral correlation functions

$$L_t = \frac{1}{\sigma_w^2}\int_0^\infty R_t(r)\,dr = \int_0^\infty e^{-|r|/L}dr = L, \tag{1.14}$$

$$L_n = \frac{1}{\sigma_w^2}\int_0^\infty R_n(r)\,dr = \int_0^\infty (1 - r/2L)\,e^{-|r|/L}dr = L/2. \tag{1.15}$$

/23

Equations (1.14) and (1.15) show that the longitudinal scale is twice that of the lateral scale, and this must always be kept in mind when Equations (1.12) and (1.13) are used where they do not reflect clearly the consequence of using some particular L parameter in both of these formulas.

Since frequency methods will be used extensively in what follows to analyze airplane dynamics, it is necessary to make a change from correlation functions to spectral densities. The spectral density of a random, stationary process is associated with its correlation function by the expression (see Appendix D)

$$S(\Omega) = \frac{2}{\pi}\int_0^\infty R(r)\cos \Omega r\,dr, \tag{1.16}$$

where Ω is the spatial angular frequency if r is a spatial coordinate;

$$\Omega = 2\pi/\lambda. \tag{1.17}$$

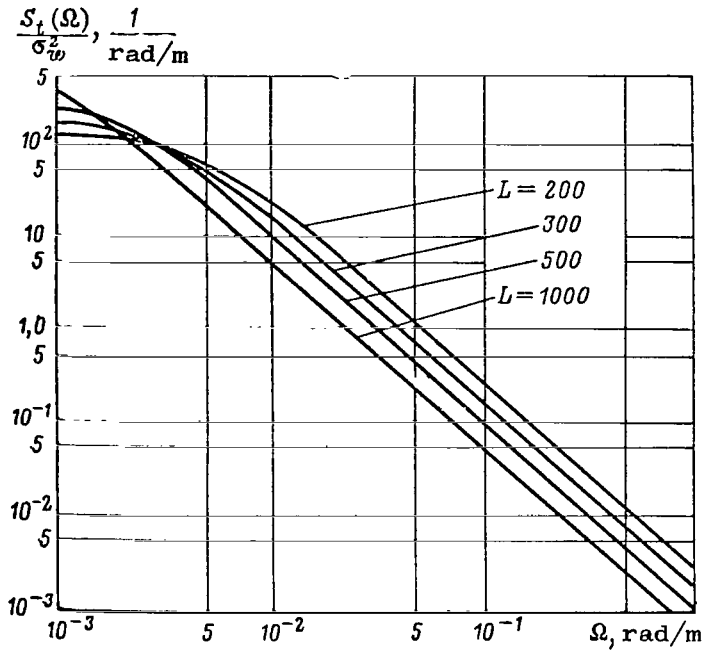

/24

Figure 1.13. Graphics of a normalized spectral density for the longitudinal component of the wind velocity.

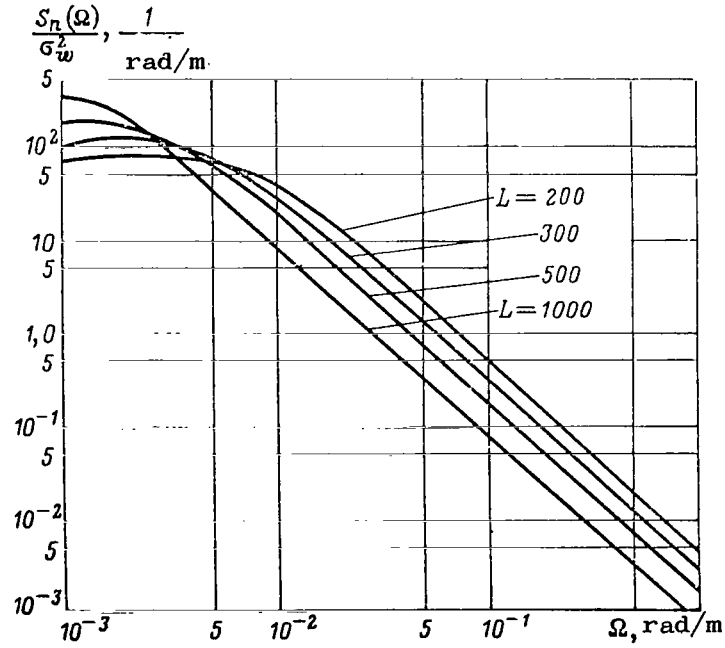

Figure 1.14. Graphics of a normalized spectral density for the lateral component of the wind velocity.

In Equation (1.17), λ is the wavelength of the spectral components of the velocity of turbulent air motion.

Substituting the values for the longitudinal and lateral correlation functions from Equations (1.12) and (1.13) in Equation (1.16), we obtain the expressions for the corresponding spectral densities[5]:

$$S_t(\Omega)=\sigma_w^2\frac{L}{\pi}\frac{2}{1+\Omega^2L^2}, \tag{1.18}$$

$$S_n(\Omega)=\sigma_w^2\frac{L}{\pi}\frac{1+3\Omega^2L^2}{(1+\Omega^2L^2)^2}. \tag{1.19}$$

Figures 1.13 and 1.14 present graphics for normalized spectral densities constructed using Equations (1.18) and (1.19) for different turbulence scales, L. A comparison of the curves in these figures reveals that the spectral density, and, as a result, the power and energy of the gusts increase in low frequency regions and decrease in high frequency regions with increases in turbulence scales.

The so-called dimensionless frequency, v, determined through the formula

$$\nu=\Omega L. \tag{1.20}$$

will be used in what follows for convenience in making the mathematical transformations.

If the change to the dimensional frequency is made in Equations (1.18) and (1.19), they become /25

$$S_t(\nu)=\frac{\sigma_w^2}{\pi}\frac{2}{1+\nu^2}, \tag{1.21}$$

$$S_n(\nu)=\frac{\sigma_w^2}{\pi}\frac{1+3\nu^2}{(1+\nu^2)^2}. \tag{1.22}$$

---

5. The National Aeronautics and Space Administration in the United States uses Equations (1.18) and (1.19) for spectral densities and Equations (1.12) and (1.13) corresponding to them for correlation functions [1].

The need to change the constant factor in Equations (1.21) and (1.22) as compared with Equations (1.18) and (1.19) stems from the identity

$$\sigma_w^2 = \int_0^\infty S(\Omega)\, d\Omega = \int_0^\infty S(\nu)\, d\nu, \tag{1.23}$$

if the formula for linking Equation (1.20) with v and Ω is considered.

The graphics for the normalized spectral densities as a function of the dimensionless frequency, constructed using Equations (1.21) and (1.22), are shown in Figure 1.15.

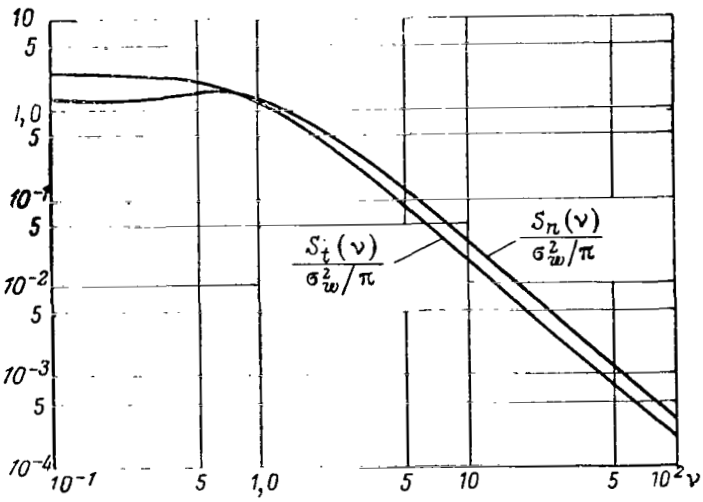

Figure 1.15. Graphics of the normalized spectral densities cited for the wind velocity components as a function of the dimensionless frequency.

The analytical expressions for the correlation functions and spectral densities cited in the foregoing for the projection of the random wind vector simply characterize the spatial distribution of the wind velocity field. Hence, these data are correct only for some, let us say arbitrary, one moment in time for which the velocity field is "frozen." At the same time, the movement of an airplane in space is always associated with definite /26 time intervals. Consequently, the characteristics of a velocity field in turbulent air, obtained in the foregoing, cannot be used unconditionally

to establish the disturbances acting on the airplane. This difficulty can be gotten around by using Taylor's hypothesis [11, 13]. According to this hypothesis, the velocity field of turbulent motion can be considered "frozen" when investigating airplane dynamics. As distinguished from the preceding field, this one can be considered "frozen" for the entire flight, not just for some one moment in time. Taylor's hypothesis can be explained as follows. Because of the high speed at which the airplane flies, as compared with the speeds at which the turbulent air moves, the airplane flies a distance over which the correlation between these speeds is quite strong, so rapidly, that during the time of flight over this distance the wind velocity field undergoes no change that is remotely significant. Based on Taylor's hypothesis, the analytical characteristics obtained in the foregoing are correct for one moment in time, strictly speaking, but can be used for the entire time of the flight for the airplane.

Moreover, if the airplane is considered as a point[6] moving in the direction of the x axis, there will remain but three of all the correlation functions in Equations (1.10) and (1.11) that depend on the variable x. The other variables (y and z) are unchanged, hence can be omitted. Based on Equation (1.10), we obtain the longitudinal correlation function for the longitudinal component of the wind, w_x as

$$R_{tx}(x)=\overline{w_x(x)\,w_x(x+\Delta x)}. \tag{1.24}$$

Based on Equation (1.11), we obtain the lateral correlation functions for the normal w_y and lateral w_z components of the wind as

$$R_{ny}(x)=\overline{w_y(x)\,w_y(x+\Delta x)}, \tag{1.25}$$

$$R_{nz}(x)=\overline{w_z(x)\,w_z(x+\Delta x)}. \tag{1.26}$$

Finally, let us take it that there is a unique link between the distance flown by the airplane, x, and time, t, for the wind velocity field that is "frozen" for the entire airplane flight time, and that the link can be written

---

6. The case when aircraft dimensions are taken into consideration will be reviewed when solving specific problems in Chapter 3.

$$x=r=Vt. \tag{1.27}$$

The relationship at (1.27) makes it possible to change from the spatial coordinate x to the time coordinate t in the general equations at (1.24)-(1.26) for the correlation functions of the wind components. Consequently, this change can be made as well in the specific analytical expressions at (1.12) and (1.13) for these functions. By replacing $|r|$ by $V(\tau)$, we obtain /27

$$R_t(\tau)=\sigma_w^2 e^{-|\tau|V/L}, \tag{1.28}$$

$$R_n(\tau)=\sigma_w^2(1-|\tau|V/2L)e^{-|\tau|V/L}. \tag{1.29}$$

It is obvious that Equation (1.28) equates to the w_x component, and Equation (1.29) equates to the w_y and w_z components.

The spatial spectral characteristics of the velocity field are functions of the spatial angular frequency Ω. The time-response spectral characteristics, reflecting the process of the interaction of this field with the airplane, naturally enough should be functions of the time-response angular frequency ω. These frequencies are linked by the obvious relationship

$$\Omega x=\omega t. \tag{1.30}$$

Substituting the value for x from Equation (1.27) in Equation (1.30), we obtain

$$\Omega=\omega/V. \tag{1.31}$$

We obtain the following expressions for the spectral densities as a function of ω after applying a Fourier transform to Equations (1.28) and (1.29):

$$S_t(\omega)=\frac{L\sigma_w^2}{\pi V}\frac{2}{1+\omega^2L^2/V^2}, \tag{1.32}$$

$$S_n(\omega)=\frac{L\sigma_w^2}{\pi V}\ \frac{1+3\omega^2L^2/V^2}{(1+\omega^2L^2/V^2)^2}. \qquad (1.33)$$

Equation (1.32) equates to the w_x component, Equation (1.33) to the w_y and w_z components.

Comparing Equations (1.32) and (1.33) with Equations (1.18) and (1.19), as well as with Equations (1.21) and (1.22), we establish the fact that the following link exists between the spectral densities written in the various forms:

$$S(\omega)=S(\Omega)/V=S(\nu)L/V. \qquad (1.34)$$

Let us see to what degree the analytical expressions for the correlation functions and spectral densities of the velocity field of atmospheric turbulence cited above agree with the concepts of three intervals of turbulent air motion introduced in Section 1,3. The most convenient way to do this is to use the graphic of the spectral density represented as a function of the space frequency Ω. The graphic of the longitudinal spectral density, constructed using Equation (1.18) when $\sigma_w^2=1\ m^2\cdot sec^{-2}$ and L=300 m, is shown in Figure 1.16 by way of an example. Plotted are the boundaries of the three intervals of turbulent air motion. Clearly seen is the fact that in the large-scale interval, covering a comparatively narrow part of the spectrum (if frequencies are plotted on a conventional, and not on a logarithmic, scale), the spectral /28
density has virtually no dependence on frequency Ω or wavelength $\lambda=2\pi/\Omega$. It should be noted that this part of the spectrum, obtained from an analytical expression for isotropic turbulence certainly cannot be expected to reflect the processes taking place in the real atmosphere at all well because, as we know, air motion in this interval is anisotropic. Moreover, wavelengths longer than the horizontal extent of the turbulent zone (see Figure 1.7) have no physical meaning in the real atmosphere. Despite these drawbacks of the analytical formula, its use to investigate airplane dynamics introduces no significant difficulties because the effect of long wave wind disturbances on an aircraft are very slight. The measurement of the results of this effect are usually beyond the capabilities of airplane instrumentation.

The inertia range in logarithmic coordinates is characterized by a linear

dependence of the spectral density on the space frequency, and this corresponds to a step function (see Figure 1.16).

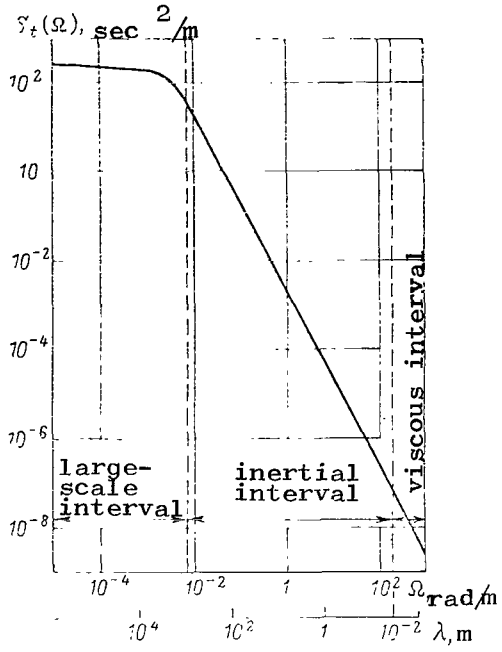

Figure 1.16. Turbulent air motion intervals.

The spectral density in the inertia range is practically proportional to Ω^{-2} in the analytical expressions at (1.18) and (1.19) introduced in this paragraph.

The slope of the spectral density curves in the viscous interval section of Figure 1.16 is the same as that in the inertia interval section. This contradicts the theoretical assessment of the spectrum in the viscous interval, in accordance with which the slope of the curves should be much steeper in the inertia interval. This drawback in the analytical formulas for atmospheric turbulence used here is associated with a desire to obtain the simplest, and therefore the most convenient formulas, to use for the computations.

This attempt at simplification has resulted in Equations (1.12) and (1.13) for the correlation functions being unable to produce a zero value for the derivative when r=0. The derivative of the correlation function changes /29
step-wise with passage through the r=0 value. For example, in Equation (1.12), when approaching zero from the right, $\left(\frac{dR_f(r)}{dr}\right)_{r=0} = -\frac{\sigma_w^2}{L}$, and when approaching from the left, $\left(\frac{dR_f(r)}{dr}\right)_{r=0} = \frac{\sigma_w^2}{L}$. This

is explained in Figure 1.17.

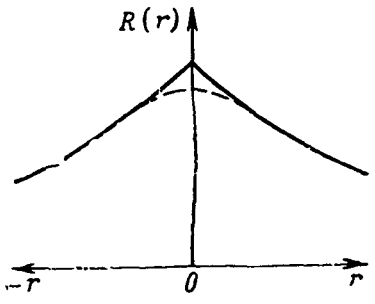

Figure 1.17. Simplified (solid) and more precise (dotted) graphic of the correlation function of wind velocity.

The correlation function for a derivative of a random function can be determined as the second derivative of the correlation function for the most random function. Therefore, the second derivative of the correlation function for the velocity corresponds to the correlation function for the acceleration of the air particles during turbulent motion.

Since the simplified description of the correlation function for the velocity of the turbulent motion of the air will lead to the appearance of a jump in the value of the first derivative of this function when $r \approx 0$, it is obvious that the second derivative of it, that is, the correlation function for the acceleration of air particles, will contain a pulse function (δ-function) when $r = 0$. As is shown in Apprneix D, in this case the dispersion in the random process will equal infinity, and this cannot happen in the case of real processes. The infinite value of the dispersion for the acceleration of air particles of turbulent motion results from the above-mentioned simplification during the analytical description of the correlation function for the velocity of turbulent motion.

This contradiction will be eliminated if the drop in the spectrum in the viscous interval is sharper, and the graphic for the correlation function for wind velocity near the value $r = 0$ is in the form shown in Figure 1.17, by the dotted line. In this case, $\left(\frac{dR(r)}{dr}\right)_{r=0} = 0$. Reference [7] contains an approximate analytical expression for the section of the correlation function $R(r)$ near $r = 0$, that associates the nature of the correlation function over this section with the scale of turbulent air motions in the viscous interval.

The analytical expressions for the correlation functions and the spectral densities of the longitudinal and lateral components of the vector for the random component of the wind velocity cited in the foregoing were found by processing the experimental data obtained when investigating turbulence in wind tunnels, as has already been pointed out. The theoretical assessment of the spectral density in the inertia range first made by A. N. Kolmogorov [14] contains results that differ somewhat from the foregoing. The spectral density in the inertia range should be proportional to $\Omega^{-5/3}$, according to this assessment. /30

This was the basis for the proposal by Von Karman [50] of the following formulas for the longitudinal and lateral correlation functions and spectral densities of the velocity field of turbulent air motion.

The correlation functions are

$$R_t(r) = \sigma_w^2 = \frac{2^{2/3}}{\Gamma\left(\frac{1}{3}\right)}\left(\frac{r}{1{,}339L}\right)^{1/3} K_{1/3}\left(\frac{r}{1{,}339L}\right), \tag{1.35}$$

$$R_n(r) = \sigma_w^2 = \frac{2^{2/3}}{\Gamma\left(\frac{1}{3}\right)}\left(\frac{r}{1{,}339L}\right)^{1/3}\left[K_{1/3}\left(\frac{r}{1{,}339L}\right) - \right.$$
$$\left. - \frac{1}{2}\left(\frac{r}{1{,}339L}\right) K_{2/3}\left(\frac{r}{1{,}339L}\right)\right], \tag{1.36}$$

where L is the turbulence scale;

$K_{1/3}(r)$ and $K_{2/3}(r)$ are modified Bessel functions of fractional order;

$\Gamma(x)$ is the gamma function.

The coefficient $2^{2/3}/\Gamma(1/3)$ equals 0.59253. Figure 1.18, containing the graphics for the lateral correlation functions constructed through Equation (1.13) (dotted) and Equation (1.36) (solid), is included for purposes of comparison. This comparison shows that these correlation functions differ little from each other.

The spectral densities corresponding to Equations (1.35) and (1.36) are in the form

$$S_t(\Omega)=\sigma_w^2=\frac{L}{\pi}\frac{2}{[1+(1,339L\Omega)^2]^{5/6}}, \tag{1.37}$$

$$S_n(\Omega)=\sigma_w^2\frac{L}{\pi}\frac{1+\frac{8}{3}(1,339L\Omega)^2}{[1+(1,339L\Omega)^2]^{11/6}}. \tag{1.38}$$

Equations (1.37) and (1.38) provide a spectral density proportionality magnitude of $\Omega^{-5/3}$ for the inertia range of scales of turbulent motion, that /31 is for values $1339\,L\Omega \gg 1$, as follows from the theoretical propositions. Graphics for spectral densities corresponding to equations (1.37) and (1.38) are not shown because they are similar to analogous graphics in Figures (1.13) and (1.14) constructed through equations (1.19) and (1.18), differing slightly in the slopes of sections in the high frequency region. Note that the analytical expressions at (1.35)-(1.38) for the velocity field of air turbulence retain the principal drawbacks noted when the expressions at (1.12)-(1.15) were reviewed; namely:

(1) the reduction in the spectral density with increase in frequency in the viscous range is not sharp enough;

(2) the step change in the derivative of the correlation function when passing through the r=0 value.

Reference [48] points out that when experimental data on atmospheric turbulence are processed very carefully, the correlation functions and the spectral densities for the lateral component of the velocity of a random wind are somewhat better approximated by the expressions at (1.35)-(1.38) than by the expressions at (1.12)-(1.15). But it should be pointed out that the atmospheric turbulence spectra obtained experimentally have quite a wide scatter in the values for the Ω exponent in the inertia interval, depending on meteorological conditions, with the result that the slight difference between the approximations at (1.12)-(1.15) and at (1.35)-(1.38) are of no special significance for the majority of flight dynamic problems. Moreover,

the expressions at (1.12)-(1.15) are better suited to the purpose than are those at (1.35)-(1.38) because of their simplicity. This is what makes the analytical investigation of the motion of an airplane in turbulent air much simpler when the formulas at (1.12)-(1.15) are used, as it does when this motion is modeled using analog computers. It is for these reasons that this book will use the formulas at (1.12)-(1.15).

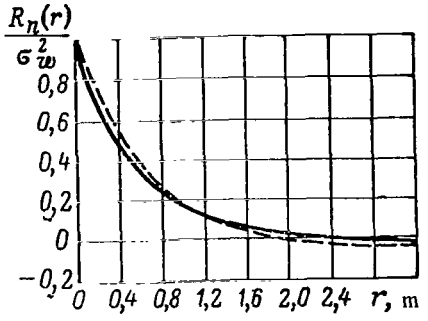

Figure 1.18. Graphics of normalized correlation functions constructed through Eq. (1.36), solid, and Eq. (1.13), dotted.

There is no difficulty in using the formulas at (1.35)-(1.36) if flight dynamics in turbulent air are analyzed using digital computers.

In concluding this section, let us point out that the instantaneous values for the components of the atmospheric wind velocity vector are considered distributed in accordance with a normal law. For any of the wind velocity components (for w_x, for example), the probability density is in the form (see Appendix D) /32

$$f(w_x) = \frac{1}{\sigma_w \sqrt{2\pi}} e^{-\frac{(w_x - W_{ex})^2}{2\sigma_w^2}}, \qquad (1.39)$$

where

W_{ex} is the constant component of the wind velocity in the direction of the x axis.

Experimental results confirming the correctness of a normal distribution for the instantaneous components of wind velocity will be given in what follows.

1.5. Results of Some Experimental Investigations of Air Turbulence

Analysis of experimental data can be used to evaluate under what conditions, and how well, the analytical expressions given in Section 1.4 will correspond to the real characteristics of atmospheric turbulence.

This section will take up the following questions:

(1) How close are the theoretical and real characteristics of turbulence?

(2) For what minimal flight speeds is Taylor's hypothesis of a "frozen" velocity field correct?

(3) For what kinds of atmospheric disturbances can the analytical expressions for isotropic and homogeneous turbulence be used?

(4) What turbulence scale and root-mean-squares of wind velocity magnitudes should be used in computations?

(5) How correct is the proposition concerning the distribution of the instantaneous values for wind velocity in accordance with a normal law?

Intensive investigation of the effect of air turbulence on flight dynamics has been going on for decades. Nevertheless, even today not all of the questions posed above can be given exhaustive answers. This is because of the complexity of the phenomenon under study and because of the great many meteorological, and other, factors that influence the characteristics of turbulence.

Both Soviet and foreign periodicals have published a great many articles in recent years containing the results of experimental investigations of the spectral composition of the air turbulence. These investigations were made in a free atmosphere and usually were carried out by an airplane acting as the probe. The methodology used for these investigations was as follows: /33

(1) the airplane serving as the probe was instrumented to record normal acceleration, altitude, and flight speed;

(2) a correlation function was constructed from the recordings of normal acceleration, and this was, in turn, used to construct the spectral density of the acceleration;

(3) the data obtained were converted into the spectral density of the vertical component of the velocity of the turbulent air motion with the dynamic characteristics of the airplane taken into consideration.

Figure 1.19 presents data from several measurements made of the spectral density of vertical wind gusts, borrowed from reference [15]. All the experimental curves in this figure plot between the two graphics (dotted) constructed using Equation (1.19). Even better concordance between the experimental

and theoretical results is shown in Figure 1.20 [1]. This latter figure shows the results of the measurement of the spectral density of the vertical wind component at an altitude of 300 meters. The slope of the straight line section can be approximated by a curve proportional to $\Omega^{-1.82}$.

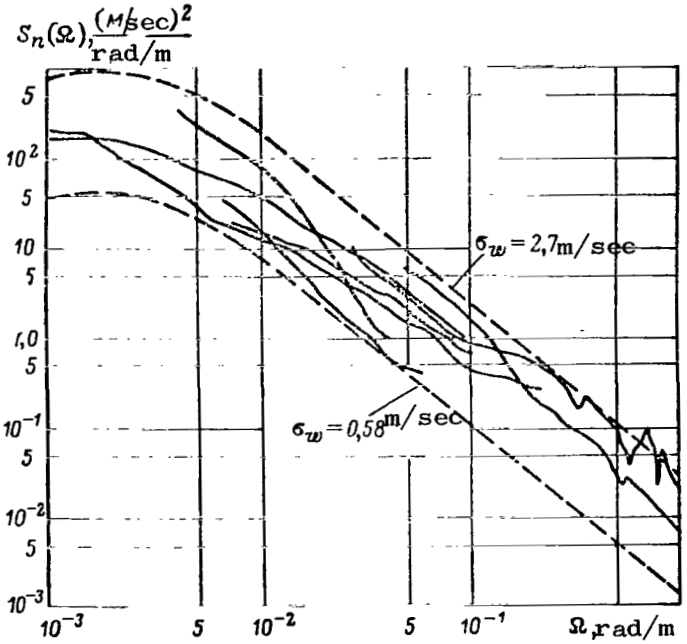

Figure 1.19. Graphics of the spectral density of the vertical component of the wind velocity, obtained experimentally.

/34

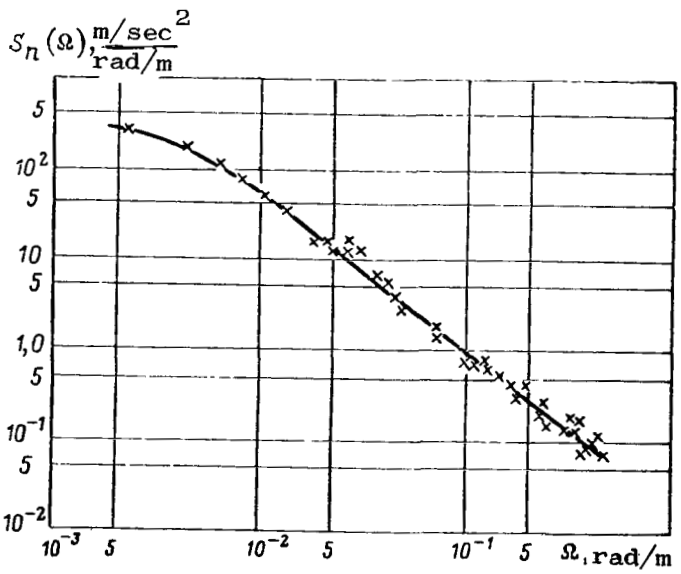

Figure 1.20. Graphic of the spectral density of the vertical component of the wind velocity, obtained experimentally.

The methodology used to measure atmospheric turbulence using a probe airplane as described above has two very definite drawbacks that reduce the accuracy of the data obtained.

The first of these involves the fact that an airplane, because it occupies a definite volume in space, is the object of an averaged action when accelerations are measured. The effect is greater the bigger the airplane. At the same time, the values for the velocity of the vertical wind obtained by converting the accelerations are equated to one point, the airplane's center of gravity. Chapter 3 will take up a theoretical method for assessing the averaging effect of airplane size, but it is quite complicated, as well as inaccurate.

A second drawback of the method described is its complexity, and the low degree of accuracy of the mathematical expressions used to convert from accelerations to wind velocities. The principal reasons for the inaccuracy in the mathematical characteristics of the airplane are contained within the complexity of taking into consideration such phenomena as the unsteadiness of the flow over the aircraft in turbulent air, and the nonrigidity of the structure. Chapter 3 will discuss the principal theoretical considerations given these factors. Finally, the pilot's actions when he is piloting the airplane introduce additional random, and very significant, errors.

Another method for recording the velocity of turbulent air motion was developed in 1960 [16]. This method involved recording pulsations in the velocity of the air flow incident on the airplane. Pulsations in the velocity in the direction of the airplane's longitudinal axis were also recorded. Figure 1.21 is a copy of an oscillogram for the longitudinal component of the wind velocity obtained in flight. /35

Figure 1.21. Variable component of the longitudinal component of the wind velocity.
H=370 meters, V_o=225 km/hour

Processing of the measurement data results is a determination of the longitudinal correlation function of the wind velocity, $R_t(\tau)$, and of the longitudinal spectral density, $S_t(\omega)$. Then, utilizing the speed, V, at which the airplane is flying, a known magnitude, we can obtain the space characteristics.

Let us, by way of an example, introduce here the data that result from processing 14 oscillograms. The methodology explained in Appendix D was used to process these oscillograms. Table 1.3 lists the conditions under which each of the oscillograms of the longitudinal component of the velocity of the turbulent air motion was obtained, as well as the root-mean-square of this velocity.

TABLE 1.3

Positions in Figures 1.22, 1.23, and 1.24	Flight altitude, meters	Flight speed		Root-mean-square of velocity of gusts, m/sec	Evaluation by crew of rough air intensity
		km/hr	m/sec		
1	500	230	63.8	1.186	Average
2	440	235	65.2	1.795	Strong
3	350	230	63.8	0.925	Average
4	960	238	66.1	0.682	Weak
5	370	230	63.8	1.66	Strong
6	920	210	58.4	1.31	Average
7	940	237	65.8	1.28	Average
8	780	240	66.8	0.507	None
9	1750	250	69.4	0.493	None
10	1650	260	72.2	0.394	None
11	440	246	68.3	1.16	Average
12	440	246	68.3	1.11	Average
13	440	235	65.2	2.07	Strong
14	370	230	63.8	2.20	Strong

Column 6 in the table lists the subjective evaluation of the rough air intensity by the crew. What follows from the data in the table is that when the root-mean-square of the velocity of the horizontal gusts is less than 0.5 m/sec[7] the crew has no sensation of rough air and feels that the

7. If flight speed of this airplane increases, threshold value of wind velocity decreases; when turbulence scale rises, unit load on wing and altitude rise.

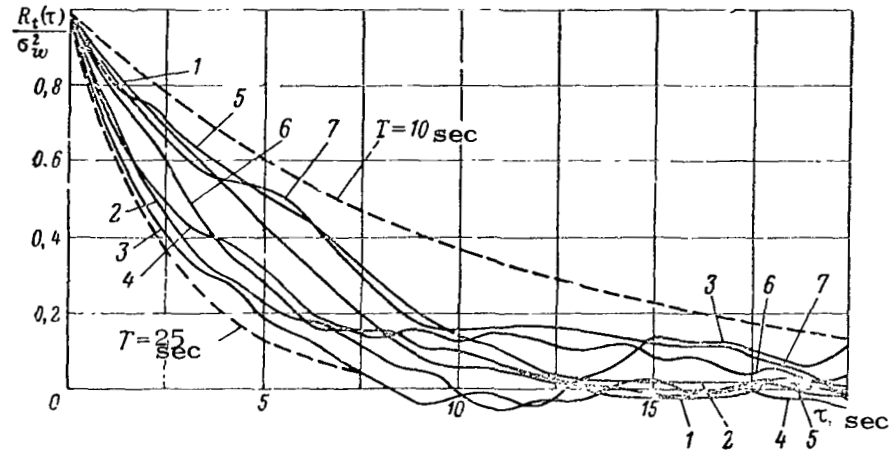

Figure 1.22. Graphics of normalized correlation functions of the longitudinal component of the wind velocity, obtained experimentally.

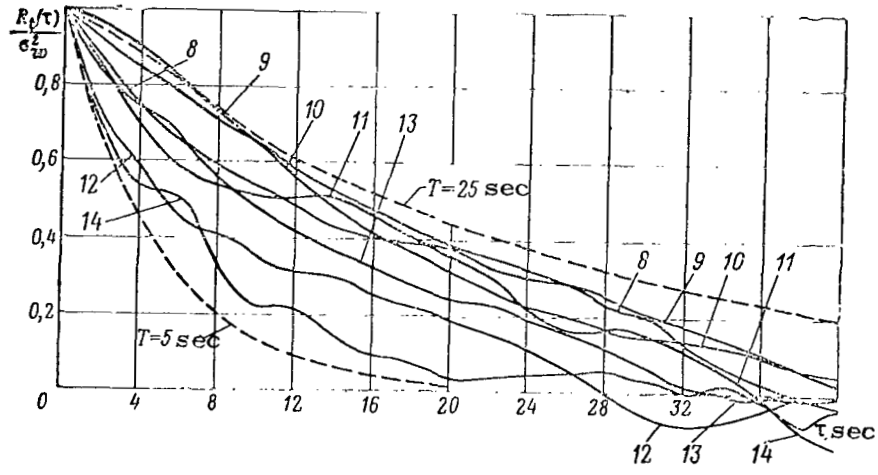

Figure 1.23. Graphics of the normalized correlation functions of the longitudinal component of the wind velocity, obtained experimentally.

flight was made in still air. This result is in concordance with the evaluation of flight conditions in terms of the root-mean-square of the velocity of vertical gusts cited in [15].

The graphics for normalized correlation functions of the longitudinal component of the velocity of turbulent motion for the oscillograms listed in Table 1.3 are shown in Figures 1.22 and 1.23. These figures show the boundary exponents with time constants T by the dotted curves, between which practically the entire family of experimental curves fall. Equation (1.27) must be used to change the scale used for the axis of abscissa for each of /37

the curves in Figures 1.22 and 1.23 in order to make the transition from the time argument to the space one. In such case the denominator of the exponent of the envelope exponentials, which is the turbulence scale, too should be determined from the relationship

$$L = VT \qquad (1.40)$$

The limits of T in Figures 1.22 and 1.23 equal 2.5 and 25 seconds. Since the speed at which the airplane is flying in all modes listed in Table 1.3 is close to 60 m/sec, then, on the basis of Equation (1.36), the turbulence scale for the realizations considered can be taken as changing in the limits from L≈150 to L≈1500 meters.

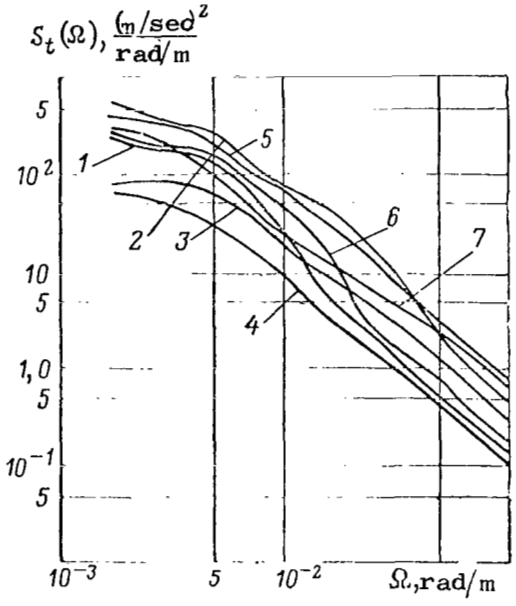

Figure 1.24. Graphics of the spectral densities corresponding to the correlation functions in Figure 1.22.

Figure 1.24 shows the unnormalized spectral densities for the longitudinal component of the wind velocity corresponding to the correlation functions in Figure 1.22. The experimental curves were constructed as a function of the space angular frequency, Ω, for convenience in comparing them with the theoretical curves (Figure 1.13). Equation (1.31) was used to make the transition from time (ω) to this frequency. Equation (1.34) was used to convert the values for $S(\Omega)$ obtained from the experimental data to the values for the spectral density $S(\omega)$. A comparison between the nature of the experimental unnormalized (Figure 1.24) and the theoretical

normalized (Figure 1.13) curves shows how extremely concordant they are. The scatter in the experimental curves along the vertical can be explained /38 by the difference in turbulence scale, L, and by the values of the dispersion σ_w^2 for each realization.

Much has been written in recent years [17, 18, 19] reviewing methods for improving the accuracy with which turbulent air wind velocity is measured by meteorological towers, as well as by airplane instrumentation.

Appendix D contains the methodology used for making direct measurement of the three components of the random wind vector when an airplane is flying through a zone of turbulence, as well as a brief description of the instrumentation used.

A reasonably well-founded response can be made to the question of lowest airplane flight speeds for which the Taylor "frozen" turbulence hypothesis can be used. This hypothesis can be used very successfully to process data on measurements made by meteorological towers of the random components of the wind velocity. At the same time, average wind velocities ensuring air transfer are measured in meters per second. Therefore, the use of the "frozen" turbulence hypothesis is permissible from a practical standpoint, even at the motion velocities indicated. By way of an illustration confirming the investigations, we have included Figure 1.25 [1] which shows the spectral densities of the vertical component of the turbulence, measured simultaneously by two methods at 60 meters; by airplane, and by a captive balloon (during these measurements the airplane flew alongside the balloon). Concordance of the graphics in Figure 1.25 can be considered quite good if the great many unavoidable errors inherent in each of the methods used are taken into consideration.

The question of the applicability of the apparatus of stationary random functions to describe the various types of turbulence is an extremely important one. A great many experiments have shown that the use of stationary random functions will provide quite a good description of real types of turbulence in the overwhelming majority of cases. However, there are some types, such as turbulence in a thundercloud [1], and turbulence near obstacles (mountains, for example), that probably cannot be described satisfactorily by the

random stationary functions apparatus. These types of turbulence in the atmosphere, in addition to random air motion, include individually ascending and descending flows of considerable extent (several kilometers) with velocities as high as 30 to 40 m/sec.

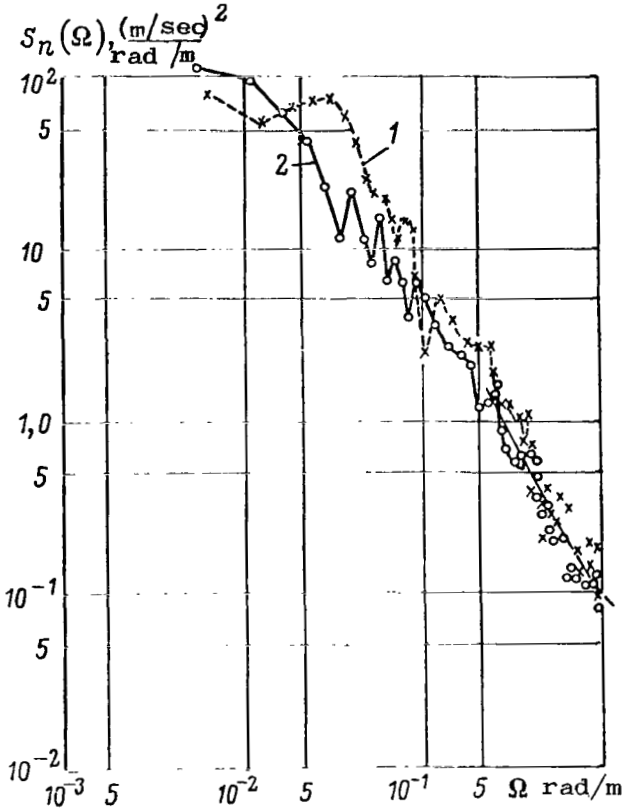

Figure 1.25. Spectral densities of the vertical component of the wind velocity. 1 - from measurement made by a probe airplane; 2 - from measurements made by a captive balloon.

A great deal of data on the simultaneous measurement of all three components of the wind vector must be available in order to provide a direct answer to the question of turbulent air isotropy. Very few such measurements have been made to date. Consequently, the question of isotropy of the atmosphere is most often answered on the basis of indirect measurements. /39 The hypothesis with respect to turbulent air isotropy for a specified flight altitude for an airplane conventionally is considered to be valid if there

is equality between the maximum velocities of the vertical and horizontal gusts, or equality between the root-mean-square of these velocities. The experimental data confirm the practical equality of the horizontal and vertical gusts. Figure 1.26 shows the maximum velocities of horizontal gusts as a function of the maximum velocity of vertical gusts [20]. Each point corresponds to maximum velocities recorded in one flight through a turbulent zone. Flights took place in a storm at altitudes ranging from ground level to 10 km.

/40

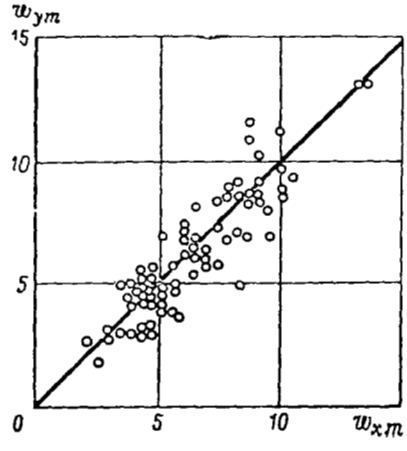

Figure 1.26. Experimental data on maximum values of velocities of vertical and horizontal wind gusts.

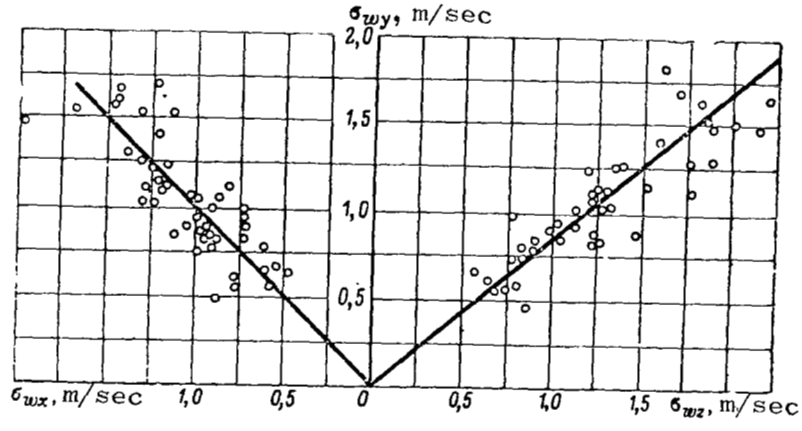

Figure 1.27. Experimental data on root-mean-squares of the three components of the wind vector.

Figure 1.27 shows the results of measuring the root-mean-squares of the variable components of the wind vector at altitudes from 50 to 800 meters [21].

The data in Figures 1.26 and 1.27 provide practically accurate confirmation of the equality of maxima, as well as of root-mean-squares, of the wind velocity components. We should point out that the equality of the root-mean-squares is maintained at lower altitudes as well, despite the fact that there the turbulence is anisotropic. This fact once again confirms the indirect nature of the evaluation used to get some idea as to the turbulence isotropy. Equality of the root-mean-squares of the variable components of the wind velocity components at low altitudes can be explained by the equality of the kinetic energies of these components (and the vertical component has a higher frequency spectrum than do the longitudinal and lateral components).

Data on the nature of the change in the random vertical wind components for the lowest altitudes are contained in [22]. Figure 1.28 shows the ratio of the amplitude of the random vertical wind component w_{ym}, to the mean value of the horizontal velocity, W_e.

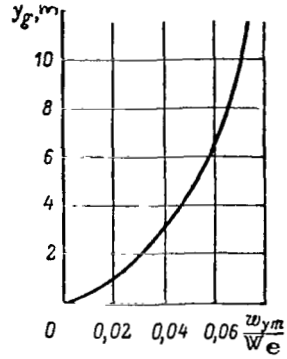

/41

Figure 1.28. Ratio of amplitude of pulsations of vertical component of the wind velocity to the mean value of the horizontal velocity at low altitudes.

The literature on the subject contains virtually no data on the length of a section over which turbulent air can be considered homogeneous. Reference [23] points out that the magnitude of σ_w will not change more than 25%, on the average, over a 15 km long section.

The author of this book used a special instrument [24] to obtain oscillograms of the random longitudinal wind component over 30 sections during flights in a thermal turbulence zone. The average length of a section with homogeneous turbulence was 25 km, with the range from 5 to 78 km. Naturally, the data cited are inadequate if we are to obtain an authentic value for the average length of a section of homogeneous turbulence, but they do make it

possible to estimate the order of this magnitude.

The question of numerical magnitudes of the turbulence scale, L, and of the root-mean-square of the velocity component σ_w is a most significant one in terms of the practical application of analytical expressions to characterize turbulent air. Unfortunately, we do not now have sufficiently complete data on these magnitudes because of the very significant dependence of L and of σ_w on meteorological conditions, and, at low altitudes, on the magnitude of the irregularities in the earth's surface as well. Given these conditions, it is quite difficult to obtain authentic mean magnitudes.

In the majority of the work done dealing with turbulent air questions, the mean value of the turbulence scale in free air is taken as 300 meters.

It should be pointed out that the turbulence scale usually has been determined from data on wind gusts obtained by recomputing the accelerations measured on the airplane, and with the airplane's dynamic characteristics taken into account. This method is relatively nonresponsive to gusts with very low, or with very high, frequencies, because these gusts establish such insignificant accelerations on an airplane that they are not recorded by the instrumentation. Since the amplitude of high frequency gusts diminishes rapidly with increase in frequency, the role of such gusts is insignificant on some predetermined turbulence scale. The picture is different in the case of low frequency gusts, since their amplitude does not decrease with decreases in frequency. This is why the fact that turbulence scales established from data based on acceleration measurements will be smaller than the actual scales must be taken into consideration. This assumption /42 has been confirmed by the results of very recent investigations made of turbulent air motion. The method of direct measurement of the components of the random wind velocity vector, described in Appendix D, was used for these investigations. Generalized data on measurements of the turbulence scale under the most varied of meteorological conditions (from clear-air turbulence to thunderstorms) are cited in reference [48]. The authors of this paper came to the conclusion that the turbulence scale change is in the limits of from 1000 to 2000 meters under these conditions, with the most probable value closer to 2000 meters than to 1000 meters. Naturally, these data do not refer to low altitudes.

At low altitudes (from 300 meters and lower) a rough approximation can be made by saying that for the vertical wind component the mean value of the turbulence scale increases in proportion to the altitude above the ground. So far as the absolute value of this scale is concerned, the change is over a wide range, one depending on the nature of the surface (fields, woods, hills, mountains), from a value equal to the flight altitude for a level surface to values larger by a factor of 3 to 4 for very broken ground. So far as the longitudinal and transverse components of the wind velocity are concerned, a reduction in the turbulence scale as a result of approach to the ground should not occur as sharply as it does, in the case of the vertical component.

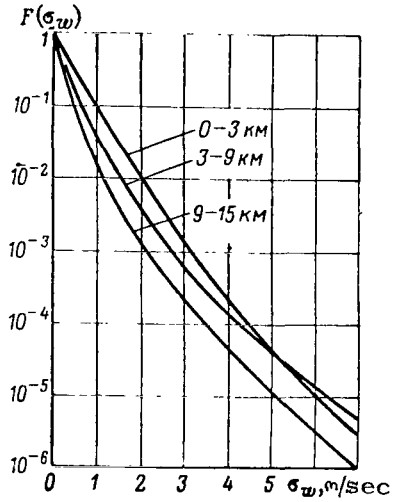

Figure 1.29. Graphics of the functions of the distribution of the probability of the excess of the root-mean-square of the velocity of the vertical wind component at different flight altitudes.

The functions of the distribution of the root-mean-square of this magnitude for different altitudes [15] are shown in Figure 1.29, by way of an example of the assignment of the characteristics of the root-mean-square for the wind, σ_w. These graphics show the probability of the excess of a specified value of σ_w and are valid for long total flight times (thousands and tens of thousands of hours).

If we compare the graphics of Figure 1.29, we see that the flight time in a turbulent atmosphere decreases significantly wihh increase in flight altitude. For example, time in a severely disturbed atmosphere (σ_w>2 m/sec) is about 1% of the total flight time for altitudes from 0 to 3 km, and 0.1% for altitudes of from 9 to 15 km.

The data in Figure 1.29 were obtained between 1935 and 1955, the result /43 of processing the recordings made by recorders installed in airplanes belonging

to United States commercial air lines. These recordings were of the accelerations as a function of flight speed, and the data naturally reflect the influence of concrete geographic conditions and of the quality of meteorological support given flights made by these air lines.

The data contained in [1] provide a root-mean-square of the vertical wind velocity component of about 2.5 m/sec when flying in cumulonimbus clouds with average length of turbulent sections about 15 km. This same source provides data to show that σ_w is 4 m/sec, and even 5 m/sec in individual cases, for thundery conditions.

There is one significant stipulation that must be made with respect to the above-cited root-mean-squares for the vertical wind component under different meteorological conditions, as well as with respect to the graphics in Figure 1.29. These data were obtained by converting the accelerations experienced by the airplane in a turbulent zone, and thus reflect all the inaccuracies of this method (already mentioned in the foregoing). Specifically, these data were designed for use in analytical investigations of airplane dynamics, with the most probable value of the turbulence scale assumed equal to 300 meters, as had been accepted earlier in most cases. But if one were to accept contemporary data on the turbulence scale, and take it as equal to 1000 to 2000 meters, the σ_w values for the analytical computations would have to undergo extensive review, and this suggests that the values ought to be increased substantially. This conclusion is based on the materials in Chapter 3, where it is pointed out that accelerations experienced by an airplane flying through atmospheric turbulence decrease quite significantly with increase in the turbulence scale. Therefore, if the turbulence scale increases from 300 meters to 1000-2000 meters, the root-mean-square of the vertical gust velocity must be increased by a factor of from 2 to 2.5, in order to retain the same root-mean-square for the accelerations. This conclusion can be substantiated. The graphics for the normalized spectral density of vertical gusts, shown in Figure 1.14, indicate that in the Ω=0.01 to 1 m^{-1} range, in which the gusts act most effectively on the airplane, the spectral density values decrease significantly with increase in the turbulence scale. Consequently, one must take larger root-mean-squares for the wind velocity, rather than larger turbulence scales, in order to obtain the same root-mean-square for the acceleration on different turbulence scales.

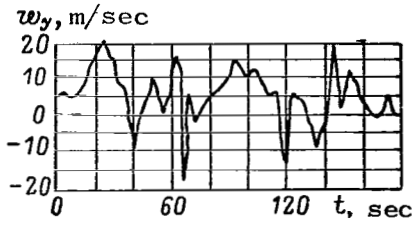

Figure 1.30. Vertical wind component over mountains in very heavy turbulence.

Maximum loads on the airplane occur when flying in a turbulent atmosphere /44 over mountains in thunderstorm conditions. Figure 1.30 shows the nature of the change in the vertical wind component over mountains when the maximum increase of the acceleration reached three G's [8]. The very large scale of the disturbances in Figure 1.30, as compared with ordinary turbulence, indicates that turbulence over mountains is definitely associated with the geometry of mountain ranges.

Figure 1.31 shows oscillograms depicting the nature of the change in altitude, y_g, indicated speed, V_{in}, and normal, n_y, and lateral, n_z, accelerations when flying along the edge of a thundercloud.

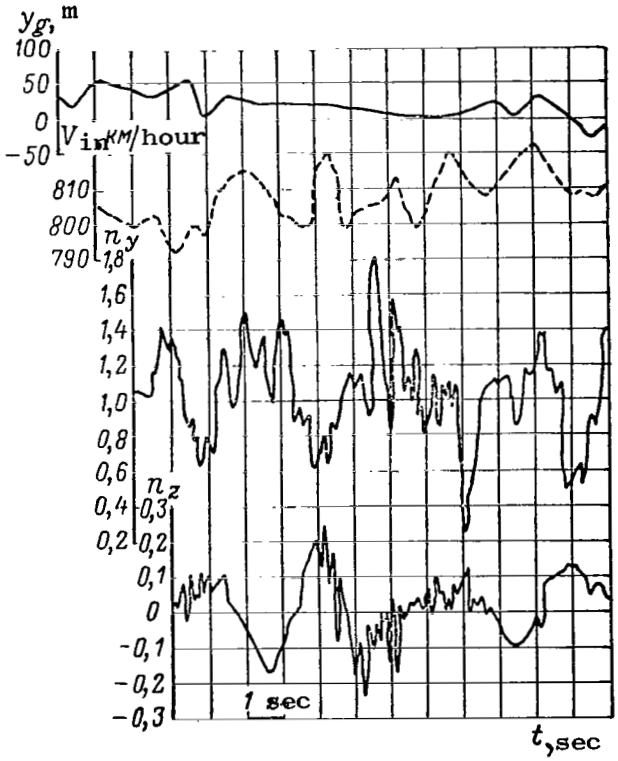

Figure 1.31. Change in altitude, indicated speed, and normal and lateral accelerations when flying along the edge of a thundercloud.

In concluding this section, we will cite the author's experimental data in accordance with the law for the distribution of the velocity of the random wind component. A careful processing of a great many oscillograms of the /45
horizontal wind component, obtained during a summer experiment, invariably resulted in a practically normal distribution law. Figure 1.32 is an example of two histograms for the probability density of velocity values, w_x, obtained as a result of processing two realizations. Processing was done for 500 points, at 0.5 second intervals. An Li-2 airplane flew about 15 km in this time. The wind's root-mean-square for Figure 1.32-a is σ_w=1.1 m/sec, and 1.18 m/sec for Figure 1.32-b.

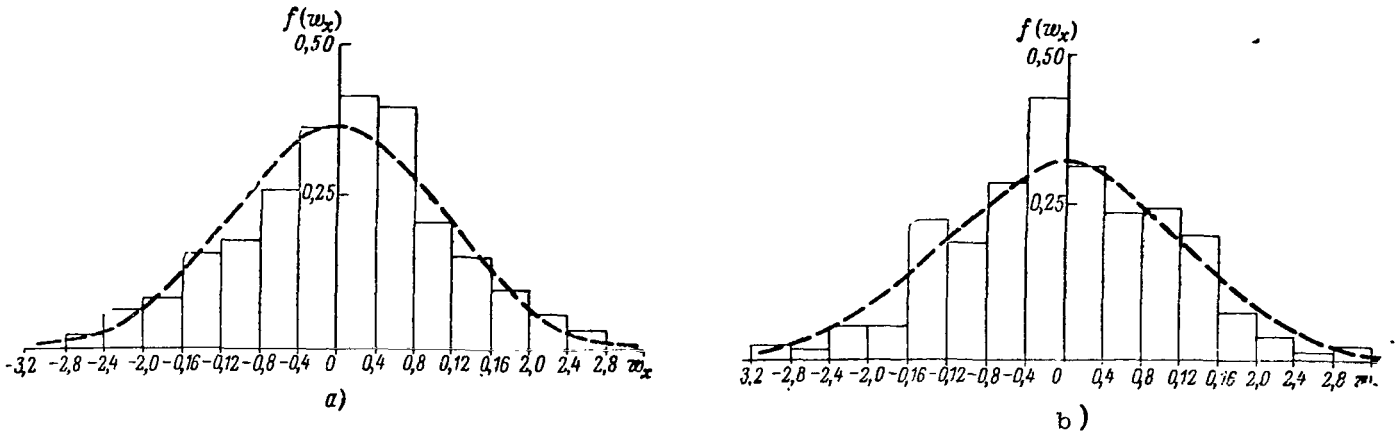

Figure 1.32. Histograms for probability density of longitudinal wind component.

Both of the histograms shown provide good compatibility between the experimental data and the theoretical curves of probability density for a /46
normal law. The degree of compatibility between theoretical and experimental distributions was evaluated using the Pearson "X^2 criterion." Probabilities, p, were determined such that purely random causes would not result in a degree of divergence between the theoretical and the experimental distribution less than that X^2 value computed for the particular oscillogram. These probabilities fall between 0.2 and 0.5, and are considered as practically adequate [25].

The experimental data presented confirm the possibility of using the normal law at (1.35), to describe the distribution of the instantaneous values of the wind velocity components.

CHAPTER II

MOTION EQUATIONS FOR AN AIRPLANE IN MOVING AIR

2.1. Statement of the Problem

Figure 2.1 is a schematic diagram of the flight of an airplane in moving air. The wind velocity vector, $\overline{W}$, can be represented at every point in space by the sum of the projections[1] on the axis of a geographic system of coordinates x_g, y_g, z_g. Only the projection of the variable component, $\overline{w}$, of the wind vector is shown in Figure 2.1. /47

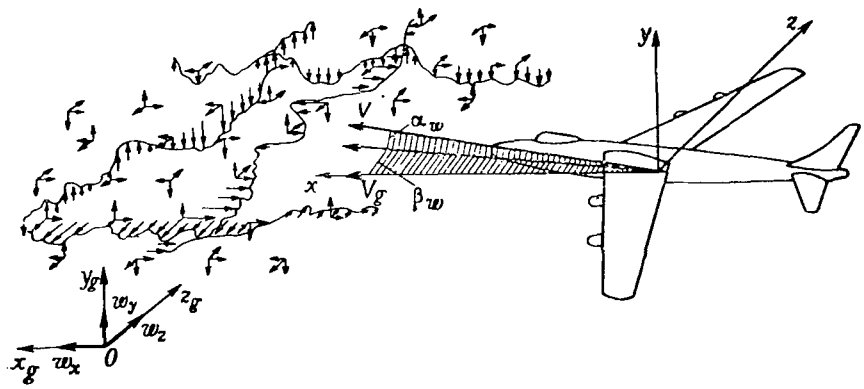

Figure 2.1. Flight of an airplane in moving air.

1. If the flight of the airplane in the undisturbed condition is not in the wings level altitude, the determination of the projections of the wind velocity must be made using a system of coordinates (associated with the earth) the x axis of which is parallel to the undisturbed flight-path.

The airplane axes, x, y, and z, are the body axes. As will be seen from Figure 2.1, the airplane speed relative to the air (air speed), V, in gusts differs from the ground speed, V_g, in magnitude and in direction (the angles α_w and β_w). Change in the magnitude and direction of the speed vector, V, results in the appearance of additional forces and moments that act on the airplane and cause a disturbance in the original flight attitude. /48

In very strong gusts the disturbance of the original attitude can become extreme, and the airplane can encounter stall conditions (with attendant loss of flight stability, as well as controllability). Investigation of these flight attitudes must be carried out with a complete system of airplane motion equations without linearization and breakdown of motion into longitudinal and lateral. Problems such as these are extraordinarily complex, do not yield to analytical investigation in general form, and are not considered in this book.

The majority of the other problems of moving air flight dynamics can be described quite satisfactorily by linearized equations, broken down for longitudinal and lateral aircraft motion. This methodology results in general solutions for the flights investigated, with the results of the theoretical analysis quite compatible with the results of flight experimentation right up to stall conditions.

In concluding this section, a few comments with respect to airplane axes systems are in order. The x axis in the system of airplane body axes x, y, and z as used in this book, is not directed along the wing chord, as is customary, but along the direction of the ground speed in the undisturbed condition, V_e. Speed V_e makes the angle α_e with the wing chord, and is the undisturbed value of the angle of attack in the original condition. It is therefore necessary to convert to new axes when deriving equations for the moment of inertia. If the moments of inertia relative to the principal axes of inertia of the airplane, I_{xp}, I_{yp}, and I_{zp} and the angle Δ in the plane of symmetry of the airplane between the direction of the principal and body axes, are known, the values of the moments of inertia about the body axes can be determined by the formulas

$$\left.\begin{aligned} I_x &= I_{xp}\cos^2\Delta + I_{yp}\sin^2\Delta, \quad I_y = I_{xp}\sin^2\Delta + I_{yp}\cos^2\Delta, \\ I_z &= I_{zp}, \quad I_{xy} = \frac{1}{2}(I_{xp} - I_{yp})\sin 2\Delta, \quad I_{yz} = I_{zx} = 0. \end{aligned}\right\} \qquad (2.1)$$

The mutual positioning of the geographic (x_g, y_g, z_g) and airplane body axes (x,y,z) is shown in Figure 2.2. The body axes are shown in the arbitrary positions they assume with the aircraft at some moment of disturbed motion. The transition of the body axes to this arbitrary angular position from the original position[2] (x_1, y_1, z_1), corresponding to the undisturbed condition, is made in three turns, which should be made in the following order:

1) a turn equal to the angle of yaw ψ around the vertical axis y_1, as a result of which the axes take up the position x_2, y_2, z_2, and the x axis takes up a final position along the course;

2) a turn equal to the angle of pitch ϑ around the horizontal axis, z_2, /49 as a result of which the axes take up the position x_3, y_3, z_3, and the x axis takes up a final position along the pitch;

3) a turn equal to the angle of roll γ around the x axis (or x_3, since they coincide), as a result of which all axes take up a final x, y, z position.

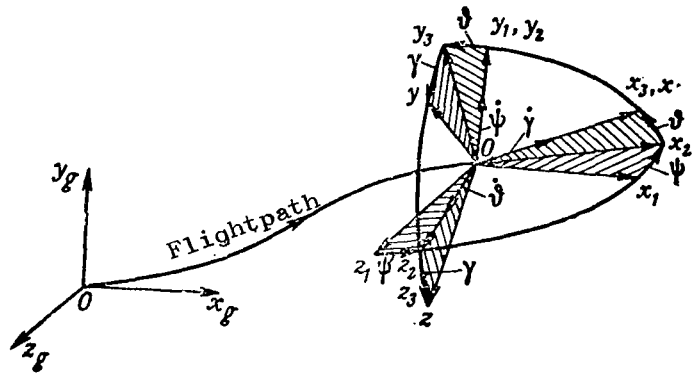

Figure 2.2. Mutual positioning of geographic and body coordinates.

2.2. Equations for Longitudinal Motion in Moving Air

We will not consider the many phenomena with relatively little effect on aircraft motion in order to obtain the simplest possible equations for

2. In this case, coinciding with the geographic axes.

airplane dynamics. We will disregard the link between longitudinal and lateral motions, and will consider the airplane to be a rigid body[3] of constant mass. Given these assumptions, the equations for the dynamics of longitudinal motion in body axes have the form [26, 27]

$$\left.\begin{aligned} m\frac{dV_{gx}}{dt} &= \Sigma X,\\ m\frac{dV_{gy}}{dt} + mV_{gx}\omega_z &= \Sigma Y,\\ I_z\frac{d\omega_{gz}}{dt} &= \Sigma M_z. \end{aligned}\right\} \qquad (2.2)$$

In Equation (2.2),

m is the mass of the airplane;

V_{gx}, V_{gy} are the projections of the airplane's ground speed on the body axes x and y;

ω_{gz} is the projection of the airplane's angular velocity relative to the ground on the body axis z; /50

I_z is the airplane's moment of inertia relative to body axis x;

ΣX, ΣY are the sums of the projections of the external forces on the x and y axes;

ΣM_z is the sum of the projections of the moments of the external forces relative to the z axis.

The external forces are made up of the aerodynamic forces, the force associated with the airplane's weight, and the force of gravity. We will use the following relationships for these forces, and for the moments they create relative to the z axis:

$$\left.\begin{aligned} \Sigma X &= -G\sin\vartheta - X(\alpha, V, M, \rho) + P_x(\delta_{\text{eh}}, M, p, T) =\\ &= -G\sin\vartheta - C_xS\frac{\rho V^2}{2} + P_x,\\ \Sigma Y &= -G\cos\vartheta + Y(\alpha, V, M, \rho) + P_y(\delta_{\text{en}}, M, p, T) =\\ &= -G\cos\vartheta + C_yS\frac{\rho V^2}{2} + P_y,\\ \Sigma M_z &= M_z\left(\delta_{\text{el}}, \alpha, \frac{d\alpha}{dt}, \omega_z, V, M, \rho\right) = m_zSb_a\frac{\rho V^2}{2}. \end{aligned}\right\} \qquad (2.3)$$

---

3. The methodology for computing the nonrigidity of the airplane structure will be discussed in Chapter 3.

In Equation (2.3),

G is the weight of the airplane;

α is the angle of attack;

δ_{en} is the angle by which the engine control mechanism is turned;

δ_{el} is the angle by which the elevator is tilted;

V is the airplane's relative air speed;

$M=V/a$ where a is the speed of sound at the flight altitude;

ρ is the density of the air;

P_x, P_y are the projections of the forces of the engine thrust on the x and y axes;

S is the wing area;

p is the air pressure;

T is the absolute air temperature;

C_x is the drag coefficient;

C_y is the lift coefficient;

m_z is the aerodynamic moment coefficient relative to the z axis;

b_a is the mean aerodynamic chord.

Let us supplement Equation (2.2) by the following kinematic relationships

$$\left.\begin{aligned} \omega_{gz} &\cong \frac{d\vartheta}{dt}, \\ \frac{dx_g}{dt} &= V_{gx}\cos\vartheta - V_{gy}\sin\vartheta, \\ \frac{dy_g}{dt} &= V_{gx}\sin\vartheta + V_{gy}\cos\vartheta, \end{aligned}\right\} \qquad (2.4)$$

where x_g and y_g are the coordinates of the center of gravity of the airplane on the geographic axes. /51

Let us take as our undisturbed condition straight, uniform flight in the vertical plane with no wind. In this undisturbed condition the airplane's motion parameters have the following values (we will designate the undisturbed condition by the subscript "e"

$$V = V_e = V_{gx} = \text{const}, \quad \alpha = \alpha_e, \quad \vartheta = \theta = \vartheta_e = \theta_e, \quad \omega_{gz} = V_{gy} = 0,$$
$$\left(\frac{dx_g}{dt}\right)_e = V_e\cos\vartheta_e, \quad \left(\frac{dy_g}{dt}\right)_e = V_e\sin\vartheta_e.$$

Introducing small deviations from their values in the undisturbed condition for all parameters, and discarding the terms with a product of parameter deviations, Equations (2.2) and (2.4) are the basis for our obtaining motion equations in deviations

$$\left.\begin{aligned}
&m\frac{d\Delta V_{gx}}{dt}=\Sigma\Delta X,\\
&m\frac{dV_{dy}}{dt}+mV_e\frac{d\Delta\vartheta}{dt}=\Sigma\Delta Y,\\
&I_z\frac{d^2\Delta\vartheta}{dt^2}=\Sigma M_z,\\
&\frac{d\Delta x_g}{dt}=(V_e+\Delta V_{gx})\cos\vartheta_e-V_e\sin\vartheta_e\cdot\Delta\vartheta-V_{gy}\sin\vartheta_e,\\
&\frac{d\Delta y_g}{dt}=(V_e+\Delta V_{gx})\sin\vartheta_e+V_e\cos\vartheta_e\cdot\Delta\vartheta+V_{gy}\cos\vartheta_e.
\end{aligned}\right\}\qquad(2.5)$$

In the equations at (2.5), the symbol Δ is used to designate the deviations of parameters from their original values in the undisturbed condition. The symbol Δ is not used here in the case of parameters whose values are zero in the undisturbed condition (ω_{gz}, V_{gy}), and will not be used in what follows.

Characteristic of the dynamics equations [the first three equations in the system at (2.5)] when analyzing motion in moving air is that, in concordance with the equations at (2.3), the right sides of these equations contain parameters characterizing the motion of the airplane relative to the air (air speed V, angle of attack α, and others). The left sides of these equations, taking into consideration the inertia forces and moments determined by the motion relative to the earth, are in the same form as that for the airplane motion in still air. These forces and moments are determined by the components of the ground speed and by the second derivative of the angle of pitch.

Let us, for convenience in analyzing the forces and moments, introduce certain additional kinematic relationships that take air motion into consideration. These relationships have an approximate validity, assuming the smallness of the wind velocity as compared with airplane speed:

/52

$$\left.\begin{aligned}
&V_x=V_{gx}-w_x\cong V_e+\Delta V_{gx}-w_x,\\
&V_y=V_{gy}-w_y,\\
&\alpha=\alpha_e+\alpha_g+\alpha_w\cong\alpha_e-\frac{V_{gy}}{V_e}+\frac{w_y}{V_e}.
\end{aligned}\right\}\qquad(2.6)$$

where

w_x, w_y are the components of the wind vector on the axes of the geographic system of coordinates in which the x_g axis coincides with the direction of the x body axis in the undisturbed condition;

α_g is the increase in the angle of attack as a result of the change in the direction of the ground speed, V_g;

α_w is the increase in the angle of attack as a result of the wind component, w_y.

The first two of the relationships at (2.6) flow from the obvious vector equality

$$\overline{V} = \overline{V}_g - \overline{W}. \tag{2.7}$$

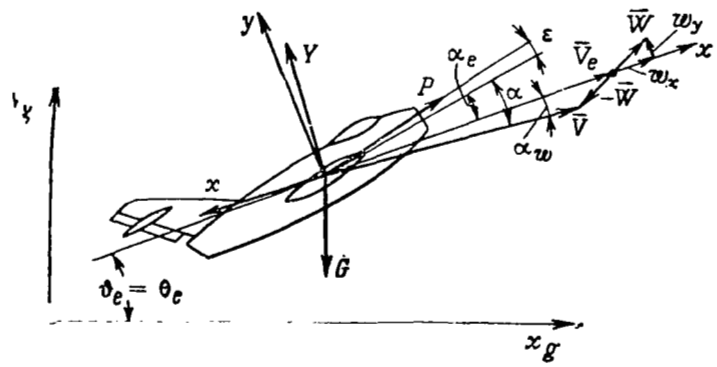

Figure 2.3. Forces and moments acting on an airplane in longitudinal motion.

Figure 2.3 explains the relationships at (2.6).[4] Figure 2.3 shows the angle ε between the direction of the wind chord and the thrust vector, P, in addition to the motion parameters already designated above.

Let us now proceed to an analysis of the right sides of the dynamics equations for an airplane in moving air [the first three of the equations at (2.5)].

Expanding the functions contained in the equations at (2.3) into a Taylor series according to their arguments, and retaining only those terms in the series with the first power of the increment for the argument, we

---

4. Figure 2.3 shows the case when ΔV_{gx} and V_{gy} equal zero.

obtain the following expressions for force and moment increments:

/53

$$\left.\begin{aligned}
\Sigma X = &- G\cos\vartheta_e\Delta\vartheta - X^{V_{gx}}\Delta V_{gx} - X^{w_x}w_x - X^{M}\Delta M - \\
&- X^{V_{gy}}V_{gy} - X^{w_y}w_y - X^{\rho y}\Delta y_g + P^{M}\cos(\alpha_e+\varepsilon)\Delta M + \\
&+ P^{p}\cos(\alpha_e+\varepsilon)\,p^{y}\Delta y_g + P^{T}\cos(\alpha_e+\varepsilon)T^{y}\Delta y_g + \\
&+ P^{\delta}\cos(\alpha_e+\varepsilon)\Delta\delta_e \\
\Sigma Y = &\; G\sin\vartheta_e\Delta\vartheta + Y^{V_{gx}}\Delta V_{gx} + Y^{w_x}w_x + Y^{M}\Delta M + \\
&+ Y^{V_{gy}}V_{gy} + Y^{w_y}w_y + Y^{\rho y}\Delta y_g + P^{M}\sin(\alpha_e+\varepsilon)\Delta M + \\
&+ P^{p}\sin(\alpha_e+\varepsilon)\,p^{y}\Delta y_g + P^{T}\sin(\alpha_e+\varepsilon)T^{y}\Delta y_g + \\
&+ P^{\delta}\sin(\alpha_e+\varepsilon)\Delta\delta_e, \\
\Sigma M_z = &\; M_z^{\delta}\Delta\delta_e + M_z^{V_{gx}}\Delta V_{gx} + M_z^{w_x}w_x + M_z^{M}\Delta M + M_z^{V_{gy}}V_{gy} + \\
&+ M_z^{w_y}w_y + M_z^{V_{gy}}\frac{dV_{gy}}{dt} + M_z^{w_y}\frac{dw_y}{dt} + M_z^{\rho y}\Delta y_g.
\end{aligned}\right\} \qquad (2.8)$$

The entries for the different magnitudes with superscripts is shorthand for the partial derivatives of those magnitudes with respect to the parameter defining the particular superscript. For example, $X^{V_{gx}} = \partial X/\partial V_{gx}$, etc.

The derivatives with respect to V_{gy} and w_y reflect the dependence of the forces and moments on the angle of attack, determined by the relationships at (2.6). The derivatives with respect to the ground speed (with respect to V_{gx} and V_{gy}) in principle should differ from the derivatives with respect to the wind velocity (with respect to w_x and w_y) because the change in the ground speed takes place comparatively slowly, whereas the gusts act on the airplane in flight with great frequency. This circumstance will be taken into consideration in what follows by the application of nonsteady aerodynamics methods. Here we will assume the derivatives with respect to the corresponding parameters are identical for ground speed and wind velocity.

Some time must be spent in dealing specifically with the moment created as a result of the delay in the downwash from the wing onto the tail. Consideration of this phenomenon for comparatively slow changes in the angle of attack for the wing reduces to the introduction of a term with dV_{yg}/dt (for the corresponding α) in the third expression at (2.8). Since the angle of attack, α, Equation (2.6), depends on the velocity of the vertical gusts,

the term with dw_y/dt, which takes into consideration the delay in the formation on the tail of the downwash from the wing, appears in this expression as a matter of formality. However, the airplane here, and virtually everywhere else in what follows[5], is considered to be a point with respect to the gusts, so the delay in the formation of lift on the horizontal tail created by the vertical gusts, as compared with the lift formation of the wing, /54 is not taken into consideration. Shown in Section 3.5 is the fact that this simplification is entirely permissible, even for big airplanes. This is all the more reason why delay in the downwash on the tail attributable to gusts need not be considered. It is for these reasons that in what follows the term with the wind derivative (dw_y/dt) in the equation for the moments with respect to the z axis will not be considered.

Substituting the values for the increments of the forces and moments from Equation (2.8) in Equation (2.5), and making simple transformations, we obtain the following system of equations describing the longitudinal motion of the airplane in moving air:

$$\left.\begin{aligned}
&a_\vartheta\Delta\vartheta+\frac{d\Delta V_{gx}}{dt}+a_x^{\cdot}\Delta V_{gx}+a_{\dot y}V_{gy}+a_y\Delta y_g=\\
&\qquad=a_{\dot\delta}\Delta\delta_e+a_x^{\cdot}w_x+a_{\dot y}w_y,\\
&V_e\frac{d\Delta\vartheta}{dt}-b_\vartheta\Delta\vartheta-b_x^{\cdot}\Delta V_{gx}+\frac{dV_{gy}}{dt}+b_{\dot y}V_{gy}+b_y\Delta y_g=\\
&\qquad=b_{\dot\delta}\Delta\delta_e-b_x^{\cdot}w_x+b_{\dot y}w_y,\\
&\frac{d^2\Delta\vartheta}{dt^2}+c_\vartheta^{\cdot}\frac{d\Delta\vartheta}{dt}+c_x^{\cdot}\Delta V_{gx}-c_y^{\cdot\cdot}\frac{dV_{gy}}{dt}-c_{\dot y}V_{gy}=\\
&\qquad=-c_{\dot\delta}\Delta\delta_e+c_x^{\cdot}w_x-c_{\dot y}w_y,\\
&\frac{d\Delta x_g}{dt}=(V_e+\Delta V_{gx})\cos\vartheta_e-V_e\sin\vartheta_e\cdot\Delta\vartheta-V_{gy}\sin\vartheta_e,\\
&\frac{d\Delta y_g}{dt}=(V_e+\Delta V_{gx})\sin\vartheta_e+V_e\cos\vartheta_e\cdot\Delta\vartheta+V_{gy}\cos\vartheta_e.
\end{aligned}\right\}\qquad(2.9)$$

The formulas for computing the coefficients in Equation (2.9) are listed in Table 2.1.

The following designations are used in Table 2.1:

g is the acceleration of gravity;

---

5. An exception is Section 3.5.

TABLE 2.1

/55

Coefficient	Formula	Measurement
a_ϑ	$g \cos \vartheta_e$	$m\text{-}sec^{-2}$
$a_{\dot{x}}$	$\frac{1}{\tau_e}\left[C_{xe} + \frac{1}{2} C_x^M M_e - \frac{P^M \cos(\alpha_e + \varepsilon)}{S\rho_e V_e a_e}\right]$	sec^{-1}
$a_{\dot{y}}$	$\frac{1}{2\tau_e}(C_{ye} - C_{xe}^\alpha)$	sec^{-1}
a_y	$\frac{V_e}{2\tau_e \rho_e}\left[C_{xe}\rho^y - \frac{2P^p \cos(\alpha_e + \varepsilon) p^y}{SV_e^2} - \frac{2P^T \cos(\alpha_e + \varepsilon) T^y}{SV_e^2}\right]$	sec^{-2}
a_δ	$P^\delta \cos(\alpha_e + \varepsilon)/m$	$m\text{-}sec^{-2}$
b_ϑ	$g \sin \vartheta_e$	$m\text{-}sec^{-2}$
$b_{\dot{x}}$	$\frac{1}{\tau_e}\left[C_{ye} + \frac{1}{2} C_y^M M_e + \frac{P^M \sin(\alpha_e + \varepsilon)}{S\rho_e V_e a_e}\right]$	sec^{-1}
$b_{\dot{y}}$	$-\frac{1}{2\tau_e}\left(C_y^\alpha + C_{xe}\right)$	sec^{-1}
b_y	$\frac{V_e}{2\tau_e \rho_e}\left[C_{ye}\rho^y + \frac{2P^p \sin(\alpha_e + \varepsilon) p^y}{SV_e^2} + \frac{2P^T \sin(\alpha_e + \varepsilon) T^y}{SV_e^2}\right]$	sec^{-2}
b_δ	$P^\delta \sin(\alpha_e + \varepsilon)/m$	$m\text{-}sec^{-2}$
b_{S}	$-C_y^{\delta_S}/2\tau_e$	sec^{-1}
$c_{\dot{\vartheta}}$	$-\bar{m}_z^{\omega_z}/2\tau_e \bar{r}_z^2$	sec^{-1}
$c_{\dot{x}}$	$-m_z^{M_{\mu_d}} M_e/2\tau_e^2 \bar{r}_z^2$	$m^{-1} sec^{-1}$
$c_{\ddot{y}}$	$-\bar{m}_z^{\dot{\alpha}}/2V_e \tau_e \bar{r}_z^2$	sec^{-1}
$c_{\dot{y}}$	$-m_z^{\alpha_{\mu_d}}/2V_e \tau_e^2 \bar{r}_z^2$	$m^{-1} sec^{-1}$
c_δ	$-m_z^{\delta_e \mu_d}/2\tau_e^2 \bar{r}_z^2$	sec^{-2}
c_{S}	$-m_z^{\delta_S \mu_d}/2\tau_e^2 \bar{r}_z^2$	sec^{-2}

$\bar{r}_z = \sqrt{I_z/m}/b_a$ is the dimensionless radius of inertia of the airplane relative to the z axis;

$\mu_d = m/\rho_e b_a S$ is the relative density for the airplane (in longitudinal motion);

$\tau_e = m/\rho_e S V_e$ is a unit of relative time;

$\bar{\omega}_z = b_a \omega_z / V_e$ is the dimensionless angular velocity;

$\dot{\bar{\alpha}} = \frac{b_a}{V_e}\frac{d\alpha}{dt}$ is the dimensionless rate of change of the angle of attack.

The system of equations at (2.9) was compiled for the general case of nonlevel flight and is quite cumbersome. The first simplification that can be made without significant reduction in the generality of the results of the analysis involves the selection of level flight as the undisturbed condition. In such case, $\vartheta_e = \sin \vartheta_e = b_\vartheta = 0$ and $\cos \vartheta_e = 1$. Moreover, the terms that take change in altitude into consideration in the first and second equations in the system at (2.9) can be discarded because they are significantly smaller than the others. Since modern control systems have no effect on the engines, we will not consider terms containing δ_e. The equations at (2.9) will now take the form

/56

$$\left.\begin{aligned}
&a_\vartheta \Delta\vartheta + \frac{d\Delta V_{gx}}{dt} + a_{\dot{x}} \Delta V_{gx} + a_{\dot{y}} V_{gy} = a_{\dot{x}} w_x + a_{\dot{y}} w_y,\\
&V_e \frac{d\Delta\vartheta}{dt} - b_{\dot{x}} \Delta V_{gx} + \frac{dV_{gy}}{dt} + b_{\dot{y}} V_{gy} = -b_{\dot{x}} w_x + b_{\dot{y}} w_y,\\
&\frac{d^2\Delta\vartheta}{dt^2} + c_{\dot{\vartheta}} \frac{d\Delta v}{dt} + c_{\dot{x}} \Delta V_{gx} - c_{\ddot{y}} \frac{dV_{gy}}{dt} - c_{\dot{y}} V_{gy} =\\
&\qquad = -c_{\dot{\delta}} \Delta\delta_{e1} + c_{\dot{x}} w_x - c_{\dot{y}} w_y,\\
&\frac{d\Delta x_g}{dt} = V + \Delta V_{gx},\\
&\frac{d\Delta y}{dt} = V_e \Delta\vartheta + V_{gy}.
\end{aligned}\right\} \qquad (2.10)$$

This system of equations describes the short-period, as well as the long-period, motions of the airplane.

As will be pointed out in Chapter 3, the system of equations at (2.10) can be greatly simplified for purposes of solving most of the problems of practical interest involving flight dynamics in turbulent air. This simplification involves ignoring the change in speed along the x axis when flying

in turbulent air ($\Delta V_{gx}=0$). The result drops the first and fourth equations out of the system at (2.10). The cases when this omission causes principal errors will be specifically stipulated in what follows. Ignoring ΔV_{gx}, what we obtain from Equation (2.10) is

$$\left.\begin{aligned} V_e\frac{d\Delta\vartheta}{dt}+\frac{dV_{gy}}{dt}+b_y^{\cdot}V_{gy}&=-b_x^{\cdot}w_x+b_y^{\cdot}w_y,\\ \frac{d^2\Delta\vartheta}{dt^2}+c_v^{\cdot}\frac{d\Delta\vartheta}{dt}-c_y^{\cdot\cdot}\frac{dV_{gy}}{dt}-c_y^{\cdot}V_{gy}&=-c_\delta^{\cdot}\Delta\delta_e+\\ &\quad+c_x^{\cdot}w_x-c_y^{\cdot}w_y,\\ \frac{d\Delta y_g}{dt}&=V_e\Delta\vartheta+V_{gy}. \end{aligned}\right\} \qquad (2.11)$$

These equations can be used to describe the short-period motion of an airplane.

It is sometimes more convenient to express all of the functions contained in Equation (2.11) in the form of angular magnitudes. If we use Equation (2.6) for these purposes we obtain (without taking the longitudinal wind component into consideration): /57

$$\left.\begin{aligned} \frac{d\Delta\vartheta}{dt}-\frac{d\alpha_g}{dt}-b_\alpha\alpha_g&=b_\alpha\alpha_w,\\ \frac{d^2\Delta\vartheta}{dt^2}+c_\vartheta^{\cdot}\frac{d\Delta\vartheta}{dt}+c_\alpha^{\cdot}\frac{d\alpha_g}{dt}+c_\alpha\alpha_g&=-c_\delta^{\cdot}\Delta\delta_e-c_\alpha\alpha_w,\\ \frac{d\Delta y}{dt}&=V_e(\Delta\vartheta-\alpha_g). \end{aligned}\right\} \qquad (2.12)$$

The coefficients in Equation (2.12) are associated with those in Equation (2.11) by the following dependencies: $b_\alpha=-b_y^{\cdot}$, $c_\alpha^{\cdot}=-V_e c_y^{\cdot}$, $c_\alpha=-V_e c_y^{\cdot}$. Equations (2.11) and (2.12) quite accurately describe the short-period motion of the airplane, and will be widely used in what follows.

Equations (2.9)-(2.12) make it possible to investigate the dynamics of an airplane with a fixed elevator, or with one moving in accordance with some law, in moving air. However, today flight is controlled by the autopilot for much of the total flight time, so a review of the dynamics when the airplane has an autopilot is of interest.

The equations for longitudinal motion of the airplane should be supplemented by an equation (by a control law) for the autopilot, in order to analyze flight dynamics when an autopilot is used. We will use the equations for the ideal autopilot to obtain a mathematical description of the autopilot;

that is, we will ignore the delay time and the nonlinearity of its characteristic curve. The admissibility of this approach to the problem under consideration will be substantiated in detail in Section 3.3.

Two types of autopilots are in use today, one with direct feedback, the other with rate feedback. The former is the one most widely used. The AP-6Ye is an example of a direct feedback autopilot.

The law for controlling this autopilot has the following form for the elevator channel

$$\Delta\delta_e = -i_\vartheta(\Delta\vartheta_s - \Delta\vartheta) + i_{\dot\vartheta}\frac{d\Delta\vartheta}{dt} + i_y\Delta y_g, \tag{2.13}$$

where

i_ϑ is the gain for the angle of pitch, ϑ, a dimensionless magnitude;

$i_{\dot\vartheta}$ is the gain for the angular velocity ω_z, dimensionality, seconds;

i_y is the gain for the altitude, y_g, dimensionality, rad/M, or degrees/M;

$\Delta\vartheta_s$ is the specified increase in the angle of pitch.

In the stabilized level flight condition $\Delta\vartheta_s = 0$. It is sometimes desirable to exclude from the law for the equation terms that are proportional to the altitude. In such cases, the angle of pitch for the stabilized level flight condition is /58

$$\Delta\delta_e = i_\vartheta\Delta\vartheta + i_{\dot\vartheta}\frac{d\Delta\vartheta}{dt}. \tag{2.14}$$

The law for the equation for the autopilot with rate feedback for the elevator channel can be written in the following form [28]:

$$\frac{d\Delta\delta_e}{dt} = -i_q(\Delta\vartheta_s - \Delta\vartheta) + i_\vartheta\frac{d\Delta\vartheta}{dt} + i_{\dot\vartheta}\frac{d^2\Delta\vartheta}{dt^2}, \tag{2.15}$$

where

i_q is the gain for the angle of pitch, dimensionality, $\sec^{-1}$;

i_ϑ is the ω_z gain, dimensionless;

$i_{\dot\vartheta}$ is the $\dot\omega_z$ gain, dimensionality, seconds.

The result of combining the equations for the airplane at (2.10) and for the autopilot at (2.13) is a system of equations describing the longitudinal motion of an airplane with an autopilot in moving air

$$\left.\begin{aligned}
&a_\vartheta\Delta\vartheta+\frac{d\Delta V_{gx}}{dt}+a_{\dot x}\Delta V_{gx}+a_{\dot y}V_{gy}=a_{\dot x}w_x+a_{\dot y}w_y,\\
&V_e\frac{d\Delta\vartheta}{dt}-b_{\dot x}\Delta V_{gx}+\frac{dV_{gy}}{dt}+b_{\dot y}V_{gy}=-b_{\dot x}w_x+b_{\dot y}w_y,\\
&\frac{d^2\Delta\vartheta}{dt^2}+(c_{\dot\vartheta}+c_{\dot\delta}i_{\dot\vartheta})\frac{d\Delta\vartheta}{dt}+c_\delta i_\vartheta\Delta\vartheta-c_{\ddot y}\frac{dV_{gy}}{dt}-c_{\dot y}V_{gy}+\\
&\qquad+c_\delta i_y\Delta y_g=c_\delta i_\vartheta\Delta\vartheta_S+c_{\dot x}w_x-c_{\dot y}w_y,\\
&\frac{d\Delta x_g}{dt}=V_e+\Delta V_{gx},\quad \frac{d\Delta y_g}{dt}=V_e\Delta\vartheta+V_{gy}.
\end{aligned}\right\}\qquad(2.16)$$

If the simplified equations for the airplane at (2.11) are combined with the equation for the autopilot, we obtain:

$$\left.\begin{aligned}
&V_e\frac{d\Delta\vartheta}{dt}+\frac{dV_{gy}}{dt}+b_{\dot y}V_{gy}=-b_{\dot x}w_x+b_{\dot y}w_y,\\
&\frac{d^2\Delta\vartheta}{dt^2}+(c_{\dot\vartheta}+c_{\dot\delta}i_{\dot\vartheta})\frac{d\Delta\vartheta}{dt}+\epsilon_\delta i_\vartheta\Delta\vartheta-c_{\ddot y}\frac{dV_{gy}}{dt}-c_{\dot y}V_{gy}+\\
&\qquad+c_\delta i_y\Delta y_g=c_\delta i_\vartheta\Delta\vartheta_S+c_{\dot x}w_x-c_{\dot y}w_y,\\
&\frac{d\Delta x_g}{dt}=V_e,\quad \frac{d\Delta y_g}{dt}=V_e\Delta\vartheta+V_{gy}.
\end{aligned}\right\}\qquad(2.17)$$

2.3. Equations for Lateral Motion in Moving Air /59

The equations for the dynamics of isolated lateral motion of an airplane in body axes have the form [26, 27]:

$$\left.\begin{aligned}
&m\frac{dV_{gz}}{dt}-m\omega_{gy}V_{gx}=\Sigma Z,\\
&I_x\frac{d\omega_{gx}}{dt}-I_{xy}\frac{d\omega_{gy}}{dt}=\Sigma M_x,\\
&I_y\frac{d\omega_{gy}}{dt}-I_{xy}\frac{d\omega_{gx}}{dt}=\Sigma M_y,
\end{aligned}\right\}\qquad(2.18)$$

where

V_{gx}, V_{gz} are the projections of the airplane's ground speed on the z and x axes;

ω_{gx}, ω_{gy} are the projections of the airplane's angular velocity relative to the ground on the x and y axes;

I_x, I_y are the moments of inertia of the airplane relative to the x and y axes;

I_{xy} is the deviation moment;

ΣZ is the sum of the projections of the external forces on the z axis;

ΣM_x, ΣM_y are the sums of the projections of the moments of the external forces relative to the x and y axes.

The sums of the projections of the external forces and moments in lateral motion can be determined by the relationships

$$\left.\begin{aligned}\Sigma Z &= G\sin\gamma + Z(\beta, \delta_r, V, M, \rho) = G\sin\gamma + C_z S\frac{\rho V^2}{2},\\ \Sigma M_x &= M_x(\beta, \delta_a, \delta_r, \omega_x, \omega_y, V, M, \rho) = m_x lS\frac{\rho V^2}{2},\\ \Sigma M_y &= M_y(\beta, \delta_a, \delta_r, \omega_x, \omega_y, V, M, \rho) = m_y lS\frac{\rho V^2}{2}.\end{aligned}\right\} \qquad (2.19)$$

where

β is the angle of sideslip;

δ_a is the aileron angle;

δ_r is the rudder angle;

l is the wing span;

C_z is the lateral-force coefficient;

m_x is the aerodynamic moment coefficient relative to the x axis;

m_y is the aerodynamic moment coefficient relative to the y axis.

We should point out that the forces and moments of lateral motion depend on certain of the longitudinal motion parameters (V, M, ρ). However, it is impossible to give consideration to these when making an isolated study of lateral motion.

Equation (2.18) should be supplemented by the following kinematic relationships /60

$$\left.\begin{aligned}\omega_{gx} &= \frac{d\gamma}{dt} + \frac{d\psi}{dt}\sin\vartheta,\quad \omega_{gy} = \frac{d\psi}{dt}\cos\gamma\cos\vartheta + \frac{d\vartheta}{dt}\cos\gamma,\\ \frac{dz_g}{dt} &= -V_{gx}\sin\psi + V_{gz}\cos\gamma\cos\psi,\end{aligned}\right\} \qquad (2.20)$$

where

z_g is the lateral deviation of the airplane's center of gravity from the z_y axis in geographic coordinates.

Let us take as the undisturbed condition straight and uniform flight, with wings level, no sideslipping or wind, and with the following parameter values $V = V_g = V_{gx} = \text{const}$,

$$\beta = \delta_a = \delta_r = \gamma = \psi = \omega_{gx} = \omega_{gy} = z_g = \left(\frac{dz_g}{dt}\right)_e = 0.$$

The following system of equations is obtained for small deviations from the original undisturbed condition, the basis being Equations (2.18) and (2.20):

$$\left.\begin{aligned} mV_e\frac{d\beta_g}{dt} - mV_e\frac{d\psi}{dt} &= \Sigma\Delta Z,\\ I_x\frac{d^2\gamma}{dt^2} - I_{xy}\frac{d\psi}{dt} &= \Sigma M_x,\\ I_y\frac{d^2\psi}{dt^2} - I_{xy}\frac{d\gamma}{dt} &= \Sigma M_y,\\ \frac{dz_g}{dt} &= V_e(\beta_g - \psi). \end{aligned}\right\} \qquad (2.21)$$

The following relationship, approximately correct for small deviations from zero in parameter values, is used in Equation (2.21):

$$V_{gx} \cong V_e,\ V_{gz} \cong V_e\beta_g,\ \omega_{gx} \cong \frac{d\gamma}{dt},\ \omega_{gy} \cong \frac{d\psi}{dt},$$

where β_g is the angle of sideslip, determined from ground speed vector.

Let us now consider the right sides of the first three equations in system (2.21). Forces and moments are determined by the motion of the airplane relative to the air, not to the ground. To simplify the analysis of the change in forces and moments in lateral motion of the airplane, flying in disturbed air, let us introduce certain additional relationships, correct only within the limitations set forth in the following discussions:

$$\left.\begin{aligned} \beta &= \beta_g + \beta_w = \beta_g - \frac{w_z}{V_e},\\ \omega_x &= \omega_{gx} + \omega_{wx} = \omega_{gx} + \frac{\partial w_y}{\partial z},\\ \omega_y &= \omega_{gy} + \omega_{wy} = \omega_{gy} + \frac{\partial w_x}{\partial z}. \end{aligned}\right\} \qquad (2.22)$$

/61

The absence of an additional subscript in the equations at (2.22) indicates that the corresponding parameter characterizes the lateral motion of the airplane relative to the moving air medium. The parameters with the g subscript characterize the motion relative to the ground, and as a result, relative to still air. Finally, the subscript w indicates that the parameter is the result of the air's mobility, that is, the result of the wind. Figure 2.4 illustrates Equation (2.22). Figure 2.4-a illustrates the first and third relationships at (2.22), and Figure 2.4-b illustrates the second. The schematic arrangement of the longitudinal and normal components of a

wind with constant spanwise gradient, Figure 2.4, shows that the positive gradient dw_y/dz, positive from the point of view of the aerodynamic moment created by it, is equivalent to the positive angular velocity of the airplane

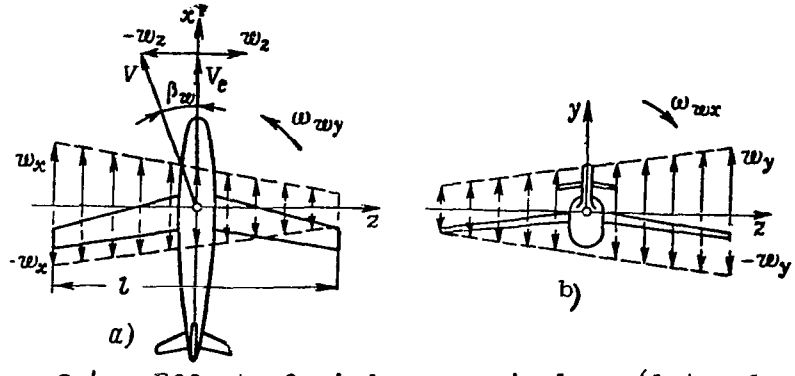

Figure 2.4. Effect of wind on an airplane (lateral motion). a - Lateral component of the wind, w_z, and nonuniform spanwise longitudinal component, w_x; b - Nonuniform spanwise normal component, w_y.

relative to the x axis, with the negative gradient, dw_x/dz, equivalent to the positive angular velocity relative to the y axis. What must be borne in mind in determining the sign of β_w and of the angular velocities ω_{wx} and ω_{wy}, the result of air motion, is that wind components w_x, w_y, and w_z characterize the direction in which the air is moving relative to the airplane, whereas angle β_w and angular velocities ω_{wx} and ω_{wy} should characterize the motion of the airplane relative to the air. Therefore, the direction /62 of the wind velocity components, w_x, w_y, and w_z, must be reversed, as was done in Figure 2.4, to compute the signs of these increments correctly.

Let us emphasize the fact that the computation of the derivatives dw_x/dz and dw_y/dz is, in principle, the same as taking the effect of the size of the airplane on the lateral motion parameters into consideration.

The geometric relationships in Figure 2.4 illustrate the limitations of the validity of the expressions at (2.22). These limitations are as follows:

(1) the expressions at (2.22) are valid only for constant spanwise gradients of the normal and longitudinal components of the wind velocity;

(2) the expressions at (2.22) were obtained from a nonuniform spanwise distribution of the wind components w_w and w_y, so are valid only for the

wing. The possibility of using these expressions for other parts of the airplane (fuselage, tail) should be given additional consideration.

Expanding the functions in Equation (2.19) in a Taylor series with respect to their arguments, and retaining only the terms in the series with first power of the increment for the argument, we obtain expressions for the right sides of the lateral motion equations

$$\left.\begin{aligned}
\Sigma\Delta Z &= Z^{\beta}{}_{g}\beta_{g} + Z^{\beta}{}_{w}\beta_{w} + Z^{\gamma}\gamma + Z^{\omega}{}_{gx}\omega_{gx} + Z^{\omega}{}_{wx}\omega_{wx} + \\
&\quad + Z^{\omega}{}_{gy}\omega_{gy} + Z^{\omega}{}_{wy}\omega_{wy} + Z^{\delta_r}\delta_r, \\
\Sigma\Delta M_x &= M_x^{\beta}{}_{g}\beta_{g} + M_x^{\beta}{}_{w}\beta_{w} + M_x^{\omega}{}_{gx}\omega_{gx} + M_x^{\omega}{}_{wx}\omega_{wx} + M_x^{\omega}{}_{gy}\omega_{gy} + \\
&\quad + M_x^{\omega}{}_{wy}\omega_{wy} + M_x^{\delta_a}\delta_a + M_x^{\delta_r}\delta_r, \\
\Sigma\Delta M_y &= M_y^{\beta}{}_{g}\beta_{g} + M_y^{\beta}{}_{w}\beta_{w} + M_y^{\omega}{}_{gx}\omega_{gx} + M_y^{\omega}{}_{wx}\omega_{wx} + M_y^{\omega}{}_{gy}\omega_{gy} + \\
&\quad + M_y^{\omega}{}_{wy}\omega_{wy} + M_y^{\delta_a}\delta_a + M_y^{\delta_r}\delta_r.
\end{aligned}\right\} \qquad (2.23)$$

Substituting the values for the increments of the forces and moments from Equation (2.23) in Equation (2.18), and taking Equation (2.22) into consideration, we obtain the following system of equations

$$\left.\begin{aligned}
&mV_e\frac{d\beta_g}{dt} - Z^{\beta}{}_{g}\beta_{g} - Z^{\omega}{}_{gx}\frac{d\gamma}{dt} - Z^{\gamma}\gamma - (mV_e + Z^{\omega}{}_{gy})\frac{d\psi}{dt} = \\
&\quad = -Z^{\beta}{}_{w}\frac{w_z}{V_e} + Z^{\omega}{}_{wx}\frac{\partial w_y}{\partial z} - Z^{\omega}{}_{gy}\frac{\partial w_x}{\partial z} + Z^{\delta_r}\delta_r, \\
&-M_x^{\beta}{}_{g}\beta_{g} + I_x\frac{d^2\gamma}{dt^2} - M_x^{\omega}{}_{gx}\frac{d\gamma}{dt} - I_{xy}\frac{d^2\psi}{dt^2} - M_x^{\omega}{}_{gy}\frac{d\psi}{dt} = \\
&\quad = -M_x^{\beta}{}_{w}\frac{w_z}{V_e} + M_x^{\omega}{}_{wx}\frac{\partial w_y}{\partial z} - M_x^{\omega}{}_{wy}\frac{\partial w_x}{\partial z} + M_x^{\delta_a}\delta_a + M_x^{\delta_r}\delta_r, \\
&-M_y^{\beta}{}_{g}\beta_{g} - I_{xy}\frac{d^2\gamma}{dt^2} - M_y^{\omega}{}_{g}\frac{d\gamma}{dt} + I_y\frac{d^2\psi}{dt^2} - M_y^{\omega}{}_{gy}\frac{d\psi}{dt} = \\
&= -M_y^{\beta}{}_{w}\frac{w_z}{V_e} + M_y^{\omega}{}_{w^x}\frac{\partial w_y}{\partial z} - M_y^{\omega}{}_{wy}\frac{\partial w_x}{\partial z} + M_y^{\delta_a}\delta_a + M_y^{\delta_r}\delta_r, \quad \frac{dz_g}{dt} = V_e(\beta_g - \psi).
\end{aligned}\right\} \qquad (2.24)$$

/63

Equations (2.24) can be simplified somewhat for airplanes that have a conventional aerodynamic arrangement. So far as these airplanes are concerned, the following magnitudes can be set equal to zero without introducing significant errors: Z^{ω_x}, Z^{ω_y}, and I_{xy}.

Taking this simplification into consideration, and after making

uncomplicated transformations in Equation (2.24), we obtain:

$$\left.\begin{aligned}
&\frac{d\beta_g}{dt}+k_\beta\beta_g-k_\gamma\gamma-\frac{d\psi}{dt}=\frac{k'\beta}{V_e}w_z+k_r\delta_r,\\
&l_\beta\beta_g+\frac{d^2\gamma}{dt^2}+l'_\gamma\frac{d\gamma}{dt}+l'_{\dot\psi}\frac{d\psi}{dt}=\frac{l'_\beta}{V_e}w_z-l'_\gamma\frac{\partial w_y}{\partial z}+\\
&\qquad+l'_{\dot\psi}\frac{\partial w_x}{\partial z}+l_a\delta_a+l_r\delta_r,\\
&n_\beta\beta_g+n'_\gamma\frac{d\gamma}{dt}+\frac{d^2\psi}{dt^2}+n'_{\dot\psi}\frac{d\psi}{dt}=\frac{n'_\beta}{V_e}w_z-n'_\gamma\frac{\partial w_y}{\partial z}+\\
&\qquad+n'_{\dot\psi}\frac{\partial w_x}{\partial z}+n_a\delta_a+n_r\delta_r.
\end{aligned}\right\}\qquad(2.25)$$

The formulas for computing the coefficients for the equations at (2.25) are listed in Table 2.2.

The following designations are used in Table 2.2:

$i_x = 4I_x/ml^2$ is the dimensionless moment of inertia relative to the x axis;

$i_y = 4I_y/ml^2$ is the dimensionless moment of inertia relative to the y axis;

$\mu_1 = 2m/\rho_e S l$ is the airplane-density ratio in lateral motion;

$\overline{\omega}_x = \omega_x l/2V_e$ is the dimensionless angular velocity relative to the x axis;

$\overline{\omega}_y = \omega_y l/2V_e$ is the dimensionless angular velocity relative to the y axis.

The primed coefficients in the right sides of the equations in the system (2.25) have the same structure as do the corresponding coefficients in the left sides, but the values entering into their partial derivatives of the coefficients of the forces and moments can be different from those for the coefficients of the left sides of the equations. This is why each of the coefficients must be considered specifically in the light of individual physical natures. However, our initial assumption will be that the airplane has encountered a single gust with constant velocity, or with a constant spanwise gradient. In this case the lateral wind will be equivalent (if one does not consider the time the aircraft entered the gust) to the angle of

TABLE 2.2

/64

Coefficient	Formula	Measurement
k_β	$-C_z^\beta/2\tau_e$	sec^{-1}
k_γ	g/V_e	sec^{-1}
k_{ω_z}	$-C_z^\delta r/2\tau_e$	sec^{-1}
l_β	$-m_x^\beta \mu_\delta/\tau_e^2 i_x$	sec^{-1}
$l_{\dot\gamma}$	$-m_x^{\bar\omega^x}/\tau_e i_x$	sec^{-1}
$l_{\dot\psi}$	$-m_x^{\bar\omega^y}/\tau_e i_x$	sec^{-1}
l_{ω_z}	$-m_x^{\delta_a}\mu_\delta/\tau_e^2 i_x$	sec^{-1}
l_r	$-m_x^{\delta_r}\mu_\delta/\tau_e^2 i_x$	sec^{-1}
n_β	$-m_y^\beta \mu_\delta/\tau_e^2 i_y$	sec^{-1}
$n_{\dot\gamma}$	$-m_y^{\bar\omega^x}/\tau_e i_y$	sec^{-1}
$n_{\dot\psi}$	$-m_y^{\bar\omega^y}/\tau_e i_y$	sec^{-1}
n_{ω_z}	$-m_y^{\delta_a}\mu_\delta/\tau_e^2 i_y$	sec^{-1}
n_r	$-m_y^{\delta_r}\mu_\delta/\tau_e^2 i_y$	sec^{-1}

sideslip and the primes over the coefficients in the equations at (2.25) can be removed, taking it that these coefficients are equal to those in the left sides. A consideration of the coefficients $l_{\dot\gamma}'$ and $n_{\dot\gamma}'$ too can lead to this same conclusion. A constant gradient along the z axis at the normal wind component, w_y (Figure 2.4-b), is equivalent to the angular velocity ω_{wx} for the entire airplane. Consequently, the coefficients $l_{\dot\gamma}'$ and $n_{\dot\gamma}'$ should be equal to the coefficients $l_{\dot\gamma}$ and $n_{\dot\gamma}$, and there is no need for them to carry the primes. The coefficient $n_{\dot\gamma}'$ in the right side of the third equation at (2.25) can be set equal to zero in order to simplify the computations and introduces no significant errors, because at flight angles of attack it is many times less (by more than an order of magnitude) than the other coefficients in the right sides of the lateral motion equations. A special analysis should be made of the terms containing $n_{\dot\gamma}'$ in the right side of the third equation at (2.25) when analyzing special

/65

conditions (landing, flying near the ceiling) that must consider such terms.

Let us consider the coefficients l_{ψ}' and n_{ψ}'. As we see from Figure 2.4-a, the presence of a constant gradient for the longitudinal wing component, w_x, along the z axis is equivalent to an angular velocity relative to the y axis only for the wing, and not for the fuselage and tail, which have very little length along the z axis, but extensive length along the x axis. Consequently, only that portion of the moment created by the wind should be taken into consideration in the derivatives $m_x'^{\omega}$ and $m_y'^{\omega_y}$. Reference [29] shows that at flight angles of attack the derivative $m_y^{\omega_y}$ is the result of the effect of the tail and the fuselage, and that the role of the wing is negligible. Therefore, the derivative $m_y'^{\omega_y}$, and, as a result, the coefficient n_{ψ}', can be taken as equal to zero, approximately. So far as the derivative $m_{\lambda}'^{\omega_y}$ is concerned, its computation requires consideration of the contribution made by the wing, so we note this by the insertion of the subscript "w":

$$m_x'^{\omega_y} = (m_x^{\omega_y})_w \tag{2.26}$$

From whence the formula for computing the coefficient l_{φ}'

$$l_{\varphi}' = -(m_x^{\bar{\omega}_y})_w / \tau_e i_x. \tag{2.27}$$

Data for computing the derivative $(m_x^{\bar{\omega}_y})_w$ can be found in [27], for example. The computations show that the case of airplanes with a conventional aerodynamic arrangement and normal flight angles of attack always satisfies the relationship $(m_x^{\bar{\omega}_y})_w \ll m_x^{\bar{\omega}_x}$. Therefore, the nonuniformity of the spanwise longitudinal wind component in creating a rolling moment plays a minor role as compared with the nonuniformity of the spanwise normal component (at small angles of attack). This is the basis for setting $l_{\psi}'=0$, in subsequent computations.

The analysis of airplane motion in moving air will consider the terms $k_r\delta_r$, $l_r\delta_r$, $n_a\delta_a$ equal to zero because of their smallness compared with the other terms in the right sides of the equations at (2.25).

When the above considerations with respect to the coefficients in the right sides of the equations at (2.25) are taken into account, the equations at the latter should be written in the following form for the case considered, that of the effect on an airplane of a gust with constant velocity, or with constant spanwise gradient /66

$$\left.\begin{aligned}
&\frac{d\beta_g}{dt}+k_\beta\beta_g-k_\gamma\gamma-\frac{d\psi}{dt}=\frac{k_\beta}{V_e}w_z,\\
&l_\beta\beta_g+\frac{d^2\gamma}{dt^2}+l_\gamma^{\cdot}\frac{d\gamma}{dt}+l_{\dot\psi}\frac{d\psi}{dt}=\frac{l_\beta}{V_e}w_z-l_\gamma^{\cdot}\frac{dw_y}{\partial z}-l_a\delta_a\\
&n_\beta\beta_g+n_\gamma^{\cdot}\frac{d\gamma}{dt}+\frac{d^2\psi}{dt^2}+n_{\dot\psi}\frac{d\psi}{dt}=\frac{n_\beta}{V_e}w_z-n_r\delta_r\\
&\frac{dz_g}{dt}=V_e(\beta_g-\psi).
\end{aligned}\right\}\qquad(2.28)$$

We should set $\delta_a=\delta_r=0$ in the equations at (2.28) when analyzing the motion of an airplane without an autopilot. The fourth equation turns out to be an isolated one. It can be used to determine the lateral deviation of the airplane's center of gravity from the original straight-line flight path caused by the gust. This equation can also be used to determine the lateral G on the earth's axes.

The equations at (2.28) should be augmented by the equations for the autopilot in order to analyze controlled flight. In the general case, these equations link the aileron and rudder angles with the β, γ, ψ and z_g coordinates. The system at (2.28) will become a closed one, thanks to the autopilot equations.

The most widely used autopilots today do not include a signal resulting from the lateral deviation, z_g, of the airplane's center of gravity from the specified flight path in their control law. In such cases, the fourth equation in the system at (2.28) will become an isolated one, even when there is an autopilot.

We will, on our study of the laws of lateral motion control, limit ourselves to a consideration of autopilots with direct feedback. Two different designs are now in use for yaw and roll, autopilots, with cross coupling, and without.

Cross coupling is introduced to eliminate deviations from straight-line flight by using coordinated deflection shifts, with the result that both

controls, the ailerons and the rudder, are deflected in event of a mismatch between any of the angles (yaw or roll).

Without cross coupling the rudder is deflected only when there is a mismatch in angle of yaw, and the ailerons are deflected only when there is a mismatch in angle of roll.

The equations for the ideal autopilot with cross coupling are in the form /67

$$\left.\begin{aligned}\delta_a &= i_\gamma\gamma + i_{\dot\gamma}\frac{d\gamma}{dt} + i_\psi(\psi_s-\psi),\\ \delta_r &= f_\gamma\gamma - f_\psi(\psi_s-\psi) + f_{\dot\psi}\frac{d\psi}{dt},\end{aligned}\right\} \qquad (2.29)$$

where

ψ_s is the specified value for the angle of yaw.

If $i_\psi = f_\gamma = 0$, in the equations at (2.29), they are transformed into a law for controlling an autopilot without cross coupling. Let us therefore make our analysis of the dynamics of the airplane autopilot system by using the equations for the autopilot with cross coupling (2.29), in order to reduce the scope of the work. All analytical expressions obtained will be valid for the airplane with an autopilot without cross coupling if the i_ψ and f_γ ratios they contain are set equal to zero.

By combining Equations (2.28) and (2.29), we obtain the following equations for an airplane autopilot system acted on by moving air:

$$\left.\begin{aligned}&\frac{d\beta_g}{dt} + k_\beta\beta_g - k_\gamma\gamma - \frac{d\psi}{dt} = \frac{k_\beta}{V_e}w_z,\\ &l_\beta\beta_g + \frac{d^2\gamma}{dt^2} + (l_{\dot\gamma} + i_\gamma l_\alpha)\frac{d\gamma}{dt} + i_\gamma l_\alpha\gamma + l_{\dot\psi}\frac{d\psi}{dt} - i_\psi l_\alpha\psi =\\ &\qquad = \frac{l_\beta}{V_e}w_z - l_{\dot\gamma}\frac{\partial w_y}{\partial z} - i_\psi l_\alpha\psi_s,\\ &n_\beta\beta_g + n_{\dot\gamma}\frac{d\gamma}{dt} + f_\gamma n_r\gamma + \frac{d^2\psi}{dt^2} + (n_{\dot\psi} + f_{\dot\psi}n_r)\frac{d\psi}{dt} + f_\psi n_r\psi =\\ &\qquad = \frac{n_\beta}{V_e}w_z + f_\psi n_r\psi_s,\\ &\frac{dz_g}{dt} = V_e(\beta_g - \psi).\end{aligned}\right\} \qquad (2.30)$$

Equations (2.28) and (2.30) can now be used to analyze the lateral motion of an airplane with an autopilot and of an airplane with an autopilot acted on by lateral wind gusts, as well as by normal gusts with a fixed spanwise gradient.

2.4. General Characteristics of Dynamic Systems

The second and third sections in this chapter showed that in many cases motion of an airplane in moving air can be described by a system of linear differential equations with constant coefficients. A system of linear equations always can be reduced to one equation of the following form for any coordinate of disturbed airplane motion: /68

$$a_0 \frac{d^n y}{dt^n} + a_1 \frac{d^{n-1} y}{dt^{n-1}} + \ldots + a_{n-1} \frac{dy}{dt} + a_n y = \\ = b_0 \frac{d^m x}{dt^m} + b_1 \frac{d^{m-1} x}{dt^{m-1}} + \ldots + b_{m-1} \frac{dx}{dt} + b_m x, \tag{2.31}$$

where

x is the disturbing effect, a known function of time;

y is a coordinate of airplane motion (the reaction to the disturbance), the unknown function;

a_i, b_i are constant coefficients that depend on the airplane's parameters.

Let us point out that the relationship of $n \geq m$ is always correct for real systems.

The dynamic properties of any system described by an equation such as that at (2.31) are very clearly characterized by the response function, H(t), which is the reaction of the system, or the output magnitude resulting from the influence on the system of a disturbance in the form of a unit function (of a unit step). At the same time, the creation of a disturbing effect in the form of a unit function is of no importance under real conditions. If the analytical expression for the response function is known, the reaction of the system to a disturbance, virtually regardless of the form of that disturbance, can be found by the Duhamel integral (the integral of convolution).

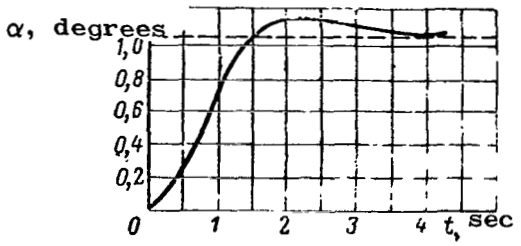

Figure 2.5. The transient for angle of attack for an airplane in the case of step elevator deviation.

Figure 2.5 is an example of the reaction of an airplane in terms of angle of attack during step change of elevator position.

If the disturbing effect can be described by a pulse, or by a δ-function, the reaction of the system is called a pulse response (weight) function, K(t). A transient and a pulse response function are linked by the relationship

$$K(t)=\frac{dH(t)}{dt}. \tag{2.32}$$

The so-called transfer function is very widely used to investigate dynamic systems. In order to obtain a transfer function for the system described by Equation (2.31), let us introduce for consideration the differentiation operator p=d/dt, which transforms the time function into a derivative of this function. Positive powers of the operator p, that is, $p^2=d^2/dt^2$, $p^3=d^3/dt^3$, etc., correspond to derivatives of second, and higher, orders. /69

Transformation of the function into multiple integrals is accomplished by the use of negative powers for the operator, p, that is, $p^{-1}=\int(\ldots)dt$, $p^{-2}=\int\int(\ldots)dt^2$, etc.

Replacing the derivatives in Equations (2.31) with the operator p of corresponding power, we obtain

$$\begin{aligned}&(a_0p^n+a_1p^{n-1}+\ldots+a_{n-1}p+a_n)y=\\&=(b_0p^m+b_1p^{m-1}+\ldots+b_{m-1}p+b_m)x,\end{aligned} \tag{2.33}$$

and

$$N(p)y=M(p)x. \tag{2.34}$$

N(p) and M(p) in Equation (2.34) are rational functions of the operator p, that is, they too are operators, but are more complex.

From Equation (2.34) we obtain

$$y=\frac{M(p)}{N(p)}x=W_{y/x}(p)x. \tag{2.35}$$

The operator $W_{y/x}(p)$, which, as ensues from Equation (2.35), transforms the disturbing effect into the reaction of the particular system, is called the transfer function for the system.

Another frequently occurring expression for the transfer function can be obtained from Equation (2.35):

$$W_{y/x}(p)=\frac{y}{x}. \tag{2.36}$$

In the case of systems described by an equation of the type at (2.31), the transfer function is a rational fractional function of the operator p:

$$W_{y/x}(p)=\frac{b_0p^m+b_1p^{m-1}+\ldots+b_{m-1}p+b_m}{a_0p^n+a_1p^{n-1}+\ldots+a_{n-1}p+a_n}. \tag{2.37}$$

Let us consider some of the properties of the transfer function when the disturbing influence is a unit function.

The value of the output magnitude in the steady-state condition ($t=\infty$), when the effect has the form of a unit function, can be obtained directly from Equation (2.31) if all the derivatives it contains are set equal to zero, $y=b_m/a_n$. This same value can be obtained from the expressions for the transfer function at (2.35) and (2.37), if we put p=0. Thus,

$$\lim_{t\to\infty}y(t)=\lim_{p\to0}W_{y/x}(p). \tag{2.38}$$

It can also be proven, although the manner of so doing is more complicated, that the initial value of the output magnitude (t=0) can be determined by the value of the transfer function when $p=\infty$, in the case of an effect of the unit function type, that is, /70

$$\lim_{t\to0}y(t)=\lim_{p\to\infty}W_{y/x}(p). \tag{2.39}$$

Let us also review the concept of the frequency characteristic curve for the system described by the differential equation at (2.31) used in what follows.

Let the disturbing action x(t) change in accordance with a sinusoidal law, that is,

$$x(t)=A_x\sin(\omega t+\psi_x), \tag{2.40}$$

where ψ_x is the initial phase of the disturbing action.

In this case, the output magnitude, or the reaction of a system in a steady-state condition, too will be a sinusoidal function of time

$$y(t)=A_y\sin(\omega t+\psi_y), \tag{2.41}$$

where ψ_y is the initial phase of the output magnitude.

Representing the sinusoidal magnitudes at (2.40) and (2.41) in complex form, we obtain

$$x(j\omega t)=A_x e^{j(\omega t+\psi_x)}=\dot{A}_x e^{j\omega t}, \tag{2.42}$$

where $\dot{A}_x=A_x e^{j\psi_x}$ is the complex amplitude of the disturbing action;

$$y(j\omega t)=A_y e^{j(\omega t+\psi_y)}=\dot{A}_y e^{j\omega t}, \tag{2.43}$$

where $\dot{A}_y=A_y e^{j\psi_y}$ is the complex amplitude of the output magnitude.

The ratio of the complex amplitudes of the output magnitude to the disturbing action is called the frequency, or amplitude-phase characteristic curve for the system, or the complex transfer function.

Substituting values x(jωt) and y(jωt) in Equation (2.31), we find the frequency characteristic curve for the system as

$$\frac{\dot{A}_y(j\omega)}{\dot{A}_x(j\omega)}=\frac{b_0(j\omega)^m+b_1(j\omega)^{m-1}+\ldots+b_{m-1}j\omega+b_m}{a_0(j\omega)^n+a_1(j\omega)^{n-1}+\ldots+a_{n-1}j\omega+a_n}. \tag{2.44}$$

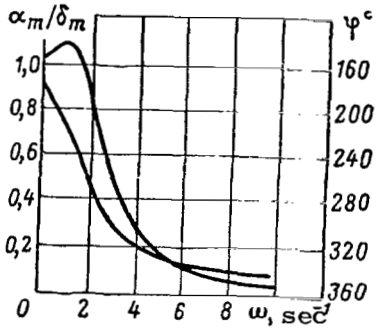

Figure 2.6. Amplitude and phase characteristic curves for angle of attack in the case of a sinusoidal movement of the elevator.

Comparing Equations (2.44) and (2.37), we establish the fact that the frequency characteristic curve can be obtained from the transfer function by replacing the operator p with the operator jω. Accordingly,

/71

$$W_{y/x}(j\omega)=\frac{\dot{A}_y(j\omega)}{\dot{A}_x(j\omega)}=\frac{A_y}{A_x}e^{j(\psi_y-\psi_x)}=W_{y/x}(\omega)e^{j\varphi}, \qquad (2.45)$$

where $W_{y/x}(\omega)=A_y/A_x$ is the modulus, or the amplitude characteristic;

$\varphi=\arg W_{y/x}(j\omega)$ is the argument, or the phase characteristic.

The amplitude characteristic expresses the amplitude of the output magnitude in terms of the frequency of the disturbing action. The phase characteristic yields a similar ratio for the phase of the output magnitude.

Figure 2.6 is included by way of an example to show the amplitude and phase characteristic curves for the angle of attack in the case of sinusoidal movement of the elevator.

2.5. Modeling the Motion of an Airplane in Turbulent Air

Modeling flight dynamics equations on analog electronic, or electromechanical, computers is a widely used procedure at this time for investigating airplane motion.

This book will review the methodology used for modeling one specific problem, that of the dynamics of the motion of an aircraft in turbulent air.

At the same time, it will be taken that turbulence is a stationary random process that can be described by the analytical expressions introduced in Chapter 1.

The motion of any system described by a linear differential equation such as Equation (2.31), and acted on by a stationary random disturbance, can be investigated by using well-known methods employing the apparatus of correlation functions, or of spectral densities. This book will use the apparatus of spectral densities. The spectral density, $S_y(\omega)$, of the output magnitude of some system with frequency characteristic $W_{y/x}(j\omega)$ (Figure 2.7) can be determined by the expression:

$$S_y(\omega)=|W_{y/x}(j\omega)|^2 S_x(\omega)=W^2_{y/x}(\omega)S_x(\omega), \tag{2.46}$$

where $S_x(\omega)$ is the spectral density of the disturbance.

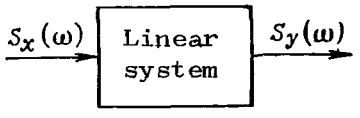

Figure 2.7. A linear system in the case of a stationary random disturbance.

The spectral density quite completely characterizes the change in the output magnitude caused by a random stationary action because it indicates the output magnitude dispersion frequency distribution. However, the more common practice is to limit the evaluation of the change in the output magnitude to an evaluation of its root-mean-square, σ_y, which is linked with the spectral density by the formula (see Appendix D): /72

$$\sigma_y^2=\int_0^\infty S_y(\omega)\,d\omega. \tag{2.47}$$

The analytical determination of the spectral density, as well as of the root-mean-square (or of the dispersion σ_y^2), is very time-consuming a process in the investigation of airplane dynamics. This is so because of the complexity of the transfer functions, and, as a result, of the airplane's frequency characteristics.

Analog computers can be used to compute the spectral density and the dispersion in the airplane motion parameters [30]. The determination of

the spectral density of the output magnitude by analog computers is based on modeling Equation (2.46). The spectral density of the wind is a rational fractional function of the frequency ω, in which ω is contained in even powers only. The spectral density of the input magnitude, therefore, can be represented in the form of the square of the modulus of the frequency characteristic of some linear system, usually called a shaping filter:

$$S_x(\omega)=|W_{x/x_1}(j\omega)|^2=W^2_{x/x_1}(\omega), \tag{2.48}$$

where

x is the input magnitude for the system under investigation;

x_1 is the sinusoidal signal of frequency ω, supplied to the input to the shaping filter with frequency characteristic $W_{x/x_1}(i\omega)$.

Equation (2.46), with Equation (2.48) taken into consideration, yields:

$$S_y(\omega)=|W_{x/x_1}(j\omega)W_{y/x}(j\omega)|^2. \tag{2.49}$$

What follows from Equation (2.49) is that if the model of the shaping filter and the system being investigated are connected in series, and if a sinusoidal signal with frequency ω is supplied to the filter input, the square of the amplitude of the output signal will equal the spectral density of the output magnitude for the system being investigated at this frequency. The block diagram of the model of the spectral density of the output magnitude is shown in Figure 2.8, in which the letters MU stand for Multiplication Unit, which squares the magnitude $y(\omega)$.

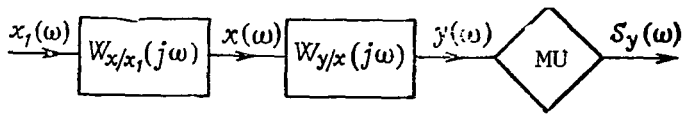

Figure 2.8. Block diagram of the model of the spectral density of the output magnitude.

Let us consider the methodology for determining the parameters of the shaping filter for modeling the spectral density of the disturbing action. /73

Let us take Equation (1.33) for the spectral density of the lateral component of a random wind as our example, and let us present it in a more

convenient form as

$$S_d(\omega)=\sigma_w^2\,\frac{a}{\pi}\,\frac{1+3a^2\omega^2}{(1+a^2\omega^2)^2}, \tag{2.50}$$

where $a=L/V_e$.

Let us equate Equation (2.50) to the square of the unknown frequency characteristic $W_{x/x_1}(j\omega)$ at (2.48):

$$S_n(\omega)=|W_{x/x_1}(j\omega)|^2=W_{x/x_1}(j\omega)\,W_{x/x_1}(-j\omega). \tag{2.51}$$

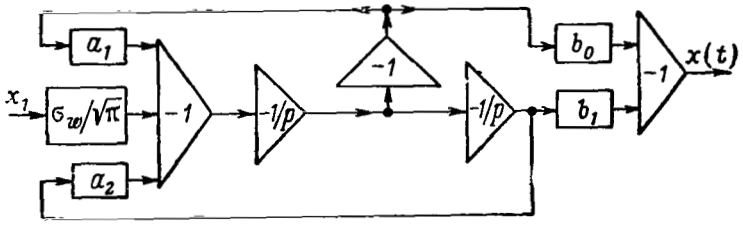

Figure 2.9. Structural diagram of a forming filter for obtaining spectral density.

Readily noted is the fact that Equation (2.51) will satisfy the following expression

$$W_{x/x_1}(j\omega)=\frac{\sigma_w}{\sqrt{\pi}}\sqrt{a}\,\frac{1+j1,73a\omega}{(1+ja\omega)^2}. \tag{2.52}$$

What follows from Equation (2.52) is that the transfer function for the shaping filter should have the following form for the lateral wind component:

$$W_{x/x_1}(p)=\frac{\sigma_w}{\sqrt{\pi}}\sqrt{a}\,\frac{1+1,73ap}{(1+ap)^2}=\frac{\sigma_w}{\sqrt{\pi}}\,\frac{b_0p+b_1}{p^2+a_1p+a_2}, \tag{2.53}$$

where

$$a_1=2/a,\quad a_2=1/a^2,\quad b_0=1.73/\sqrt{a},\ b_1=1/a^{3/2}. \tag{2.54}$$

The structural diagram of the model of the transfer function for the form at (2.53) on an analog computer is shown in Figure 2.9.

It should be pointed out that when a filter such as that shown in Figure 2.9 is used, the root-mean-square wind is reduced in concordance with the amplitude of the sinusoidal voltage supplied from an infrared frequency generator. The amplitude of the voltage after the multiplication unit should be measured at the output of the circuit in Figure 2.9. The amplitude of the sinusoidal voltage at the input should be reduced by a factor of $1/\sqrt{\pi}$ [Equation (2.53)] if the shaping filter is to correspond to the original expression for the spectral density. /74

The shaping filter used in several other circuits can be used to obtain the dispersion in the output parameters for the system subjected to a stationary disturbance.

The determination of the dispersion of the parameters of the system under investigation on an analog computer is based on the relationship

$$\sigma_y^2 = \int_0^\infty S_y(\omega)d\omega = \int_0^\infty |W_{x/x_1}(j\omega)W_{y/x}(j\omega)|^2 d\omega. \qquad (2.55)$$

On the other hand, we know that the frequency characteristic and the pulse transfer function of a linear system are linked by Rayleigh's theorem

$$\int_0^\infty K_y^2(t)\,dt = \frac{1}{\pi}\int_0^\infty |W_{x/x_1}(j\omega)W_{y/x}(j\omega)|^2 d\omega. \qquad (2.56)$$

The lower limit $-\infty$ is replaced by 0 in the integral in the left side of Rayleigh's theorem because the pulse transfer function $K_y(t)$ is identically equal to zero when $t<0$.

The right sides of Equations (2.55) and (2.56) differ only by the coefficient $1/\pi$. Therefore

$$\sigma_y^2 = \int_0^\infty K^2(t)\,dt = \frac{1}{\pi}\int_0^\infty |\sqrt{\pi}W_{x/x_1}(j\omega)W_{y/x}(j\omega)|^2 d\omega. \qquad (2.57)$$

Equation (2.57) shows that in order to obtain the dispersion in the form of an integral from the square of the pulse function of some system using Equation (2.47) between the dispersion and the spectral density, the

frequency characteristic of that system should be multiplied by $\sqrt{\pi}$.

Equation (2.57) is inconvenient for modeling because it requires that a pulse function act on the system. External actions are given in the form of a unit function in conventional integrators. What follows from Equation (2.32) is that if $K_y(t)$ is a pulse response function of a system with frequency characteristic $W(j\omega)$, it is also a response function of a system with frequency characteristic $j\omega W(j\omega)$. This is why the transfer function of the shaping filter in the diagram for modeling the dispersion (Figure 2.10) /75 has an additional factor, p, and why a unit function is supplied at the input. The transfer function for a shaping filter corresponding to the spectral density at (2.50) will be in the following form when the additional factors $\sqrt{\pi}$ and p are taken into consideration:

$$W_{x/x_1}(p)=\sigma_w\sqrt{a}\,\frac{p+1{,}73ap^2}{(1+ap)^2}=\sigma_w\,\frac{b_0p^2+b_1p}{p^2+a_1p+a_2}\,. \qquad (2.58)$$

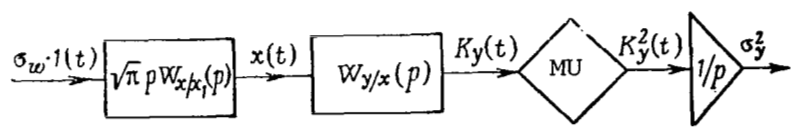

Figure 2.10. Block diagram of the model of the dispersion of the output magnitude.

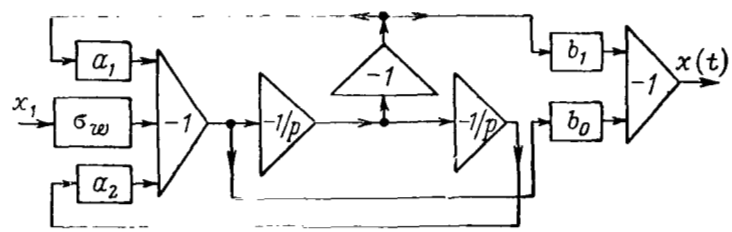

Figure 2.11. Structural diagram of a model filter for obtaining the dispersion.

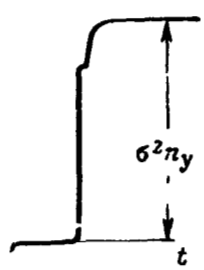

Figure 2.12. Oscillogram of the voltage across the output of the block diagram in Figure 2.10.

The coefficients a_i and b_i are determined through Equation (2.54). The structural diagram of the model of this filter is shown in Figure 2.11.

What follows from Equation (2.57) is that the voltage across the output of the circuit (Figure 2.10) upon completion of the transient that caused the supply of a step function to the input corresponds to the square of the dispersion of the magnitude under investigation. This time is equal to infinity, theoretically, but practically it varies over limits of seconds or tens of seconds when airplane dynamics are investigated. Figure 2.12 shows a typical oscillogram of the output voltage across the circuit (Figure 2.10) during the investigation of the accereration caused by a random vertical wind.

The methodology cited for modeling the dynamics of a system acted on by a disturbance that is a stationary random function makes it possible to quite rapidly investigate the motion of an airplane in turbulent air.

CHAPTER III

LONGITUDINAL MOTION OF AN AIRPLANE IN MOVING AIR

3.1. Transfer and Response Functions for the Parameters of Wind-caused Longitudinal Motion

The principal task of this section is to obtain and analyze transfer /76
functions for the parameters of the longitudinal motion of an airplane in moving air. The transfer functions will be used in subsequent sections of this chapter to obtain the characteristics of longitudinal motion in turbulent air. This will be done by using Equation (2.46) and Equation (2.47).

The response functions for the longitudinal motion, considered jointly with the transfer functions, provide a graphic presentation of the behavior of an airplane that encounters a single wind gust with a form that of a unit step function. Although gusts such as this do not exist in the real atmosphere, gusts with steep gradients are encountered, and these, in the first few seconds of their action on the airplane, can be considered as steps.

This chapter compares the dynamics of an airplane with fixed controls with those when control is exercised by an autopilot. Investigation of the behavior of an airplane with fixed controls is of theoretical and practical interest because the instructions given a pilot flying in moving air recommend that in so far as possible he not interfere with the control of the airplane, but that he hold the controls in a fixed position. However, the autopilot is being used more and more frequently to control the airplane under these conditions.

Let us evaluate the role of the longitudinal and normal components of the wind velocity in the disturbance of the longitudinal motion parameters. To this end, let us consider the transfer and response functions for an airplane with a fixed elevator, and an airplane controlled by an autopilot with an altitude corrector [the law at (2.13)] and without one [the law at (2.14)].

We will obtain the following transfer functions for the action of the

horizontal wind component by using the entire system of equations at (2.10), since the system is valid for level flight of an airplane with fixed elevator.

For the angle of pitch[1]

$$W_{\vartheta/w_x}(p) = -\frac{B(p)}{A(p)} = -\frac{b_0 p^2 + b_1 p}{p^4 + a_1 p^3 + a_2 p^2 + a_3 p + a_4}. \qquad (3.1)$$ /77

The minus sign for the Equation (3.1) transfer function indicates that immediately upon encountering the wake of air at constant velocity ($W_x > 0$), the airplane drops its nose ($\Delta\vartheta < 0$). In the steady-state condition (p = 0) the increase in the angle of pitch is zero.

For the increase in speed with respect to body axis x

$$W_{\Delta V_{gx}/w_x}(p) = \frac{C(p)}{A(p)} = \frac{c_0 p^3 + c_1 p^2 + c_2 p + a_4}{A(p)}. \qquad (3.2)$$

Coincidence of the absolute terms in the numerator and denominator of the Equation (3.2) transfer function indicates that in the steady-state condition the increase in the ground speed, ΔV_{gx}, is equal to the constant velocity of the horizontal wind component, w_x.

For the y body axis velocity we have

$$W_{V_{gy}/w_x}(p) = -\frac{D(p)}{A(p)} = -\frac{d_0 p^3 + d_1 p^2}{A(p)}. \qquad (3.3)$$

For the vertical speed of the airplane (in earth axes) we have

$$W_{\dot{y}_g/w_x}(p) = -\frac{E(p)}{A(p)} = -\frac{e_0 p^3 + e_1 p^2 + e_2 p}{A(p)}. \qquad (3.4)$$

For the horizontal acceleration we have

$$W_{n_x/w_x}(p) = \frac{p}{g} W_{\Delta V_{gx}/w_x}(p). \qquad (3.5)$$

For the vertical acceleration we have

$$W_{n_y/w_x}(p) = \frac{p}{g} W_{\dot{y}_g/w_x}(p). \qquad (3.6)$$

The form of the transfer functions at (3.3) - (3.6) confirms the fact that in the steady-state condition (p = 0), with constant wind W_x acting, the increases in the parameters V_{gy}, y_g, n_x and n_y are zero.

The transfer functions for an aircraft with a fixed elevator acted on by the vertical wind component have the following form.

---

1. The expressions for the coefficients of this, and of the other transfer functions characterizing longitudinal motion, are listed in Appendix A.

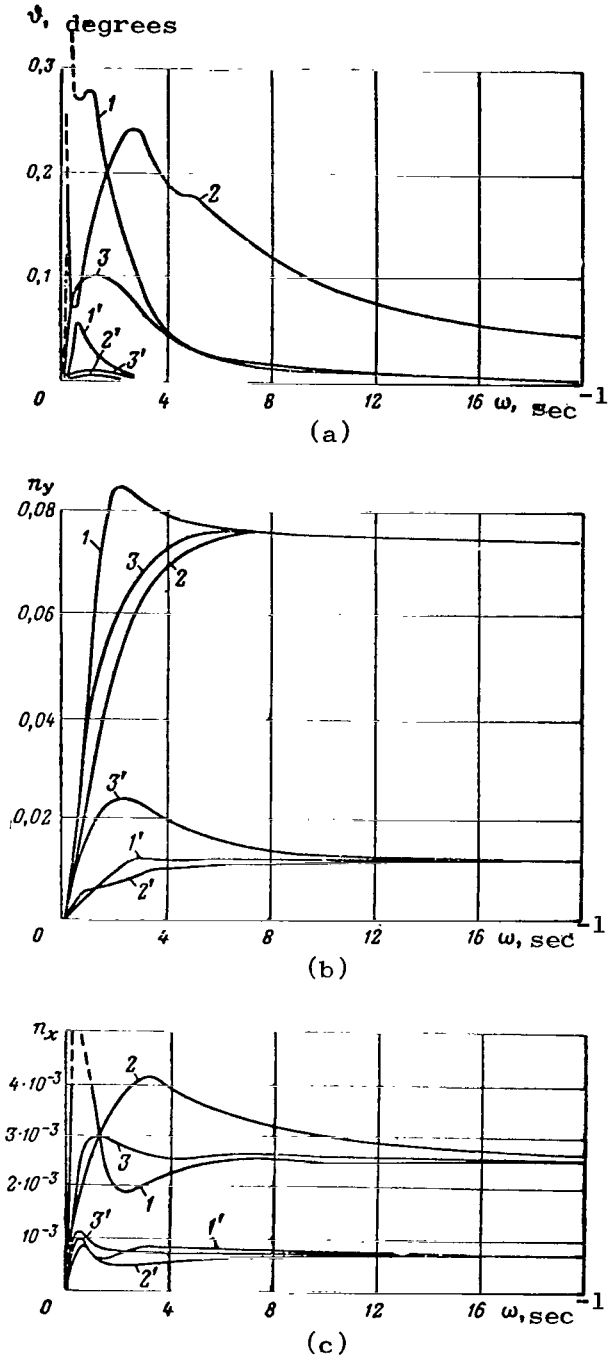

Figure 3.1. Amplitude characteristic curves for angle of pitch (a), and vertical (b) and horizontal (c) accelerations as a result of the action of the vertical and horizontal wind components (Airplane No. 1). The curves for the horizontal wind are shown as the dashed segments. 1 - airplane with fixed controls; 2 - airplane with autopilot [law (2.13)]; 3 - airplane with autopilot [law (2.14)].

For the angle of pitch

$$W_{\vartheta/w_y}(p) = -\frac{F(p)}{A(p)} = -\frac{f_0 p^2 + f_1 p}{A(p)}. \tag{3.7}$$

The minus sign for the Equation (3.7) transfer function indicates that immediately upon entering an updraft of constant velocity ($W_y > 0$), the stable airplane will drop its nose ("dive into the wind"). In the steady-state condition (p = 0), with constant vertical wind velocity the increase in the angle of pitch is zero. /79

For the increment of the velocity along the x body axis we have

$$W_{\Delta V_{gx}/w_y}(p) = \frac{G(p)}{A(p)} = \frac{g_0 p^3 + g_1 p^2 + g_2 p}{A(p)}. \tag{3.8}$$

For the velocity along the y body axis we have

$$W_{V_{gy}/w_y}(p) = \frac{H(p)}{A(p)} = \frac{h_0 p^3 + h_1 p^2 + h_2 p + a_4}{A(p)}. \tag{3.9}$$

For the vertical speed of the airplane (in earth axes) we have

$$W_{\dot{y}_g/w_y}(p) = \frac{I(p)}{A(p)} = \frac{i_0 p^3 + i_1 p^2 + i_2 p + a_4}{A(p)}. \tag{3.10}$$

The absolute terms in the numerators and denominators of Equation (3.9) and Equation (3.10) coincide, indicating that in the steady-state condition the airplane's vertical speed will equal the velocity of a wind with constant magnitude W_y.

For the horizontal acceleration we have

$$W_{n_x/w_y}(p) = \frac{p}{g} W_{\Delta V_{gx}/w_y}(p). \tag{3.11}$$

For the vertical acceleration we have

$$W_{n_y/w_y}(p) = \frac{p}{g} W_{\dot{y}_g/w_y}(p). \tag{3.12}$$

Figure 3.1 contains examples of the amplitude-frequency characteristic curves for the practically most important parameters of longitudinal motion of a big transport airplane flying under normal cruising conditions (this airplane will be called Airplane No. 1 for short in the following. These curves were constructed from the above-considered transfer functions for the angle of pitch, and from the vertical and horizontal accelerations resulting the vertical (curve 1) and horizontal (curve 1') wind components. Figure 3.2 (curves numbered 1) shows the initial sections of these curves at a larger

scale for ω. The curves for the airplane in Figure 3.2 were constructed for vertical wind component action only because the curves in Figure 3.1 show that the angle of pitch and the vertical acceleration caused by the horizontal wind component are smaller by approximately an order of magnitude than those caused by the vertical wind component. The role of the horizontal component in creating the horizontal acceleration (Figure 3.1c) is somewhat larger, but the latter is small in absolute magnitude and is of no practical interest in the majority of cases. This is the basis in what follows for usually analyzing the behavior of an airplane acted on by vertical wind gusts. /80

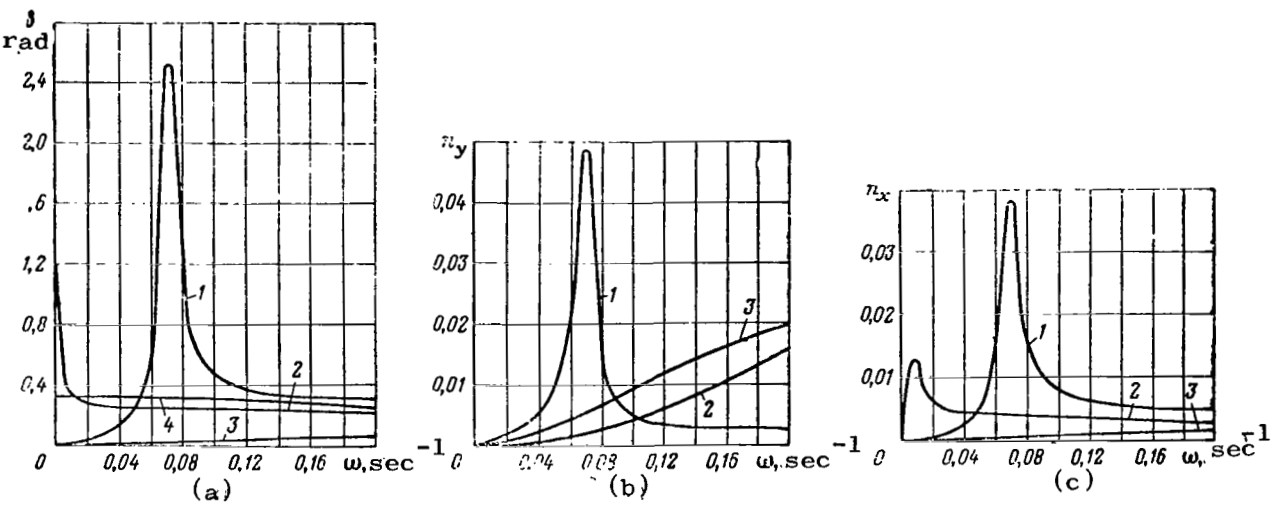

Figure 3.2. Initial sections of the amplitude characteristic curves for the increases in angle of pitch (a), and for the vertical (b), and horizontal (c) accelerations resulting from the vertical wind component (Airplane No. 1). 1 - airplane with fixed controls; 2 - airplane with autopilot [law (2.13)]; 3 - airplane with autopilot [law (2.14)]; 4 - airplane with autopilot [law (2.13)], simplified equations for the airplane at (2.11).

The curves in Figure 3.2 indicate that at very low frequencies the curves for the airplane with fixed controls contain peaks of considerable amplitude, the result of long-period motion (phugoids). This is well confirmed by the transients corresponding to the entry of Airplane No. 1 into a vertical air flow with a velocity of W_y = 10 m/sec (Figure 3.3).

Attention must be given to the fact that the increase in the angle of attack $\Delta\alpha$, attributable to the vertical gusts, drops practically to zero /81

during short-period motion and is not disturbed during the process of phugoid oscillations. The response function for the angle of attack practically coincides with the response function for the vertical acceleration. Therefore the analysis of the longitudinal motion, made primarily from the point of view of the accelerations, can be limited by the simpler equations at (2.11). It will be shown in what follows that in the case of the airplane with an autopilot without altitude corrector this assumption is even more valid because the autopilot suppresses phygoid oscillations, and the transients obtained by using the complete Equation (2.10) and the simplified Equation (2.11) coincide better than they do in the case of the airplane without an autopilot.

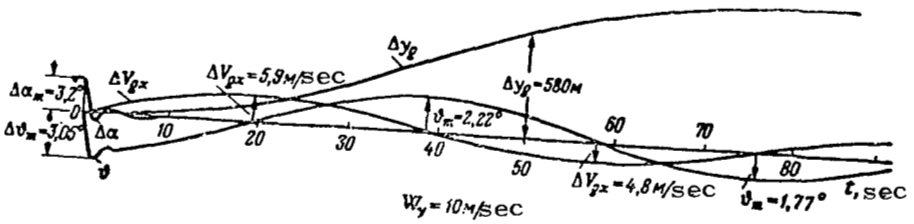

Figure 3.3. Transients resulting from vertical wind action for Airplane No. 1 with fixed controls obtained using the complete Equation (2.10).

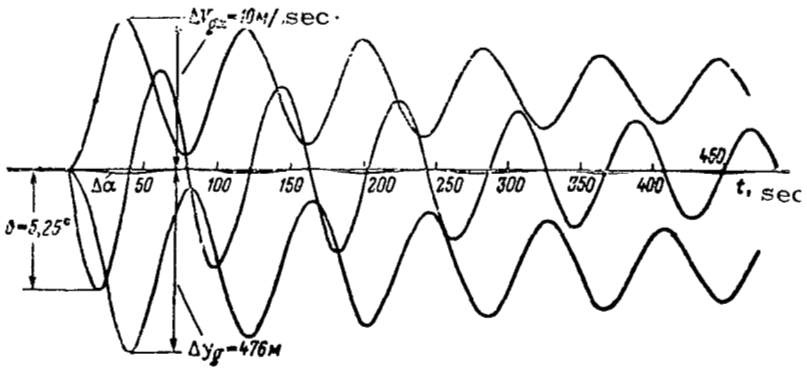

Figure 3.4. Transients resulting from horizontal wind action for Airplane No. 1 with fixed controls obtained using the complete Equation (2.10).

Figure 3.4 shows the transients for Airplane No. 1 with fixed controls corresponding to the entry of the airplane into an air current with a velocity of W_x = 10 m/sec. The time scale has been reduced to provide a more graphic representation of the phugoid oscillations. The transients in Figure 3.4

show that in the case of an airplane with fixed controls encountering a horizontal gust there is virtually no disturbance in the angle of attack, and that the increases in angle of pitch, ground speed, and altitude complete weakly damped oscillations with a long period. At the same time, the variations in flight speed and altitude occur relative to the values of these magnitudes in the new steady-state condition. /82

Let us obtain the transfer functions for the parameters of the motion of an airplane with fixed controls in the case of action by the horizontal wind component, using the simpler Equation (2.11).

For the angle of pitch (expressions for the coefficients of the Equations (3.13) - (3.19) transfer functions are listed in Appendix A) we have

$$W_{\vartheta/w_x}(p) = -\frac{B'(p)}{pA'(p)} = -\frac{b_0' p + b_1'}{p\left(p^2 + a_1' p + a_2'\right)}. \tag{3.13}$$

For the velocity along the y body axis we have

$$W_{V_{gy}/w_x}(p) = -\frac{D'(p)}{A'(p)} = -\frac{d_0' p + d_1'}{A'(p)}. \tag{3.14}$$

For the airplane's vertical speed we have

$$W_{\dot{y}_g/w_x}(p) = -\frac{E'(p)}{pA'(p)} = -\frac{e_0' p^2 + e_1' p + e_2'}{pA'(p)}. \tag{3.15}$$

For the vertical acceleration we have

$$W_{n_y/w_x}(p) = \frac{p}{g} W_{\dot{y}_g/w_x}(p). \tag{3.16}$$

Let us consider the transfer functions for the parameters of longitudinal motion when the vertical wind component is acting. The functions are obtained through Equation (2.11).

For the angle of pitch we have

$$W_{\vartheta/w_y}(p) = -\frac{F'(p)}{A'(p)} = -\frac{f_0'}{A'(p)}. \tag{3.17}$$

For the velocity along the y body axis we have

$$W_{V_{gy}/w_y}(p) = \frac{H'(p)}{A'(p)} = \frac{h_0' p + a_2'}{A'(p)}. \tag{3.18}$$

For the airplane's vertical speed we have

$$W_{\dot{y}_g/w_y}(p) = \frac{I'(p)}{A'(p)} = \frac{i_0' p + i_1'}{A'(p)}. \tag{3.19}$$

For the vertical acceleration we have /83

$$W_{n_y/w_y}(p) = \frac{p}{g} W_{\dot{y}_g/w_y}(p). \tag{3.20}$$

Let us also find the transfer function for the additional acceleration attributable to the angular motions of the aircraft, that is, to its oscillations relative to the center of gravity. This acceleration we determine only for the case of the vertical wind component. The transfer function for the acceleration of length l of the center of gravity attributable to the angular motions is in the form

$$W_{n_\vartheta/w_y}(p) = \frac{lp^2}{g} W_{\vartheta/w_y}(p). \tag{3.21}$$

Length l has a plus sign for points located between the center of gravity and the tail.

It must be pointed out that the transfer functions at (3.13) and (3.15) cannot be used to compute the motion of an airplane acted on by a random wind because they contain a purely integrating link as a factor, and this results in infinitely large values for the dispersion of the angle of pitch and of the vertical speed as a result of the action of a random wind. This result stems from a negligible change in flight speed. The transfer functions at (3.1) and (3.4) for these same parameters, while obtained through the use of exact Equation (2.10), lack this drawback.

The frequency characteristic curves for the angle of pitch and the acceleration, obtained by using the simplified formulas, practically coincide with those shown in Figure 3.1, a and b (curves 1 and 1'). This confirms the assertion made above with respect to the short-period motion of an airplane without an autopilot acted on by a wind that can be described quite well by the system of equations at (2.11).

The low frequency peaks (Figure 3.2, a and b) corresponding to the phugoids disappear on the frequency curves obtained through the use of the simplified equations. However, the area of these peaks is negligible, so their role in determining the dispersion of the angle of pitch and of the acceleration as a result of the action on the airplane of a random wind is negligible. In order to illustrate all these statements, let us consider the transients for Airplane No. 1, obtained through Equation (2.11). These functions correspond to the

airplane entering a vertical wind, W = 10 m/sec (Figure 3.5). When Figure 3.5 is compared with Figure 3.3, we see that within the time limits the damping of the short-period motion of the process is very similar in both figures.

Now let us proceed to an analysis of the transfer and response functions with an autopilot. Combining Equation (2.10) for the airplane and the autopilot with the Equation (2.13) control law, we obtain the transfer functions for the parameters of the longitudinal motion.

These functions have the following form for the action of the horizontal wind component.

For the angle of pitch (expressions for the coefficients of the Equations (3.22) - (3.27) transfer functions are listed in Appendix A). /84

$$W_{\vartheta/w_x}(p) = -\frac{J(p)}{K(p)} = -\frac{j_0 p^3 + j_1 p^2 + j_2 p}{p^5 + k_1 p^4 + k_2 p^3 + k_3 p^2 + k_4 p + k_5}. \qquad (3.22)$$

For the horizontal acceleration

$$W_{n_x/w_x}(p) = \frac{1}{g}\frac{L(p)}{K(p)} = \frac{1}{g}\frac{l_0 p^5 + l_1 p^4 + l_2 p^3 + l_3 p^2 + k_5 p}{K(p)}. \qquad (3.23)$$

For the vertical acceleration

$$W_{n_y/w_x}(p) = -\frac{1}{g}\frac{M(p)}{K(p)} = -\frac{1}{g}\frac{m_0 p^5 + m_1 p^4 + m_2 p^3}{K(p)}. \qquad (3.24)$$

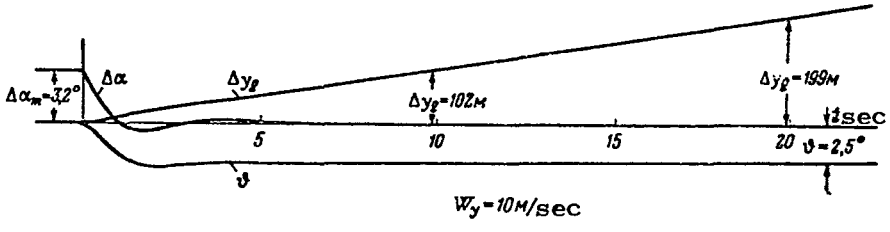

Figure 3.5. Transients for Airplane No. 1 with fixed controls acted on by a vertical wind obtained using simplified Equation (2.11).

The transfer functions have the following form when the vertical wind component is acting.

For the angle of pitch

$$W_{\vartheta/w_y}(p) = \frac{N(p)}{K(p)} = -\frac{n_0 p^3 + n_1 p^2 + n_2 p + n_3}{K(p)}. \qquad (3.25)$$

For the horizontal acceleration

$$W_{n_x/w_y}(p)=\frac{1}{g}\frac{Q(p)}{K(p)}=\frac{1}{g}\frac{q_0p^5+q_1p^4+q_2p^3+q_3p^2+q_4p}{K(p)}. \qquad (3.26)$$

For the vertical acceleration

$$W_{n_y/w_y}(p)=\frac{1}{g}\frac{R(p)}{K(p)}=\frac{1}{g}\frac{r_0p^5+r_1p^4+r_2p^3+r_3p^2}{K(p)}. \qquad (3.27)$$

The amplitude-frequency characteristic curves, constructed from the Equations (3.22) - (3.27) transfer functions (the values of ratio for the autopilot are listed in Appendix A) for Airplane No. 1 are shown in Figure 3.1 (curves 2 and 2'). The curves numbered 2 are for the action of the vertical, and curves numbered 2' are for the action of the horizontal wind components. The curves for low frequencies, equating to the vertical wind, are shown in Figure 3.2 (curves 2). The curves in Figure 3.2 show that an autopilot with Equation (2.13) control law cuts off the peaks of the phugoid oscillations for vertical acceleration and reduces the peaks for horizontal acceleration. An unsatisfactory result is the displacement of the peak on the angle of pitch curve to zero frequency (Figure 3.2a), as a result of which the effect of the vertical wind causes a significant deviation of all parameters from their values in the steady-state condition. Figure 3.2a also shows the amplitude-frequency curve, 4, constructed using a simplified transfer function, when the change in speed is not taken into consideration [Equation (2.11) and the autopilot Equation (2.13)]. There is no peak in curve 4 at zero frequency, and this has a very significant effect on airplane dynamics. /85

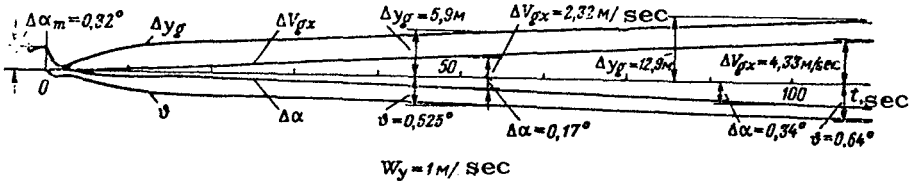

Figure 3.6. Transients resulting from the action of a vertical wind for Airplane No. 1 with autopilot [law (2.13)] obtained using the complete Equation (2.10).

Let us illustrate these results by using the transients for Airplane No. 1 shown in Figures 3.6 and 3.7. The transients in Figure 3.6 were obtained using the complete equations at (2.10). The oscillograms in Figure 3.6 show the very unfavorable nature of the transient for an airplane with an autopilot

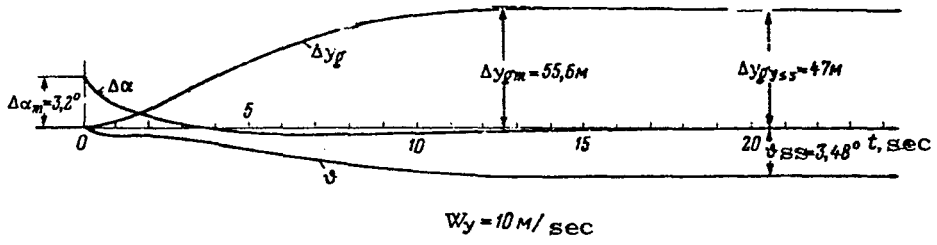

Figure 3.7. Transients resulting from the action of a vertical wind for Airplane No. 1 with autopilot [law (2.13)] obtained using the simplified Equation (2.11).

equipped with an altitude corrector when it encounters a vertical wind flow. The autopilot causes the airplane to nose down in order to stabilize the airplane at the new altitude when the wind direction is upward, for example, /86 thereby increasing speed. The angle of attack must now be reduced significantly in order to arrive at equilibrium for the new speed. All of these undesirable phenomena develop very slowly, the result of the low autopilot altitude gain (i_y = 0.07 degrees-control/meter). Therefore, in the overwhelming majority of cases the airplane flies out of the zone in which the vertical gust is acting earlier than these phenomena succeed in developing. But even if the action of the vertical gusts on the airplane is short-lived, the effect of the altitude corrector will be negative. Adding to the problem is the fact that today the sensor used to provide the signals with respect to change in altitude is a barometric statoscope, an instrument that functions satisfactorily only under still air conditions. There are pressure pulsations present in turbulent air, and these are reproduced by the sensor as oscillations in altitude. Under these conditions the altitude corrector can feed significantly strong, false signals to the autopilot, causing undesirable evolutions by the airplane.

A second feature of the motion we are considering with respect to an airplane with an autopilot fitted with an altitude corrector when the airplane encounters a vertical air flow is the principal impossibility of investigating this problem with the help of Equation (2.10) if the vertical wind velocity is significant. If such is the case, the deviations in speed and angle of attack from the original values are so large that in order to investigate flight dynamics we must use the original nonlinear equations. Therefore, the airplane motion shown in Figure 3.6 was investigated at a wind velocity of

W_y = 1 m/sec. But even so, the steady-state values of the deviations of the parameters from their values in the undisturbed condition, computed in accordance with the above-cited transfer functions, are

$$\Delta\vartheta_{ss} = -1{,}15^\circ,\ \Delta V_{gx} = 17{,}5\ м/\text{sec},\ \Delta y_g = 29\ м.$$

These values are not shown in Figure 3.6 because the process failed to arrive at the steady-state condition during oscillographing.

Figure 3.7 shows the transients for this same case, but without change in flight speed taken into consideration [Equation (2.11)]. Here the value of the vertical wind velocity was taken equal to 10 m/sec, because there are no such features in the behavior of the airplane-autopilot system. The phugoid oscillations are damped by the autopilot, the transients soon are over, and the airplane continues its flight with but a slight deviation in altitude.

A comparison of Figures 3.6 and 3.7 reveals clearly that the investigation of airplane dynamics when an autopilot with an altitude corrector is involved must be made with change in speed taken into consideration.

/87

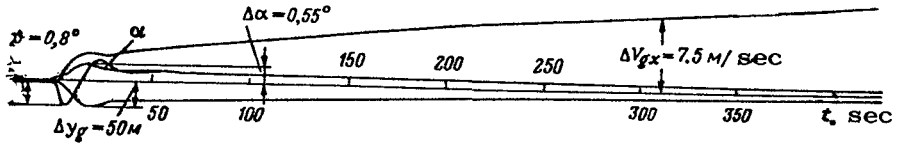

Figure 3.8. Transients as a result of the action of a horizontal wind for Airplane No. 1 with autopilot with altitude corrector, obtained using the complete Equation (2.10).

Figure 3.8 shows the transients for Airplane No. 1 with an autopilot with an altitude corrector. These point out the behavior of an airplane when it enters an air current with W_x = 10 m/sec. These functions were obtained using the complete equations for the airplane, Equation (2.10). There are no large deviations from the original state here that match those for the case of the airplane with autopilot with altitude corrector that enters a vertical wind stream (Figure 3.6). However, the process of the transition to a new steady-state condition is very drawn out and takes about 10 minutes in our example. Because of the negative effect of the altitude corrector on flight dynamics in disturbed air, as established in the foregoing, let us consider the behavior of an airplane with an autopilot with an altitude corrector, that is, one with the Equation (2.14) control law. Combining equations (2.10) and (2.14), we obtain

the following transfer functions in the case of the action of the horizontal wind component.

For the angle of pitch we have (expressions for the coefficients of the Equations (3.28) - (3.33) transfer functions are listed in Appendix A)

$$W_{\vartheta/w_x}(p)=-\frac{S(p)}{T(p)}=-\frac{s_0p^2+s_1p}{p^4+t_1p^3+t_2p^2+t_3p+t_4}. \tag{3.28}$$

For the horizontal acceleration

$$W_{n_x/w_x}(p)=\frac{1}{g}\frac{U(p)}{T(p)}=\frac{1}{g}\frac{u_0p^4+u_1p^3+u_2p^2+u_3p}{T(p)}. \tag{3.29}$$

For the vertical acceleration

$$W_{n_y/w_x}(p)=-\frac{1}{g}\frac{V(p)}{T(p)}=-\frac{1}{g}\frac{v_0p^4+v_1p^3+v_2p^2}{T(p)}. \tag{3.30}$$

The transfer functions when the vertical wind component is acting are in the following form for an airplane with an autopilot without altitude corrector.

For the angle of pitch

$$W_{\vartheta/w_y}(p)=-\frac{W(p)}{T(p)}=-\frac{w_0p^2+w_1p}{T(p)}. \tag{3.31}$$

For the horizontal acceleration /88

$$W_{n_x/w_y}(p)=\frac{1}{g}\frac{X(p)}{T(p)}=\frac{1}{g}\frac{x_0p^4+x_1p^3+x_2p^2}{T(p)}. \tag{3.32}$$

For the vertical acceleration

$$W_{n_y/w_y}(p)=\frac{1}{g}\frac{Y(p)}{T(p)}=\frac{1}{g}\frac{y_0p^4+y_1p^3+y_2p^2+y_3p}{T(p)}. \tag{3.33}$$

The amplitude-frequency characteristic curves constructed using the Equations (3.28) - (3.33) transfer functions for Airplane No. 1 are shown in Figure 3.1 (curves 3 and 3'). The initial sections of the curves, equated to the vertical wind, are shown large scale for ω in Figure 3.2 (curves 3). The curves in Figure 3.2 indicate that the curves for an airplane with an autopilot without altitude corrector [law (2.14)] extend into the region of low frequencies in the most favorable manner. So far as higher frequencies are concerned (Figure 3.1), the difference between curves 2 and 3 is slight. It is particularly slight for the vertical accelerations (Figure 3.1b), which are of the most practical interest.

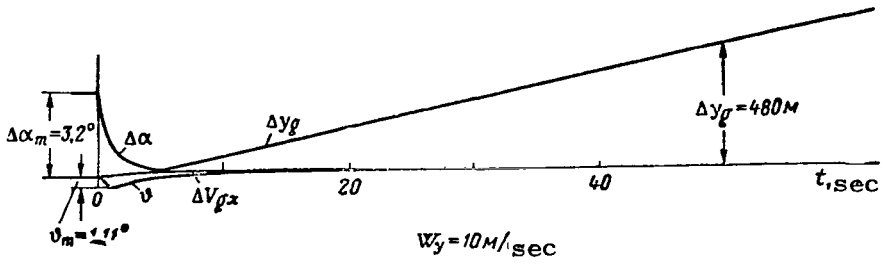

Figure 3.9. Transients as a result of the action of a vertical wind for Airplane No. 1 with autopilot [law (2.14)], obtained using the complete Equation (2.10).

Figures 3.9 and 3.10 show the transients during a vertical gust for Airplane No. 1 with autopilot, the control law for which is expressed by Equation (2.14). The transients in Figure 3.9 were obtained by using the complete Equation (2.10), while those in Figure 3.10 were obtained by using the simplified Equation (2.11). A comparison of these processes shows that when investigating the behavior of an airplane with an autopilot without an altitude corrector it is entirely permissible to use the simplified equations for the airplane.

The nature of the transients is extremely favorable, and there are no undesirable underswings in the angle of attack. All of which serves to confirm the conclusions arrived at using the frequency characteristic curves.

/89

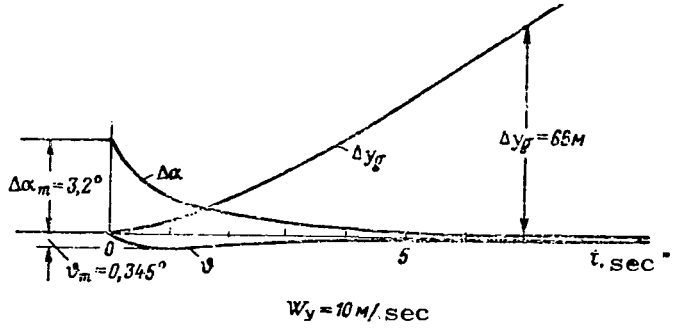

Figure 3.10. Transients as a result of the action of a vertical wind for Airplane No. 1 with autopilot [law (2.14)] obtained using simplified Equation (2.11).

Figure 3.11 shows the transients for Airplane No. 1 with autopilot without altitude corrector corresponding to entry of the airplane into an air current with a velocity W_x = 10 m/sec. These processes were obtained using complete Equation (2.10). The nature of transients is such that there is confirmation of a smooth, and relatively quick, transition to a new steady-state condition

when there is no altitude corrector.

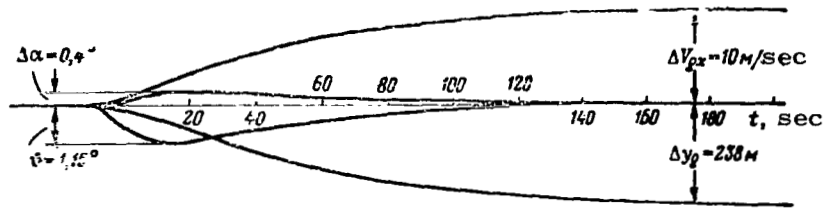

Figure 3.11. Transients as a result of the action of a horizontal wind for Airplane No. 1 with autopilot without altitude corrector, obtained using complete Equation (2.10).

In concluding this section, let us review the characteristic curves for an airplane with an autopilot with speed feedback, the control law for which can be expressed by Equation (2.15). Combining Equation (2.15) with simplified Equation (2.11) for longitudinal motion, we find the transfer function for the vertical acceleration caused by the vertical wind component as

$$W_{n_y/w_y}(p)=\frac{1}{g}\frac{Z(p)}{\Phi(p)}=\frac{1}{g}\frac{z_0p^4+z_1p^3+z_2p^2+z_3p}{p^4+\varphi_1p^3+\varphi_2p^2+\varphi_3p+\varphi_4}. \qquad (3.34)$$

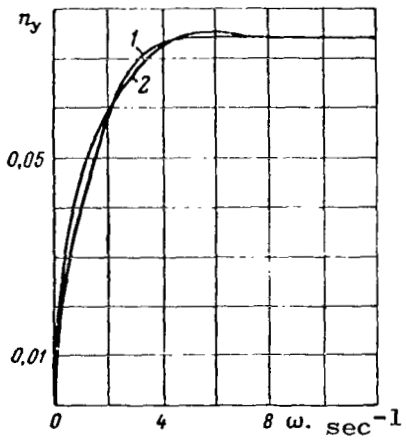

Figure 3.12. Amplitude-frequency characteristic curve for the increases in the vertical acceleration as a result of the effect of the vertical wind component for Airplane No. 1 with autopilot. 1 - autopilot with speed feedback [law (2.15)]; 2 - autopilot with direct feedback [law (2.14)].

The amplitude-frequency characteristic curve for Airplane No. 1, constructed on the basis of Equation (3.34), is shown on Figure 3.12 (curve 1). As before, the data for Airplane No. 1 listed in Appendix A were used to construct this curve. The values for the /90 gains $i_{\vartheta}^{\bullet}$ and i_{ϑ} were kept the same as in the preceding examples, and i_q = 0.15 sec^{-1} was selected in order to obtain a completely satisfactory transient in the development of a system for controlling the angle of pitch action.

Figure 3.12 also shows the frequency characteristic curve (curve 2) for Airplane No. 1 with autopilot with control law (2.14) for purposes of com-

parison. A comparison of curves 1 and 2 reveals that the airplane-autopilot with speed feedback system has virtually the same amplitude-frequency characteristic curve as does the airplane-autopilot with direct feedback system. Thus, the autopilot with speed feedback provides no advantages when flying in turbulent air.

3.2. Longitudinal Motion of an Airplane in Turbulent Air

Let us use the modeling methodology explained in Section 2.5 to analyze the longitudinal motion of an airplane in turbulent air. An analysis such as this usually concentrates on determination of oscillations in the angle of pitch and in the vertical acceleration experienced by the airplane, and these parameters of the longitudinal motion are of the greatest interest in the majority of practical problems associated with airplane flight in "rough air" conditions.

The use of the above-mentioned methodology will yield quite complete characteristic curves for the motion of an airplane in turbulent air. Simplified Equation (2.11) will be used in this paragraph to obtain the characteristic curves for longitudinal motion of the airplane. All such curves equate to airplane dynamics when the action is that of vertical gusts because, as we established in Section 3.1, disturbance the result of horizontal gusts is much less than that resulting from vertical gusts (by an order of magnitude, as a rule).

Let us begin our consideration with the spectral densities of the acceleration ond of the angle of pitch for Airplane No. 1 with an autopilot, and without one. The spectral densities obtained will follow those shown in /91
Figure 2.8. Figure 3.13 shows the normalized spectral densities of the increases in the vertical acceleration and of the angle of pitch for Airplane No. 1 with an autopilot, and without one,[2] the results of vertical wind. The dashed line curves are for the airplane without autopilot. The normalization of the spectral densities here, as well as in what follows, is for dispersion

2. This paragraph assumes the autopilot has control law (2.14), that is, that the altitude corrector is disengaged. Use of the autopilot with another control law will be stipulated.

of the random component of the vertical wind. Figure 3.13 shows six graphics for three different turbulence scales, L: the 1 curves for L = 50 m; the 2 curves for L = 300 m; and the 3 curves for L = 1,500 m. Selection of so wide a turbulence scale range can be explained by the lack of current, reliable data on the possible limits of change in this magnitude.[3]

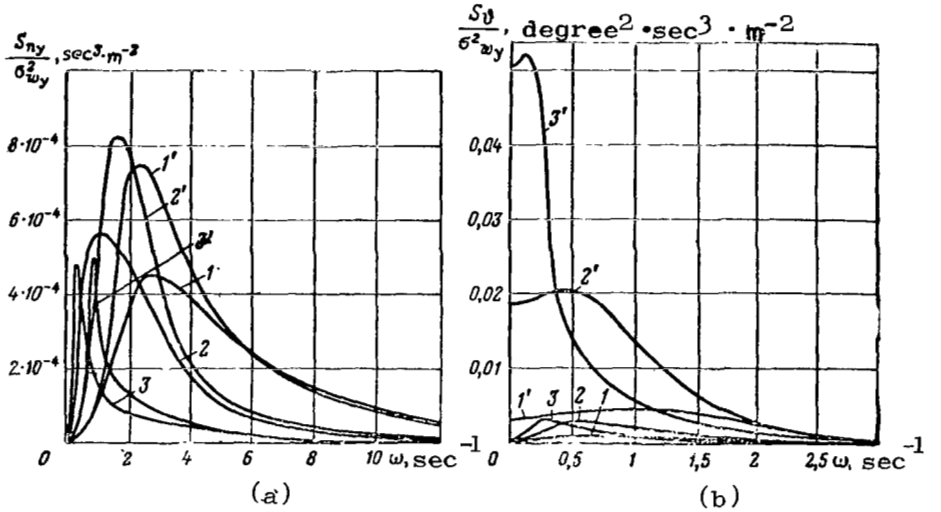

Figure 3.13. Normalized spectral densities of increase in vertical acceleration (a) and angle of pitch (b) for Airplane No. 1 with fixed controls and with an autopilot (the dashed curves are for the airplane with fixed controls): 1 - L = 50 m; 2 - L = 300 m; 3 - L = 1,500 m.

Analysis of the curves in Figure 3.13 reveals that the autopilot significantly reduces pitch oscillations, and reduces vertical acceleration somewhat. The reduction in pitch oscillations is quite regular because the autopilot is /92 designed to stabilize the specified value of this angle. Reduction in the acceleration is not evident, and this result will be made the subject of a special analysis in what follows. Also to be noted is that the vertical acceleration spectrum can be broader by approximately an order of magnitude than that of pitch oscillations (at small turbulence scales). Since the autopilot acts on airplane dynamics only as a result of a change in pitch, its range of activity is in frequency limits from 0 to 0.5 Hz. This result is well

3. A scale of L = 300 m is recommended in [15] as most probable.

confirmed by the acceleration spectral density curves in Figure 3.13a. The spectral densities for an airplane with an autopilot, and for one without an autopilot, practically coincide beginning at a frequency somewhat higher than 0.5 Hz. Consequently, airplane accelerations reproduce the vertical wind gusts in this frequency range. The autopilot reduces the peak of the acceleration spectral density curve somewhat at the very low frequencies and displaces it into the range of lower frequencies. This displacement can be explained by the fact that the acceleration on an airplane without an autopilot and at very low frequencies will be reduced as a result of pitch oscillations, something that will not occur when the airplane has an autopilot because the latter stabilizes the angle of pitch. The negative action on the part of the autopilot is balanced by its positive action at somewhat higher frequencies, frequencies at which the airplane without an autopilot will be subjected to a considerable vertical acceleration because of its inherent oscillatory properties. The accelerations on the airplane with the autopilot prove to be lower at these frequencies (see Figure 3.13).

Finally, the spectral density curves in Figure 3.13a are the basis for the assertion that the acceleration increase will decrease with increase in the turbulence scale, L. However, it is difficult to arrive at a quantitative assessment of the dispersion in the angle of pitch increase from these curves.

All the conclusions stemming from Figure 3.13 for Airplane No. 1 are valid for Airplane No. 2, even though the two are of different types. Airplane No. 1, as we have already pointed out, is a heavy transport plane, whereas Airplane No. 2 is a light, single-seater, fighter plane.

Figure 3.14 presents the spectral densities of the increases in the vertical acceleration and in the angle of pitch for Airplane No. 2, the result of the vertical wind component. The number 1 is for spectral densities of the airplane with fixed controls, the number 2 for the aircraft with an autopilot. The spectral densities in Figure 3.14 are equated to a turbulence scale L = 300 meters.

Although Airplane No. 2 is lighter than Airplane No. 1 by a factor greater than 10, there are no principal differences in the curves for acceleration spectral densities and angles of pitch. Airplane No. 2 does have a wider angle of pitch oscillation spectrum, but this is because of very great

static stability, associated with the high speed at which Airplane No. 2 flies. It should be pointed out that spectrum width, regardless of the parameter, will be proportional to flight speed, all other conditions being equal. /93

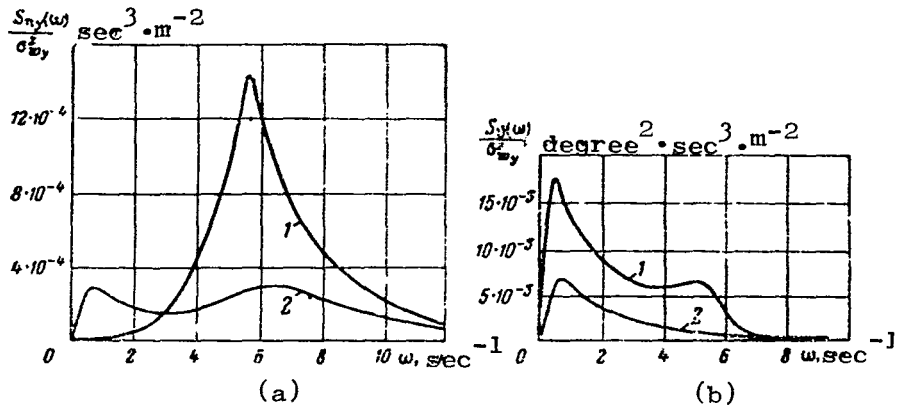

Figure 3.14. Normalized spectral densities of the increases in vertical acceleration (a) and angle of pitch (b) for Airplane No. 2. 1 - with fixed controls; 2 - with autopilot.

Let us consider the root-mean-squares of the oscillations in the parameters of longitudinal motion for the airplane and their relationships in terms of scale L, as seen in Figures 3.13 and 3.14. Graphics included in what follows will reflect this relationship more accurately.

The root-mean-squares of the parameters of the longitudinal motion can be determined in terms of the dispersions in these parameters, and the dispersions in turn, can be obtained by modeling, using the block diagram shown in Figure 2.10.

Figure 3.15 shows the root-mean-squares of the increases in vertical acceleration, angle of pitch, and additional acceleration resulting from angular oscillations, for Airplane No. 1 equated to the root-mean-square of the vertical wind component. These root-mean-squares are represented as a function of the turbulence scale, L. The curves numbered 1 are for the airplane with fixed controls, those numbered 2 for the airplane with autopilot and Equation (2.14) control law, and those numbered 3 for the airplane with autopilot and Equation (2.13) control law (with altitude corrector).

The graphics in Figure 3.15 show that the greatest acceleration attributable to turbulent air is experienced by the airplane without the autopilot (curve 1), and that this is so over the entire range of change in scale L. The airplane with the autopilot with altitude corrector (curve 3) experiences a somewhat lighter acceleration, while the airplane with autopilot without altitude corrector (curve 2) experiences the lightest acceleration. /94

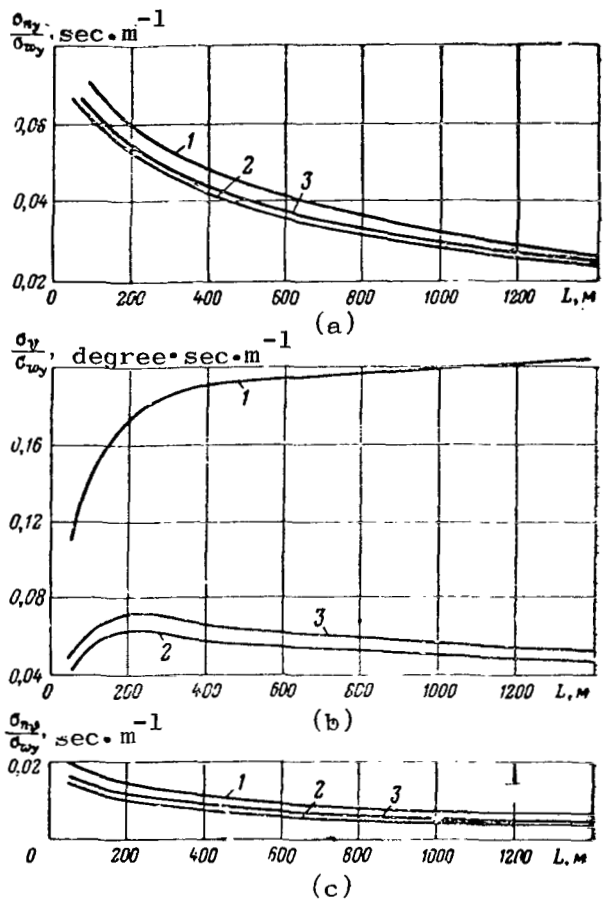

Figure 3.15. Normalized root-mean-squares of increases in vertical acceleration (a), angle of pitch (b), and acceleration the result of angular oscillations (c), as a function of the turbulence scale for Airplane No. 1. 1 - with fixed controls; 2 - with autopilot without altitude corrector; 3 - with autopilot with altitude corrector.

The data in Figure 3.15b are the basis for the assertion that the autopilot reduces oscillations in the pitching of Airplane No. 1 by a factor of from 3 to 4. These oscillations have virtually no dependence on the turbulence scale, except for very small L values. This last is valid as well for the root-mean-squares of accelerations (Figure 3.15c) attributable to the airplane's angular oscillations. Accelerations attributable to angular motions were determined for a point in the tail section of the fuselage 15 meters from the center of gravity, but even with a length such as this, the accelerations were comparatively light. These accelerations will decrease in proportion to the shortening of the length /95

The root-mean-squares of the increases in the vertical acceleration and of the angle of pitch as a function of the turbulence scale, L, for Airplane No. 2 are shown in Figure 3.16. The curves numbered 1 are for an airplane with fixed controls, those numbered 2 for an airplane with an autopilot with-

out altitude corrector. A comparison of these curves with those for Airplane No. 1 (see Figure 3.15) leads to the following conclusions. Despite the much greater static stability of Airplane No. 2, as compared with that of Airplane No. 1, the effect of the autopilot on the reduction in the root-mean-squares of the accelerations on it turns out to be greater than is the case for Airplane No. 1. This will be explained in what follows. A comparison of the absolute values of the accelerations for the different airplanes would be futile because such basic factors as speed, altitude, and unit wing loading, all of which enter into a determination of vertical wind acceleration, are different for the different airplanes.

The greater static stability of Airplane No. 2 results from the fact that pitching oscillations are reduced to a lesser degree when the autopilot is used than is the case for Airplane No. 1.

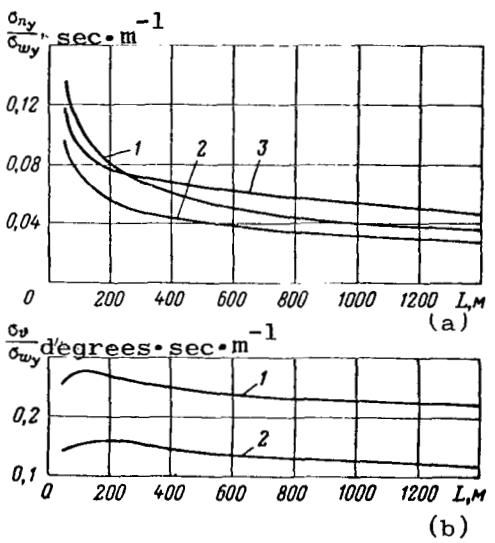

Figure 3.16. Normalized root-mean-squares of vertical acceleration (a) and angle of pitch (b) as a function of turbulence scale L for Airplane No. 2. 1 - with fixed controls; 2 - with autopilot; 3 - with autopilot ideally stabilizing angle of pitch ($i_\vartheta = \infty$).

In concluding this section, let us consider the causes of the reduction in the acceleration on the airplane in turbulent air when an autopilot is used. It is apparent that the autopilot, since it stabilizes the specified angle of pitch for the airplane, hampers angular motion by the airplane, serving to reduce the angle of attack and the acceleration attributable to vertical gusts. This assumption occasionally leads to the conclusion that the autopilot, since it stabilizes the angle of pitch, reduces safety in rough air, and should, therefore, be disengaged under these conditions. In point of fact, the behavior of the airplane when a vertical gust acts on it cannot be reduced simply to angular motion. /96 Moreover, the nature of this angular motion should be taken into consideration. The

increase in the acceleration when an airplane encounters a vertical air flow results in the appearance of the vertical velocity of the center of gravity ("swelling"), which too reduces the increase in the angle of attack attributable to the wind. We have illustrated these assertions by including oscillograms taken for the short-period motion of Airplane No. 1 upon encountering a step wind, W_y = 1 m/sec. Figure 3.17 shows the transients for an airplane with fixed controls and with an autopilot. Included in this figure are the processes of change in increase, angle of attack, acceleration, angle of pitch, and vertical velocity of the center of gravity. The scale for the vertical velocity deliberately was selected such that its ordinates would correspond to the increase in the angle of attack attributable to this velocity. Consequently, all the curves in Figure 3.17 are shown at the same angular scale.

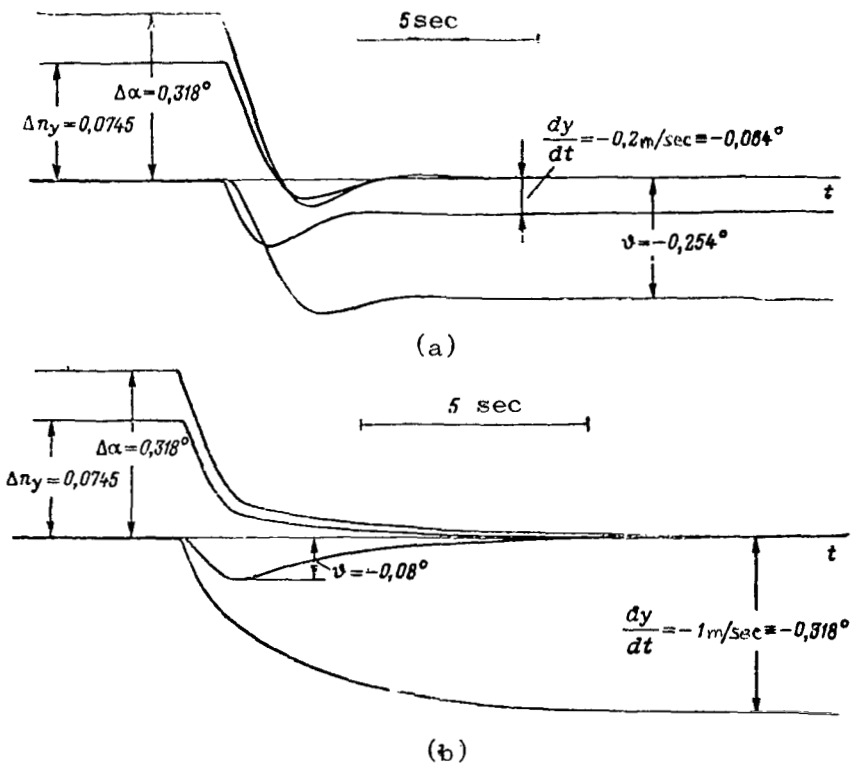

Figure 3.17. Transients of the short-period motion of Airplane No. 1 acted on by a vertical step wind. a - with fixed controls; b - with autopilot.

Analysis of the curves in Figure 3.17a reveals that in the time interval /97 over which the acceleration drops to zero for the first time (about 1 second) the ordinates of the vertical velocity are larger than those of the angle of

pitch and, as a result, the larger the role of the component of the short-period motion of the airplane in eliminating the increase in the angle of attack. When the transient if over, 20% of the original disturbance of the angle of attack continues to balance the vertical velocity, and 80% the change in the angle of pitch.

As we see from the graphics in Figure 3.9, in the case of the airplane with autopilot without altitude corrector, consideration of the change in flight speed [the use of complete Equation (2.10)] does little to change the transients.

The effect of the pitch autopilot on the short-period motion of the airplane is shown in Figure 3.17b. All curves have the same angular scale. The autopilot reduces the oscillations in the airplane's angle of pitch significantly, but there is a corresponding increase in the airplane's vertical speed. When the condition is steady-state $\Delta \vartheta = 0$ and $dy_g/dt = W_y$. The only explanation for the increase in the vertical speed of the airplane with autopilot, as compared with one without autopilot, is the increase in the time the acceleration is acting. Actually, the acceleration shown in Figure 3.17b drops more slowly than the one shown in Figure 3.17a. When its root-mean-square is computed for $W_y = 1$ m/sec for the airplane without autopilot, it is equal to $\sigma_{ny} = 0.0289$, and $\sigma_{ny} = 0.0332$ for the airplane with the autopilot. Thus, the autopilot causes a 15% increase in the root-mean-square of the acceleration when a step gust acts on the airplane. However, these results are not adequate for drawing final conclusions because in the real atmosphere there are no step gusts.

All of the above-cited experimental data on root-mean-squares of acceleration for turbulent air, regardless of turbulence scales, indicate the opposite, that is, that there is a reduction in the acceleration when the autopilot is cut in. The reason is that the process involved in eliminating the acceleration on the airplane without autopilot usually is oscillatory, so that as the airplane oscillates the amplitudes of change in angle of attack and acceleration on the airplane without autopilot in turbulent air become greater (within a definite range of frequencies) than they do in the case of the airplane with autopilot. This can be confirmed by the curves for the acceleration spectral densities for the two airplanes shown in Figures 3.13a and 3.14a. The oscillo-

grams in Figure 3.18 can also be used to arrive at a determination of the negative effect of the oscillatory nature of the reaction of the airplane to a step gust. These show the reactions of Airplane No. 2 to a single gust, W_y = 1 m/sec. As in the preceding figures, all curves are plotted on one angular scale. Figure 3.18a shows the transients for the airplane with fixed controls, Figure 3.18b those for the airplane with autopilot. Since Airplane No. 2 has greater static stability, change in its angle of pitch plays a decisive role in opposing the wind acceleration. Vertical speed is low, and is of little importance in this process, although in both figures this speed has larger ordinates at the very beginning of the process than does the angle of pitch. Even when there is an autopilot, the effect of the static stability moment usually is so great that the role of pitch oscillations is much more important than the role of the vertical speed (Figure 3.18b). However, because of the oscillatory nature of the reaction of Airplane No. 2 with fixed controls to a step gust when flying in turbulent air, the reduction in the acceleration as a result of using the autopilot turns out to be even greater than in the case of Airplane No. 1 with less static stability, but with less oscillation in a step gust. /98

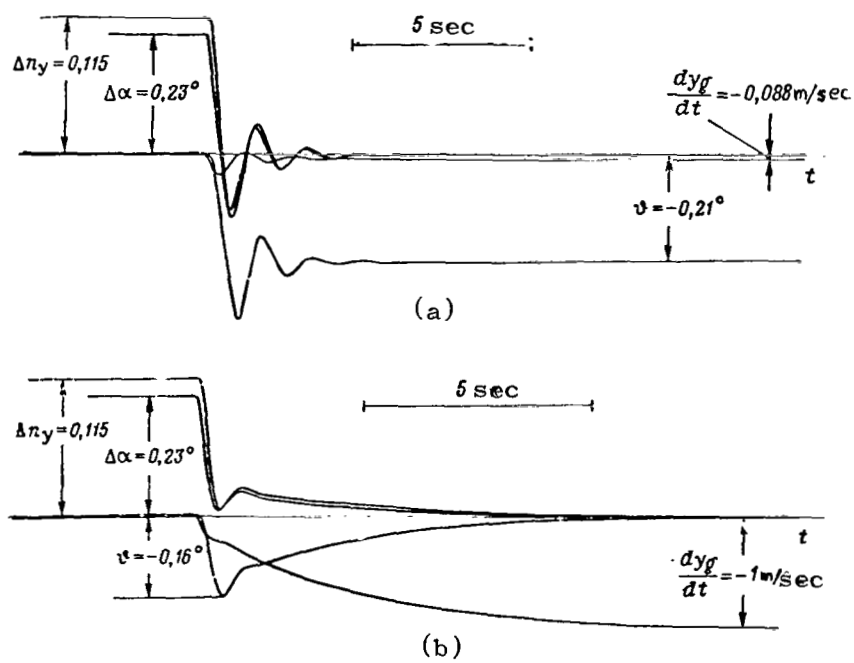

Figure 3.18. Transients as the result of the action of a vertical step gust of the short-period motion of Airplane No. 2. a - with fixed controls; b - with autopilot.

It is easy to show that an increase in the static stability is useful only for the airplane with the autopilot, and that nothing positive will result in the case of the airplane without autopilot. Figure 3.19 presents the graphics of the root-mean-squares of the acceleration on Airplane No. 1 as a function of the static stability moment coefficient, $c_y^{\bullet}$. The value of this coefficient was varied from zero (neutral airplane) to approximately 15 times the nominal value ($c_y^{\bullet} = 0.675$). Computations were made for a turbulence scale L = 300 meters. Curve 2 is for the airplane with autopilot, and shows the comparatively small change in acceleration for a considerable increase in $c_y^{\bullet}$. The acceleration does not decrease, but instead increases slightly in the case of the airplane with fixed controls (curve 1) when there is an increase in the static stability coefficient. This result can be explained by the increase in the oscillating nature of the angular motions with increase in the airplane's static stability.

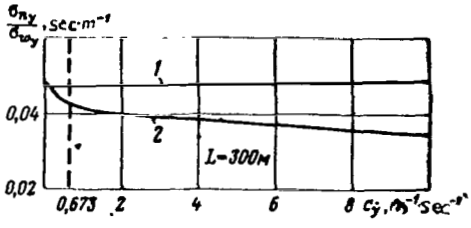

Figure 3.19. Normalized root-mean-squares of acceleration attributable to vertical gusts for Airplane No. 1 as a function of the static stability moment coefficient. 1 - with fixed controls; 2 - with autopilot.

Finally, let us see what will be the effect of rigid pitch stabilization by the autopilot. Slight changes in the i_{ϑ} ratio will cause no significant changes in acceleration, but significant change in i_{ϑ} will cause acceleration to approach those for the airplane without autopilot. As we have already pointed out, conventional autopilots provide good pitch stabilization in turbulent air, so even a significant increase in the i_{ϑ} gain should not cause very great changes to take place in acceleration. By way of an example, suppose we consider the limiting (practically an unattainable one) case when $i_{\vartheta} = \infty$ for Airplane No. 2, with pitch oscillations completely eliminated. Figure 3.16a (curve 3) shows the root-mean-squares of the acceleration as a function of the turbulence scale, L, for this case. Comparing curve 3 with curve 2 (the airplane with the autopilot has a nominal value i_{ϑ}) we see that the accelerations increase in the case of infinitely large i_{ϑ}. However, in the region of small turbulence scales the accelerations when $i_{\vartheta} = \infty$ are less than they are in the case of the airplane without autopilot (curve 1), and this can be ex-

plained only by the negative effect of the angle of pitch when there is no autopilot. Curve 3 rises above the other curves in the large L region. In this region the disturbance spectra are narrower, their frequency is lower, and accelerations on the airplane without autopilot are reduced substantially, despite the negative effect of the pitch oscillations, because of static stability.

3.3. Effect of the Characteristics of a Real Autopilot on Flight Dynamics in Turbulent Air.

The considerations of the autopilot equations in Section 2.2 stipulated /100
that the control laws adopted for the analysis describe ideal autopilots. The "idealness" of these autopilots involves the fact that when the dynamics of the airplane-autopilot system are analyzed the delay in the autopilot, and the nonlinearity of its characteristics are not taken into consideration. Modern autopilots are well engineered and their delay and various nonlinearities usually have no significant effect on the dynamic properties of the airplane-autopilot system when the condition is one of stabilization of angular coordinates.

This section will evaluate the effect of these features of real autopilots on flight dynamics in turbulent air in order to provide a basis for using the ideal autopilot equations for real autopilots.

Let us consider the effect of the following characteristics of real autopilots:

(1) delay time;

(2) non-response zone;

(3) limitations on control motion angle.

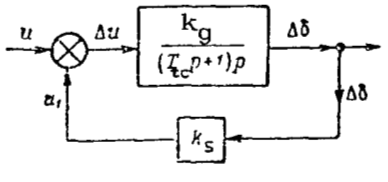

Figure 3.20. Structural diagram of an actuator with direct feedback.

We will make our analysis using autopilots with direct feedback since since this is the type now most widely used.

The primary source of delay in the autopilot is its actuator (the control

drive). The structural diagram of the actuator in a direct feedback autopilot is shown in Figure 3.20.

The following designations are used in this figure:

u is the signal supplied to the actuator from the sensing element, or from the autopilot's computer;

$\Delta\delta$ is the control motion angle;

u_1 is the feedback signal, supplied by this circuit with coefficient k_s;

k_g is the gain for the actuator, equal to the ratio of the angular velocity of the control to the voltage, Δu, across the input;

T_{tc} is the actuator time constant.

The structural diagram of the actuator shown in Figure 3.20 is valid for electrical, hydraulic, and pneumatic control surface actuators. This diagram /101 is the basis for a differential equation describing the dynamics of the actuator for the autopilot

$$\frac{T_{tc}}{k_g k_s}\frac{d^2\Delta\delta}{dt^2}+\frac{1}{k_g k_s}\frac{d\Delta\delta}{dt}+\Delta\delta=\frac{1}{k_s}u. \tag{3.35}$$

Autopilot actuators are so designed that the time constant, T_{tc}, is as low as possible (practically in the hundredths of a second). This constant is divided by the product of the coefficients $k_g k_s$, which is usually between 3 to 10 sec^{-1}. For these reasons the second derivative is very small, and this term can be ignored. Equation (3.35) yields the equation for the inertia link as

$$T_a\frac{d\Delta\delta}{dt}+\Delta\delta=i_a u, \tag{3.36}$$

where

$T_a = 1/k_g k_s$ is the actuator time constant;

k_s is the actuator gain.

The time constant, T_a, for modern autopilots is 0.1 to 0.3 second, and this is what establishes the delay in the autopilot for the most part. The time required to damp the short-period motion of modern airplanes with autopilots is from 3 to 10 seconds (see Figure 3.17b and Figure 3.18b, for example). So it can be asserted that autopilot delay should have no appreciable effect of the dynamics of the airplane-autopilot system. Figure 3.21 is included

to verify this assertion for turbulent air flight conditions. Here we have the root-mean-squares of the acceleration (curve 1) and angle of pitch (curve 2) for Airplane No. 1 as functions of autopilot delay, T_a. The turbulence scale, L, is 500 meters. The graphics in this figure show that with increase in the autopilot time constant, that is, in its delay, the pitch oscillations increase, and the acceleration decreases significantly. At the same time, the time constant has changed from 0 to T_a = 1 second, and this is not found in real autopilots.

Reduction in acceleration with increase in autopilot delay can be explained by the fact that angle of pitch stabilization deteriorates somewhat, whereas the positive role of the static stability moment increases somewhat. However, use of this effect as a means for artificially increasing the delay in the autopilot when flight is in turbulent air is undesirable because the reduction in acceleration can turn out to be negligible.

What has been said is the basis for the assertion that delay time in real autopilots has no significant effect on the more significant parameters of airplane motion in turbulent air, on vertical acceleration. /102

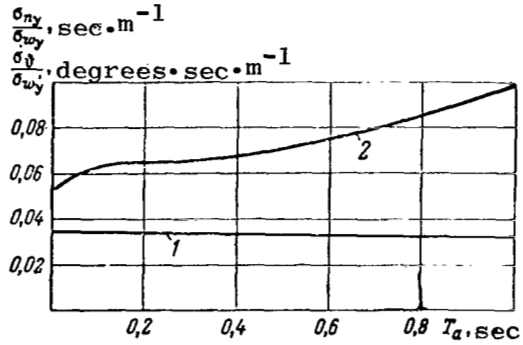

Figure 3.21. Normalized root-mean-squares of acceleration and angle of pitch for Airplane No. 1 as functions of the time constant for the autopilot actuator.
1 - acceleration; 2 - angle of pitch.

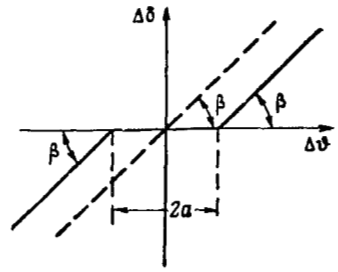

Figure 3.22. Characteristic curve for an autopilot with a non-response zone.

Let us now proceed to an analysis of the effect of a non-response zone on the characteristic of an autopilot during turbulent air flight. Figure 3.22 shows the curve for the autopilot with a non-response zone, in which

2a is the width of the non-response zone;

β is the slope of the linear section of the characteristic curve (the tangent of this angle is equal to the autopilot reduction factor).

The dotted line passing through the coordinate origin is the ideal autopilot characteristic curve (one without a non-response zone).

The angle of pitch oscillates at random in gusts, and the control motion angle too will be a random function. The connection between these magnitudes can be determined by the nonlinear characteristic curve shown in Figure 3.22.

The connection between the probable characteristic curves for the disturbed action and some output parameter in general form cannot be expressed in analytical form when systems are nonlinear. This connection can be found in approximate form, however, if the method of statistical linearization of nonlinearities is used. The fundamental concept of this method is the approximation of the nonlinear characteristic of the linearized relationship between the random functions statistically equivalent to this characteristic.

The problem of statistical linearization was solved in [36] for inertialess nonlinear elements with the most diverse of characteristic curves. On the basis of [36], the nonlinear characteristic curve in Figure 3.22 for a random stationary nature of the change in the argument (in this case in the angle of pitch) /103 can be linearized in the following manner

$$\Delta\delta = k_\vartheta i_\vartheta \Delta\vartheta, \tag{3.37}$$

where

$i_\vartheta = \tan\beta$ is the gain for a linear autopilot

k_ϑ is the coefficient that depends on the ratio of the root-mean square of the angle of pitch σ_ϑ to half the width of the non-response zone a. Its value can be determined through the formula [36]

$$k_\vartheta = 1 - 2\Phi\left(\frac{a}{\sigma_\vartheta}\right), \tag{3.38}$$

where

$\Phi\left(\frac{a}{\sigma_\vartheta}\right)$ is a probability integral with a zero lower limit, determined from Table D.1 (see Appendix D).

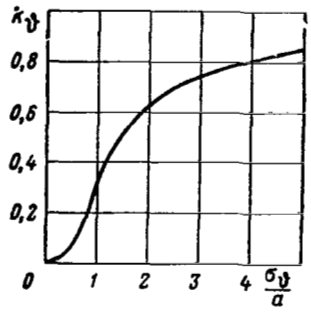

Figure 3.23. The statistical linearization coefficient.

The ratio of k_ϑ to σ_ϑ/a is shown in Figure 3.23. This graphic shows that the non-response zone on the autopilot characteristic curve is smoothed out as a result of the linearizing influence of the oscillations in the angle of pitch. There is an autopilot gain for every root-mean-square of the angle of pitch, determined through Equation (3.38).

The non-response zone substantially reduces the autopilot gain when the root-mean-squares are small, and this must be taken into consideration in the computations. In what is, in practice, the most important case of intensive turbulence, that is, when the root-mean-square of the angle of pitch is considerably in excess of half the non-response zone, the coefficient k_ϑ is close to unity, and the autopilot's non-response zone cannot be taken into consideration.

There is only a slight difference among modern autopilots so far as the absolute value of the non-response zone in angular coordinates is concerned. Autopilots in use today have values for the non-response zone in the limits 0.2 to 0.5° for all three channels (pitch, roll, yaw).

The above-cited methodology for computing the autopilot's non-response zone in terms of angular coordinates can be used as well to evaluate the effect of the non-response zone on the autopilot's characteristics in terms of linear coordinates and in terms of angular velocities.

It must be noted that the gain for a linearized autopilot with a non-response zone will depend on the value of an unknown input signal, acting on a nonlinear element of a system parameter, such as the root-mean-square of the angle of pitch for example, which, in turn, depends on the gain. This is why the successive approximations method should be used to solve the problem of airplane motion when the non-response zone is taken into consideration. But because the method is cumbersome, its use is practical only when computers are used. /104

Let us consider the effect of limitation of control motion angle on the operation of the autopilot in turbulent air flight. Control motion when

flying on the autopilot is very greatly limited as compared with the motion that can be developed by the pilot using the control column or the rudder bar. In the case of Airplane No. 1, for example, the pilot can tilt the elevator up 25° and down 15°. The full range over which the elevator can be shifted by the autopilot is 6°, that is, ±3°. Limitation in control motion by the autopilot is dictated by the need to provide for safety in flight should the autopilot fail.

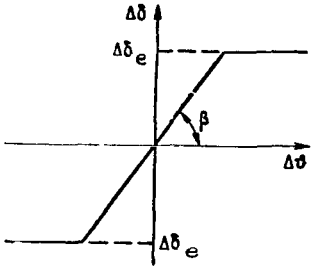

Figure 3.24. Characteristic curve for an autopilot with angle of motion limitation.

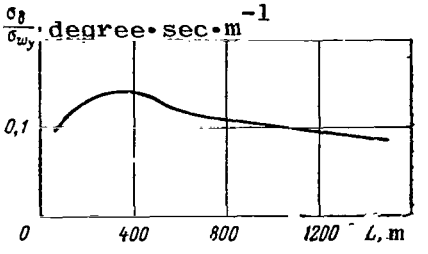

Figure 3.25. Normalized root-mean-squares of elevator motion angle for Airplane No. 1 as a function of the turbulence scale.

Figure 3.24 is the characteristic curve for an autopilot with the limitation pointed out considered (there is no non-response zone). In order to evaluate the effect of this limitation on flight dynamics in turbulent air, let us determine just how much the controls are tilted at various wind velocities. Figure 3.25 shows the root-mean-square of the elevator motion angle for Airplane No. 1 as a function of the turbulence scale, L. The largest root-mean-square of wind velocity in Figure 3.25 equals 0.135. The probability of encountering a region with σ_w = 5 m/sec is negligible small, even under thunderstorm conditions. At σ_w = 5 m/sec, the root-mean-square of the control motion angle is 0.675°. Based on the "three-sigma rule," it can be asserted (see Appendix D, p. 264) that the maximum control motion angle for Airplane No. 1 /105 will not exceed $\Delta\delta_m$ = 2.025°, and that the probability will be 0.997. Thus, the elevator of Airplane No. 1 will not go into the limits under turbulent air flying conditions, even when σ_w = 5 m/sec, so there is no need to take the elevator motion angle limitation into consideration in the analysis of the dynamics of the airplane-autopilot system under these conditions.

Although this conclusion has been arrived at from data for a specific airplane, it is quite a general one in nature, because the limitation imposed on

the movement of the control surfaces when the autopilot is in use is selected for all airplanes on the basis of the same safety criterion. Moreover, if the characteristics of the airplane and autopilot are known, this conclusion can be verified by the above-cited methodology. The results obtained make it possible to disregard the limitations imposed on elevator movement in the analysis of airplane dynamics in turbulent air if the autopilot control law is in conventional form.

The angles by which the controls are moved will be much greater when the pilot is flying the airplane under similar conditions. The pilot is unable to move the controls in time to stabilize the airplane under rough air conditions, with the result that the deviations in angular coordinates add up rapidly, and the controls must be moved over a larger angle in order to overcome their sum.

3.4. The Effect of the Nonstationary Nature of Flow on the Dynamics of Flight in Turbulent Air.

Section 2.2 provided equations for the longitudinal motion of an airplane in turbulent air. The coefficients of the rotary derivatives for aerodynamic forces and moments acting on an airplane have been taken as constant magnitudes not dependent on the nature of the flow over the airplane and is based on the stationary nature hypothesis. This assumption is not strictly valid because there is a nonsteady state condition of the flow over the airplane during the disturbed motion process, and the stationary nature hypothesis is not valid for it in the general case. Nevertheless, in a great many flight dynamic problems of practical interest, the results of the computation made for the disturbed motion of an airplane, obtained by using this hypothesis as a basis, are in good concordance with the results of in-flight experiments. This concordance can be explained by the fact that the disturbed motion of the airplane usually is a comparatively slow occurrence, and the effect of the nonstationary nature of the flow over the airplane proves to be slight.

The situation is fundamentally different when the airplane is flying through turbulent air, that is when there are random gusts, the spectra of which contain rather high frequencies. It is these latter that create the forces and moments that establish the disturbed motion of the airplane. Consequently, in the problem under consideration, the effect of the nonstationary

nature of the air flow should be analyzed specifically.

The solution of the problem of determining the forces and moments in the case of a nonstationary flow over a lifting surface has now been elucidated in a great many Soviet papers (see [51, 52], for example), as well as in the foreign technical literature. The general statement of this problem is extremely complex, and digital computers are used to arrive at a solution. This book will use the less precise methodology suggested in [13] in order to obtain simpler analytical expressions that can be used for modeling, and for taking into account the effect of the nonstationary nature of the flow over the airplane at subsonic flight speed. /106

We need but consider this process during a step or sinusoidal change in the angle of attack in order to take into account the nonstationary nature of the flow over the wing during the formation of lift. Since this book makes use of the apparatus of spectral functions, let us consider an expression for the complex amplitude of nonstationary lift for a wing of infinite span when there is a sinusoidal change in the angle of attack (in a stream of incompressible air)

$$\Delta Y(j\omega) = C_y^{\alpha} q S \Phi(jk) \Delta\alpha(j\omega), \tag{3.39}$$

where

$\Phi(jk)$ is a Sears function, equal to the relative value of the complex amplitude of the wing lift during a sinusoidal change in the angle of attack with frequency ω and unit amplitude;

$k = \omega b_a / 2V_e$ is the argument of the Sears function;

q is the velocity head.

If half the mean aerodynamic chord, $b_a/2$, is taken as the characteristic linear dimension, the argument k will be equal to the Strouhal number.

The Sears function is a quite complex analytical expression containing Bessel functions. Only the square of the modulus of the Sears function is required in what follows, however, and for this [37] provides the following approximately expression

$$|\Phi(jk)|^2 \cong \frac{1}{1+2\pi k} = \frac{1}{1+\omega\pi b_a/V_e}. \tag{3.40}$$

Figure 3.26 is a graphic showing the precise value of the square of the

modulus of the Sears function, and values determined through Equation (3.40). A comparison of the curves shows that Equation (3.40) provides quite a good approximation.

As has been pointed out, the Sears function takes into consideration the nonstationary nature of the flow over a wing of infinite span in incompressible air. Finite wing span dimensions will introduce errors that will be larger the shorter the wing.

Compressibility of the air begins to have a significant effect on the magnitude of the wing lift with transition to supersonic flight speeds, so the Sears function cannot be used for these speeds. However, it must be emphasized that the effect of the nonstationary nature of the airflow diminishes /107 quite rapidly with such transition. Let us use k_n to designate a coefficient equal to the ratio of the wing lift with the nonstationary nature of the flow over it taken into consideration to the lift without such consideration.

Figure 3.27 shows this coefficient in terms of the M number at which the airplane is flying, and the graphic is valid for an airplane with fixed μ_d (density ratio) and mean aerodynamic chord to turbulence scale ($s = b_a/L$) ratio. The magnitude of k_n is kept constant in the subsonic speed range and is fixed by the effect of the Sears function. There is a sharp increase in k_n to a value close to unity with change in M from 0.9 to 1.6, and in the limit for unbounded increase in M the coefficient k_n tends to unity.

Let us now proceed to our analysis of the longitudinal motion of airplane with the nonstationary nature of the airflow taken into consideration. Now Equation (2.11) should be written in the form (only the vertical wind component is taken into consideration)

$$\left.\begin{aligned} V_e \frac{d\Delta\vartheta}{dt} + \frac{dV_{gy}}{dt} + b_{\dot{y}} V_{gy} &= b'_{\dot{y}} w_y, \\ \frac{d^2\Delta\vartheta}{dt^2} + c_{\dot{\vartheta}} \frac{d\Delta\vartheta}{dt} - c_{\ddot{y}} \frac{dV_{gy}}{dt} - c_{\dot{y}} V_{gy} &= -c_{\delta}\Delta\delta_e - c'_{\dot{y}} w_y. \end{aligned}\right\} \qquad (3.41)$$

The dashed lines are for the coefficients of the forces and moments created by the gusts. We will consider the nonstationary nature of the airflow only for these terms in Equation (3.41). We will consider the coefficients of all the terms in the left sides of Equation (3.41) to be constants because the disturbed motion of the airplane has no harmonics high enough to warrant con-

sideration of the nonstationary nature of the airflow attributable to these motions. The coefficient b'_y characterizes the lift created by the angle of attack attributable to the vertical gusts. On the basis of Equation (3.39), therefore, we obtain

$$b'_{\dot{y}}(j\omega)=b_{\dot{y}}\Phi(jk). \tag{3.42}$$

Airplane moment in terms of the lateral axis can be established as the difference in the moments of the wing and tail lifts. This is why we will assume that the nonstationary nature of the airflow in the determination of the moment coefficient can also be given consideration by using the Sears function, as was done in Equation (3.42) for the lift coefficient

$$c'_{\dot{y}}(j\omega)=c_{\dot{y}}\Phi(jk). \tag{3.43}$$

When we take Equation (3.42) and Equation (3.43) into consideration, Equation (3.41) provides us with the complex transfer functions for the angle of pitch and the acceleration of the airplane without autopilot with the nonstationary nature of the airflow taken into consideration

$$W_{\vartheta/w_y}(j\omega)=-\frac{F'(j\omega)}{A'(j\omega)}\Phi(jk)= \qquad \text{/108}$$

$$=-\frac{c_{\dot{y}}-\frac{b_{\dot{y}}c_{\ddot{y}}}{b_{\dot{y}}}}{-\omega^2+j\omega(b_{\dot{y}}+c_{\dot{\vartheta}}+c_{\ddot{y}}V_e)+b_{\dot{y}}c_{\dot{\vartheta}}+c_{\dot{y}}V_e}\Phi(jk), \tag{3.44}$$

$$W_{n_y/w_y}(j\omega)=\frac{1}{g}\frac{F'(j\omega)}{A'(j\omega)}\Phi(jk)=$$

$$=\frac{1}{g}\frac{b_{\dot{y}}\left[-\omega^2+j\omega(c_{\dot{\vartheta}}+c_{\ddot{y}}V_e)\right]}{A'(j\omega)}\Phi(jk). \tag{3.45}$$

The transfer functions of Equations (3.44) and (3.45) differ from those of Equations (3.17) and (3.20), which did not take into consideration the nonstationary nature of the airflow, but instead only considered the $\Phi(jk)$ factors. Analogous transfer functions for the airplane with autopilot, Equation (2.14), are in the form

$$W_{\vartheta/w_y}(j\omega)=-\frac{j\omega F'(j\omega)}{A''(j\omega)}\Phi(jk), \tag{3.46}$$

where

$$A''(j\omega)=-j\omega^3-\omega^2(b_{\dot{y}}+c_{\dot{\vartheta}}+c_{\dot{\delta}}i_{\dot{\vartheta}}+c_{\ddot{y}}V_e)+$$
$$+j\omega(b_{\dot{y}}c_{\dot{\vartheta}}+b_{\dot{y}}c_{\dot{\delta}}i_{\dot{\vartheta}}+c_{\dot{\delta}}i_{\vartheta}+c_{\dot{y}}V_e)+b_{\dot{y}}c_{\dot{\delta}}i_{\vartheta}; \tag{3.47}$$

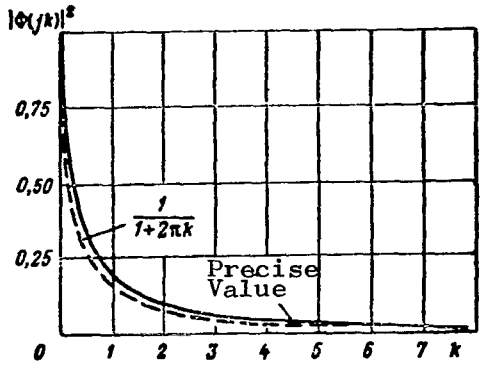

Figure 3.26. Graphics of the precise and approximate values of the Sears function.

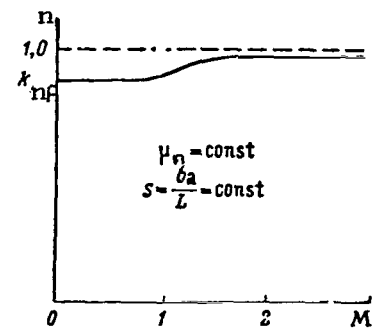

Figure 3.27. Ratio of wing lift with nonstationary nature of the flow over the wing taken into consideration to lift without such consideration in terms of the M number.

$$W_{n_y/w_y}(j\omega) = \frac{1}{g}\frac{I''(j\omega)}{A''(j\omega)}\Phi(jk), \qquad (3.48)$$

where

$$I''(j\omega) = b_y'[-j\omega^3 - \omega^2(c_{\dot\vartheta} + c_y'V_e + c_\delta i_\vartheta) + j\omega c_\delta i_\vartheta].$$

/109

The square of the modulus of the complex transfer function is needed in the computation of the change that takes place in the parameters of the longitudinal motion of the airplane due to random wind when using Equation (2.46). Therefore, the square of the modulus of the Sears function, determined by the approximate expression that is Equation (3.40), enters into all computations that take the nonstationary nature of the flow over the airplane into consideration.

The root-mean-squares of the increases in vertical acceleration and angle of pitch were determined for Airplane No. 1 with autopilot through the Equations (3.46) and (3.48) transfer functions. Figure 3.28 (curve 1) shows the results of the computation of the acceleration in the form of graphics as a function of the turbulence scale. The root-mean-squares of the acceleration, without the nonstationary nature of the flow over the airplane taken into consideration (curve 2), are plotted in this same figure. A comparison of the two curves shows that consideration of the nonstationary nature of the flow over the airplane reduces the value of the vertical acceleration by a magnitude of from 5 to 20%, depending on the turbulence. The higher figure is for the lowest

scale value and, consequently, for the broadest wind spectrum. This result is completely compatible because the Sears function diminishes rapidly with increase in frequency. Data on airplane acceleration when there is no autopilot are not included because they add nothing new to the comparison already pointed out with respect to the airplane with autopilot.

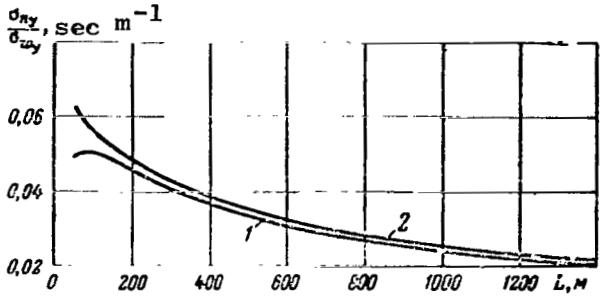

Figure 3.28. Normalized root-mean squares of the vertical acceleration of Airplane No. 1 acted on by a vertical wind. 1 - with the nonstationary nature of the flow over the airplane taken into consideration; 2 - without this phenomenon taken into consideration.

The increases in the angle of pitch with the nonstationary nature of the flow over the airplane taken into consideration are practically the same as those obtained earlier for the case when this phenomenon was not taken into consideration (Figure 3.17b). This result can be explained by the fact that, as we have already mentioned, the spectrum of angle of pitch fluctuations is very narrow, and the effect of the nonstationary nature of the flow over the airplane lies within the limits of accuracy of the modeling.

There are no complications involved in taking the nonstationary nature of the flow over the airplane into consideration when the Sears function is used, so the phenomenon will be taken into consideration in the results of the computations that follow.

3.5. Effect of Airplane Size on Dynamics of Flight in Turbulent Air.

/110

The preceding sections of this chapter considered the airplane to be a point in a velocity field of turbulent air motion because it was assumed that the velocity was the same everywhere on the surface of the airplane. It is obvious that this is an approximation in the case of big airplanes. This section will take up the methodology to use to assess the effect of airplane size on the force and moment due to flight in turbulent air.

Two factors must be given primary consideration in the analysis of the longitudinal motion of the airplane when its size is taken into consideration;

nonuniformity of the spanwise vertical component of the gust, and the non-coincidence of these components at wing and tail at the same moment in time.

Let us consider initially the change in the spectral density of the vertical wind component if the nonuniformity of the distribution of this component over the wing span is taken into consideration. The general expression for the increase in the wing lift when the angle of attack is an arbitrary function of time and of the z coordinate for the given section of the wing in terms of the span, can be obtained in the form of a Duhamel integral [39]

$$\Delta Y(t)=\int_{-\infty}^{\infty} dt_1 \int_{-l/2}^{l/2} K(t_1, z)\,\Delta\alpha[(t-t_1), z]\,dz, \tag{3.50}$$

where

K(t, z) is the pulse response function (Green's function) of the wing lift

$\Delta\alpha$ (t, z) is the increase in the angle of attack;

l is the wing span.

The pulse response function physically is a lift force due to wing element dz a distance z from the root chord when the change in the angle of attack on this element can be characterized by a δ-function. Let us first find the response function for the lift, that is, the lift due to this dz element, if the change in the angle of attack is in the nature of a unit step. Reference [38] has pointed out that the relative distribution of the lift over the span when there is a step change in the angle of attack does not, in essence, depend on the time, but coincides with the stationary form of this distribution. Only the overall magnitude of the lift will depend on time when such an assumption is made. Consequently, the response function can be represented in the form of two cofactors, one of which is a function only of time, whereas the other is a function only of the z coordinate determining the position of the dz element in the wing

$$H(t, z)=\frac{1}{l} H_Y(t)\,\varepsilon(z). \tag{3.51}$$

/111

The factor ε (z) in Equation (3.51) is the stationary distribution of the lift in the case of a unit step in the angle of attack, determined through the formula

$$\varepsilon(z)=\frac{b(z)C_{yz}}{b_a C_y}, \tag{3.52}$$

where

b (z) is the wing chord in the z section;

C_y is the lift coefficient for the airplane as a whole;

C_{yz} is the lift coefficient for the z section.

The second factor in Equation (3.51), $H_Y(t)$ characterizes the change in the overall magnitude of the lift in the case of a step change in the angle of attack, and is determined through the formula

$$H_Y(t)=C_y^{\alpha}qS\varphi\left(\frac{V_e t}{b_a/2}\right). \tag{3.53}$$

The function φ in Equation (3.53) determines the relative change in the lift in terms of time for a unit step in the angle of attack. Since there is a simple connection between the pulse response function K(t) and the response function H(t), determined through Equation 2.32), Equation (3.51) provides the final formula for the pulse response function as

$$K(t, z)=\frac{1}{l}K_Y(t)\varepsilon(z), \tag{3.54}$$

where

$$K_Y(t)=C_y^{\alpha}qS\frac{d\varphi(t)}{dt}. \tag{3.55}$$

We note that the Fourier transform of the function $d\varphi(t)/dt$ yields the Sears function $\Phi(jk)$, introduced in Section 3.4.

Let us now proceed to a determination of the increase in the lift due to the nonuniform distribution of the vertical wind component over the span. With Equation (2.6) as our basis, let us replace the increase in the angle of attack in Equation (3.50) by the vertical wind component, w_y, and introducing the linear coordinate $V_e(t - t_1)$, we obtain

$$\Delta Y_w(t)=\frac{1}{V_e}\int_{-\infty}^{\infty}dt_1\int_{-l/2}^{l/2}K(t_1, z)w_y[V_e(t-t_1), z]\,dz. \tag{3.56}$$

Since w_y is a random function, $\Delta Y_w(t)$ too will be a random function of time. The correlation function for the lift due to the wind can be determined through the formula

$$R_Y(\varepsilon)=\frac{1}{V_e^2}\int_{-\infty}^{\infty}\int_{-\infty}^{\infty}\int_{-l/2}^{l/2}\int_{-l/2}^{l/2}K(t_1, z_1)K(t_2, z_2)\times$$

$$\overline{\times w_y[V_e(t-t_1), z_1]\, w_y[V_e(t+\tau-t_2), z_2]}\, dz_1\, dz_2\, dt_1\, dt_2. \qquad (3.57)$$ /112

The correlation function of the wind velocity under the integral (under the vinculum) is a function of the space coordinate (z), as well as of time (τ). However, by using Taylor's hypothesis, Equation (1.27) is the basis for associating the x and τ arguments, and for taking it that this function is dependent only on the space coordinates x and z. In the case of isotropic (or even of axisymmetrical) turbulence, the correlation function indicated will depend solely on the absolute value of the spatial displacement, that is, on $\sqrt{\Delta x^2+\Delta z^2}$. Therefore

$$\overline{w_y[V_e(t-t_1), z_1]\, w_y[V_e(t+\tau-t_2), z_2]}=$$
$$=R_{w_y}\left(\sqrt{V_e^2(\tau+t_1-t_2)^2+(z_2-z_1)^2}\right). \qquad (3.58)$$

Equation (3.57), with Equations (3.54) and (3.58) taken into consideration, yields

$$R_Y(\tau)=\frac{1}{V_e^2}\int_{-\infty}^{\infty}\int_{-\infty}^{\infty}K_Y(t_1)K_Y(t_2)R_{we}(V_e\tau)\,dt_1\,dt_2, \qquad (3.59)$$

where

$R_{we}(V_e\tau)$ is the averaged wing span correlation function for the vertical wind component:

$$R_{we}(V_e\tau)=\frac{1}{l^2}\int_{-l/2}^{l/2}\int_{-l/2}^{l/2}R_{w_y}\left[\sqrt{V_e^2\tau^2+(z_2-z_1)^2}\right]\varepsilon(z_1)\varepsilon(z_2)\,dz_1\,dz_2 \qquad (3.60)$$

Finally, using a direct Fourier transform, we obtain, through Equation (3.60), an expression for the averaged wing span spectral density of the vertical wind component

$$S_{we}(\omega)=\frac{1}{\pi V_e}\int_{-\infty}^{\infty}e^{-j\frac{\omega}{V_e}(V_e\tau)}R_{we}(V_e\tau)\,d(V_e\tau). \qquad (3.61)$$

It is obvious that in the general case of an arbitrary form of distribution of lift over the span when there is a unit step in the angle of attack, that is, in the case of an arbitrary form for $\varepsilon(z)$, the determination of R_{we} and S_{we} can be made through Equations (3.60) and 3.61) by numerical methods only. Reference

[13] contains the results of the analytical integration of Equations (3.60) and (3.61) for the very simple case of a uniform distribution of the lift over the span. Specifically, the following formula was obtained for the averaged spectral density of the vertical wind

$$S_{we}(\omega)=\frac{\sigma_w^2 L}{k^2\pi V_e}\frac{2}{1+\nu^2}\{3\nu^2 k\sqrt{1+\nu^2}\,[K_{i0}(k\sqrt{1+\nu^2})-$$
$$-k\sqrt{1+\nu^2}\,K_0(k\sqrt{1+\nu^2})+(1-3\nu^2)\,[2-$$
$$-2k\sqrt{1+\nu^2}\,K_1(k\sqrt{1+\nu^2})-k^2(1+\nu^2)\,K_0(k\sqrt{1+\nu^2})]], \qquad (3.62)$$

/113

where

$\nu = \omega L/V_e$ is a dimensionless frequency;

l/L is the span ratio;

K_0 and K_1 are the modified Bessel functions of the second kind of first and zero orders [33];

K_{i0} is the Bessel function integral, determined through the formula

$$K_{i0}(x)=\int_0^x K_0(x_1)\,dx_1. \qquad (3.63)$$

The dispersion in the averaged wing span vertical wind component, on the basis of Equation (3.62), can be determined through the formula

$$\sigma_{we}^2=\sigma_w^2\frac{1-e^{-k}}{k}. \qquad (3.64)$$

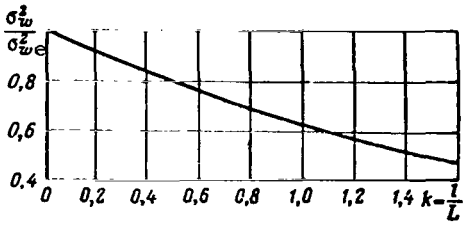

Figure 3.29. Graphic of the ratio of the dispersion in vertical wind averaged over the wing span to the dispersion of the wind at one point as a function of the wing span ratio.

Figures 3.29 and 3.30 show the graphics for the σ^2_{we}/σ^2_w ratio, and for the reduced average spectral density. These graphics can be used to determine the averaging effect of the wing span on the spectral density of a random wind. This effect is expressed primarily in a reduction in the dispersion of this component with increase in wing span (see Figure 3.29), and is readily explainable when it is recognized that as the span tends to infinity the lift due to the wind should tend to zero because an identical number of rising and descending flows will be acting along the span simultaneously.

The graphics in Figure 3.30 show that an increase in the span will result in a sharper drop in the spectral density at high frequencies, and this is in addition to the reduction in the dispersion. If the spectral density at high frequencies for any point on the airplane decreases in proportion to v^2 [see Equation (1.22)], the spectral density at these frequencies, averages over the span, will decrease more intensively.

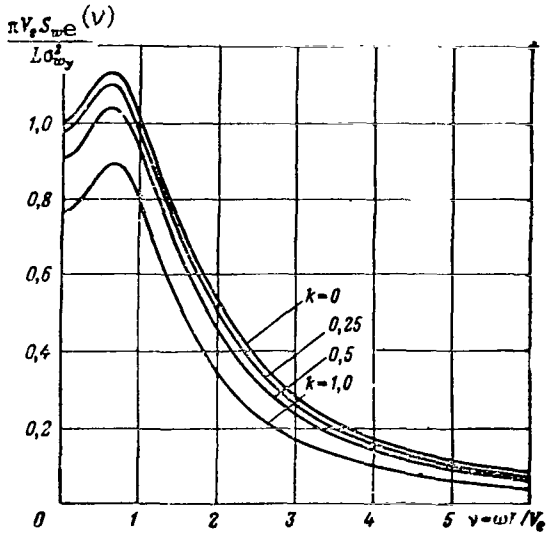

Figure 3.30. Graphic of the ratio of the reduced spectral density of the vertical wind, averaged over the wing span, to the dispersion of this wind at one point as a function of the dimensionless frequency.

Now let analyze the effect on the moment relative to the lateral axis of the delay in the tail moment, the result of the horizontal tail entering the wind later than the wing. This results in the delay setting up an additional moment /114 that cannot be taken into consideration if the airplane is considered as a point.

The moment relative to the lateral axis due solely to the vertical wind is created by wing and tail lifts due to this wind. This is the basis for using the following expression to determine the pitching moment

$$\Delta M_w(t)=\frac{1}{l}\int_{-\infty}^{\infty} K_{M_w}(t_1)\,dt_1 \int_{-l/2}^{l/2} \varepsilon(z)\,w_y[V_e(t-t_1), z]\,dz +$$

$$+\int_{-\infty}^{\infty} K_{Mt}(t_1)\,w_y[L_{ht}+V_e(t-t_1)]\,dt_1, \qquad (3.65)$$

where

$K_{Mw}(t)$ is the pulse response function of the pitching moment created by the wing and due to the wind, w_y, in the form of a δ-function;

$K_{Mt}(t)$ is the pulse response function of the pitching moment created by the tail and due to wind, in the form of a δ-function;

L_{ht} is the length of the horizontal tail.

The only difference between the pulse response function for the wing moment and the pulse response function $K_Y(t)$ for the lift of Equation (3.55) is in the geometric relationships. The following expression is valid for the pulse response function for the wing moment /115

$$K_{Mw}(t)=K_Y(t)\,x_w/V_e, \tag{3.66}$$

where

x_w is the distance between the center of pressure for the wing and the airplane's center of gravity.

Expressing the function $K_Y(t)$ in terms of the coefficient $b_y^{\bullet}$, we obtain

$$K_{Mw}(t)=b_y^{\bullet}\,mx_w\frac{d\varphi(t)}{dt}. \tag{3.67}$$

The simplest way to obtain the pulse response function for the horizontal tail moment is to remember that this moment is equal to the difference in the moment for the entire airplane and the wing moment

$$K_{Mt}(t)=K_{Mc}(t)-K_{Mw}(t). \tag{3.68}$$

Determining the moment for the entire airplane in terms of its parameters, we obtain the expression

$$K_{Mt}(t)=-(c_y^{\bullet}I_z+b_y^{\bullet}mx_w)\frac{d\varphi(t)}{dt}. \tag{3.69}$$

Equation (3.65) is the basis for obtaining an expression for the correlation function of the moment due to the wind, $\overline{M_w(t)M_w(t-\tau)}$. The application of a Fourier transform to this correlation function results in an expression for the spectral density of the moment due to the vertical wind

$$\begin{aligned}S_M(\omega)=&|W_w(j\omega)|^2S_{we}(\omega)+|W_t(j\omega)|^2S_w(\omega)+\\&+2\,\mathrm{Re}\,[e^{j\omega L_{ht}/V_e}W_t(j\omega)W_w(-j\omega)]S_w(\omega),\end{aligned} \tag{3.70}$$

in which the symbol Re designates the real part of the complex expression.

The complex transfer functions for wing and tail moments can be determined through the following relationships on the basis of Equations (3.67 and (3.69)

$$W_w(j\omega)=b_{\dot{y}}\, mx_w\Phi(jk)=W_w\Phi(j\omega), \tag{3.71}$$

$$W_t(j\omega)=-(c_{\dot{y}}\, I_z+b_{\dot{y}}\, mx_w)\,\Phi(jk)=-W_t\Phi(j\omega). \tag{3.72}$$

Substituting Equations (3.71) and (3.72) in Equation (3.70), we obtain

$$S_M(\omega)=[W_w^2S_{we}(\omega)+W_t^2S_w(\omega)+2\cos(\omega L_{ht}/V_e)\times \\ \times W_wW_tS_w(\omega)]\,|\Phi(j\omega)|^2. \tag{3.73}$$

Let us introduce the following relationship for purposes of simplification /116

$$W_w = rW_t.$$

The coefficient r is negative for the normal airplane. The limit case for the neutral airplane has r = -1. For other trims $|r|$ is usually less than 1, but greater than zero. Considering Equations (3.74) and (3.74), we obtain

$$S_M(\omega)=W_t^2[r^2S_{we}(\omega)+S_w(\omega)+ \\ +2r\cos(\omega L_{ht}/V_e)S_w(\omega)]\,|\Phi(j\omega)|^2. \tag{3.75}$$

Finally, in order to simplify the analysis of the effect of the tail moment delay relative to the wing moment, we can, without introducing significant error, ignore the effect averaging the wing span has on the wing moment. Now $S_{we}(\omega) = S_w(\omega)$, and, from Equation (3.75)

$$S_M(\omega)=W_t^2[1+r^2+2r\cos(\omega L_{ht}/V_e)]\,|\Phi(j\omega)|^2S_w(\omega). \tag{3.76}$$

It is obvious that the spectral density of the moment can be obtained from Equation (3.76) as follows if we set $L_{ht} = 0$, and if the tail moment delay relative to the wing moment is not taken into consideration

$$S'_M(\omega)=W_t^2(1+r)^2\,|\Phi(j\omega)|^2\,S_w(\omega). \tag{3.77}$$

We now find the ratio of the root-mean-squares of the moments computed using Equations (3.76) and (3.77), that is

$$\frac{\sigma_M}{\sigma'_M}=\frac{\sqrt{\int_0^\infty S_M(\omega)d\omega}}{\sqrt{\int_0^\infty S'_M(\omega)d\omega}}. \tag{3.78}$$

This ratio yields the relative error when the tail moment delay relative to the wing moment is not taken into account. After substitution of the expressions for the corresponding spectral densities in Equation (3.78), we obtain

$$\frac{\sigma_M}{\sigma'_M} = \frac{1}{1+r}\sqrt{1+r^2+2r\Psi(L_{ht}/L,\ L_{ht}/b_a)}, \tag{3.79}$$

where the function Ψ can be determined through the formula

$$\Psi\left(\frac{L_{ht}}{L},\ \frac{L_{ht}}{b_a}\right) = \frac{\int_0^\infty \cos(\omega L_{ht}/V_e)\, S_w(\omega)\,|\,\Phi(j\omega)\,|^2\, d\omega}{\int_0^\infty S_w(\omega)\,|\,\Phi(j\omega)\,|^2\, d\omega}. \tag{3.80}$$

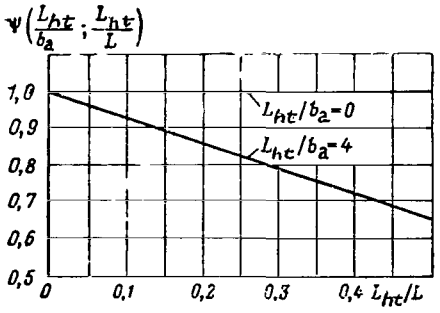

Figure 3.31. Graphic of the function Ψ, constructed using Equation (3.80).

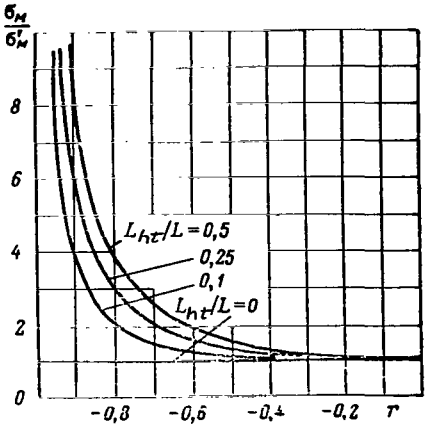

Figure 3.32. Graphic of the ratio of the root-mean-square of the moment due to the vertical wind and determined with the length of the horizontal tail taken consideration, to the root-mean-square of the moment determined without this length taken into consideration.

/117

Figure 3.31 is an example of the construction of the graphic for Ψ as a function of L_{ht}/L using Equation (3.80) for two values of L_{ht}/b_a. Figure 3.32 shows the graphics of the root-mean-squares of moments $\sigma M/\sigma'_M$ in terms of the coefficient r for various L_{ht}/L values, constructed using Equation (3.79). These graphics show that the root-mean-square of the moment due to the vertical wind component, σ_M, obtained with the tail moment delay relative to the wing moment taken into consideration, is larger than that of moment σ'_M, for which delay was not considered. This effect tends to zero when $r \to 0$. The moments

tend to infinity when $r \to -1$. This conclusion does not contradict the physics of the phenomenon we are considering because it is the result of the tending to zero of the moment σ'_M for the neutral airplane. The root-mean-square of the moment σ_M, due to the vertical wind can be computed for the neutral airplane with delay taken into consideration by using the spectral density at Equation (3.76). It will be greater than zero the greater L_{ht}/L.

So what follows from the graphics in Figures 3.31 and 3.32 is that consideration of the tail moment delay relative to the wing moment is more significant the greater the L_{ht}/L ratio, and the absolute value of the coefficients of r. This coefficient can be determined in terms of the parameters /118 for the airplane through the formula

$$r \approx -\frac{b_{\dot{y}}^{\cdot} m x_w}{C_{\dot{y}}^{\cdot} I_z + b_{\dot{y}}^{\cdot} m x_w}. \tag{3.81}$$

The above-obtained formulas for the spectral densities of a vertical wind component (the effect of averaging for the wing span considered) and moment (the effect of the horizontal tail length considered) provide the means for proceeding to an analysis of the dynamics of a big[4] rigid airplane in turbulent air. The equations of the longitudinal motion of a big airplane will differ from Equation (3.41) for a small airplane only in the forms of the right sides.

$$\left.\begin{aligned} V_e \frac{d\Delta\vartheta}{dt} + \frac{dV_{gy}}{dt} + b_{\dot{y}}^{\cdot} V_{gy} &= \Delta Y_w(t)/m, \\ \frac{d^2\Delta\vartheta}{dt^2} + c_{\dot{\vartheta}}^{\cdot} \frac{d\Delta\vartheta}{dt} - c_{\dot{y}}^{\cdot\cdot} \frac{dV_{gy}}{dt} - c_{\dot{y}}^{\cdot} V_{gy} &= -c_{\delta}^{\cdot}\Delta\delta_e + \Delta M_w(t)/I_z. \end{aligned}\right\} \tag{3.82}$$

The right sides of Equation (3.82) can be determined by Equations (3.56) and (3.65). The transfer functions for the various parameters of longitudinal motion can be obtained through Equation (3.82). We will limit ourselves to an analysis of the most important parameter, the vertical acceleration. The complex transfer function for acceleration has the form

---

4. For brevity's sake the term "big" will designate an airplane that takes these two factors (span and length) into consideration.

$$W_{n_y/w_y}(j\omega)=\left[\frac{1}{G}\cdot\frac{-\omega^2+j\omega(c_y^{\cdot}V_e+c_{\dot{\vartheta}})+c_y^{\cdot}V_e}{-\omega^2+j\omega(b_{\dot{y}}+c_{\dot{\vartheta}}+c_y^{\cdot}V_e)+b_{\dot{y}}c_{\dot{\vartheta}}+c_{\dot{y}}V_e}\right]\times$$
$$\times W_Y(j\omega)-\left[\frac{V_e}{gI_z}\cdot\frac{b_{\dot{y}}^{\cdot}}{-\omega^2+j\omega(b_{\dot{y}}+c_{\dot{\vartheta}}+c_y^{\cdot}V_e)+b_{\dot{y}}c_{\dot{\vartheta}}+c_{\dot{y}}V_e^{\cdot}}\right]\times$$
$$\times W_M(j\omega), \qquad (3.83)$$

where

$W_Y(j\omega)$ and $W_M(j\omega)$ can be determined by a Fourier transform of the functions $\Delta Y_w(t)$ and $\Delta M_w(t)$.

We must find the spectral density of the acceleration in order to determine its dispersion and root-mean-square. This spectral density can be determined through the expression

$$S_{n_y}(\omega)=(|W_1(j\omega)|^2|W_Y(j\omega)|^2+|W_2(j\omega)|^2\times$$
$$\times\{|W_w(j\omega)|^2+|W_t(j\omega)|^2+2\mathrm{Re}[e^{j\omega L_{ht}/V_e}W_t(j\omega)W_w(-j\omega)]\}+$$
$$+2\mathrm{Re}[W_1(j\omega)W_2(-j\omega)W_Y(j\omega)W_w(j\omega)+$$
$$+W_1(j\omega)W_2(-j\omega)W_Y(j\omega)W_t(-j\omega)])S_{we}(\omega), \qquad (3.84)$$

where

$W_1(j\omega)$ and $W_2(j\omega)$ are complex transfer functions in the first and second brackets of the right side of Equation (3.83); /119

$W_Y(j\omega)=b_{\dot{y}}^{\cdot}m\Phi(j\omega)/V_e$ is the transfer function for the wing lift due to the vertical wind.

After substituting values for the Equation (3.84) transfer functions and completing the operations required to separate the real parts of the complex expressions, we obtain a computing formula for the acceleration spectral density for a big airplane as

$$S_{n_y}(\omega)=\frac{b_{\dot{y}}^2}{g^2}\cdot\frac{S_{we}(\omega)|\Phi(j\omega)|^2}{\omega^4+\omega^2[(b_{\dot{y}}+c_{\dot{\vartheta}}+c_y^{\cdot}V_e)^2+b_{\dot{y}}c_{\dot{\vartheta}}+c_{\dot{y}}V_e]+(b_{\dot{y}}c_{\dot{\vartheta}}+c_{\dot{y}}V_e)^2}\times$$
$$\times\Big\{(-\omega^2+c_{\dot{y}}V_e)^2+\omega^2(c_y^{\cdot}V_e+c_{\dot{\vartheta}})^2+\frac{V_e^2}{I_z^2}[b_{\dot{y}}^2m^2x_w^2+$$
$$+(c_{\dot{y}}I_z+b_{\dot{y}}mx_w)^2-2\cos(\omega L_{ht}/V_e)(c_{\dot{y}}I_z+b_{\dot{y}}mx_w)\times$$
$$\times b_{\dot{y}}mx_w]-2c_{\dot{y}}V_e(-\omega^2+c_{\dot{y}}V_e)\Big\}. \qquad (3.85)$$

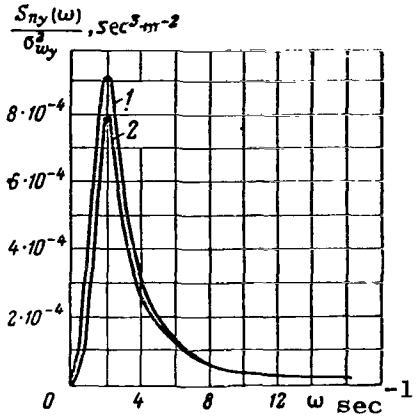

Figure 3.33. Normalized acceleration spectral densities for Airplane No. 1 due to vertical wind. 1 - with effect of wing span and horizontal tail length considered; 2 - with span only considered.

Figure 3.33 presents a graphic (curve 1) for the acceleration spectral density for Airplane No. 1, computed through Equation (3.85), that is, with span and horizontal tail length considered. The turbulence scale was selected small (L = 150 m) in order to express the effect of airplane size more sharply. Curve 2 in this figure shows the spectral density when only the span averaging effect is considered, that is, the effect of the horizontal tail length is not considered. The Equation (3.45) transfer function for a small airplane was used to determine this latter, but the spectral density $S_{we}(\omega)$, averaged over the span, was used instead of the wind spectral density at the particular point $S_w(\omega)$. Not plotted in Figure 3.33 is the acceleration spectral density for Airplane No. 1 with its size not taken into consideration, because it very nearly merges with curve 1.

The root-mean-squares of the acceleration for these three cases are as follows: /120

(1) airplane size not considered $\sigma_{n_y} = 0.0536$;

(2) span average only considered $\sigma_{n_y} = 0.0485$;

(3) span and horizontal tail length considered $\sigma_{n_y} = 0.0521$.

The following conclusions derive when the curves in Figure 3.33 and the root-mean-squares of the acceleration for the cases considered are compared.

There is virtually no change in the nature of the spectral density curves when the lateral and longitudinal dimensions of the airplane are taken into consideration. The averaging effect of the wing span for big airplanes, and small turbulence scales, result in quite an appreciable reduction in the vertical acceleration due to vertical gusts. In the example considered this reduction was about 10%. However, the effect of the horizontal tail length is to increase the root-mean-square of the moment due to the wind, to an increase

in the fluctuation of the airplane relative to the center of gravity, and, in the final analysis, to an increase in the acceleration to a value close to the acceleration for a small airplane.

The effect of the lateral and longitudinal dimensions, even for big airplanes, will be so slight for the most probable turbulence scale values (L = 300 m) that no attention need be paid to it in the overwhelming majority of cases.

3.6. The Effect of Airplane Structure Elasticity on Flight Dynamics in Turbulent Air.

The deformations that take place in the structures of modern airplanes are extensive, because of the high speeds at which they fly. Most of the evolutions carried out by the airplane involve movements that can be characterized by very low frequencies, yet the fundamental frequencies of the elastic oscillations of the airplane's elements are considerably higher (by an order of magnitude and more). Therefore, during slow evolutions of the airplane, the elastic deformations of its structure have no significant effect on flight dynamics. This is the explanation of why the airplane usually is considered to be a solid body in flight dynamics work.

The acceleration changes very sharply when an airplane is flying in disturbed air, practically repeating wind velocity pulsations. As we will point out in what follows, under these conditions structural deformations can have a significant effect on airplane dynamics.

Let us introduce the equations for the longitudinal motion of an elastic airplane flying at constant speed. These equations can be obtained by a consideration of the vertical displacement of all points on the airplane. The vertical displacement of any point on the airplane, in geographic coordinates, /121 can be determined by the expression

$$\Delta y(x, z, t)=\sum_{i=1}^{n}\xi_i(x, z)q_i(t), \tag{3.86}$$

where

q_i is the i^{th} generalized coordinate of the airplane's motion corresponding to one of the n considered degrees of freedom;

ξ_i is the i^{th} normal shape of the oscillations, the use of which assists in transforming the coordinate q_i into the vertical displacement.

Since Equation (3.86) should consider the total vertical displacement of any point on the aircraft, the concept of "normal shape" in this equation can be extended not only to elastic oscillations, but to the oscillations of the airplane as a solid body as well.

The Lagrangian equation for an elastic body is in the form

$$\frac{d}{dt}\frac{dT}{\partial \dot{q}_i} - \frac{\partial T}{\partial q_i} + \frac{\partial U}{\partial q_i} = F_i, \tag{3.87}$$

where

T is the body's kinetic energy;

U is the body's potential energy, attributable to its deformations;

q_i is the rate of change for the i^{th} generalized coordinate;

F_i is the generalized force, or moment, causing the change in the i^{th} generalized coordinate.

The kinetic energy of any point on the airplane with mass $\Delta m(x, z)$, when it is displaced vertically, can be expressed by the formula

$$\Delta T = \frac{1}{2}\Delta m(x, z)\left[\sum_{i=1}^{n}\xi_i(x, z)\,q_i(t)\right]^2. \tag{3.88}$$

From whence we obtain

$$\frac{d}{dt}\frac{\partial \Delta T}{\partial \dot{q}_i} = \Delta m(x, z)\sum_{j=1}^{n}\xi_i(x, z)\xi_j(x, z)\ddot{q}_i(t), \quad i = 1, 2, \ldots, n. \tag{3.89}$$

After the integration of Equation (3.89) in terms of the surface of the airplane in plan, we obtain the first term in the left side of Equation (3.87) as

$$\frac{d}{dt}\frac{\partial T}{\partial \dot{q}_i} = \sum_{j=1}^{n} M_{ij}\ddot{g}_j(t), \quad i = 1, 2, \ldots, n. \tag{3.90}$$

M_{ij} in Equation (3.90) designates the generalized inertia coefficients, /122 which can be determined through the expression

$$M_{ij} = \iint_S \mu(x, z)\xi_i(x, z)\xi_j(x, z)\,dx\,dz, \tag{3.91}$$

where

$\mu(x, z)$ is the mass per unit of airplane surface S in the xoz plane, in which the integral of Equation (3.91) is taken.

The second term in the left side of Equation (3.87) equals zero because the airplane's kinetic energy does not depend on the coordinate q_i. The third term in the left side of this equation, which takes into consideration the potential energy of the deformation of the airplane, can be determined by the Rayleigh method [39]. The idea behind this method is that the elastic oscillations of the parts of the airplane usually are only slightly damped, so are considered as undamped in determining the third term in Equation (3.87). The result is that the extreme values of the kinetic and potential energies of the oscillations of the elements of the airplane's structure equal each other. It is obvious that a potential energy maximum occurs when these elements occupy one of the extreme positions and their kinetic energy equals zero, and that a kinetic energy maximum occurs when these elements come through the equilibrium position and their potential energy equals zero. Let us suppose that the generalized coordinates of the elastic degrees of freedom change according to a sinusoidal law

$$q_i = A_i \sin \omega_{i,k} t, \tag{3.92}$$

where

ω_{ik} is the fundamental frequency of the k^{th} harmonic of the oscillations in the i^{th} degree of freedom.

Let us limit ourselves to the first harmonic of these oscillations, and let us drop the index k = 1. Substituting Equation (3.92) in Equation (3.90), and integrating with respect to the airplane's surface, S, we obtain the maximum value for the kinetic energy for an elastic oscillatory mode

$$T_{im} = \frac{1}{2} M_{ii} \omega_i^2 A_i^2, \quad i = 1, 2, \ldots, n, \tag{3.93}$$

where

M_{ii} can be determined through Equation (3.91).

On the other hand, the potential energy in the case of deformation is proportional to the square of the generalized coordinate. We obtain the following for the i^{th} coordinate

$$U_i = \frac{1}{2} c_i q_i^2(t). \tag{3.94}$$

where

c_i is an unknown proportionality factor.

The maximum value of the potential energy equals

$$U_{im}=\frac{1}{2}c_iA_i^2. \tag{3.95}$$

From what has been said above, the maximum values of the kinetic [Equation (3.93)] and potential [Equation (3.95)] energies can be equated in order to determine c_i, and we obtain /123

$$c_i=M_{ii}\omega_i^2. \tag{3.96}$$

Substituting the value for c_i in Equation (3.94), we find

$$U_i=\frac{1}{2}M_{ii}\omega_i^2q_i^2(t). \tag{3.97}$$

Differentiating Equation (3.97) with respect to q_i, we determine the third term in Equation (3.87) as

$$\frac{\partial U_i}{\partial q_i}=M_{ii}\omega_i^2q_i(t). \tag{3.98}$$

The generalized force F_i in the right side of Equation (3.87) can be determined by the work done by the external forces on the virtual displacement q_i. Accordingly, the general expression for this force should be in the form

$$F_i=\frac{\partial W}{\partial q_i}, \tag{3.99}$$

where

W is the work done by the external forces.

Substituting the values of all the terms in Equation (3.87) from Equations (3.90), (3.98) and (3.99), we obtain equations for the longitudinal motion of the elastic airplane in the form

$$\sum_{j=1}^{n}M_{ij}\ddot{q}_j(t)+M_{ii}\omega_i^2q_i(t)=\frac{\partial W}{\partial q_i},\ i=1,2,\ \ldots,\ n. \tag{3.100}$$

Bending and twisting of the wing, and in some cases even bending of the fuselage, are the most significant types of deformations so far as modern airplanes are concerned. Equation (3.100) makes it possible to consider the effect of the first harmonics (tones) of any types of airplane deformations.

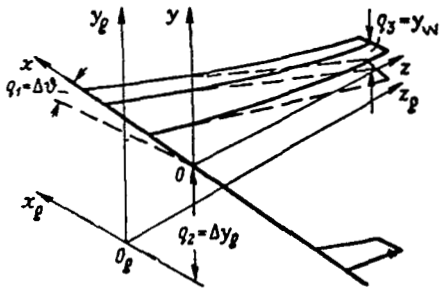

Figure 3.34. Three coordinates fixing the motion of the airplane with wing bending considered.

In the following example the analysis of the motion of an elastic airplane in turbulent air will consider only the basic deformation, the first form of bending of the wing. Ignoring the other forms of bending oscillations corresponding to the higher frequencies is based on the physically obvious proposition that the elastic degrees of freedom affect the stability and controllability of the airplane only when their frequencies are relatively low. Given this assumption, the longitudal motion of an airplane flying at constant speed can be described by three generalized coordinates (Figure 3.34) /124

$q_1 = \Delta\vartheta$ the change in the angle of pitch;

$q_2 = \Delta y_g$ the vertical displacement of the airplane's center of gravity;

$q_3 = y_w$ the vertical deflection of the axis of rigidity for the wing at its tip.

Substituting these coordinates in Equation (3.100), we obtain the following system of equations (n = 3)

$$\left.\begin{aligned} M_{11}\frac{d^2\Delta y_g}{dt^2}+M_{12}\frac{d^2\Delta\vartheta}{dt^2}+M_{13}\frac{d^2y_w}{dt^2}&=F_1,\\ M_{21}\frac{d^2\Delta y_g}{dt^2}+M_{22}\frac{d^2\Delta\vartheta}{dt^2}+M_{23}\frac{d^2y_w}{dt^2}&=F_2,\\ M_{31}\frac{d^2\Delta y_g}{dt^2}+M_{32}\frac{d^2\Delta\vartheta}{dt^2}+M_{33}\frac{d^2y_w}{dt}+M_{33}\omega_w^2y_w&=F_3. \end{aligned}\right\} \qquad (3.101)$$

The subjects of the computations made in this section will be big Airplanes No. 1 and No. 3 (see Appendix A). The characteristics of Airplane No. 3 were taken from [40]. The formulas for the computations of the inertia coefficients and their values for Airplanes No. 1 and No. 3, as well as the general considerations for computing the first oscillatory bending mode for the wing, are contained in Appendix B.

Equation (3.101) differs from the equations for the rigid airplane only in the consideration of the bending oscillations for the wing. If we put

$y_w = dy_w/dt = d^2y_w/dt^2 = 0$, these equations will be converted into simplified equations of the short-period motion for the airplane at Equation (2.11). Therefore, the right sides of the first two equations should contain all the terms contained in Equation (2.11). Moreover, the forces and moments attributable to wing oscillations will appear in the right sides of these equations. The aerodynamic forces that cause wing oscillations, as well as motion of the airplane as a whole, are included in the right side of the third of the equations at (3.10).

Because the frequency of the first harmonic of the wing bending oscillations is comparatively low, the determination of the forces and moments associated with these oscillations will be made on the basis of the stationary nature hypothesis (see Appendix B). Once we have determined the values of the generalized forces and substituted them in the system of Equation (3.101), and once we have reduced this system to a more convenient form, we obtain the equations for the airplane with elastic wing flying in the velocity field of a vertical wind

/125

$$\left.\begin{aligned}
&V_e\frac{d^2\Delta\vartheta}{dt^2}+\frac{dV_{gy}}{dt}+b_{\dot y}V_{gy}+b_{\ddot w}\frac{d^2y_w}{dt^2}+b_{\dot w}\frac{dy_w}{dt}+\\
&\qquad+b_w y_w=b_{\dot y}w_y,\\
&\frac{d^2\Delta\vartheta}{dt^2}+c_{\dot\vartheta}\frac{d\Delta\vartheta}{dt}-c_{\ddot y}\frac{dV_{gy}}{dt}-c_{\dot y}V_{gy}+c_{\ddot w}\frac{d^2y_w}{dt^2}+c_{\dot w}\frac{dy_w}{dt}+\\
&\qquad+c_w y_w=-c_{\dot\delta}\Delta\delta_e-c_{\dot y}w_y,\\
&e_{\ddot\vartheta}\frac{d^2\Delta\vartheta}{dt^2}+e_{\dot\vartheta}\frac{d\Delta\vartheta}{dt}+e_{\ddot y}\frac{dV_{gy}}{dt}+e_{\dot y}V_{gy}+\frac{d^2y_w}{dt^2}+\\
&\qquad+e_{\dot w}\frac{dy_w}{dt}+(\omega_w^2+e_w)y_w=e_{\dot y}w_y.
\end{aligned}\right\}\qquad(3.102)$$

The formulas for the coefficients of the equations at (3.102) and their values for Airplanes No. 1 and No. 3 are listed in Appendix B.

The system of equations at (3.102) was supplemented by Equation (2.14) for the autopilot without altitude corrector for purposes of investigating controlled flight.

Let us consider the dynamic characteristics of an airplane with an elastic wing acted on by a vertical step gust. The results of the integration of

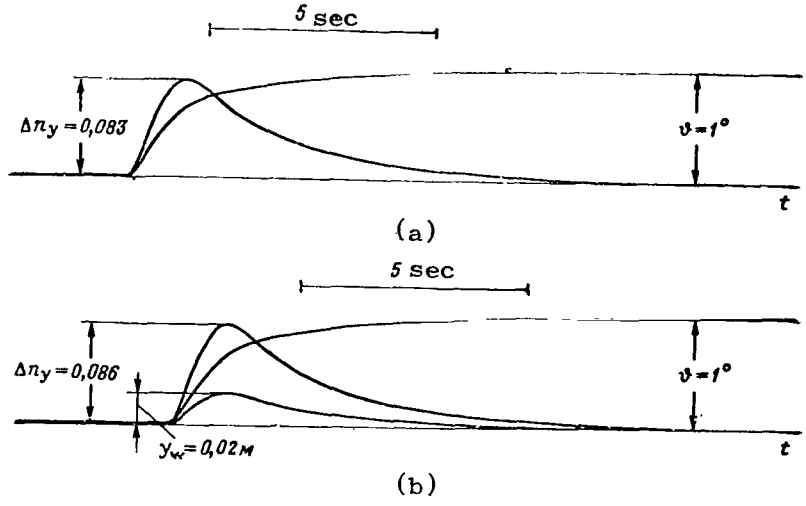

Figure 3.35. The reaction of Airplane No. 1 with autopilot to a pitch control signal. a - rigid; b - bending of the wing considered.

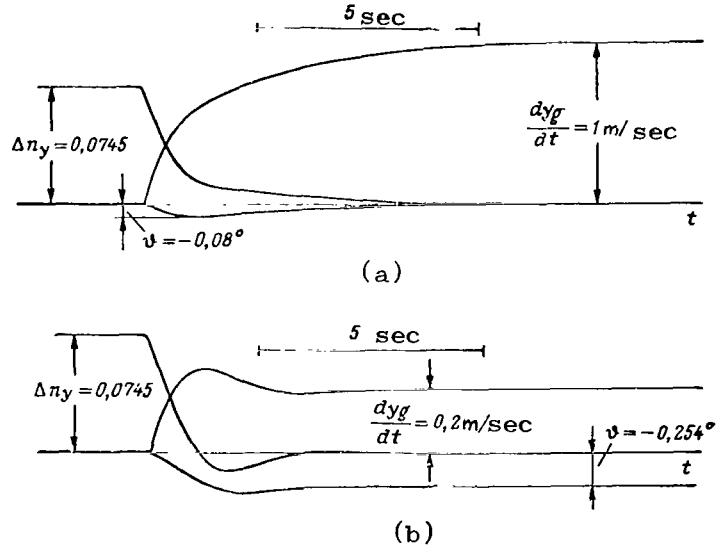

Figure 3.36. Reaction of rigid Airplane No. 1 to a single vertical gust. a - with autopilot; b - with fixed controls.

Equation (3.102) in the form of oscillograms of the transients are shown in the figures that follow. All data in these figures are for a vertical wind with a velocity W_y = 1 m/sec acting on the airplane.

First of all, let us consider the oscillograms of the transients for Airplane No. 1. Figure 3.35 shows the reaction of the airplane with autopilot to control signal $\Delta\vartheta_s = 1°$. Figure 3.35a is for a rigid, and Figure 3.35b is for an elastic airplane. The latter is the oscillogram for wing tip (y_w) deflections. A comparison of these figures reveals that during ordinary, slow, evolutions of the airplane, bending of the wing has no significant effect on the nature of the change in the parameters of short-period motion. It is therefore perfectly permissible to use the assumption of the airplane as a solid body, as was pointed out at the beginning of this section, to analyze slow motions of the airplane.

Figure 3.36 shows the reaction of a rigid airplane with autopilot (a) and with fixed controls (b) in a single gust. This figure gives the dynamic characteristics of a rigid and an elastic airplane, the reactions of which to a single gust are shown in Figure 3.37, for purposes of comparison. Figure 3.37a is for the airplane with autopilot, while Figure 3.37b is for the airplane with fixed controls. Comparison of the curves in Figures 3.36 and 3.37 provides the basis for the assertion that the elasticity of the wing has practically no effect on the nature of the reaction with respect to the angle of pitch and the vertical velocity but does change the nature of the reaction with respect to the vertical acceleration significantly. The initial value of the acceleration for the elastic airplane is reduced substantially (almost halved). This reduction can be explained by the fact that the effective angle of attack, and as a result, the increase in the lift when the wing bends, is less than that for the case of the rigid wing. But in the case of the rigid airplane, the acceleration drops sharply at first, whereas it rises initially in the case of the airplane with the flexible wing, so that the maximum for the acceleration becomes greater than the initial value for the rigid airplane. /127

The wing tip deflection (see Figure 3.37) practically duplicates the law for change in the acceleration. Excluded is the initial moment when the acceleration increases instantaneously, but the wing tip deflection is smoother.

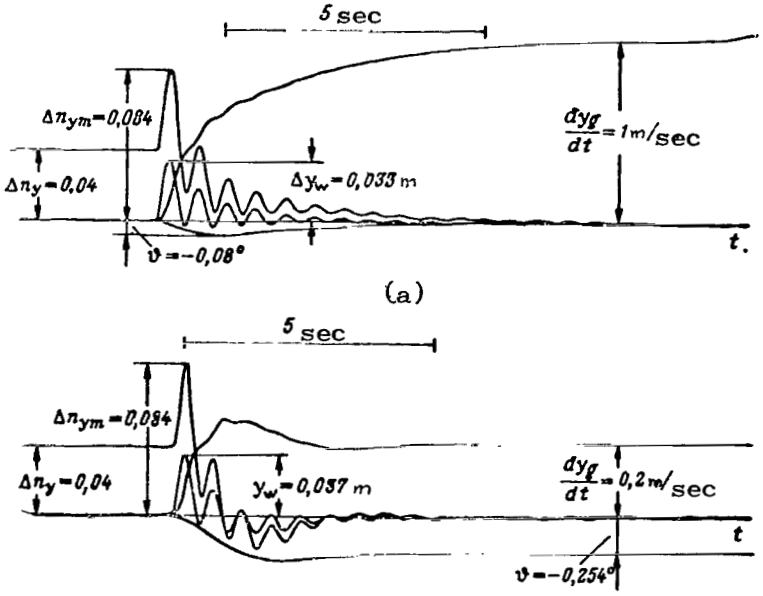

Figure 3.37. Reaction of Airplane No. 1 to a single vertical gust with bending of the wing considered. a - with autopilot; b - with fixed controls.

Maximum wing tip deflection is 0.037 meter when the vertical gust velocity is W_y = 1 m/sec. Deflection is comparatively slight because flight at an altitude of y_g = 8,000 meters is being considered, and at this altitude the air density is comparatively low. This deflection increases considerably at ground level.

/128

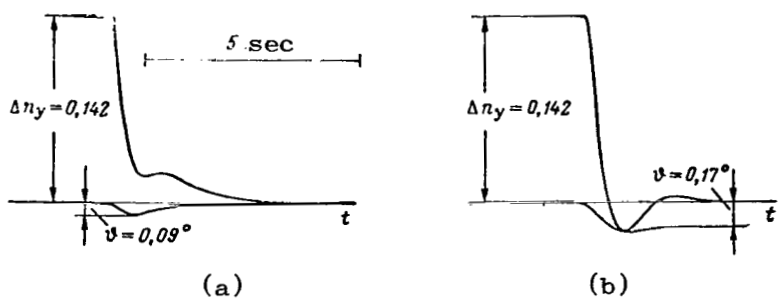

Figure 3.38. Reaction of rigid Airplane No. 3 to a single gust. a - with autopilot; b - with fixed controls.

Airplane No. 1 has a straight wing. Bending of a swept wing is accompanied by a certain special feature, the appearance of an additional negative angle of attack serving to reduce the overall increase in the angle of attack that would be obtained for the straight wing. In order to illustrate the effect the swept wing has on the dynamics of an airplane with a flexible wing, in what follows we have included oscillograms of the transients resulting from the effect of a single step gust on Airplane No. 3, which has a swept wing.

The reaction of a rigid airplane with autopilot (a) and with fixed controls (b) is shown in Figure 3.38. Figure 3.39 shows the same characteristics for the elastic airplane. Comparing the two figures, we can assert that because of the swept-wing design the acceleration of the aircraft acted on by a single gust is reduced quite substantially. Figure 3.40 is included to confirm reduction in the acceleration precisely because the wing is swept. This figure

/129

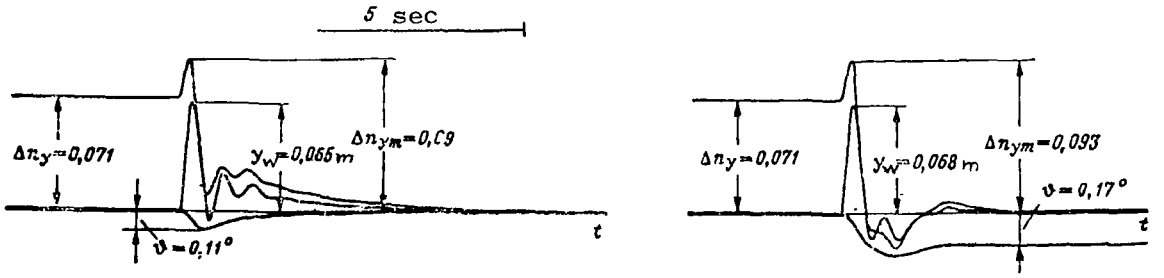

(a) (b)

Figure 3.39. Reaction of Airplane No. 3 (with swept wings) to a single vertical gust with wing bending taken into consideration. a - with autopilot; b - with fixed controls.

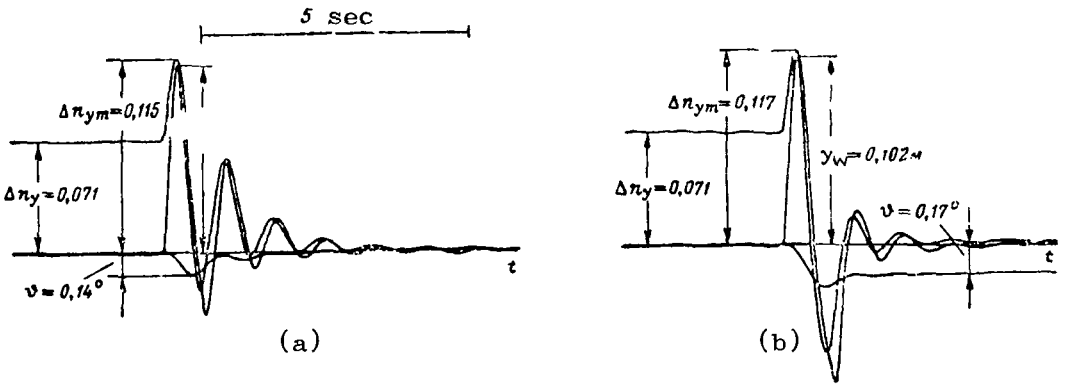

(a) (b)

Figure 3.40. Reaction of Airplane No. 3 to a single vertical gust, assuming no sweepback. a - with autopilot; b - with fixed controls.

is for Airplane No. 3 and its reaction to a single gust and assumes zero sweepback for the wing. All weight, aerodynamic and strength characteristics of the wing, and of the airplane as a whole, are as before. A comparison of the graphics in Figures 3.39 and 3.40 is persuasive evidence of the positive effect of sweepback on the dynamic characteristics of an elastic airplane in a disturbed atmosphere. Note that if bending of the wing is not considered, the reaction of the airplane to a single gust, as shown in Figure 3.38, will be the same for the swept wing and for the straight wing.

Let us now move on to a qualitative evaluation of the effect of wing bending on the dynamics of flight in a turbulent atmosphere.

Let us consider the spectral densities and the root-mean-squares of the parameters of the longitudinal motion of the airplane under these conditions.

Figure 3.41 shows the spectral densities of the increases in the angle of pitch and of the vertical acceleration of Airplane No. 1 flying in the velocity /130

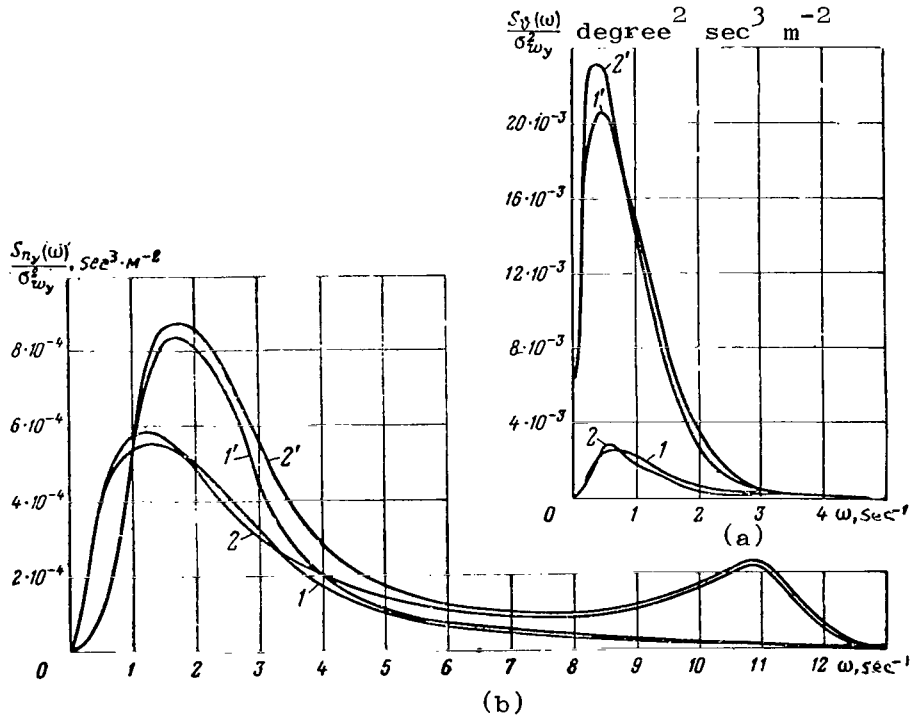

Figure 3.41. Normalized spectral densities of the increase in the angle of pitch (a) and of vertical acceleration (b) for Airplane No. 1 with fixed controls and with autopilot. The primes are the curves for the airplane with fixed controls. 1 - rigid airplane; 2 - with bending of wing taken into consideration.

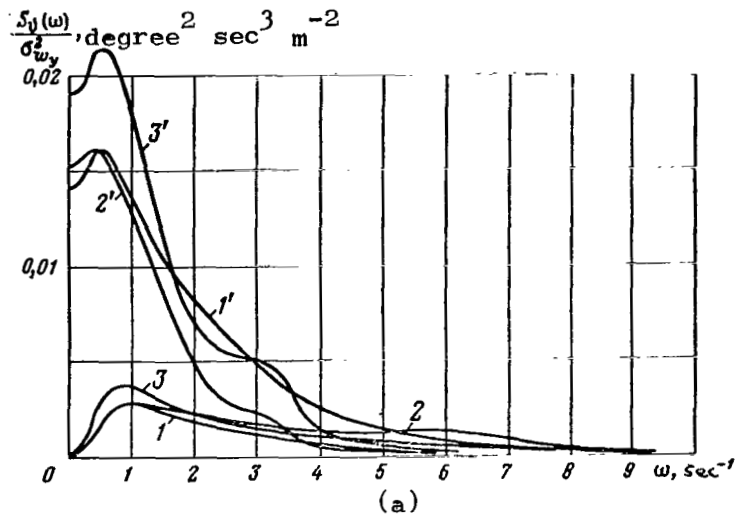

(a)

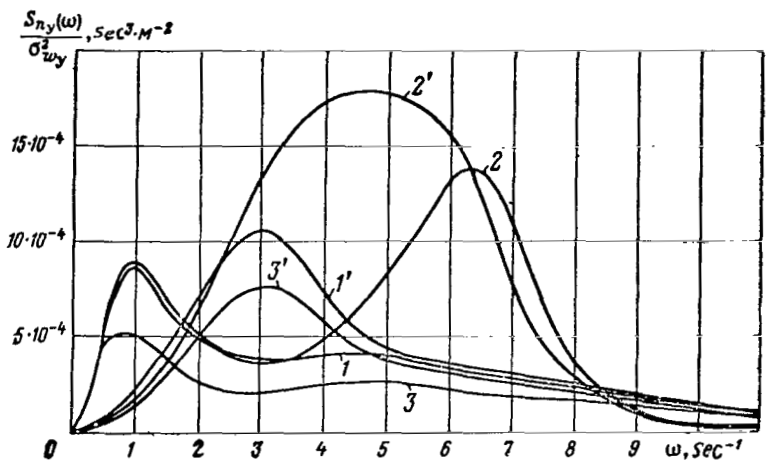

(b)

Figure 3.42. Normalized spectral densities of the increase in the angle of pitch (a) and in the vertical acceleration (b) for Airplane No. 3 with fixed controls and with autopilot. The prime designates the curves for the airplane with the fixed controls.

1 - rigid airplane; 2 - bending of straight wing taken into consideration; 3 - bending of swept wing taken into consideration.

fields of vertical gusts. These same data are included in Figure 3.42 for Airplane No. 3. The curves numbered 1 are for the rigid airplane, those numbered 2 for the airplane with flexible straight wing, and those numbered 3 for the airplane with flexible swept wing. Figures without primes are for the curves for the airplane with the autopilot, and those with primes are for the airplane with fixed controls. Table 3.1 lists the root-mean-squares of the angle of pitch and of the acceleration for all cases shown in Figures 3.41 - 3.42. The turbulence scale L = 300 meters applies to the curves for spectral densities in all figures, as well as to the data in Table 3.1, and a random wind with dispersion $\sigma_w^2 = 1\ m^2/sec^2$ acting on the airplane is used throughout.

The graphics in Figures 3.41a and 3.42b, as well as the data in Table 3.1, show that wing elasticity has no significant effect on the spectral density, or on the root-mean-square of the oscillations in the angle of pitch.

TABLE 3.1

/132

Commas represent decimal points.

Curves in Figures 3.41 - 3.42		1	1'	2	2'	3	3'
σ_ϑ in angular minutes	№ 1	4,0	11,0	4,0	11,7	—	—
	№ 3	5,4	12,0	6,6	10,0	6,0	12,6
σ_{n_y}	№ 1	0,044	0,052	0,054	0,059	—	—
	№ 3	0,066	0,073	0,078	0,093	0,052	0,061

Airplanes

The graphics for the spectral density of the acceleration in Figures 3.41b and 3.42b differ significantly for different cases considered and therefore require a more detailed discussion. Let us compare the curves with each other, equating them to the same control method (with autopilot, or without). The curves in Figure 3.41b show that wing bending for Airplane No. 1 is absolutely the same whether flying on the autopilot, or with fixed controls. Bending results in a second peak at a frequency somewhat lower than 2 Hz, leading to some increase in the acceleration. This result can be confirmed by the oscillograms in Figures 3.36 and 3.37.

Wing flexibility in the case of Airplane No. 3 (Figure 3.42b) on the other hand leads to a reduction in the acceleration (curves 3 and 3') as compared

with the acceleration for the rigid airplane (curves 1 and 1'). As has already been pointed out, reduction in acceleration in the case of Airplane No. 3 because of bending of swept wing is associated with the appearance of a negative angle of attack. This agrees with the conclusions drawn on the basis of the transfer functions for Airplane No. 3 (Figure 3.38 and 3.39). The straight flexible wing of Airplane No. 3 (Figure 3.42, curves 2 and 2') increases the acceleration considerably. This is associated with the presence of a peak on the spectral density curves with maximum in the 1 Hz region. Engaging the autopilot leads to a 10 to 15% reduction in the acceleration in all of the cases considered.

Let us introduce graphics of the root-mean-square of the acceleration in terms of the turbulence scale in order to obtain a better concept of the effect bending of the wing has on the acceleration of an airplane flying in turbulent air. The data are for an airplane with an autopilot only. Curves for an airplane with fixed controls are similar in nature, but are somewhat higher than the corresponding curves for the airplane with autopilot.

Figure 3.43 shows the data for rigid Airplane No. 1 (curve 1), as well as for this same airplane with an elastic wing (curve 2). In the region of the most likely scale, L = 300 meters, the increase in the acceleration attributable to the bending of the wing is about 15%, and in the region of the smallest scale, L = 50 m, this increase is 35%. /133

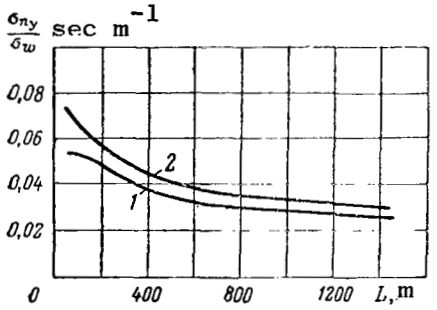

Figure 3.43. Normalized root-mean-squares of vertical acceleration of Airplane No. 1 with autopilot as a function of the turbulence scale.

1 - rigid airplane; 2 - with bending of wing taken into consideration.

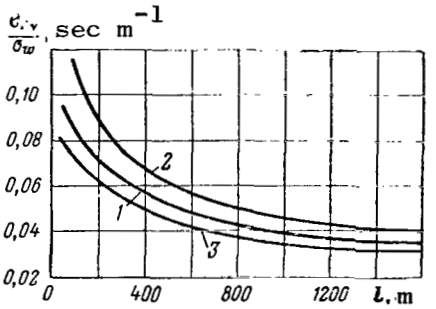

Figure 3.44. Normalized root-mean-squares of the vertical acceleration of Airplane No. 3 with autopilot as a function of the turbulence scale.

1 - rigid airplane; 2 - with bending of a straight wing taken into consideration; 3 - with bending of a sweptback wing taken into consideration.

Figure 3.44 gives the root-mean-squares of the acceleration for rigid Airplane No. 3 (curve 1), as well as for this same airplane with straight (curve 2) and sweptback (curve 3) flexible wings. Here the effect of wing bending appears to an even greater degree than in the Airplane No. 1 case.

Accordingly, bending of the wing, particularly in the case of big airplanes, results in a significant change in the magnitude of the acceleration experienced when flying in a turbulent atmosphere. In the case of the straight-wing airplane, bending of the wing increases the root-mean-square of the acceleration under these conditions. Bending of the sweptback wing can reduce the acceleration attributable to atmospheric disturbances (for the usual values of sweepback angles for modern airplanes).

3.7. Deviation of an Airplane From its Assigned Flightpath when Flying in Turbulent Atmosphere.

Modern autopilots usually have a so-called altitude corrector, that is, a statoscope, providing the signal to the actuator to change the assigned altitude. It was pointed out section 3.2 that the altitude corrector increases the accelerations experienced by the airplane in a turbulent atmosphere. An increase in the accelerations can occur even when the statoscope is used ideally as an altimeter. As a matter of fact, the statoscope measures pressure, and pressure too can fluctuate in a disturbed atmosphere, leading to the delivery /134 to the controls of undesired signals not associated with change in altitude. This is why it is difficult to expect the data obtained from the theoretical computation of the altitude oscillations of an airplane, made on the assumption of ideal operation of the statoscope, to be in good concordance with the results of experimentation. Nevertheless, even under these conditions, it is useful to assess the order of magnitude of the oscillation of the center of gravity of the airplane with respect to altitude since prior to this it has been difficult to say what magnitudes we could be talking about. This is why Figure 3.45 shows the root-mean-squares of altitude deviations for Airplane No. 1 with an autopilot with an altitude corrector [Equation (2.13) law] as a function of the turbulence scale. Curves are plotted for two values of autopilot altitude gain. Curve 1 equates to the nominal value i_y = 0.07 degrees/m, and curve 2 to the reduced value i_y = 0.025 degree/m. The reduction in this gain is the

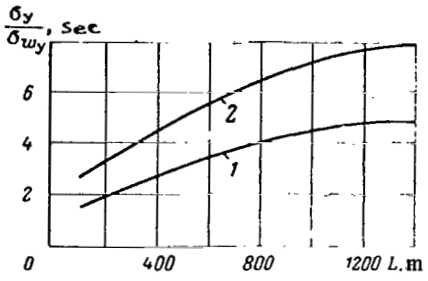

Figure 3.45. Normalized root-mean-squares of oscillations in the altitude at which Airplane No. 1 is flying when acted on by vertical gusts as a function of the turbulence scale.

1 - nominal autopilot altitude gain; 2 - gain reduced by a factor of 3.

result of the presence in the corrector of a non-response zone of the order of ±(10 to 20) m. According to the data in section 3.3, the effect of the non-response zone results in a considerable reduction in the gain when flying in a turbulent atmosphere. The data in Figure 3.45 show that the root-mean-squares of oscillations in flight altitude can be measured in units of meters per unit of root-mean-square of the velocity of the vertical wind component. These oscillations are heavily dependent on the autopilot altitude gain.

The flying mode along the glide path in the glide during the landing approach is of great importance under the conditions that prevail during summer operations.

The root-mean-square oscillations of the center of gravity of the airplane relative to the glide path per unit root-mean-square of the velocity of the vertical wind gusts are several meters under these conditions, and diminish as the airplane approaches the runway. The vertical wind gusts diminish rapidly in the final stage of the landing, the touchdown, and this is shown in Figure 1.28. At this stage the wind gusts cannot create marked disturbances in the altitude at which the airplane is flying. Since the angle of attack is large at the touchdown stage, the horizontal gusts begin to play a big role, as do the lateral gusts in the side motion of the airplane.

3.8. An Approximate Method for Computing the Vertical Acceleration When Flying in a Turbulent Atmosphere.

/135

There are certain practical problems that arise, the solutions to which necessitate making a rapid assessment of the acceleration attributable to the vertical wind component, even though the result has a rather significant error. One such method, extraordinarily simple and reliable, is contained in [37].

Let us find the wing lift for an airplane flying level at constant speed

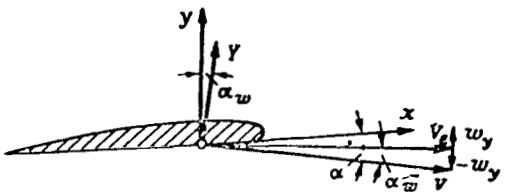

Figure 3.46. Diagram of velocities and forces for a wing acted on by a vertical wind.

attributable to the effect of the vertical wind velocity w_y. A diagram of velocities and forces is shown as Figure 3.46. We will, in order to simplify subsequent analysis, ignore the angular motions of the wing, and, as a result, those of the airplane as a whole. This assumption is also the major cause of the error in the method under consideration. With this assumption in mind, the airplane can move vertically only under the effect of force Y. Change in this force as compared with its undisturbed value can be caused by the wind, as well as by wing movement. Based on the foregoing, the equation for Newton's second law for the vertical motion of the airplane should be in the form

$$m\frac{d^2y_g}{dt^2}=Y(y_g)+Y(w_y), \tag{3.103}$$

where

$Y(y_g)$ is a force attributable to vertical wing movement;

$Y(w_y)$ is a force attributable to the wind, w_y (the disturbing force).

For an incompressible flow, these forces can be determined through the expressions

$$Y(y_g)=-\frac{C_{y\rho}^{\alpha}b_aS}{8}\frac{d^2y_g}{dt^2}-\frac{C_{y\rho}^{\alpha}SV_e}{2}C(t)\frac{dy_g}{dt}, \tag{3.104}$$

$$Y(w_y)=C_y^{\alpha}\frac{\rho SV_e}{2}\varphi(t)w_y(t), \tag{3.105}$$

where

$C_{y\rho}^{\alpha}b_aS/8$ is the apparent aerodynamic mass;

$C_{y\rho}^{\alpha}SV_eC(t)$ is the aerodynamic damping coefficient;

$C(t)$ and $\varphi(t)$ are special functions that take into consideration the nonstationary nature of the flow over the wing.[5]

Substituting Equations (3.104) and (3.105) in the original Equation (3.103), we obtain a differential equation for the vertical motion of the /136

5. The function $\varphi(t)$ has already been referred to in this chapter; see Equation (3.53), and subsequent.

airplane as a result of the vertical wind

$$\left(m+\frac{C_y^{\alpha}\rho b_a S}{8}\right)\frac{d^2y_g}{dt^2}+\frac{C_y^{\alpha}\rho S V_e}{2}C(t)\frac{dy_g}{dt}=$$

$$=\frac{C_y^{\alpha}\rho S V_e}{2}\varphi(t)\,w_y(t). \tag{3.106}$$

The complex transfer function for the airplane must be found in order to use spectral methods. Equation (3.106) provides this function in the form

$$W_{n_y/w_y}(j\omega)=\frac{1}{g}\,\frac{\omega\Phi(j\omega)}{\dfrac{b_a\omega}{V_e(2\mu_d/C_y^{\alpha}+0{,}25)}-jG(j\omega)}, \tag{3.107}$$

where

$G(j\omega)$ is a Fourier transform for the function $C(t)$.

The functions $\varphi(t)$ and $C(t)$ can be transformed into Sears and Theodorsen functions if the vertical wind is sinusoidal in nature. The Sears function can be approximated by Equation (3.40), and the Theodorsen function is equal to unity, approximately [41], within the limits of the low range of frequencies.

Equations (2.46) and (2.47), together with the transfer function of Equation (3.107) and the spectral density of Equation (1.33), provide an expression for acceleration dispersion in the form

$$\sigma_{n_y}^2=\sigma_w^2\,\frac{V_e^2}{\pi g^2 b_a^2(2k+0{,}25)^2}\int_0^{\infty}\frac{\nu^2}{\nu^2+a^2}\,\frac{1}{1+\pi S\nu}\,\frac{1+3\nu^2}{(1+\nu^2)^2}\,d\nu, \tag{3.108}$$

where

$$a=1/S(2k+0{,}25),\quad s=b_a/L,\quad k=\mu_d/C_y^{\alpha}.$$

Making very simple transformations, and ignoring the 0.25 in the parenthesis in the denominator because of its smallness compared with the magnitude of $2\mu_d/C_y^{\alpha}$, we obtain the final expression linking the root-mean-square of the vertical acceleration with the root-mean-square of the vertical wind velocity

$$\sigma_{n_y}=\sigma_w\,\frac{C_y^{\alpha}\rho V_e}{2G/S}\sqrt{\frac{I(k,s)}{\pi}}. \tag{3.109}$$

The definite integral of the right side of Equation (3.109) is designated $I(k, s)$. We will call $\sqrt{I(k,s)/\pi}$ the coefficient of reaction of the airplane

to a random wind. Figure 3.47 shows nomograms reflecting this coefficient in terms of its two parameters, the reduced density, k, and the ratio of the mean aerodynamic chord, b_a, to the turbulence scale, L. This coefficient will be a constant for a specfic airplane and a fixed altitude at which it is flying. /137

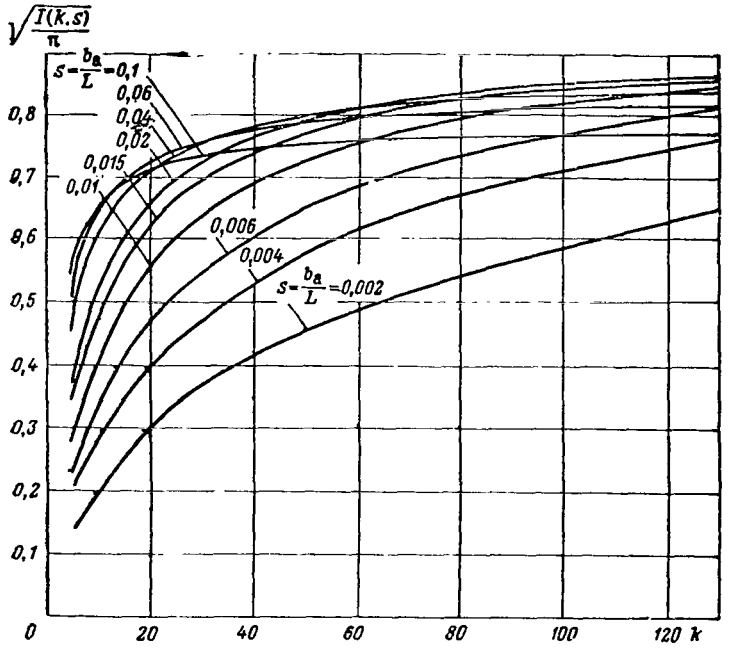

Figure 3.47. Nomograms for the coefficient of reaction of an airplane in a vertical gust.

The principal advantage of Equation (3.109) is its simplicity. The equations show clearly that when the root-mean-square of the wind is constant, acceleration will increase in proportion to the flight speed. The effect of altitude is not quite so obvious because the air density is contained in the numerator of the formula, as well as in the parameter k, determining the wind reaction factor.

An increase in the wing loading (G/S) characteristic for modern airplanes results in a reduction in the acceleration [see Equation (3.109)]. On the other hand, the wind reaction factor increases with increase in μ_d, and consequently, with increase in the unit load. There is a simple physical explanation for this latter event. The acceleration is slight when the density ratio for the airplane, μ_d, is small because the airplane can easily absorb

the wind gusts, and this explains the bending of the wings in Figure 3.47 for small k. An increase for the airplane with vertical gusts by increasing μ_d will play an even lesser role, so $\sqrt{I(k, s)/\pi}$ will be increased. /138

The structure of Equation (3.109) will be retained when there is a transition to near-sonic and supersonic speeds. However, the nomograms in Figure 3.47, derived with the Sears function taken into consideration, will not be as precise because the use of this function is valid for an incompressible flow only.

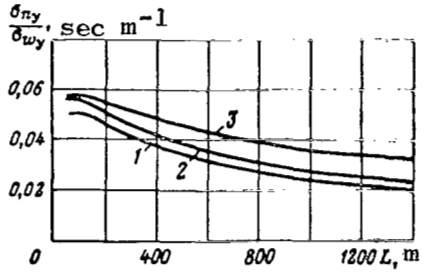

Figure 3.48. Normalized root-mean-squares of the acceleration for Airplane No. 1 caused by vertical gusts as a function of the turbulence scale.

1 - with autopilot; 2 - with fixed controls; 3 - Equation (3.109).

To conclude this section, let us consider an example of the use of Equation (3.109). Figure 3.48 shows the root-mean-squares of the acceleration caused by vertical gusts for Airplane No. 1, wherein curve 1 is for the airplane with an autopilot, and curve 2 is for the airplane with fixed controls. Data for the construction of these curves were obtained by modeling with the methodology adopted in this book. Curve 3 was derived from Equation (3.109). It is obvious that when this formula is used it makes no difference whether the airplane does or does not have an autopilot because the derivation of this formula assumed there were no oscillations in the angle of pitch. Accordingly, the computation made using Equation (3.109) should yield the same result as that reviewed at the end of section 3.2 for the limit case of ideal stabilization of the airplane in pitch ($i = \infty$). Therefore, the physical explanation of the positions of curves 1, 2, and 3 in Figure 3.16a, given in this section, remains true for the curves in Figure 3.48 as well. The only difference in these figures is that because of Airplane No. 1's good natural damping of the oscillations in the angle of pitch, the acceleration computed with these oscillations taken into consideration (Figure 3.48, curves 1 and 2) is always less than the acceleration determined using Equation (3.109) without the angular motions taken into consideration.

3.9. Some Experimental Data with Respect to the longitudinal Motion of an Airplane in a Turbulent Atmosphere

The results of flight investigations of longitudinal motion are persuasive confirmation of the principal correctness of the statistical approach to the dynamics of an airplane in a turbulent atmosphere discussed in the preceding sections of this chapter. One example we can present is the result of the processing of the data obtained from over 200 flights made by a heavy transport airplane under "rough air" conditions. Not considered in the averaging were /139 differences in conditions of specific flights, speed, altitude, or airplane weight. Data were separated for three types of airplane control (pilot, autopilot with altitude corrector, and autopilot without altitude corrector). The results of processing the data obtained during these flights are listed in Table 3.2.

TABLE 3.2.

Commas represent decimal points.

Control mode	σ_{n_y}	σ_ϑ degrees	σ_{δ_e} degrees
Pilot	0,177	1,826	0,720
Autopilot without altitude corrector	0,155	0,481	0,572
Autopilot with altitude corrector	0,172	0,785	0,793

The data in Table 3.2 confirm the advantages of controlling the airplane when flying in "rough air" by using the autopilot (particularly one without an altitude corrector), as set forth above the basis of a theoretical review of this question.

Figure 3.49 presents the graphics of a normalized spectral density, obtained from the realization recorded for the vertical acceleration during one of the flights recalled in the foregoing.

The flight mode to which the graphics in Figure 3.49 equate is the following: y_g = 3,600 m; V = 400 km/h. These graphics also equate to three types of airplane control. The increase in the acceleration spectral density

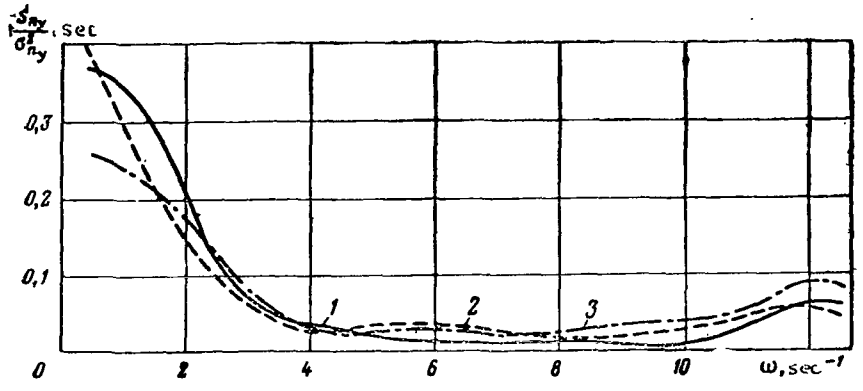

Figure 3.49. Normalized spectral densities of vertical acceleration when flying in a turbulent atmosphere.

1 - pilot; 2 - autopilot with altitude corrector; 3 - autopilot without altitude corrector.

for a frequency of about 2 Hz ($\omega \cong 12$ sec^{-1}) can be explained by the effect of /140 the first tone of the airplane wing's bending oscillations. The spectral density graphics differ but slightly from each other when shown in normalized form, but the root-mean-squares of the acceleration, equated to the root-mean-square of the vertical wind component[6] differ quite substantially:

pilot - $\sigma_{n_y}/\sigma_{w_y} = 0.091$ sec-m^{-1};

autopilot with [sec] altitude corrector - $\sigma_{n_y}/\sigma_{w_y} = 0.108$ sec-m^{-1};

autopilot with [sec] altitude corrector - $\sigma_{n_y}/\sigma_{w_y} = 0.108$ sec-m^{-1}.

Let us show how it is possible to use the experimental data obtained in flight in a turbulent atmosphere to refine the characteristics of the airplane's longitudinal motion. Actually, what follows from Equation (2.46) is that

$$W^2_{y/x}(\omega) = S_y(\omega)/S_x(\omega). \qquad (3.110)$$

Consequently, if the result of the experiment is the obtaining of spectral densities of the disturbance (of the vertical wind) and of an output reaction for the airplane (any motion parameter of interest to us), Equation (3.110) is the basis for plotting the airplane's amplitude-frequency characteristic curve.

6. The root-mean-square of the horizontal wind velocity component was determined during the experiment. It was assumed that the root-mean-square of the vertical wind component had this same magnitude, the basis being the hypothesis with respect to the isotropic nature of turbulence.

A comparison of this curve, obtained by experiment, with the curve plotted using the plant data for the airplane, will help establish just how accurate these data are.

By way of an example of such a comparison we present materials from [48]. Figure 3.50 shows the amplitude-frequency characteristic curves for a supersonic fighter plane with a delta wing, constructed using the plant data for the airplane. The experimental data are plotted as well. These curves provide the values of the vertical acceleration caused by a vertical sinusoidal wind of unit amplitude (W_{my} = 1 m/sec), of different frequencies. The solid curve is for the airplane with pitch damping action taken into consideration, the dashed curve does not. The experimental data show that during the flights, which were made under storm-air turbulence conditions, the elevons went into the mechanical stops when under damper control, after which the damper was cut out. Therefore, it should be expected that the actual frequency characteristic curve for the airplane in the range of frequencies in which the damper is effective should lie between the solid and the dashed curves.

The circles in Figure 3.50 mark the values of the vertical acceleration /141
obtained by using Equation (3.110) in terms of the experimental values of the spectral densities of the vertical wind gusts and the vertical acceleration.

The concordance of the theoretical and experimental frequency characteristic curves for the airplane in Figure 3.50a, b, and d is extremely good. Only that flight mode shown as Figure 3.50c shows a poorer concordance, but it should be pointed out that the actual static stability of the airplane in this mode turns out to be better than one would have supposed from the theoretical data.

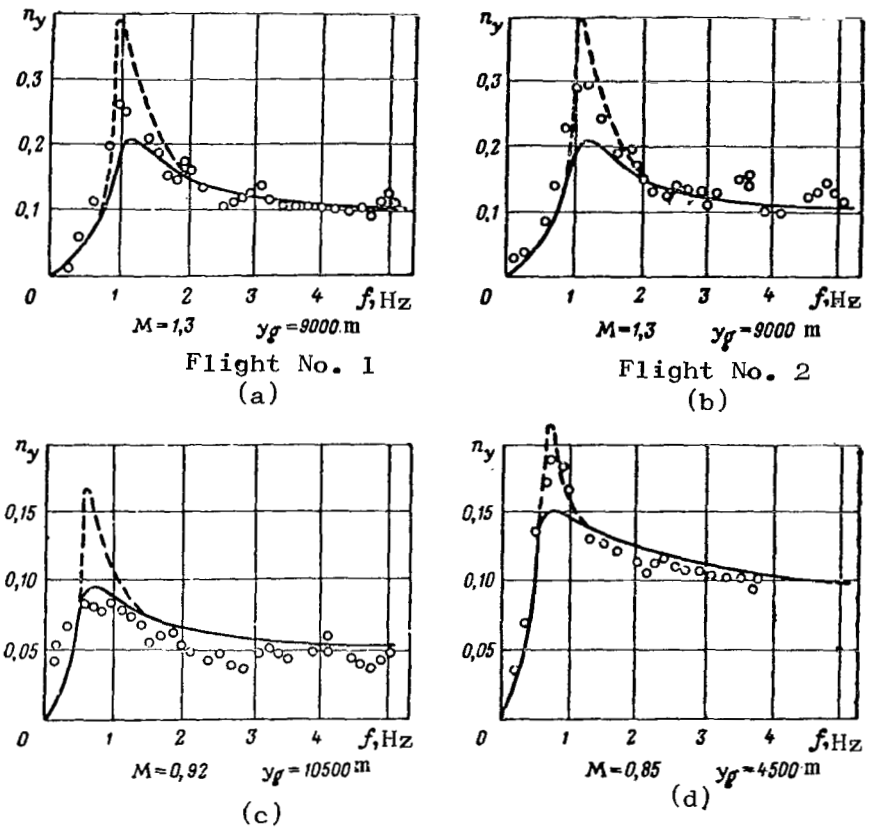

Figure 3.50. Comparison of the frequency characteristic curves for an airplane plotted from computations (solid and dashed lines) and experimental data (circles). (The dashed lines are for the case of no damper).

CHAPTER IV

LATERAL MOTION OF AN AIRPLANE IN MOVING AIR

4.1. Transfer and Response Functions for the Parameters of Lateral Motion Resulting from Wing Action

The heaviest accelerations take place in longitudinal motion when an airplane is flying in turbulent air. This is the reason why much less research has been done in the Soviet Union, as well as abroad, on the lateral motion of an airplane flying in moving air, than on longitudinal motion. /142

The response functions introduced in this section provide a graphic presentation of the lateral motion of an airplane when acted on by a single wind gust. The transfer functions will be the basis for investigating the dynamics of the airplane with fixed controls and when controlled by an autopilot in subsequent sections.

Initially, let us consider the transfer functions for the parameters of lateral motion (β, γ, ψ, z_g) of the airplane without autopilot when acted on by a crosswind, w_z. Equation (2.28) provides these functions.

The transfer function[1] for the ground angle of sideslip, β_g is

$$W_{\beta_g/w_z}(p)=\frac{1}{V_e}\frac{B(p)}{A(p)}=\frac{1}{V_e}\cdot\frac{b_0p^3+b_1p^2+b_2p+a_4}{p^4+a_1p^3+a_2p^2+a_3p+a_4}. \qquad (4.1)$$

Let us introduce the transfer function for the angle of sideslip[2], β, attributable to the cross wind, w_z. This function is obtained from Equation (4.1) and the first of the relationships at (2.22)

$$W_{\alpha/w_z}(p)=-\frac{1}{V_e}\frac{p^4+(a_1-b_0)p^3+(a_2-b_1)p^2+(a_3-b_2)p}{A(p)}. \qquad (4.2)$$

---

1. The values of the coefficients a_i and b_i of the Equation (4.1) transfer function are expressed in terms of the Equation (2.28) coefficients listed in Appendix C. Also listed there are the expressions for the coefficients of all the transfer functions that will be considered in what follows.

2. We recall that β designates the angle of sideslip with respect to the wind.

Using Equations (4.1) and (4.2) transfer functions, let us consider the limits of change in the angle of sideslip for an airplane that encounters a cross flow with constant velocity W_z moving in the positive direction along the z axis (wind from port). The angle of sideslip relative to the air, β [Equation (4.2)] increases in steps to the value $\beta = -W_z/V_e$, when $t = 0$ ($p = \infty$), and equals zero upon completion of the transient ($t = \infty$; $p = 0$). Figure 4.1 is a schematic diagram of the position of the airplane and of its ground and air speeds, as well as wind velocity vectors within these limit cases. The angle of sideslip with respect to the ground [Equation (4.1)] remains equal to zero when $t = 0$, but it then increases to equal W_z/V_e (Figure 4.1) in the steady-state condition. /143

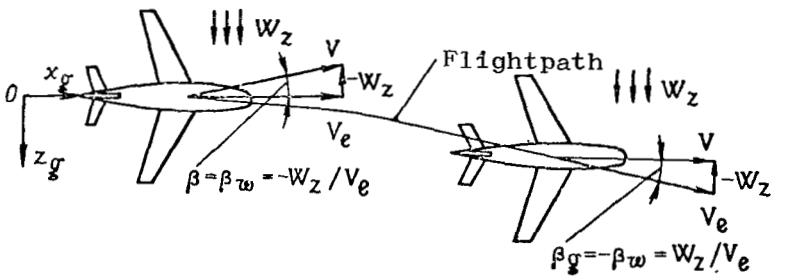

Figure 4.1. Position of the airplane and flight speed and wind velocity vectors when $t = 0$ and $t = \infty$.

The transfer function for the angle of roll is

$$W_{\gamma/w_z}(p)=\frac{1}{V_e}\frac{C(p)}{A(p)}=\frac{1}{V_e}\frac{c_0p^2+c_1p}{A(p)}. \qquad (4.3)$$

The Equation (4.3) transfer function indicates that when the airplane enters a cross gust of positive direction (from port) the airplane banks in the positive direction (on the starboard wing). This roll, or bank, is zero in the steady-state condition.

The transfer function for the angle of yaw is

$$W_{\psi/w_z}(p)=\frac{1}{V_e}\frac{D(p)}{A(p)}=\frac{1}{V_e}\frac{d_0p^2+d_1p}{A(p)}. \qquad (4.4)$$

What follows from Equation (4.4) is that when the airplane enters a cross gust of positive direction, the airplane, able to hold course ($n_\beta = d_0 > 0$), begins to turn to port, and when the transient is over the direction of its longitudinal axis in the horizontal plane returns to where it was prior to

encountering the gust (ψ = 0). The stable airplane endeavors to bring its longitudinal axis into coincidence with the air velocity vector, V, upon encountering a cross gust. /144

The transfer function for the lateral deflection of the center of gravity from the original straight-line flightpath is

$$W_{z_g/w_z}(p) = \frac{b_0 p^3 + (b_1 - d_0) p^2 + (b_2 - d_1) p + a_4}{pA(p)}. \qquad (4.5)$$

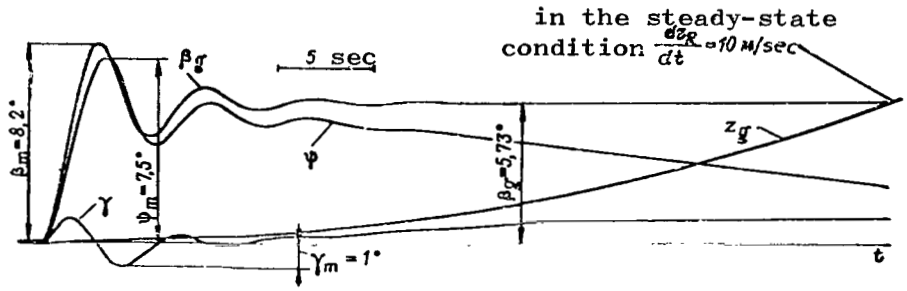

Figure 4.2. Motion of an airplane with fixed controls after entering a rectangular step cross gust.

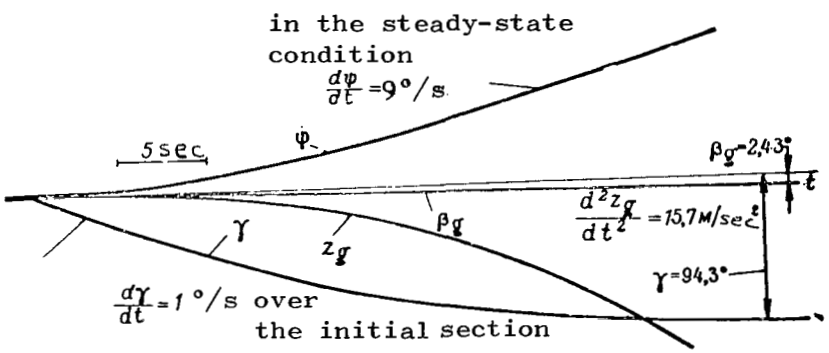

Figure 4.3. Motion of an airplane with fixed controls after entering a vertical gust with constant spanwise gradient.

The operator, p, as a factor in the denominator of Equation (4.5) indicates that in the steady-state condition the coordinate will increase in accordance with a linear law (because of the drift of the airplane in a constant crosswind) as shown in Figure 4.1.

We have included the transients for the lateral motion of Airplane No. 1 with fixed controls (Figures 4.2 and 4.3) to illustrate the conclusions arrived at from an analysis of the Equations (4.1) - (4.5) transfer functions.

Certain remarks are pertinent prior to proceeding to an analysis of the oscillogram in Figure 4.2. The airplane investigated, like many other airplanes, has spiral instability without a control system. This is expressed /145
mathematically by the coefficient a_4 of the characteristic polynomial A(p) [Equations (4.1) - (4.5)] being found negative. The airplane with spiral instability, being on its own, deviates very slowly from the assigned direction of flight. But the very slowness of the process is the reason why piloting the airplane is not complicated, the more so because the pilot, using the controls (particularly the ailerons) constantly, overcomes the effect of spiral instability. However, it is extremely inconvenient to have to deal with an unstable system when integrating equations describing airplane motion on analog computers. Moreover, the presence, or absence, of a slight spiral instability is of no moment on what is in practice the important period of the airplane's reaction to the wind, the initial period (up to 5 to 10 seconds). The coefficient a_4 of the polynomial A(p) must be made positive in order to eliminate this instability and at the same time simplify the investigation of airplane motion on an analog computer. All that need be done is to set $t_{\dot{\psi}}$ equal to zero, as follows from Equation (C.1) in Appendix C. This has no significant effect on the airplane's lateral motion. This was done in the example considered and the numerical values of the transfer function for Airplane No. 1, cited in Appendix C, were computed on the assumption that $t_{\dot{\psi}} = 0$. But even given this assumption, the small root of the characteristic polynomial, equal approximately to the ratio a_4/a_3, causes such a slow damping of the transient, particularly that of the angle of yaw, that the zero drifts in the integrators have more effect on the steady-state condition than do the values of the transfer function coefficients. The coefficient a_4 in the example therefore was increased artificially in order to speed up transient damping time. This is why the oscillograms for the airplane with autopilot shown in Figures 4.2 and 4.3 should be regarded as a sufficiently accurate illustration for the first 5 to 10 seconds, and qualitatively correct for the steady-state condition. The values of the parameters in the steady-state condition, indicated in Figure 4.2, were determined in terms of the transfer functions, so they too are accurate, but the time of attainment of this condition will be considerably longer than is the case on the oscillograms shown. This distortion of the real picture is not very significant because when the

gust acts on the airplane with autopilot what is of practical importance is the reaction of the airplane in the first seconds after encountering the gust. This is when the pilot exercises control, and the subsequent motion of the airplane is primarily the result of actions taken by the pilot. This same approach should be taken to the consideration of the transfer functions for the airplane without autopilot shown in Figures 4.2 and 4.3.

The oscillogram in Figure 4.2 illustrates the behavior of Airplane No. 1 acted on by a crosswind, W_z, of the unit function type with intensity 10 m/s. /146 The curves for angles β_g, γ, ψ and for the linear coordinate of the center of gravity, z_g, qualitatively confirm the conclusions drawn as a result of the analysis of the Equations (4.1) - (4.5) transfer functions. However, the transient damping time should be much longer than follows from the oscillograms. This time can be evaluated quite accurately by setting it equal to the three time constants for the exponent determined by the small root of the polynomial A(p). This root is $p_4 \cong a_4/a_3 = 0.01$ sec^{-1}. The time constant is $T = 1/p_4 = 100$ sec, and the transient damping time is about 300 seconds.

There is an undesirable oscillation over the initial section in the reaction of the airplane without autopilot to a crosswind.

Let us now consider the transfer functions for the same parameters of the airplane's lateral motion on which the normal wind component with constant gradient over the wind span, $\omega_{wx} = dw_y/dz$, is acting.

The transfer function for the angle of sideslip is (because $w_z = 0$, the ground and air angles of sideslip coincide)

$$W_{\beta/\omega_{wx}}(p) = -l_\gamma \frac{E(p)}{A(p)} = -l_\gamma \frac{e_0(p) + e_1}{A(p)}. \qquad (4.6)$$

The minus sign in Equation (4.6) means that when ω_{wx} is positive (when the wind is stronger on the starboard wing[3]), the angle of sideslip will be negative, that is, the airplane will sideslip on the port wing.

The transfer function for the angle of roll is

---

3. When the conditions are such that the wind velocity is upward.

$$W_{\gamma/\omega_{wx}}(p) = -l_{\gamma}^{\cdot}\frac{F(p)}{A(p)} = -l_{\gamma}^{\cdot}\frac{p^2 + f_1 p + f_2}{A(p)}. \qquad (4.7)$$

What follows from Equation (4.7) is that when ω_{wx} is positive the airplane will drop its port wing (negative angle of roll).

The transfer function for the angle of yaw is

$$W_{\psi/\omega_{wx}}(p) = l_{\gamma}^{\cdot}\frac{G(p)}{pA(p)} = l_{\gamma}^{\cdot}\frac{g_0 p^2 + g_1 p + g_2}{pA(p)}. \qquad (4.8)$$

Equation (4.8) shows that when ω_{wx} is positive the airplane will turn counter clockwise continuously.

The transfer function for the coordinate of the center of gravity is

$$W_{z_g/\omega_{wx}}(p) = -l_{\gamma}^{\cdot} V_e \frac{(e_0 + g_0)p^2 + (e_1 + g_1)p + g_2}{p^2 A(p)}. \qquad (4.9)$$

Equation (4.9) says that when ω_{wx} is positive in the steady-state condition the lateral coordinate of the airplane's center of gravity will increase in proportion to the square of the time in the direction of the negative section of the z_g axis. /147

Figure 4.3 shows the oscillograms obtained upon integrating the system of equations at (2.28) for Airplane No. 1 with the effect of the normal wind component with constant spanwise gradient taken into consideration. This gradient, $\omega_{wx} = dw_y/dz$, was taken as equal to 1 °/s, corresponding to inhomogeneity of the vertical wind component in terms of the span equal to 0.0175 m/sec per 1 meter of wing span. The steady-state values of all parameters, other than β, are extraordinarily large (see Figure 4.3), despite the low gradient. This is further confirmation of the conditional nature of the oscillograms presented for the total duration of the transients of the lateral motion of an airplane without autopilot. It is obvious that long before these transients have subsided the angle of roll will have become so large that the linear ratio of the forces and moments to the motion parameters will have been upset, and that Equation (2.28), obtained by the linearization method for small deviations of the parameters from their values in the undisturbed condition, will no longer be valid. Moreover, in the real atmosphere there are no wind gusts with gradient dw_y/dz of constant sign over long distances that the airplane

will traverse, even over a period of several tens of seconds.

Accordingly, the transients shown in Figure 4.3, as well as those in Figure 4.2, can be considered as quantitatively correct only for the first 5 to 10 seconds after the initiation of the gust action. The actual duration of the transients shown in Figure 4.3 too will be close to 300 seconds, and this is greatly in excess of the time shown on the oscillogram.

Now let us consider the transfer functions for the airplane with autopilot. These transfer functions can be obtained from Equation (2.30). We will begin our analysis of the transfer functions relative to the crosswind, w_z.

The transfer function for the ground angle of sideslip is

$$W_{\beta_g/w_z}(p)=\frac{1}{V_e}\frac{B'(p)}{A'(p)}=\frac{1}{V_e}\frac{b_0'p^4+b_1'p^3+b_2'p^2+b_3'p+a_5'}{p^5+a_1'p^4+a_2'p^3+a_3'p^2+a_4'p+a_5'}. \tag{4.10}$$

The transfer function for the angle of sideslip relative to the wind is

$$W_{\beta/w_z}(p)=-\frac{1}{V_e}\frac{p^5+(a_1'-b_0')p^4+(a_2'-b_1')p^3+(a_3'-b_2')p^2+(a_4'-b_3')p}{A'(p)} \tag{4.11}$$

The transfer function for the angle of roll is /148

$$W_{\gamma/w_z}(p)=\frac{1}{V_e}\frac{C'(p)}{A'(p)}=\frac{1}{V_e}\frac{c_0'p^3+c_1'p^2+c_2'p}{A'(p)}. \tag{4.12}$$

The transfer function for the angle of yaw is

$$W_{\psi/w_z}(p)=\frac{1}{V_e}\frac{D'(p)}{A'(p)}=\frac{1}{V_e}\frac{d_0'p^3+d_1'p^2+d_2'p}{A'(p)}. \tag{4.13}$$

The transfer function for the coordinate of the center of gravity is

$$W_{z_g/w_z}(p)=\frac{b_0'p^4+(b_1'-d_0')p^3+(b_2'-d_1')p^2+(b_3'-d_2')p+a_5'}{pA(p)}. \tag{4.14}$$

A comparison of the Equations (4.1) - (4.5) transfer functions for the airplane without autopilot with the Equations (4.10) - (4.14) transfer functions for the airplane with autopilot will show that the structure of the functions is unchanged. Therefore, the reaction of an airplane with autopilot to a crosswind will remain as it was in the consideration of the above reaction to this wind in the case of the airplane without autopilot, at least in a qualitative

way. The only effect of the autopilot is to improve the quality of the transients of the lateral motion of the airplane, primarily in reducing transient time. Moreover, the nature of the transients can be made more favorable, that is, nonoscillatory.

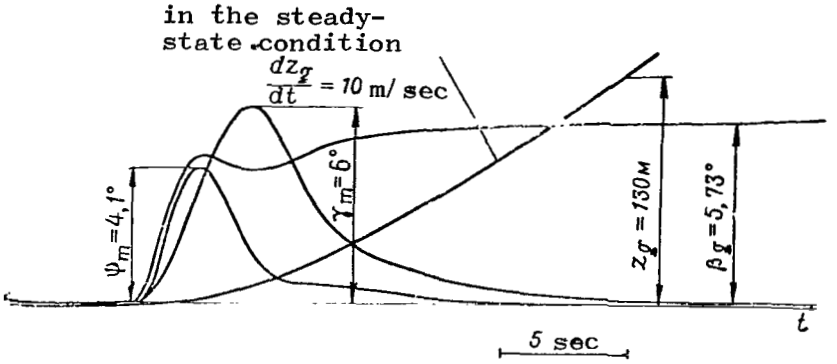

Figure 4.4. Motion of an airplane with autopilot after encountering a rectangular step gust.

We will illustrate what has been said by an example, using the same Airplane No. 1. The transients in Figure 4.4 show the change in angles β_g, γ and ψ, and in the coordinate z_g when the airplane with autopilot encounters a crosswind with constant velocity w_z = 10 m/s. Comparison of these curves with the curves for the airplane without autopilot (see Figure 4.2) confirms the conclusion arrived at above with respect to what is, in principle, the identical nature of the transients in both cases. This comparison also shows the sharp /149 reduction in time and improvement in the quality of the transients when there is an autopilot.

Now let us consider the transfer functions for an airplane with an autopilot acted on by the normal wind component with constant spanwise gradient $\omega_{wx} = dw_y/dz$.

The transfer function for the angle of sideslip is

$$W_{\beta_g/\omega_{wx}}(p) = -l_\gamma \frac{E'(p)}{A'(p)} = -l_\gamma \frac{e_0' p^2 + e_1' p + e_2'}{A'(p)}. \qquad (4.15)$$

The transfer function for the angle of roll is

$$W_{\gamma/\omega_{wx}}(p) = -l_\gamma \frac{F'(p)}{A'(p)} = -\frac{p^3 + f_1' p^2 + f_2' p + f_3'}{A'(p)}. \qquad (4.16)$$

The transfer function for the angle of yaw is

$$W_{\psi/\omega_{wx}}(p)=l_{\dot{\gamma}}\frac{G'(p)}{A'(p)}=l_{\dot{\gamma}}\frac{g_0'p^2+g_1'p+g_2}{A'(p)}. \qquad (4.17)$$

The transfer function for the coordinate of the center of gravity is

$$W_{z_g/\omega_{wx}}(p)=-l_{\dot{\gamma}}V_e\frac{(e_0'-g_0')p^2+(e_1'-g_1')p+e_2'+g_2'}{A'(p)}. \qquad (4.18)$$

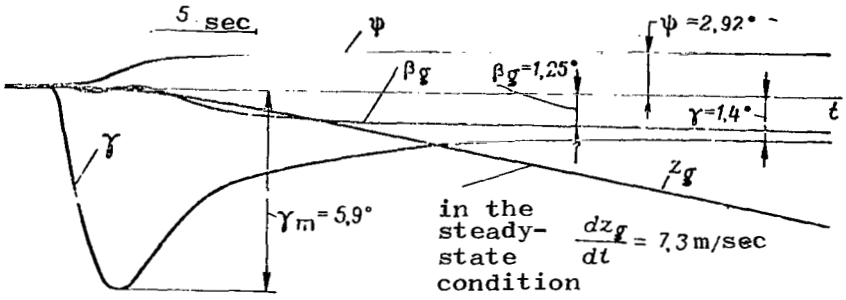

Figure 4.5. Motion of an airplane with autopilot after encountering a vertical gust with constant spanwise gradient.

Pointed out in the foregoing was the fact that when an airplane encounters a crosswind the transfer functions (and, as a result, the transient) are, in principle, identical in nature, with, and without, an autopilot. The transients differ only in the time and degree of damping of oscillations. But when an airplane encounters a vertical gust with constant spanwise gradient, there is a difference. A comparison of Equations (4.6) - (4.9) transfer functions for the airplane without autopilot with the Equations (4.15) - /150
(4.18) transfer functions for the airplane with autopilot reveals that the structure of the transfer functions does not change for angles β and γ, that there is a limit to angle ψ when there is an autopilot, and that a constant velocity is retained for the coordinate of the center of gravity in the steady-state condition, that is, there is no acceleration. Moreover, just as in the case of the crosswind, the autopilot should reduce the duration of the transients sharply. Finally, the autopilot reduces many fold the deviation of the steady-state condition parameters from their values in the undisturbed condition.

Figure 4.5 illustrates this, showing the transfer functions for the

parameters of the lateral motion when the airplane encounters a vertical gust with constant spanwise gradient. We should emphasize the fact that in order to obtain marked deviations from the undisturbed condition the gust gradient, ω_{wx}, is taken 10 times that of the case of the airplane without autopilot, that is, at 10 °/s, corresponding to an inhomogeneity in the vertical spanwise wind component of 0.175 m/s per 1 m of wing span.

The deviations of angles β, γ and ψ from the initial zero value are slight, despite so substantial a gradient. Thus, the autopilot copes well with the external action of the type considered.

In conclusion, we should point out that the oscillograms in Figures 4.4 and 4.5 for the airplane with autopilot, as distinguished from the oscillograms in Figures 4.2 and 4.3, contain no conditionalities, and accurately describe the motion of an airplane acted on by wind gusts of the type indicated in the foregoing, the assumptions made taken into consideration, of course.

4.2. Forces and Moments Determining the Lateral Motion of an Airplane in Turbulent Air.

As pointed out in section 4.1, the expressions for forces and moments acting on an airplane in disturbed air, cited in that section, can be used only to analyze the motion of an airplane the result of single gusts of a previously selected form. There are no such gusts under real flight conditions, however. So the conclusions in the preceding section are of interest primarily for evaluating the effect of constant crosswind causing the airplane to drift. An analysis of the effect of the normal wind component with constant spanwise gradient was made in order to obtain the transfer functions used in what follows.

The purpose of this section is to obtain analytical expressions for the forces and moments causing a disturbance in the lateral motion of an airplane in turbulent air; that is, under conditions much closer to reality than those considered in section 4.1. Therefore, expressions for the right sides of /151
Equations (2.28) and (2.30) will be considered in what follows, because it is these right sides that are the result of wind action. So far as the left sides of the equations are concerned, they take into consideration the forces

and moments occurring as a result of the motion of the airplane proper, and not of the air. Since airplane motion resulting from the wind has approximately the same linear and angular velocities as would be present when the controls are used, the left sides of Equations (2.28) and (2.30) can be used to describe this motion.

The vertical tail and the fuselage play the biggest role in creating the lateral forces and moments relative to the x and y axes of the crosswind. In the general statement of the problem with regard to the action of the crosswind on the airplane, the coefficients of the forces and moments the result of the wind are functions of the frequency of change in this wind [31]. However, [29] contains experimental data showing that the lateral force and moments from wind w_z relative to the x and y axes depend only slightly on the frequency (within the limits of frequencies practically appearing to act on the lateral motion of the airplane). We will, in this book, therefore take it that the coefficients k_β, t_β and n_β in the right sides of Equations (2.28) and (2.30) are constants, established using the formulas in Table 2.2.

An expression for the correlation function and the spectral density of the random crosswind component, w_z, must also be selected. Figure 1.10 suggests the use of Equations (1.13) and (1.29) for the lateral correlation functions, and of Equations (1.19), (1.22), and (1.33) for the spectral density, in the case of crosswind.

Let us proceed to the determination of the moment relative to the x axis, attributable to the spanwise normal wind gradient. This moment can be expressed as follows within the limits of the linear section of the $C_y = f(\alpha)$ curve

$$M_x = m_x l S q_e = \int_{-l/2}^{l/2} Y^z(z)\, z\, dz, \tag{4.19}$$

where

Y^z is the antisymmetrical spanwise lift per unit length (at the z section).

This antisymmetrical spanwise lift can be determined through the formula

$$Y^z(z) = C_y(z)\, q_e b(z), \tag{4.20}$$

where

$C_y(z)$ is the antisymmetrical lift factor at the z section;

$b(z)$ is the chord of the wing at the z section;

q_e is the velocity head in undisturbed motion.

The antisymmetrical lift factor at the z section can be expressed in the form /152

$$C_y(z)=C_y^{\alpha}(z)\alpha_w, \tag{4.21}$$

where

$C_y^{\alpha}(z)$ is the slope of the curve of $C_y(z) = f(\alpha)$;

$\alpha_w = w_y(x, z)/V_e$ is the angle of attack at the z section, attributable to the wind, w_y.

When Equation (4.20) and Equation (4.21) are taken into consideration, Equation (4.19) acquires the form

$$m_x lSq_e=\int_{-l/2}^{l/2} C_y^{\alpha}(z)\alpha_w q_e b_z(z)\,dz. \tag{4.22}$$

Making elementary transformations in Equation (4.22), we obtain an expression for the rolling-moment coefficient attributable to normal wind as a function of the x coordinate, establishing the position of the airplane's center of gravity on the flightpath

$$m_x(x)=\frac{-m_x^{\bar{\omega}_x}}{4V_e}\int_{-1}^{1}\varepsilon(\bar{z})w_y(x,\bar{z})\,d\bar{z}, \tag{4.23}$$

where

$$\varepsilon(\bar{z})=\frac{C_y^{\alpha}(\bar{z})\bar{z}b(\bar{z})}{-m_x^{\bar{\omega}_x}b_a} \tag{4.24}$$

and

$$\bar{z}=2z/l.$$

The function $\varepsilon(\bar{z})$ is the distribution of the wing lift when there is a linear, antisymmetrical spanwise change in the angle of attack.

Now let us proceed to a determination of the correlation functions for the rolling-moment coefficient attributable to the nonuniform and random spanwise vertical wind component. With Equation (4.23) as a basis, this function can be established through the expression

$$R_{m_x}(x_2-x_1)=\lim_{X\to\infty}\frac{1}{2X}\int_{-X}^{X}m_x(x_2)\,m_x(x_1)\,dx_1=\lim_{X\to\infty}\frac{1}{2X}\times$$

$$\times\int_{-X}^{X}\frac{\left(m_x^{\bar{\omega}_x}\right)^2}{16V_e^2}\int_{-1}^{1}\varepsilon(\bar{z}_1)\,w_y(x_1,\ \bar{z}_1)\,d\bar{z}_1\int_{-1}^{1}\varepsilon(\bar{z}_2)\,w_y(x_2,\ \bar{z}_2)\,d\bar{z}_2dx_1=$$

$$=\frac{\left(m_x^{\bar{\omega}_x}\right)^2}{16V_e^2}\int_{-1}^{1}\int_{-1}^{1}\varepsilon(\bar{z}_1)\,\varepsilon(\bar{z}_2)\,R_{w_y}(x_2-x_1,\ \bar{z}_2-\bar{z}_1)\,d\bar{z}_1d\bar{z}_2, \tag{4.25}$$

where /153

$$R_{w_y}(x_2-x_1,\ \bar{z}_2-\bar{z}_1)=\lim_{X\to\infty}\frac{1}{2X}\int_{-X}^{X}w_y(x_1,\ \bar{z}_1)\,w_y(x_2,\ \bar{z}_2)\,dx_1. \tag{4.26}$$

The correlation function for the vertical wind component depends on two coordinates. This function has already been taken up in Chapter 3 in the analysis of the averaging effect of the wing span on the lift created by the vertical wind [Equation (3.58)]. Based on an assumption of axisymmetry of turbulence, it can be taken that this correlation function is dependent only on the absolute value of the spatial displacement; that is, on $\sqrt{(x_2-x_1)^2+(z_2-z_1)^2}$.

Introducing new variables by substitutions

$$x_2-x_1=V\tau,$$

$$\bar{z}_2-\bar{z}_1=2\Delta z/l=\eta,$$

Equation (4.25) can be presented in the form

$$R_{m_x}(V_e\tau)=\frac{\left(m_x^{\bar{\omega}_x}\right)^2}{8V_e^2}\int_0^2\Gamma(\eta)\,R_{w_y}(V_e\tau,\ \eta)\,d\eta, \tag{4.27}$$

where

$$\Gamma(\eta)=\int_{-1}^{1-\eta}\varepsilon(\bar{z}_1)\,\varepsilon(\bar{z}_1+\eta)\,d\bar{z}_1 \tag{4.28}$$

and

$$R_{w_y}(V_e\tau,\ \eta)=\sigma_w^2R_n\left[\sqrt{(V_e\tau)^2+(l\eta/2)^2}\right]. \tag{4.29}$$

R_n in Equation (4.29) is the lateral correlation function, determined through Equation (1.13) and Equation (1.29). The explanation of the transformations made in the transition from Equation (4.25) to Equation (4.27) is contained in Appendix C.

Since we are using the spectral densities apparatus for the computation, a transition is necessary from the correlation function of Equation (4.27) to the spectral density of the rolling-moment coefficient. A Fourier transform provides

$$S_{m_x}(\omega)=\frac{1}{\pi V_e}\int_{-\infty}^{\infty} R_{m_x}(V_e\tau)\,e^{-j\frac{\omega}{V_e}V_e\tau}\,d(V_e\tau). \tag{4.30}$$

Substituting the expression for $R_{m_x}(V_e\tau)$ in Equation (4.30), we obtain

$$S_{m_x}(\omega)=\frac{\left(\overline{m_x^{\omega}}\right)^2}{8\pi V_e^3}\int_0^2 \Gamma(\eta)\,P(\omega/V_e,\ \eta)\,d\eta, \tag{4.31}$$

$$P(\omega/V_e,\ \eta)=\int_{-\infty}^{\infty} e^{-j\frac{\omega}{V_e}V_e\tau}R_{w_y}(V_e\tau,\quad \eta)\,d(V_e\tau). \tag{4.32}$$ /15

The following types of spanwise lift are usually taken into consideration in a theoretical analysis of the forces and moments created by the wing; uniform, elliptical, parabolic, and triangular. These terms establish the nature of the lift distribution for a step change in the wing angle of attack. Reference [32] points out that the nature of the spanwise lift has little effect on the spectral density of the moment coefficient. Therefore, only the simplest case of uniform spanwise lift will be considered.

The derivation of the formula for the function $\varepsilon(\overline{z})$ in the case of uniform spanwise lift is given in Appendix C. Substituting the value of this function in Equation (4.28) from Equation (4.31), we obtain a formula for the spectral distribution of the rolling-moment coefficient attributable to the nonuniformity of the spanwise normal wind [32]

$$S_{m_x}(\omega)=\sigma_w^2\,\frac{\left(\overline{m_x^{\omega}}\right)^2 L}{\pi V_e^2}\,S_k(\nu). \tag{4.33}$$

The function $S_k(\nu)$ in the right side of Equation (4.33) in turn is determined through the expression (derivation of this formula is contained in Appendix C)

$$S_k(\nu)=\frac{18}{a^4(1+\nu^2)^2}\left\{a^3\nu^2\int_0^a K_0(x)\,dx+[a^4+16a^2(1-\nu^2)]\,K_0(a)+\right.$$

$$\left.+[2a^3(3-\nu^2)+32a(1-\nu^2)]\,K_1(a)+2a^2(1-3\nu^2)-32(1-\nu^2)\right\}, \tag{4.34}$$

where

$a=k\sqrt{1+\nu^2}$, $k=l/L$ and $K_0(a)$, $K_1(a)$ are modified Bessel functions of the second kind of zero and first orders [33].

The dimensionless frequency v, since it is the Equation (4.34) argument, is linked with the timed frequency, ω, by Equation (1.20) and Equation (1.31), from whence it follows that

$$\nu=\omega L/V_e. \tag{4.35}$$

Figure 4.6 shows the graphics for the function $S_k(\nu)$, constructed using Equation (4.34) for various k values, the ratio of the wing span to the turbulence scale.

/155

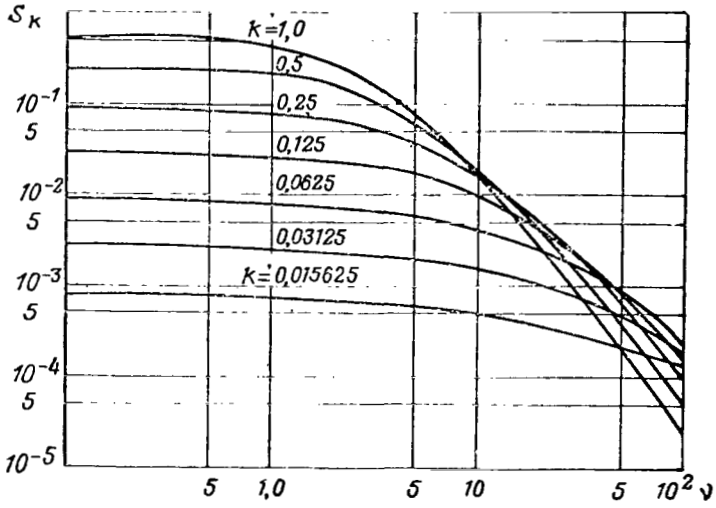

Figure 4.6. Graphics of the function $S_k(\nu)$ contained in the expression for the spectral density of a dimensionless rolling-moment coefficient.

As follows from Equation (4.19), Equation (4.33) expresses the spectral density of a dimensionless rolling-moment coefficient. This coefficient must be multiplied by $\frac{1}{2}S\rho_e V_e^2/2$ and divided by I_x to arrive at the form in which moments can be computed using Equations (2.28) and (2.30). These additional factors are squares in the spectral density expression. The final form of the spectral density of the rolling-moment coefficient attributable to the nonuniform spanwise vertical wind component is as follows after transform-

ations.

$$S_{m_x}(\omega)=\sigma_w^2\frac{8\left(\overline{m_x^{\omega}}\right)^2L}{\pi i_x^2 l^3\tau_{el}^4\delta}S_k(\nu)=\sigma_w^2AS_k(\nu). \tag{4.36}$$

The use of Equation (4.36) to compute the parameters of the lateral motion will be explained in the next section.

4.3. Lateral Motion of an Airplane in Turbulent Air

The lateral motion of an airplane in disturbed air is a composite of two components, as Equations (2.28) and (2.30), as well as the transfer and response functions reviewed in Section 4.1, show. One is attributable to the crosswind, w_z, the other to the spanwise normal wind gradient. /156

Let us investigate the lateral motion of an airplane in turbulent air by modeling, the general methodology for which was explained in Section 2.5. The only difference will be in the analysis of the lateral motion component attributable to the nonuniform spanwise normal wind gradient, and this difference will be discussed in what follows.

Let us proceed to an analysis of each of the above-mentioned lateral motion components.

Lateral motion the result of crosswind. Modeling provides quite complete characteristics of lateral motion the result of crosswind in turbulent air.

The probability characteristics for a crosswind have the same form as for a normal wind, as was pointed out in Section 4.2. Therefore, the transfer functions and the structural diagrams for shaping filters for determining the spectral density and dispersion of the lateral motion parameters the result of crosswind action will be those reviewed in Section 2.5 for the normal wind.

These filters are combined with a dynamic model of the lateral motion, assembled on the basis of Equations (2.28) and (2.30) on an analog computer.

Let us consider the results of modeling the lateral motion the result of crosswind for Airplane No. 1, a big passenger plane. This airplane has an autopilot with cross-couplings in the course and roll channels. The values of the autopilot gains and of the coefficients of the equations are listed in Appendix C.

Figure 4.7 shows the graphics of normalized spectral densities of angles of roll and yaw, as well as the lateral acceleration for Airplane No. 1 with autopilot. Figure 4.8 shows the same data, but for Airplane No. 1 without autopilot. All graphics were normalized in terms of the crosswind dispersion.

Figures 4.7 and 4.8 show three spectral density graphics for three different turbulence scales; curve 1 for L = 50 m, curve 2 for L = 500 m, and curve 3 for L = 1,500 m.

Analysis of the graphics in Figures 4.7 and 4.8 shows that the autopilot with the cross-couplings significantly increases the spectral densities of the roll and of the acceleration at low frequencies. The peak of the oscillations in the angle of yaw occurs in this range ($\omega < 1$ sec^{-1}). The cross-couplings for the autopilot also cause the oscillations in the angle of yaw to increase the roll (and acceleration) oscillations. The cross-coupling of the roll to the course usually is slight, so course oscillations are not increased, but decrease when an autopilot with this type of coupling is used.

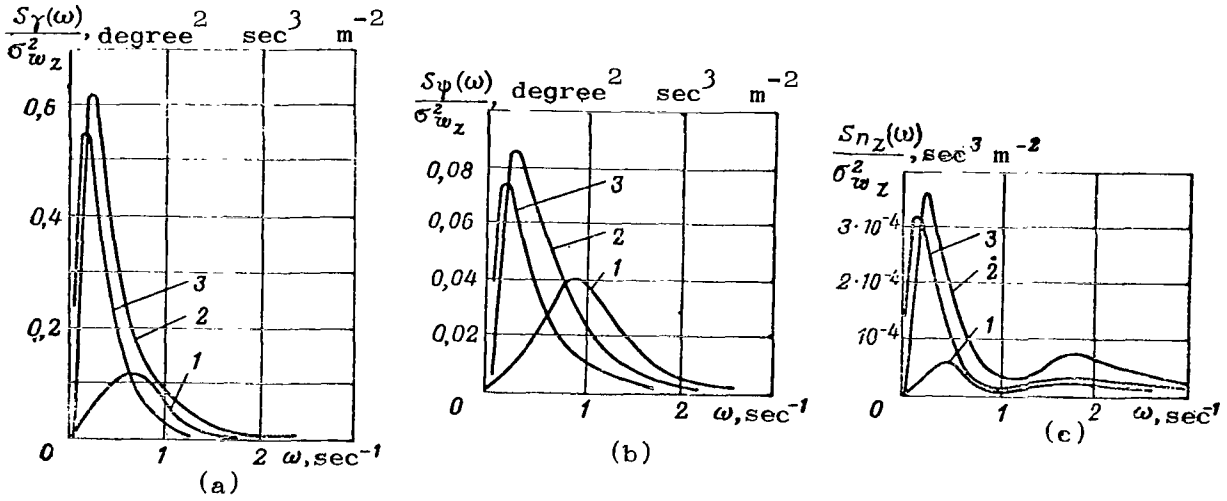

/157

Figure 4.7. Normalized spectral densities of angles of roll (a) and yaw (b) and lateral acceleration of Airplane No. 1 (c) with autopilot, the result of crosswind.

1 - L = 50 m; 2 - L = 500 m; 3 - L = 1,500 m.

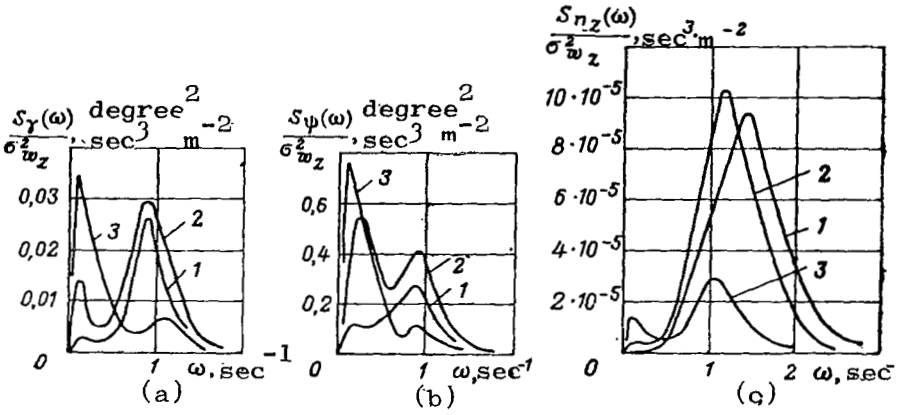

Figure 4.8. Normalized spectral densities of angles of roll (a) and yaw (b) and lateral acceleration (c) for Airplane No. 1 with fixed controls, the result of crosswind.

1 - L = 50 m; 2 - L = 500 m; 3 - L = 1,500 m.

/158

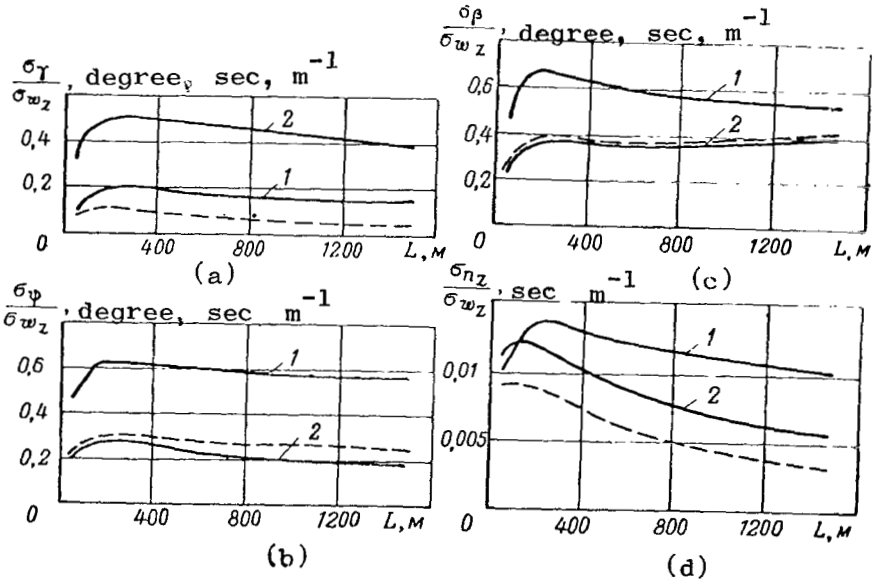

Figure 4.9. Normalized root-mean-squares of parameters of lateral motion of Airplane No. 1 (a - angle of roll; b - angle of yaw; c - angle of sideslip; d - lateral acceleration) as a function of the turbulence scale (as a result of crosswind).

1 - with fixed controls; 2 - with autopilot; dashed with autopilot without cross-couplings.

Figures 4.7 and 4.8 can be used to explain the effect the turbulence scale, L, has on the dispersion of the lateral motion parameter. The effect of L is more clearly expressed in Figure 4.9, however, for here the root-mean-squares of these parameters are presented as a function of the turbulence scale. These values are for the root-mean-square of the crosswind. Curves numbered 1 are for the airplane without autopilot, those numbered 2 for the airplane with autopilot. The graphics in Figure 4.9 confirm the above conclusion with respect to the effect the autopilot with cross-couplings has on the lateral motion of the airplane acted on by a crosswind. Moreover, these graphics provide the basis for the assertion that the root-mean-squares of changes in the lateral motion parameters the result of the crosswind depend less on the turbulence scale than on the root-mean-squares of the longitudinal motion parameters. The only significant reduction in root-mean-squares occurs in the very low scale region (L < 100 m), something very seldom encountered, and generally speaking not encountered under real flight conditions.

/159

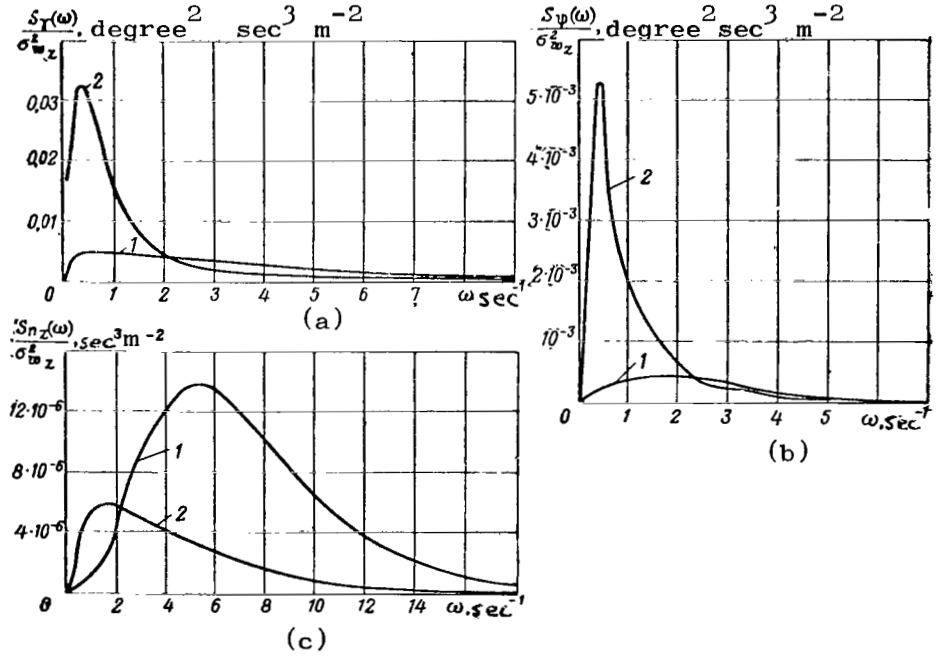

Figure 4.10. Normalized spectral densities of angles of roll (a) and yaw (b) and lateral acceleration (c) for Airplane No. 2 with autopilot, the result of crosswind.

1 - L = 50 m, 2 - L = 500 m.

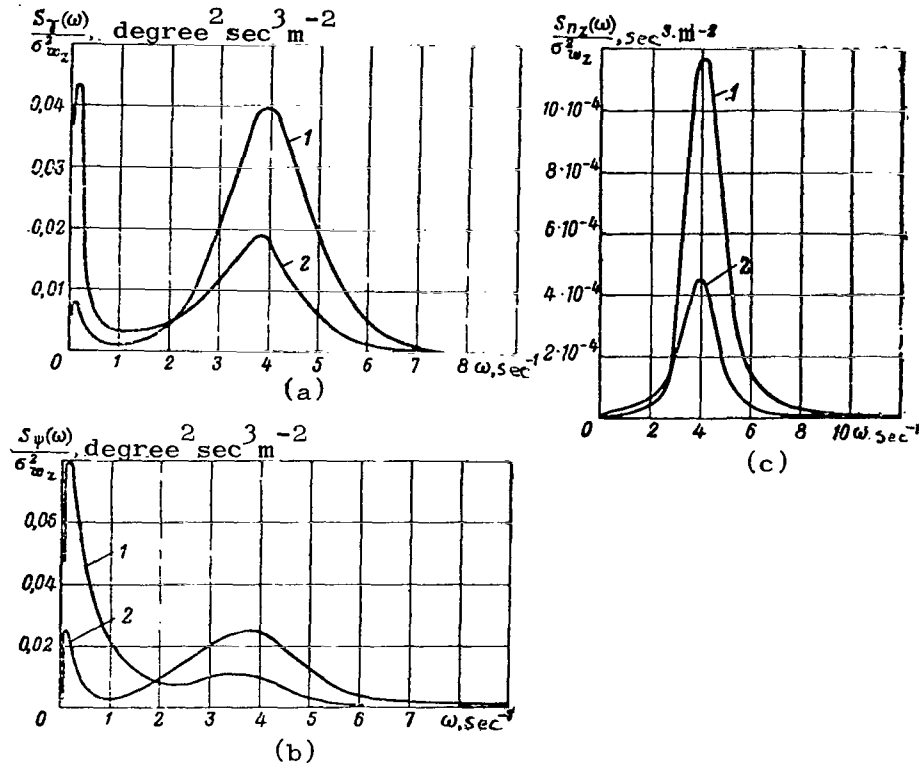

Figure 4.11. Normalized spectral densities of angles of roll (a), yaw (b), and lateral acceleration (c) for Airplane No. 2 with fixed controls, the result of cross-wind.

1 - L = 50 m, 2 - L = 500 m.

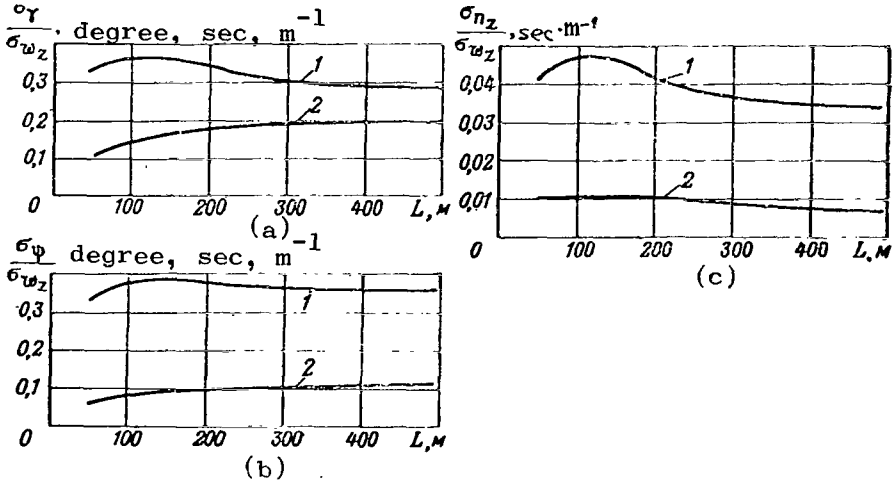

Figure 4.12. Normalized root-mean-squares of parameters of lateral motion of Airplane No. 2 (a - angle of roll; b - angle of yaw; c - lateral acceleration) as a function of the turbulence scale) (as a result of crosswind).

1 - with fixed controls: 2 - with autopilot.

Let us review the results of modeling the lateral motion resulting from crosswind in the case of Airplane No. 2, a single-seat fighter plane. Figure 4.10 presents the graphics of the normalized spectral density of angles of roll and yaw, as well as the lateral acceleration for Airplane No. 2 with autopilot without cross-couplings. Figure 4.11 presents these same data for Airplane No. 2 without autopilot. Graphics numbered 1 correspond to a turbulence scale L = 50 m, those numbered 2 to L = 500 m.

Figure 4.12 presents the root-mean-squares of these same parameters as a function of the turbulence scale, L. The curves numbered 1 in Figure 4.12 are for the airplane with fixed controls, those numbered 2 for the airplane with autopilot.

The following conclusions can be drawn from a comparison of the graphics for the spectral densities and root-mean-squares of the deviations in the parameters of the lateral motion of Airplanes No. 1 and No. 2, the result of crosswind:

(1) the spectra of all parameters for Airplane No. 2 are much broader than for Airplane No. 1, explained by the very good course stability and high speed of Airplane No. 2;

(2) the root-mean-squares of the disturbances of the parameters for both airplanes differ but little, although the airplanes are completely different so far as characteristics are concerned;

(3) lack of cross couplings in the autopilot of Airplane No. 2 results in a more efficient autopilot in the sense that there is a reduction in the roll and lateral acceleration oscillations attributable to crosswind. /161

Lateral motion when there is a spanwise normal wind gradient. The methodology used to model the lateral motion of an airplane in turbulent air when there is a spanwise normal wind gradient differs somewhat from the methodology described in the foregoing for modeling this motion resulting from crosswind. The difference arises because the rolling moment created by the spanwise normal wind gradient is computed using Equations (4.34) - (4.36) for the spectral density of the rolling-moment coefficient of this moment. As Equation (4.34) indicates, the spectral density of the rolling-moment coefficient is a quite complex function of the dimensionless frequency, v, and does not have

the form required for the transition to the transfer function for the shaping filter.[4] Therefore, the modeling requires that Equation (4.34) approximate a rational fractional function containing only even powers. The approximating functions obtained by the selected points method [34] for all values of k = l/L, shown in Figure 4.6, are in the form

$$\left.\begin{aligned}
k=1{,}0, &\quad S_k(\nu)=\frac{0{,}52+0{,}0175\nu^2}{1+0{,}25\nu^2+0{,}01\nu^4},\\
k=0{,}5, &\quad S_k(\nu)=\frac{0{,}23+0{,}0055\nu^2}{1+0{,}169\nu^2+0{,}002\nu^4},\\
k=0{,}25, &\quad S_k(\nu)=\frac{0{,}09+0{,}0034\nu^2}{1+0{,}12\nu^2+0{,}0019\nu^4},\\
k=0{,}125, &\quad S_k(\nu)=\frac{0{,}03+0{,}0016\nu^2}{1+0{,}12\nu^2+0{,}0007\nu^4},\\
k=0{,}0625, &\quad S_k(\nu)=\frac{0{,}009+0{,}0000353\nu^2}{1+0{,}018\nu^2+0{,}0000163\nu^4},\\
k=0{,}03125, &\quad S_k(\nu)=\frac{0{,}0028+0{,}00007\nu^2}{1+0{,}059\nu^2+0{,}0000275\nu^4},\\
k=0{,}015625, &\quad S_k(\nu)=\frac{0{,}0008+0{,}000183\nu^2}{1+0{,}34\nu^2+0{,}00011\nu^4}
\end{aligned}\right\} \qquad (4.37)$$

Let us emphasize the fact that Equation (4.37) can be used to analyze the lateral motion of any airplane, because the dimensionless frequency, v, and the relative wing span, k, appear in them.

If Equation (4.37) is written in the form /162

$$S_k(\nu)=\frac{c_0\nu^2+c_1}{d_0\nu^4+d_1\nu^2+1}, \qquad (4.38)$$

the general form of the transfer function for the shaping filter for obtaining the spectral density of the lateral motion parameters will be

$$W_{x/x_1}(\bar{p})=\sigma_w\sqrt{A}\,\frac{b_1\bar{p}+b_1}{a_1\bar{p}^2+a_1\bar{p}+1}, \qquad (4.39)$$

where

$\bar{p} = pL/V_e$ is a dimensionless differentiation operator;

---

4. The argument v has even, as well as fractional exponents of the power. Moreover, Bessel functions of this argument are contained in Equation (4.34).

$\sqrt{A}=\sqrt{\frac{8L\left(m^{\bar{\omega}_x}_{\bar{x}}\right)^2}{\pi i_x^2 l^3 \tau_c \mu_e}}$ is a factor derived from Equation (4.36);[5]

$$a_0=\sqrt{d_0},\quad a_1=\sqrt{d_1+2\sqrt{d_0}},\quad b_0=\sqrt{c_0},\quad b_1=\sqrt{c_1}. \tag{4.40}$$

From Equation (4.37), and with the help of Equation (4.40), we obtain the following transfer functions for the shaping filter for modeling the spectral density of the lateral motion parameters for various values relative to the wing span, k

$$\left.\begin{aligned}
k=1{,}0,\quad & W_{x/x_1}(\bar{p})=\sigma_w\sqrt{A}\,\frac{0{,}72+0{,}132\bar{p}}{1+0{,}67\bar{p}+0{,}1\bar{p}^2},\\
k=0{,}5,\quad & W_{x/x_1}(\bar{p})=\sigma_w\sqrt{A}\,\frac{0{,}48+0{,}0741\bar{p}}{1+0{,}507\bar{p}+0{,}0447\bar{p}^2},\\
k=0{,}25,\quad & W_{x/x_1}(\bar{p})=\sigma_w\sqrt{A}\,\frac{0{,}3+0{,}0583\bar{p}}{1+0{,}455\bar{p}+0{,}0435\bar{p}^2},\\
k=0{,}125,\quad & W_{x/x_1}(\bar{p})=\sigma_w\sqrt{A}\,\frac{0{,}173+0{,}04\bar{p}}{1+0{,}415\bar{p}+0{,}0264\bar{p}^2},\\
k=0{,}0625,\quad & W_{x/x_1}(\bar{p})=\sigma_w\sqrt{A}\,\frac{0{,}095+0{,}00594\bar{p}}{1+0{,}161\bar{p}+0{,}00404\bar{p}^2},\\
k=0{,}03125,\quad & W_{x/x_1}(\bar{p})=\sigma_w\sqrt{A}\,\frac{0{,}0529+0{,}00836\bar{p}}{1+0{,}263\bar{p}+0{,}0052\bar{p}^2},\\
k=0{,}015625,\quad & W_{x/x_1}(\bar{p})=\sigma_w\sqrt{A}\,\frac{0{,}0283+0{,}0135\bar{p}}{1+0{,}6\bar{p}+0{,}0105\bar{p}^2}.
\end{aligned}\right\} \tag{4.41}$$

It should be emphasized that the turbulence scale, L, changes for various k and fixed t. This is why the factor $\sqrt{A}$ and the coefficient for the transition from a dimensionless $\bar{p}$ to dimensional p differentiation operator will have different values in each of the transfer functions in Equation (4.41). Appendix C lists the transfer functions for Airplanes No. 1 and No. 2, obtained through Equation (4.41). /163

Filters with Equation (4.41) transfer functions were modeled using the arrangement in Figure 2.8, so it should be pointed out that Equation (4.41)

---

5. If the angular magnitudes computed (γ, ψ, β) must be measured in degrees, the coefficient $\sqrt{A}$ must be multiplied by 57.3.

transfer functions have no clear-cut $1/\sqrt{\pi}$ factor, as distinguished from the Equation (2.53) transfer function. The input signal need not be reduced by a factor of $\sqrt{\pi}$, as shown in Figure 2.8.

With the content of section 2.5 in mind, we can say that the transfer function for the shaping filter used to obtain the dispersion of the parameters of the system under investigation (when a unit function is supplied to the input) will differ from the Equation (4.41) transfer functions only in the additional factor $\sqrt{\pi p}$. These filters are modeled using the arrangement in Figure 2.10. The input signal here should be increased by a factor of $\sqrt{\pi}$.

The results of the investigation of the effect of nonuniform spanwise normal wind on Airplanes No. 1 and No. 2 are described below. This investigation was made using modeling based on the methodology described in the foregoing.

Figure 4.13 shows the graphics of the spectral densities for deviation of angle of roll and lateral acceleration of Airplane No. 1 with autopilot the result of a spanwise random vertical wind gradient. Figure 4.14 contains the data for this same Airplane No. 1, but without an autopilot. Data are not provided here on deviations in angle of yaw and angle of sideslip because such deviations from the spanwise nonuniform vertical wind are negligible in magnitude.

Curves numbered 1 in Figures 4.13 - 4.14 are for L = 37.5 m, those numbered 2 are for L = 299.2 m, and those numbered 3 are for L = 1,196.8 m. The scale used for Figure 4.13 is such that the 3 curves cannot be plotted. The use of other than round numbers for the turbulence scale stems from the fact that the curves for the $S_k(v)$ functions in Figure 4.6 used for the computations were constructed for relative span values k = 1, 0.5, etc., corresponding to turbulence scales equal to, and multiples of, the wing span. All graphics of spectral densities in Figures 4.13 - 4.14 have been normalized in terms of the normal wind component dispersion.

The graphics of the angle of roll spectral density for Airplane No. 1 are practically analogous to the graphics for the acceleration, so the autopilot influence can be established by comparing the curves for angle of roll. This comparison shows that the influence of the autopilot on roll oscillations /164

is different than it is in the case of lateral wind action. Course oscillations are small in the case considered. Hence, the autopilot is effective in reducing angle of roll and acceleration oscillations regardless of turbulence scales.

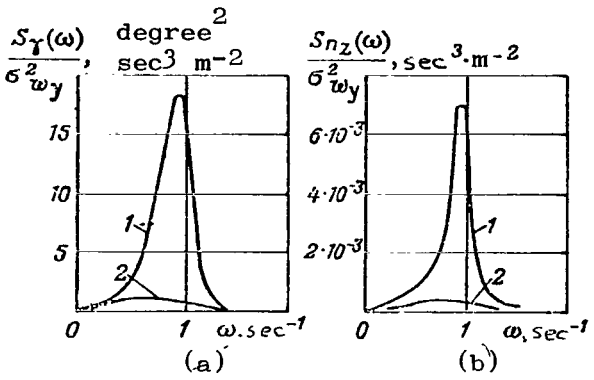

Figure 4.13. Normalized spectral densities of angle of roll (a) and lateral acceleration (b) for Airplane No. 1 with autopilot the result of spanwise nonuniform vertical wind.

1 - L = 37.5 m; 2 - L = 299.2 m.

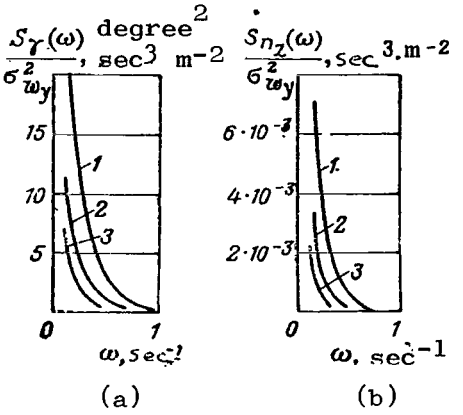

Figure 4.14. Normalized spectral densities of angle of roll (a) and lateral acceleration (b) for Airplane No. 1 with fixed controls the result of spanwise nonuniform vertical wind.

1 - L = 37.5 m; 2 - L = 299.2 m; 3 - L = 1,196.8 m.

A more descriptive idea of the influence the turbulence scale has on the root-mean-squares of the deviations in lateral motion parameters resulting from spanwise nonuniform normal wind is reflected in Figure 4.15. The root-mean-squares of these parameters equate to the root-mean-square of the normal wind. Number 1 curves are for the airplane without autopilot, number 2 curves for the airplane with autopilot. Absence of the curve numbered 1 in Figure 4.15b for the airplane without autopilot results from the fact that the Equation (4.8) transfer function for the angle of yaw contains an integrating link in this case. This, as we know, leads to infinitely large dispersion /165 values for the system acted on by a random stationary disturbance. The graphics in Figure 4.15 show that the root-mean-squares of the deviations in the lateral motion parameters for Airplane No. 1, the result of spanwise random normal wind gradient, have their greatest magnitudes at small turbulence scales close to the wing span. These values decrease quite sharply with increase in L to 200-400 meters, after which their decrease becomes less sharp

with increase in scale.

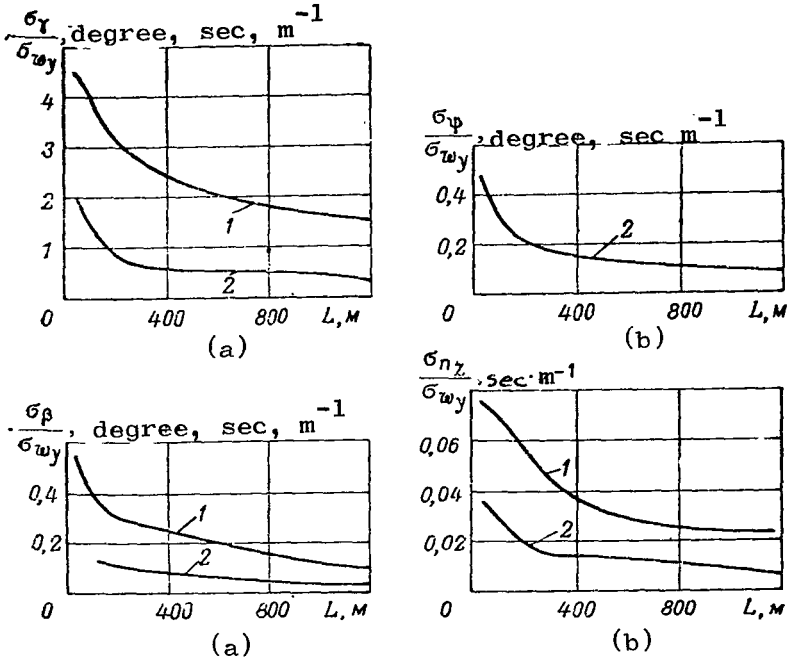

Figure 4.15. Normalized root-mean-squares of lateral motion parameters for Airplane No. 1 (a - angle of roll; b - angle of yaw; c - angle of sideslip; d - lateral acceleration). 1 - with fixed controls; 2 - with autopilot.

In the case of Airplane No. 2, the deviations in angles of yaw and sideslip caused by spanwise nonuniform normal wind are extremely small compared with the values of these magnitudes in the case of crosswind. This result is completely valid if one considered that this airplane has a wing span one-fourth that of Airplane No. 1. Hence, only one parameter, angle of roll, will be considered for Airplane No. 2.

Figure 4.16 presents the graphics of the spectral density of the angle of roll for Airplane No. 2 with autopilot, and Figure 4.16 does the same for this airplane with autopilot. Curves numbered 1 are for L = 38.4 m, those numbered 2 for L = 614.4 m. /166

Figure 4.18 shows the root-mean-squares of the deviations in the angle of roll as a function of the turbulence scale. Curves numbered 1 are for the airplane without autopilot, those numbered 2 for the airplane with autopilot. These graphics prove how extremely efficient the autopilot is from

the standpoint of reducing Airplane No. 2 roll oscillations. /167

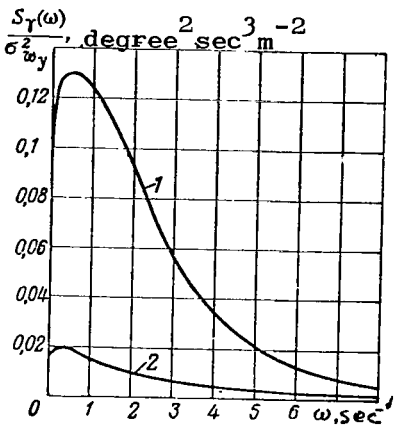

Figure 4.16. Normalized spectral density of angle of roll for Airplane No. 2 with autopilot attributable to the spanwise nonuniform wind.

1 - L = 38.4 m; 2 - L = 614.4 m.

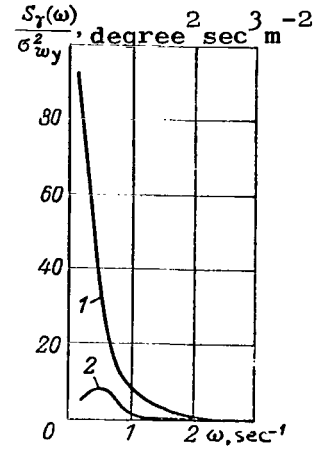

Figure 4.17. Normalized spectral density of angle of roll for Airplane No. 2 with fixed controls attributable to the spanwise nonuniform wind.

1 - L = 38.4 m; 2 - L = 614.4 m.

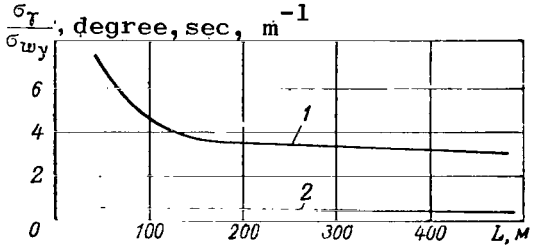

Figure 4.18. Normalized root-mean-squares of angle of roll as a function of the turbulence scale. 1 - with fixed controls; 2 - with autopilot.

The following conclusions flow from a comparison of the graphics for spectral densities and root-mean-squares of deviations in lateral motion parameters for airplanes No. 1 and No. 2 attributable to a spanwise nonuniform normal wind:

(1) disturbances in angles of sideslip and yaw are negligibly small in the case of an airplane with a small wing span (Airplane No. 2);

(2) lack of cross-couplings in the autopilot installed in Airplane No. 2 results in a more significant reduction in the disturbances in the angle of roll than is the case for Airplane No. 1.

Let us assess the role of the lateral and normal wind components in disturbing the parameters of airplane lateral motion. Comparison of Figure 4.9 a and d with Figure 4.15 a and d, respectively, makes it relatively simple to establish the fact that the role of the spanwise nonuniform normal wind distribution in causing roll and lateral acceleration deviations is much more

significant than the role of the crosswind, in the case of an airplane with a large wing span (Airplane No. 1). Cross-couplings in the autopilot increase the angle of roll and acceleration disturbances.

Roll oscillations attributable to the normal wind prove to be greater than those attributable to the crosswind in the case of an airplane with a small wing span (Airplane No. 2).

A comparison of Figure 4.9 b and c with Figure 4.15 b and c, will show that even in the case of Airplane No. 1, which has a large wing span and low course stability, the disturbances in the angles of yaw and sideslip attributable to the crosswind exceed those attributable to the normal wind. In the case of Airplane No. 2, which has a small wing span and high course stability, the disturbances in the angles of yaw and sideslip attributable to the normal wind have proven to be practically negligible compared with those attributable to the crosswind.

Figure 4.19 contains the resultant graphics showing the root-mean-squares of the deviations in the lateral motion parameters for Airplane No. 1 attributable to the summed influence of the lateral and normal wind components in terms of the turbulence scale. Curves numbered 1 are for the airplane with fixed controls, those numbered 2 for the airplane with autopilot. Since it was shown in Section 1.4 that the wind component is uncorrelated with respect to the different axes, the resultant root-mean-square of any airplane motion parameter can be found as the square root of the sum of the dispersions for the parameter attributable to the individual wind components. Moreover let us suppose that the turbulence is isotropic, that is, that the root-mean-squares of the wind components are identical: $\sigma_{wy} = \sigma_{wz} = \sigma_w$.

The graphics in Figure 4.19a show that the autopilot reduces roll oscillations by a factor of approximately 3, compared with the oscillations that occur when flying without an autopilot. But this is not the way to compare /168
angles of yaw (see Figure 4.19b) because this angle tends to infinity, theoretically, when flying without an autopilot. The angle of sideslip (see Figure 4.19c) is reduced by a factor of 1.3-2, and the lateral acceleration (see Figure 4.19d) is reduced by a factor of approximately 2, when the autopilot is used.

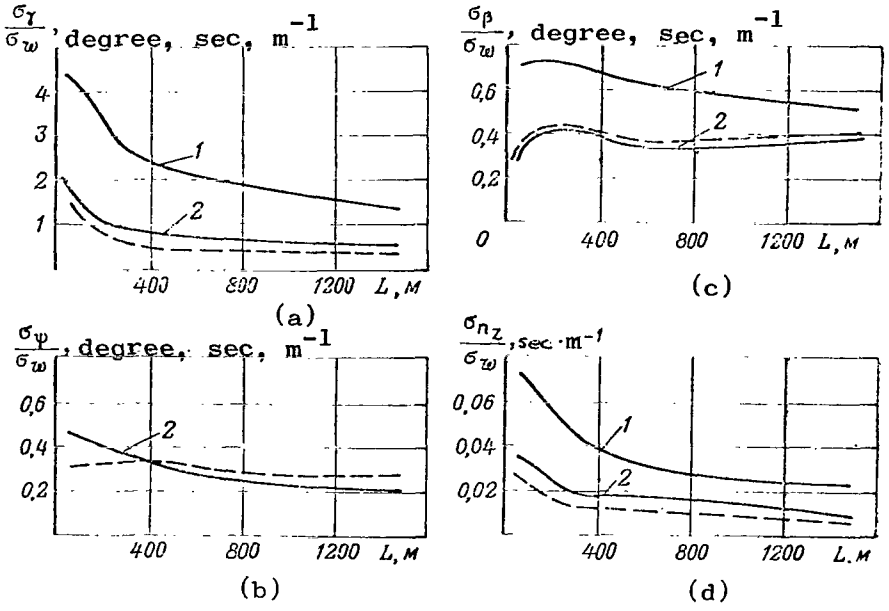

Figure 4.19. Normalized root-mean-squares of Airplane No. 1 lateral motion parameters (a - angle of roll; b - angle of yaw; c - angle of sideslip; d - lateral acceleration) attributable to the simultaneous influence of the crosswind and the nonuniformity in the spanwise vertical wind distribution. Values are given as a function of the turbulence scale.

1 - with fixed controls; 2 - with autopilot, dashed curves for autopilot without cross-couplings.

The dashed curves in Figure 4.19 are for the root-mean-squares of the corresponding lateral motion parameters that would occur when the cross-couplings in the autopilot in Airplane No. 1 are disconnected.

In concluding this chapter, let us review the results obtained by comparing the experimental data on lateral motion parameters with data computed using the methodologies described in the foregoing. The experimental data were obtained by recording the motion parameters of a big passenger airplane with autopilot in flight and then processing these data using the methodology set forth in Appendix D. Figure 4.20 shows the experimental spectral density curves for lateral motion parameters (solid lines). The vertical acceleration spectral density graphic was used to select the turbulence scale, L, and the root-mean-square of the wind velocity, σ_w in flight. The values of L and σ_w found in this manner were used to establish the lateral motion parameters /169

on an analog computer, using the assumption that the turbulence was isotropic.

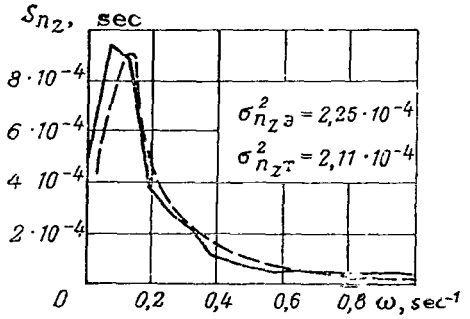

(a)

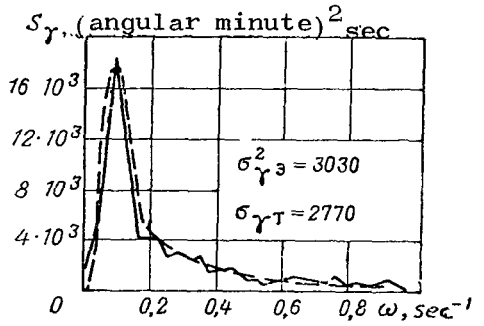

(c)

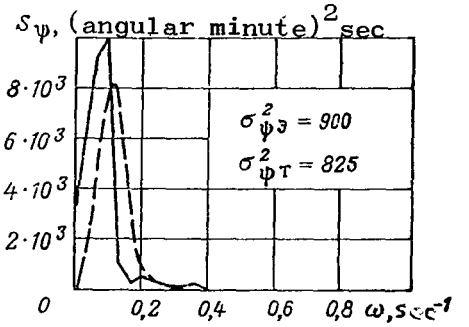

(b)

Figure 4.20. Spectral densities of lateral motion parameters. The solid curves are for the experimental data, the dashed curves for the computed data (a - lateral acceleration; b - angle of yaw; c - angle of roll).

The spectral density curves obtained using this method are included in Figure 4.20 (dashed). These graphics further show the dispersions in the parameters, determined experimentally (exponent "e") and by modeling (exponent "m"). The dispersions in the angle of yaw (Figure 4.20b) and in the angle of roll (Figure 4.20c) have the dimensionality of "angular minutes squared."

The coincidence between the spectral density curves and the curves for the dispersions in the lateral motion parameters obtained experimentally and on the basis of analytical computations, is quite good.

We should also point out that a great many experiments have proven there is a significant reduction in the oscillations the airplane makes in angle of roll and in angle of yaw when the autopilot is used to control the aircraft in turbulent air as compared with those recorded when the pilot is in control. And there is no significant change in the deflection angles for the controls. /170 Confirmation is contained in Table 4.1, which lists the experimental results obtained for a big transport airplane flying at 4,000 meters in cumulous clouds.

TABLE 4.1

Control condition	σ_γ degree	σ_ψ degree	σ_{δ_a} degree	σ_{δ_r} degree
Pilot	3,43	3,52	0,82	0,42
Autopilot without altitude corrector	0,67	0,37	0,99	0,51
Autopilot with altitude corrector	0,85	0,53	1,28	0,68

Commas represent decimal points.

Table 4.1 lists the root-mean-squares of the lateral motion parameters in degrees. As the data in Table 4.1 show, use of the autopilot without altitude corrector when flying in rough air results in a reduction in angle of roll oscillations by a factor of 5, and a reduction in the angle of yaw oscillations by a factor of almost 10. The autopilot corrector is acted on by pressure pulses and introduces additional disturbances in the elevator control channel, and also affects the quality with which the latter's motion parameters are stabilized.

CHAPTER V

COUNTERING WIND LOADS ON AN AIRPLANE

5.1. General Information

The airplane flying in moving air experiences wind gust accelerations /171
along all axes, longitudinal, normal, and lateral. But it is a well-known fact that the greatest accelerations occur along the normal axis, and that they are the result of wind gusts along that axis. These accelerations have virtually no relationship to the flightpath angle. Therefore, for purposes of simplification in what follows, we will take up level flight and vertical accelerations from vertical gusts.

Vertical acceleration limits for an airplane are determined by the structural strength, or by its stall condition. There is yet another aspect to the problem of the effect of wind loads on an airplane in addition to the analysis of acceleration limits, one that requires consideration of all loads, including very small ones.

This problem arises in the computation of the resources the airplane can draw on, and these are based on airframe fatigue strength. Experimental data show that atmospheric turbulence is the principal factor drawing on the resources built into the airplane's structure. Listed below are the relative values of individual types of loads on the airframe that result in defects in its structure (with the total number of defects taken as 100% [49]):

takeoff and landing loads	5%
loads attributable to turbulence	57%
loads caused by maneuvers during monitored flights	22%
loads caused by maneuvers during conventional flights	16%

It should be pointed out that in the case of aircraft flying on local airlines the relative weight of wind loads in creating defects attributable to structural fatigue is even higher, some 85% [49], and this is because of the lower altitudes at which they fly.

Finally, a similar problem involves the evaluation of how comfortable a flight will be for passengers and crew in turbulent air, although in this case small accelerations are not significant. /172

This chapter reviews methods for determining acceptable acceleration values, as well as methods that may be used to reduce the loads caused by vertical gusts. A methodology for making a quantitative evaluation of a particular system for automatically controlling an airplane, from the point of view of the probability of achieving fixed acceleration values, is presented. These values are selected in advance, based on the conditions stipulated in the problem. Specifically, they can be permissible acceleration limits.

5.2. Permissible Acceleration and Vertical Wind Gust Velocities

As was pointed out in the preceding section, two factors are involved in determining permissible vertical accelerations for an airplane;

(1) structural strength, or physiological endurance of man with respect to the acceleration;

(2) arrival of the airplane at angles of attack so high that flying at them will result in loss of control and in stalling.

The vertical acceleration limit can be established by the first, or by the second, of these two factors, depending on flight conditions.

Strength conditions provide a more or less constant acceleration limit, one that changes over certain limits with change in the weight of the airplane, but does not depend on flight conditions.

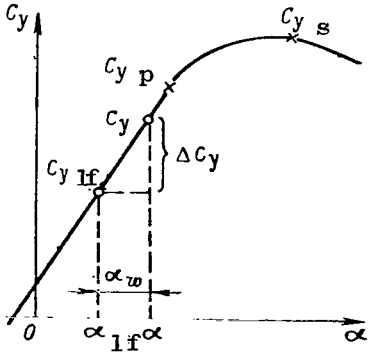

Figure 5.1. Change in the lift coefficient as a result of a vertical step wind gust.

The conditions under which the airplane will arrive at high angles of attack caused by vertical gusts is closely associated with the conditions under which the airplane is flying. The acceleration corresponding to permissible angles of attack can vary greatly. Let us take up this question in more detail. Let us say the original condition is one of level flight at speed V_e, angle of attack α_{lf} and lift co-

efficient $C_{y\,1f}$ for the particular airplane, and that the values are those shown in Figure 5.1. We will assume the vertical gust to be idealized, but of the most unfavorable step type. As soon as the airplane encounters this gust, its angle of attack will change by the magnitude $\alpha_w = w_y/V$. The increase in the angle of attack is accompanied by an increase in the lift coefficient by the magnitude ΔC_y, as is shown in Figure 5.1. Higher gust velocity results in /173 a greater increase, and the total value of the lift coefficient can reach the value $C_{y\,s}$, at which the airplane will stall out. We therefore select $C_{y\,p} < C_{y\,s}$ as the permissible value. Sometimes $C_{y\,p}$ is determined as that value of the lift coefficient at which the airplane begins to experience buffeting caused by local wing stalls.

Acceleration will be maximum the instant the airplane enters the gust (if the nonstationary nature of the flow over the wing is not taken into consideration), after which it will diminish as a result of the change in the angle of pitch and of the appearance of vertical velocity at the airplane. The maximum for the acceleration can be obtained through Equation (1.4) if one puts k = 1

$$\Delta n_y = \frac{C_y^{\alpha} \rho_e V}{2G/S} W_y. \qquad (5.1)$$

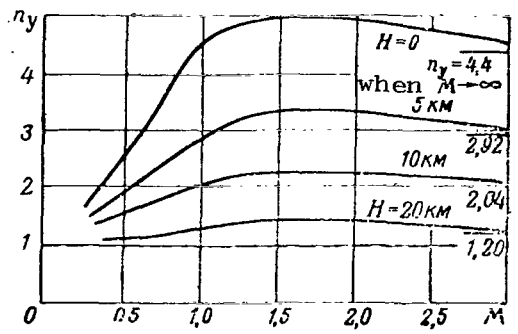

Figure 5.2. Graphics of the increases in the vertical acceleration experienced by the airplane upon entering a step gust at different altitudes in terms of the M number at which the airplane is flying.

Let us take a concrete example in order to show the effect change over a wide range of speeds and altitudes has on the accelerations caused by entering a step vertical wind gust. Figure 5.2 shows the graphics of $n_y = f(M)$ for various altitudes at which the airplane with the following data is flying: G/S = 300 kg/m^2; delta wing with a 50° sweepback angle, a taper ratio of 7, and an aspect ratio of 2.45; gust velocity W_y = 12 m/s. The graphics in Figure 5.2 show that when M < 1.0, the acceleration due to the gust increases in proportion to the speed. Then the reduction in C_y^{α} will slow the increase in the acceleration attributable to the gust at first, the result of the compressibility, but with further increase in speed there is some reduction in the acceleration. The acceleration

is slight at high altitudes because of the smallness of ρ. However, the graphics in Figure 5.2 do not take into consideration the fact that there are times when a gust with a velocity of 12 m/s will be unacceptable because a high angle of attack will occur.

The following obvious relationships will be introduced for purposes of considering the limit gust question /174

$$\Delta n_y = \frac{\Delta C_y}{C_{y\,1f}} \tag{5.2}$$

and

$$W_y = \frac{\Delta C_y V}{C_y^{\alpha}} \tag{5.3}$$

The graphic of the $C_{y\ p} = f(M)$ relationship must be available in order to determine the magnitude of the acceleration and the gust velocity permissible from the point of view of the outcome being a high angle of attack. Figure 5.3 is an example of such a graphic, reflecting the influence of the air compressibility on $C_{y\ p}$. Figure 5.3 also shows the graphics for the lift coefficient values, $C_{y\ 1f} = f(M)$, needed for level flight at various altitudes.

What follows from the graphics in Figure 5.3 is that there is a completely defined increase, ΔC_y, for every speed and altitude, bringing the value of the lift coefficient to the magnitude $C_{y\ p}$.

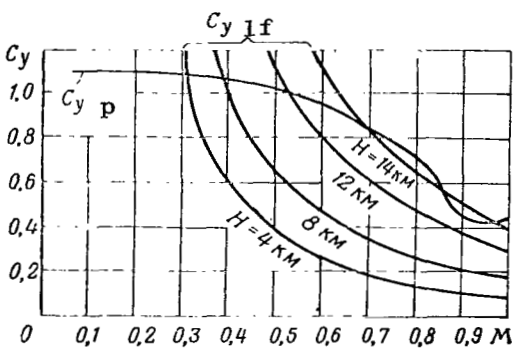

Figure 5.3. Graphics of required and available values for the lift coefficient in terms of the M number.

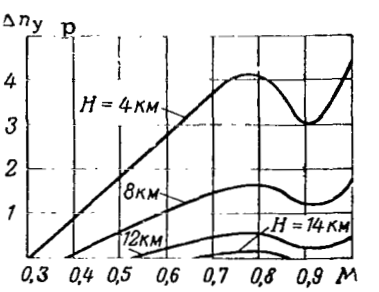

Figure 5.4. Graphics of the permissible increases in the vertical acceleration at various altitudes.

Based on Equation (5.2) and the data in Figure 5.3, these increases, ΔC_y, can be converted into the increase in the acceleration, $\Delta n_{y\,p}$, permissible for the conditions of attaining the value $C_{y\,p}$. The results are shown in Figure 5.4.

These increases in the acceleration are quite significant for low altitudes and for a definite range of speeds, and can exceed the accelerations permissible flight speeds at high a'titudes, and the maximum values of $\Delta n_{y\,p}$ decrease significantly. /175

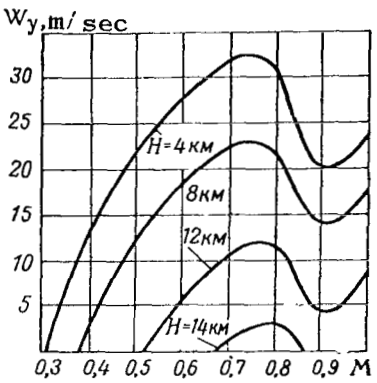

Figure 5.5. Graphics of the permissible velocities of vertical step gusts at various altitudes in terms of the M number.

Equation (5.3) and the graphics in Figure 5.4 can be used to obtain the values for velocities of vertical step gusts putting the airplane at the lift coefficient value $C_{y\,p}$. Figure 5.5 shows the graphics for these velocities. These show that there is a minimum flight speed at which even slight vertical gusts will result in a relationship $C_y > C_{y\,p}$ for every altitude. So, in high altitude flight the permissible vertical gust velocities are low.

The values of the permissible vertical gust velocities shown in Figure 5.5 were found assuming the airplane as entering a step gust. But gusts such as these are not encountered under real conditions. It is far more correct to reflect the condition of the real atmosphere by the concept of the random nature of the gust velocity field. The probability approach must be used for this concept to assess the effect of the wind on an airplane.

5.3. Passive Methods for Reducing Vertical Wind Gust Loads.

Equation (5.1) shows that when all other conditions are equal, increase in the wing loading (G/S) reduces acceleration attributable to vertical gusts. In the case of modern airplanes the load on the wing is increasing constantly, but there is a simultaneous increase in flight speed as well, such that the problem of reducing wind loads continues to be quite pertinent.

The reasons for the desirability of reducing the loads experienced by an airplane flying in moving air were given in 5.1. This problem is being given a great deal of attention at this time. For example, [42] lists 14 possible systems and methods for countering wind loads. Systems such as these can be broken down into active and passive. The active systems include automatic systems that act on the airplane's controls, such as the elevator, flaps, elevons, and others. Passive systems include those that vary the geometry, or the aerodynamic characteristics, of the wing. /176

This section will review, in brief, some of the passable methods used to reduce vertical gust loads.

Variable-sweep wing. This wing is already in use on modern airplanes and is designed to improve aerodynamic quality over a wide range of changes in flight speed. At the same time, this wing provides for some reduction in vertical gust loads by reducing C_y^α with increase in wing sweepback and reduction in its aspect ratio. It is also possible to reduce the wing area while increasing sweepback, leading to an increase in the G/S ratio.

Telescopic wing. The tips of this wing can be retracted inside the rigid section. Use of the telescopic wing would help improve aerodynamic quality at supersonic speeds, as well as for reducing wind loads by increasing the G/S ratio. There is a simultaneous reduction in C_y^α because the aspect ratio is reduced. However, telescopic wings have not yet been used because of great structural difficulties which must be overcome if such wings are to be built.

Folding wing. A wing with tips that fold back 90° has been proposed as one of the passive systems for reducing vertical gust loads. The bent back wing tips play the role of tip plates. There is no marked reduction in C_y^α as a result of the effect the tip plates have on a wing with bent back tips when compared with a straight wing. Reduction in the gust load is the result of the increase in G/S because of the reduction in the wing area when its tips are bent.

Reference [42] lists still other devices for reducing vertical gust loads, in addition to those mentioned above, including:

(1) interceptors for breaking the smooth flow over the wing in order to reduce C_y^α;

(2) elevons that take over as the wing bends under the gusts;

(3) hinged wing surface sections rigidly connected to the wing in still air, but which are hinged gusts, resulting in something of a reduction in the effective wing area.

All these methods require a great deal more research in order to provide the answers to questions of their applicability in countering wind loads.

5.4. Active Systems for Reducing Vertical Wind Gust Loads. /177

Let us consider some of the automatic systems designed for reducing wind loads. At the same time, we will take up only the principal capabilities and properties of these systems, so the analysis of the dynamics will be made without regard for the nonlinearities of the control system and the non-rigidity in the airplane's structure. Consideration of these factors greatly complicates the problem we are about to consider, and can make significant changes in the results below.

We will divide automatic systems for reducing wind loads into two groups. The first will include autopilot type systems that control lift with the aid of the elevator. The autopilot control law can be changed significantly in order to better counter accelerations, and the possibilities of making this change, as compared with the law presently in use, are available. But since these laws are not yet in use, we will limit ourselves to an analysis of an arrangement with an autopilot in which a signal proportional to the acceleration at the center of gravity in introduced, in addition to the conventional signals.

We will include in the second group those automatic systems exercising direct control over wing lift by using flaps, or some other control surfaces, or devices. For convenience of analysis we will assume the airplane to have a conventionally installed autopilot in addition to the system controlling wing lift. Let us consider the signals proportional to the vertical acceleration at the airplane's center of gravity, and the velocity of the vertical gust, as those acting on the automatic device.

Autopilot with signal of acceleration at airplane's center of gravity.

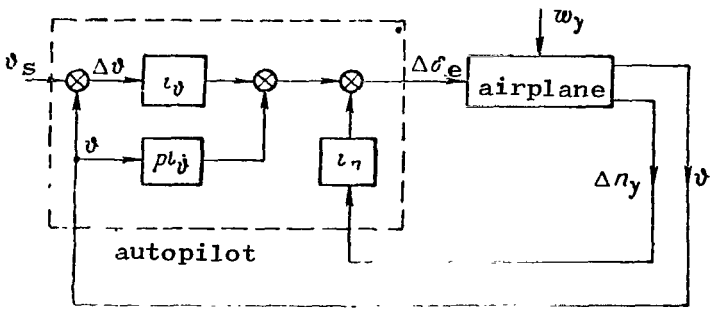

Figure 5.6. Structural schematic of a control system with an autopilot and an additional signal for vertical acceleration at the airplane's center of gravity.

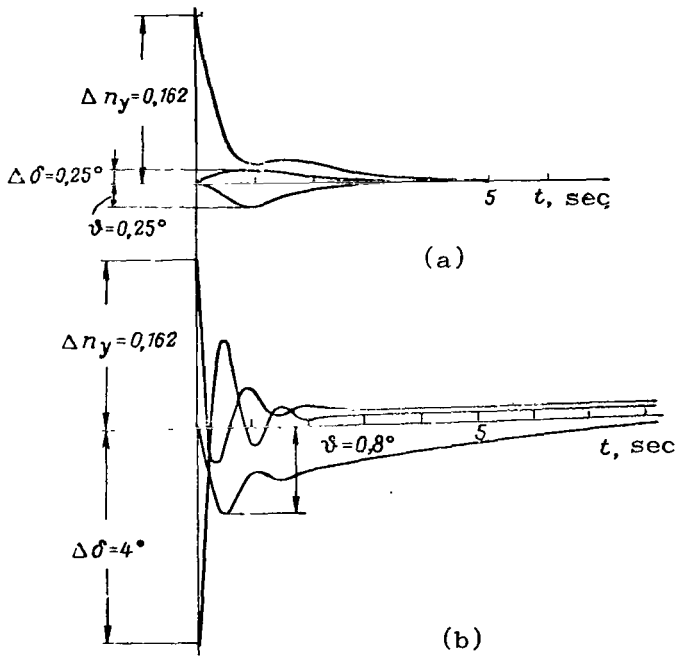

Figure 5.7. Transients for Airplane No. 4 upon entering a vertical step gust.

a - with conventional autopilot; b - with autopilot with additional signal for acceleration at the airplane's center of gravity.

In this case the airplane is under the control of the autopilot controlling the elevator. An additional term proportional to the vertical acceleration at the airplane's center of gravity, is introduced in the control law for the autopilot. This signal can be obtained from an accelerometer installed near the airplane's center of gravity.

Figure 5.6 is the structural schematic of the airplane's control system. The dynamics of this system can be described by the equations for the airplane at (2.11), and by the equation for the autopilot, which should be written in the following form

$$\Delta\delta_e = i_\vartheta \frac{d\Delta\vartheta}{dt} - i_\vartheta(\Delta\vartheta_s - \Delta\vartheta) + i_n \Delta n_y, \tag{5.4}$$

where

i_n is the autopilot gain in terms of the acceleration.

This system corresponds to the following transfer function for acceleration caused by the vertical wind component:

$$W_{n_y w_y}(p) = \frac{b_y^\cdot}{g} \frac{p^3 + (c_\vartheta + c_y^\cdot V_e + c_\alpha i_\vartheta) p^2 + c_\alpha i_\vartheta p}{\Delta(p)}, \tag{5.5}$$ /179

$$\Delta(p) = p^3 + (b_y^\cdot + c_\vartheta + c_y^\cdot V_e + c_\alpha i_\vartheta) p^2 +$$

$$+ [V_e(c_y^\cdot + b_y^\cdot c_\vartheta i_n/g) + b_y^\cdot (c_\vartheta + c_\alpha i_\vartheta) + c_\alpha i_\vartheta] p + b_y^\cdot c_\alpha i_\vartheta. \tag{5.6}$$

Analysis of the nature of the coefficients of the Equation (5.6) polynomial and of the Equation (5.05) transfer function reveals that supplying a signal to the elevator proportional to the acceleration is equivalent to increasing the static stability coefficient $c_y^\cdot$ by the magnitude $b_y^\cdot c_\delta i_n/g$. It was pointed out in section 3.2 that a significant increase in static stability is accompanied by an increase in the oscillatory nature of the airplane's angular motions. This is confirmed by the type of response functions for Airplane No. 4 (data for Airplane No. 4, and its flight conditions, are given in Appendix A) shown in Figure 5.7, where the reaction of the airplane to a vertical step gust with velocity w_y = 1 m/s is shown. The response functions in Figure 5.7a are for an airplane with a mass-produced autopilot for this airplane (i_ϑ = 1; $i_\vartheta^\cdot$ = 0), while those in Figure 5.7b are for the control system under consideration (i_ϑ = 1; $i_\vartheta^\cdot$ = 0; i_n = 25°).[1] It must be emphasized that the more rapid re-

1. The gain, i_n has the dimensionality of degrees (or radians) for the control deflection angle per unit of vertical acceleration.

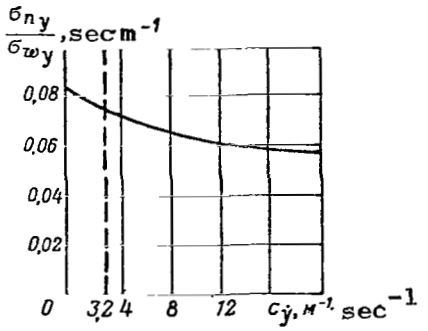

Figure 5.8. Normalized root-mean-squares of the acceleration at the center of gravity of Airplane No. 4 in terms of the static stability moment coefficient (when σ_w = 1 m/sec).

moval of the acceleration by the autopilot receiving an acceleration signal is achieved by the high flow and high rate at which the elevator moves (Figure 5.7b).

Figure 5.8 is the graphic of the root-mean-square of the acceleration at the center of gravity of Airplane No. 4 equated to the root-mean-square of the velocity of random vertical gusts in terms of the static stability coefficient, $c_y^{\bullet}$ (since equivalency of the terms $b_y^{\bullet}\, c_\delta i_n/g$ and $c_y^{\bullet}$ was established), and is included to provide a means for making a more complete evaluation of the capability of the arrangement under consideration. The graphic was constructed for a turbulence scale L = 300 m. When $c_y^{\bullet}$ is changed from 3.2, the actual value for this particular airplane, to 20, that is, by a factor of approximately 6, the root-mean-square of the acceleration is reduced approximately 35%. /180

The effectiveness of this system in reducing the acceleration over the range of turbulence scales for Airplane No. 4 is illustrated in Figure 5.9.

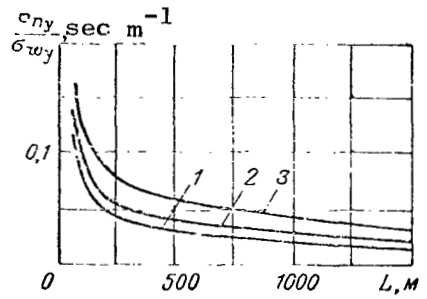

Figure 5.9. Normalized root-mean-squares of the acceleration at the center of gravity of Airplane No. 4 in terms of turbulence scale (when σ_w = 1 m/sec).
1 - autopilot with gain i_n = 20°; 2 - same, but i_n = 40°; 3 - conventional autopilot.

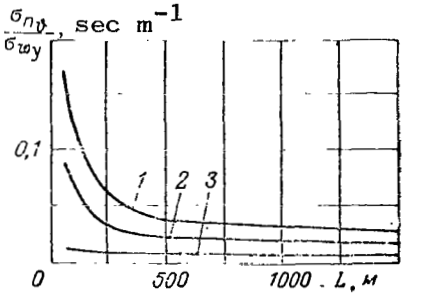

Figure 5.10. Normalized root-mean-squares of the acceleration for Airplane No. 4 from angular motions for the section of the fuselage 7 meters from the center of gravity in terms of the turbulence scale (when σ_n = 1 m/sec).
1 - autopilot with gain i_n = 20°; 2 - same, but i_n = 40°; 3 - conventional autopilot.

Curve 3 is for the airplane with a conventional autopilot stabilizing angle of pitch, while curves 1 and 2 are for the airplane with an autopilot with acceleration signal (curve 2 is for $i_n = 20°$, curve 1 for $i_n = 40°$). These graphics indicate that the root-mean-square of the acceleration is decreased approximately 30% when $i_n = 20°$, and 50% when $i_n = 40°$. However, the additional acceleration caused by the angular acceleration of the airplane increases sharply with increase in the gain, i_n. Figure 5.10 shows the root-mean-squares of this acceleration for a section of the fuselage $l = 7$ meters from the center of gravity. Curves 1, 2 and 3 equate to the same autopilot gains used for Figure 5.9. The instantaneous value of the acceleration at the section of the fuselage at some distance from the center of gravity is equal to the sum of the instantaneous values of the acceleration at the center of gravity (Δn_y) and the acceleration from angular acceleration (n_ϑ). The root-mean-square of the summed acceleration is a complex function of these components. However, the investigation established that in the case of an airplane with conventional angular motion characteristics, the root-mean-square of the summed acceleration for points along the axis of the fuselage located ahead of the center of gravity are equal, approximately, to the difference between the root-mean-squares of σ_{n_y} and σ_{n_ϑ}, and to the sum of these values for points located behind the center of gravity. With this in mind, and on the basis of the graphics in Figures 5.9 and 5.10, the conclusion can be drawn that there are three reasons why any significant increase in the gain (more than 20° in the case of Airplane No. 4, for example) is undesirable: /181

(1) substantial increases in i_n will not result in proportional reductions in the acceleration at the center of gravity;

(2) increase in i_n results in a sharp increase in the additional acceleration attributable to the angular accelerations, and this reflects unfavorably on the comfort of passengers seated in the tail section of the fuselage;

(3) the limitations imposed on elevator deflection by modern autopilots is such that the operating range of the autopilot will be substantially restricted when there is an increase in i_n.

In addition to everything else, the addition of an acceleration signal to the autopilot control law results in deterioration in controllability of

the airplane because the gain, i_n, must be quite high in order for this signal to be adequately effective, and this, in turn, is equivalent to making an extraordinarily large increase in static stability. Figure 5.11 shows oscillograms of the reaction of Airplane No. 4 with Equation (5.4) control law to pitch controlling signal $\Delta\vartheta_s = 1°$ ($i_\vartheta = 1$, $i_{\dot\vartheta} = 2.0$, $i_n = 20°$). As we see, the transient lasts for over 15 seconds.

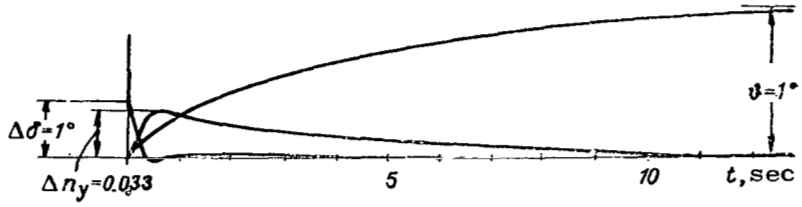

Figure 5.11. Reaction of Airplane No. 4 with autopilot with acceleration signal to a step pitch control signal.

Airplane No. 4, used for the computations, has a short fuselage. Airplanes with long fuselages will find the control system under consideration particularly unsuccessful because the reduction in the acceleration at the center of gravity will be accompanied by a significant increase in the acceleration in the tail section of the fuselage.

Flap control robot reacting to vertical gust velocity and autopilot. In this case the airplane is controlled by a conventional autopilot, with the flap (or elevon) control robot used to reduce accelerations attributable to wind gusts. Robot control is by a signal proportional to the velocity of the vertical gusts, measured by a special instrument (instruments in the airplane for measuring vertical gust velocities are described in [18, 19]). The /182
structural schematic of the airplane control system is shown in Figure 5.12, and the flap control robot is seen to operate on a closed circuit, using the external disturbance compensation principle.

When there is an upward gust the robot deflects the flaps upward; when there is downward gust they are deflected downward. This requires no turning of the airplane, so delay in compensating for the lift created by the gust will be determined by the delay in the robot actuator. It can therefore be expected that this arrangement for opposing accelerations will be more effective than the first.

Here the longitudinal motion equations for the airplane are changed

somewhat from those used before this in this book, because in this case the equations must take flap action into account. Simplified Equation (2.11) is converted into the following form in this case

$$\left.\begin{aligned} V_e \frac{d\Delta\vartheta}{dt} + \frac{dV_{gy}}{dt} + b_{\dot{y}} V_{gy} &= -b_f \Delta\delta_f + b_{\dot{y}} w_y, \\ \frac{d^2\Delta\vartheta}{\partial t^2} + c_{\dot{\vartheta}} \frac{d\Delta\vartheta}{dt} - c_{\ddot{y}} \frac{dV_{gy}}{dt} - c_{\dot{y}} V_{gy} &= -c_{\dot{\delta}} \Delta\delta_e - c_f \Delta\delta_f - c_{\dot{y}} w_y, \end{aligned}\right\} \quad (5.7)$$

where

$\Delta\delta_f$ is the flap deflection angle.

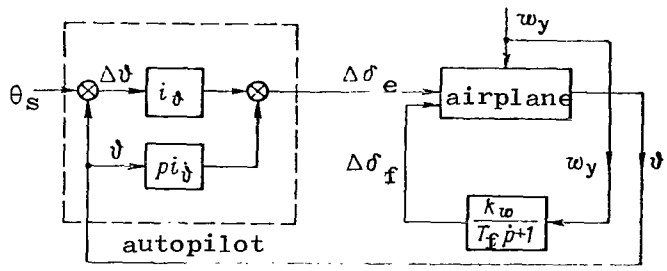

Figure 5.12. Structural schematic of an airplane control system containing a conventional autopilot and a flap robot reacting to vertical gust.

The values of the coefficients b_f and cf_v are listed in Table 2.1. It can be assumed that flap design is such that the flaps can be deflected up and down from the neutral position.

The robot equation for flap control can be put in the form of the inertia link equation

$$T_f \frac{d\Delta\delta_f}{dt} + \Delta\delta_f = k_w w_y, \quad (5.8)$$

where /183

T_f is the time constant for the robot;

k_w is the robot gain; its dimensionality is degrees (or radians) of flap deflection angle per unit vertical wind component velocity.

Equations (2.14), (5.7) and (5.8), taken in toto, describe the dynamics of the system reviewed. Corresponding to this system of equations is the transfer function for the acceleration attributable to the vertical wind

$$W_{n_y/w_y}(p) = \frac{1}{g} \frac{\Delta_2(p)}{\Delta_3(p)}, \quad (5.9)$$

where

$$\Delta_2(p)=p\left\{b_{\dot{y}}\,(T_{\mathrm{f}}p+1)[p^2+(c_{\dot{\vartheta}}+c_{\ddot{y}}V_e+c_{\dot{\alpha}}\,i_{\dot{\vartheta}})\,p+c_{\alpha}\,i_{\vartheta}]-\right.$$

$$\left.-k_w b_{\mathrm{f}}\left[p^2+(c_{\dot{\vartheta}}+c_{\ddot{y}}V_e+c_{\dot{\alpha}}\,i_{\dot{\vartheta}})\,p+c_{\alpha}\,i_{\vartheta}+V_e\left(c_{\dot{y}}-\frac{c_{\mathrm{f}}}{b_{\mathrm{f}}}\,b_{\dot{y}}\right)\right]\right\}, \tag{5.10}$$

$$\Delta_3(p)=(T_{\mathrm{f}}p+1)\{p^3+(b_{\dot{y}}+c_{\dot{\vartheta}}+c_{\ddot{y}}V_e+c_{\dot{\alpha}}\,i_{\dot{\vartheta}})\,p^2+$$

$$+[V_e c_{\dot{y}}+b_{\dot{y}}\,(c_{\dot{\vartheta}}+c_{\dot{\alpha}}\,i_{\dot{\vartheta}})+c_{\alpha}\,i_{\vartheta}]\,p+b_{\dot{y}}\,c_{\alpha}\,i_{\vartheta}\}. \tag{5.11}$$

The so-called invariance [43] of the airplane's longitudinal motion to a vertical gust can be based on Equation (5.9). This can be done by making the Equation (5.10) polynomial for the Equation (5.9) transfer function numerator an identity equal to zero, and this can be done by satisfying three conditions

$$T_{\mathrm{f}} = 0,\ k_{\mathrm{w}} = b^{\bullet}_{\dot{y}}/b_{\mathrm{f}},\ b_{\mathrm{f}}c^{\bullet}_{\dot{y}} = b^{\bullet}_{\dot{y}}c_{\mathrm{f}}.$$

The first condition, no delay in the operation of so powerful an actuator as the flap control robot, is, in principle, not feasible. Yet, as will be demonstrated in what follows, even a small delay greatly effects the power of this arrangement. The second condition reflects the equality of the increase in lift attributable to the vertical wind, w_y, and to flap deflection $\Delta\delta_{\mathrm{f}}$. The third condition expresses the equality of the increase in z-axis moment attributable to the gust, w_y, and the flap deflection, $\Delta\delta_{\mathrm{f}}$. It should be pointed out that even if these three conditions are satisfied, invariance of airplane longitudinal motion to a vertical gust cannot be ensured, strictly speaking, because of the effect of change in the airplane's drag resulting from flap deflection. Change in drag results in change in flight speed, and as a result to change in all the coefficients contained in the equation for airplane longitudinal motion. This latter in turn results in longitudinal motion disturbances. It is practically impossible to compensate for changes /184 in drag when flap movements are rapid.

The response functions for Airplane No. 4 with the system under consideration are shown in Figure 5.13. These functions show the reaction of the system (k_{w} = 7.0 degrees-sec-m^{-1}) to a step gust with velocity W_y = 1 m/s. Figure 5.13a is for a time constant equal to 0.1 second, Figure 5.13b 0.5 second. The acceleration drops very sharply when T_{f} = 0.1 second, and there

is but a slight disturbance in the angle of attack. The acceleration decreases more smoothly when T_f = 0.5 second, but the angle of attack is disturbed significantly.

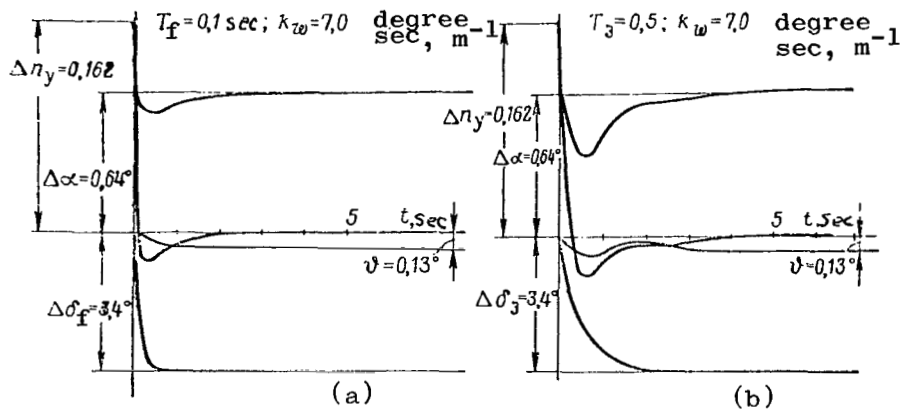

Figure 5.13. Transients for Airplane No. 4 with flap robot in a step gust for various values of the k_w ratio and time constant, T_f, for the flap robot.

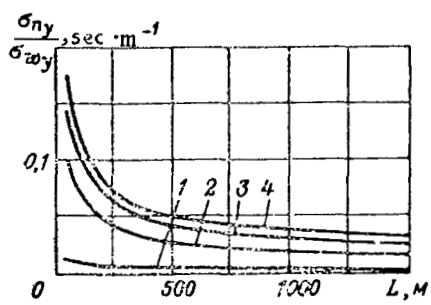

Figure 5.14. Normalized root-mean-squares of the acceleration at the center of gravity of Airplane No. 4 when there is a flap robot installed and reacting to a gust, in terms of the turbulence scale (when σ_w = 1 m/s).

1 - time constant T_f = 0;

2 - T_f = 0.1 second;

3 - T_f = 0.5 second;

4 - k_w = 0 (robot disengaged).

Figure 5.14 is for this same airplane, and shows the root-mean-squares of the acceleration equated to the root-mean-square of the gust velocity in terms of the turbulence scale for various time constant, T_f, values: curve 1 - T_f = 0; curve 2 - T_f = 0.1 second; curve 3 - T_f = 0.5 second; curve 4 is for the airplane without flap robot. The graphics in Figure 5.14 show that when there is no delay (T_f = 0) the arrangement is very effective in reducing acceleration (by a factor of approximately 10). However, it is very sensitive to delay in robot operation. When T_f = 0.1 second, the acceleration is halved as compared with curve 4, and robot power is very slight when T_f = 0.5 second. The arrangement is very sensitive as well to an increase in k_w, as will be seen from the

/185

graphics in Figure 5.15, showing the curves of $\sigma_{n_y}/\sigma_{w_y} = f(L)$ for four values of k_w: optimal - k_w = 7.0 degrees-sec-m^{-1} (curve 1); k_w = 10 degrees-sec-m^{-1} (curve 2); k_w = 4.2 degrees-sec-m^{-1} (curve 3); and k_w = 0, or robot disengaged (curve 4). T_f = 0 in all cases. The data in Figure 5.15 show that both over and under-compensation reduce system power very drastically.

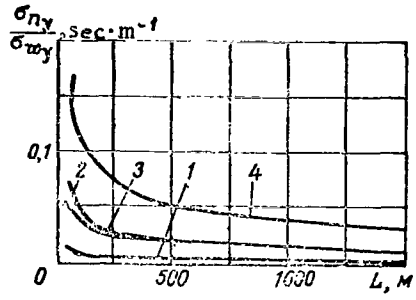

Figure 5.15. Normalized root-mean-squares of the acceleration at the center of gravity of Airplane No. 4 with flap robot reacting to wind gusts in terms of turbulence scale (when σ_w = 1 m/s.

1 - k_w =7.0; 2 - k_w = 10.0;

3 - k_w = 4.2; 4 - k_w = 0 (robot disengaged).

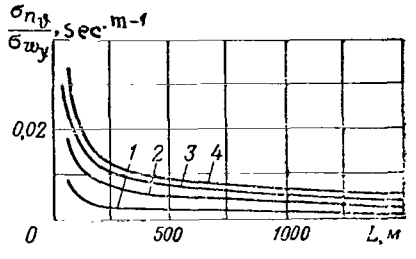

Figure 5.16. Normalized root-mean-squares of Airplane No. 4 acceleration attributable to angular motions for a section of the fuselage 7 meters from the center of gravity in terms of the turbulence scale (when σ_w = 1 m/s).

1 - T_f = 0; 2 - T_f = 0.1 sec;

3 - T_f = 0.5 sec; 4 - k_w = 0 (robot disengaged).

The accelerations attributable to angular airplane accelerations do not increase, as was the case for the first arrangement, but decrease to approximately the same degree as is the case for the acceleration at the center of gravity. Figure 5.16 shows this by providing the root-mean-squares of the acceleration attributable to the angular motions at a distance of 7 meters from the airplane's center of gravity (curve 1 is for the time constant T_f = 0, curve 2 for T_f = 0.1 second, curve 3 for T_f = 0.5 second, and curve 4 for k_w = 0, that is, the robot is disengaged). These results are easy to explain when it is recognized that controlled flaps change the angle of pitch very smoothly and slightly (as compared with the first arrangement), so that the accelerations attributable to the angular acceleration are small.

This arrangement in no way changes airplane controllability because the flap robot will only react to a vertical wind. /186

The drawback in this arrangement is the high degree of sensitivity of the flap robot to delay. Moreover, the equipment required to measure the vertical wind component is complicated. These drawbacks are overcome, to a considerable degree, by this next control system.

Flap control robot reacting to acceleration at the airplane's center of gravity and autopilot. The structural schematic of this system is shown in Figure 5.17. Here we see that as distinguished from the preceding system, this one has a closed circuit for regulating the deviation of the acceleration from its level flight value equal to unity. The sensitive element is a conventional accelerometer installed in the airplane's center of gravity.

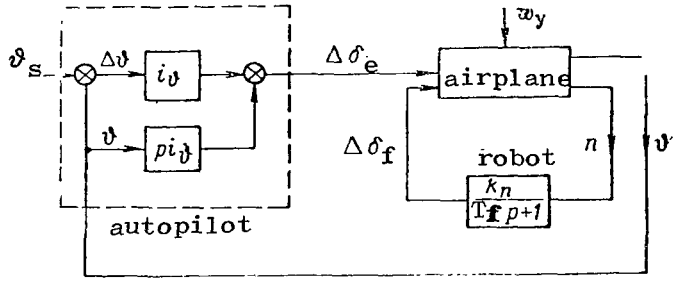

Figure 5.17. Structural schematic of an airplane control system containing a conventional autopilot and flap robot reacting to acceleration at the airplane's center of gravity.

The equation for the robot in this arrangement is

$$T_f \frac{d\Delta\delta_f}{dt} + \Delta\delta_f = k_n \Delta n_y, \tag{5.12}$$

where

k_n is the robot gain in terms of the flap deflection per unit acceleration, with k_n having the dimensionality of degrees (or radians) of flap deflection per unit of vertical acceleration.

The dynamics of this arrangement can be described by the equations for the autopilot, Equation (2.14), for the airplane, Equation (5.7), and for the robot, Equation (5.12). These equations correspond to the following transfer function for the acceleration attributable to vertical wind action

$$W_{n_y/w_y}(p) = \frac{1}{g} \frac{\Delta_4(p)}{\Delta_5(p)}, \tag{5.13}$$

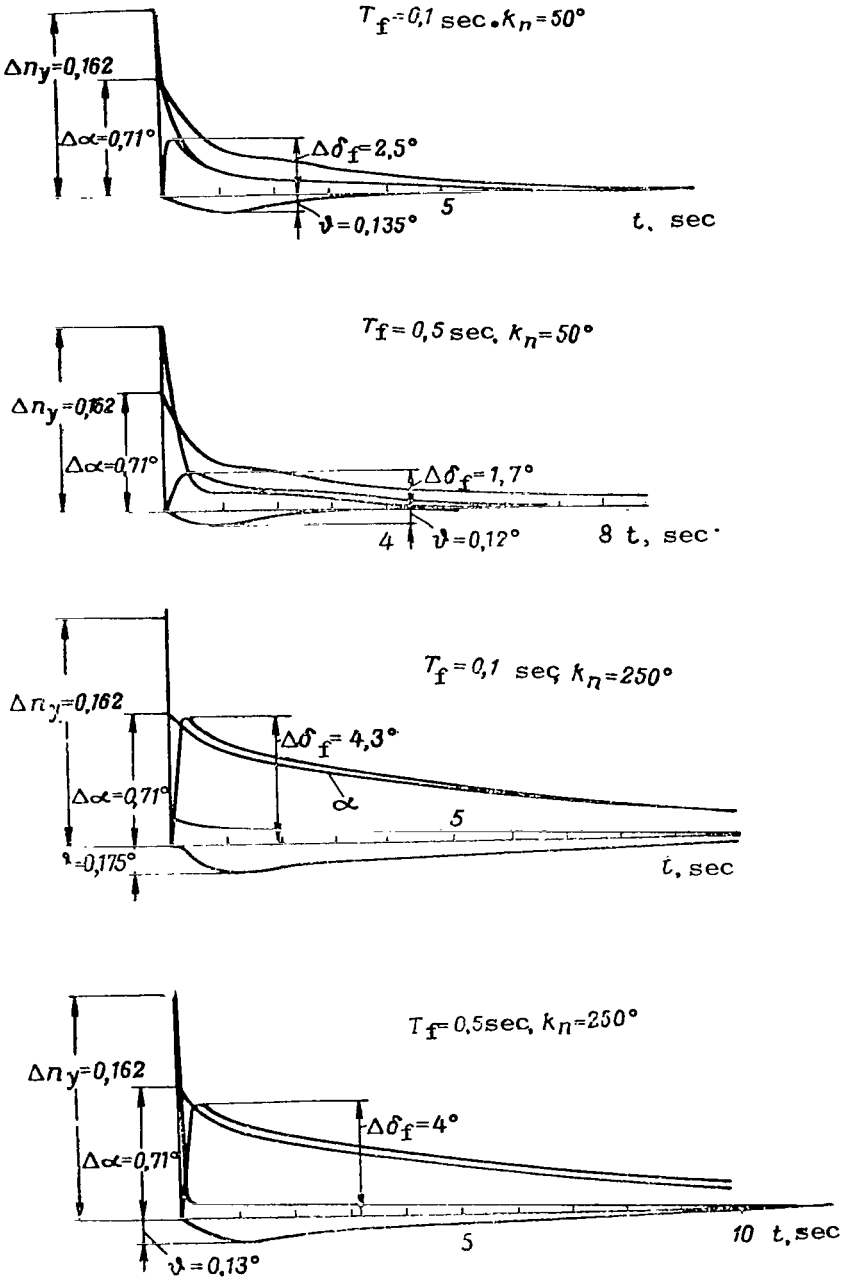

Figure 5.18. Transients for Airplane No. 4 with a conventional autopilot and flap robot in a step gust for various values of the gain k_n, and time constant T_f, for the flap robot.

where

/188

$$\Delta_4(p)=b_{\dot{y}}(T_f p+1)[p^2+(c_{\dot{\vartheta}}+c_{\ddot{y}}V_e+c_{\delta}i_{\vartheta})p+c_{\delta}i_{\vartheta}]p, \tag{5.14}$$

$$\begin{aligned}\Delta_5(p)=\Big\{&(T_f p+1)[p^3+(b_{\dot{y}}+c_{\dot{\vartheta}}+c_{\ddot{y}}V_e+c_{\delta}i_{\vartheta})p^2+\\&+(b_{\dot{y}}c_{\dot{\vartheta}}+b_{\dot{y}}c_{\delta}i_{\vartheta}+c_{\dot{y}}V_e)p+b_{\dot{y}}c_{\delta}i_{\vartheta}]+\\&+\frac{k_n b_f}{g}\Big[p^3+(c_{\dot{\vartheta}}+c_{\ddot{y}}V_e+c_{\delta}i_{\vartheta})p^2+\\&+\Big(c_{\delta}i_{\vartheta}+c_{\dot{y}}V_c-\frac{b_{\dot{y}}}{b_f}c_z V_e\Big)p\Big]\Big\}.\end{aligned} \tag{5.15}$$

Analysis of the Equation (5.13) transfer function will show the impossibility of this arrangement completely countering wind acceleration, even when $T_f = 0$. However, the acceleration will tend to zero if the increase in k_n is unlimited, and the value T_f is limited.

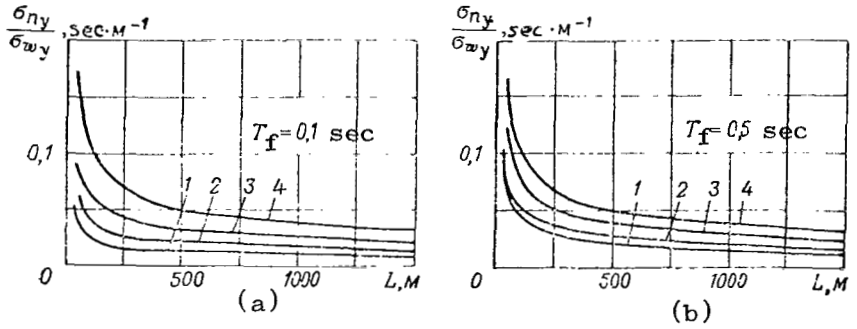

Figure 5.19. Normalized root-mean-square of acceleration at the center of gravity of Airplane No. 4 when there is an automatic flap control device installed and reacting to the acceleration as a function of the turbulence scale (a - T_f = 0.1 sec, b - T_f = 0.5 sec):
1 - k_n = 250; 2 - k_n = 150; 3 - k_n = 50;
4 - k_n = 0.

Figure 5.18 shows the response functions for this control system for Airplane No. 4 for various combinations of k_n and T_f. These graphics are for the reaction of the airplane to a step wind with velocity W_y = 1 m/s. The graphics show that an increase in k_n can provide the required type of acceleration curve for real values of the delay in the flap robot.

Let us consider the power of the control system for an airplane flying in turbulent air. Figure 5.19 shows the graphics for the relationship

$\sigma_{n_y}/\sigma_{w_y} = f(L)$ for various k_n and T_f values (Airplane No. 4). These graphics show that there is a constant increase in robot power with increase in k_n. /189 However, the reduction in the root-mean-square of the acceleration is not proportional to the increase in k_n. For example, change in k_n from 0° to 50° provides the same reduction in the acceleration as does a subsequent change from 50° to 250°, as will be seen from the graphics. Moreover, selection of very large k_n is undesirable because of the increase in flap rate.

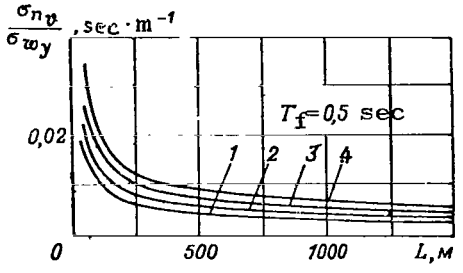

Figure 5.20. Normalized root-mean-squares of acceleration of Airplane No. 4 attributable to angular motions for a section of the fuselage 7 meters from the center of gravity in terms of the turbulence scale (when σ_w = 1 m/s).
1 - k_n = 250; 2 - k_n = 150;
3 - k_n = 50; 4 - k_n = 0.

Just as in the case of the preceding control system, oscillations in the angle of pitch are decreased with decrease in accelerations. Figure 5.20 shows this well in its presentation of the acceleration attributable to angular motions for a section of the fuselage 7 meters from the center of gravity.

Use of the third control system results in deterioration in airplane controllability, as will be seen from Figure 5.21, showing the reaction of the airplane to a controlling pitch signal $\Delta\vartheta_f$ = 10. If the angular rotation of the aircraft with respect to the angle of pitch takes place in practically the same way as it does without the flap robot, the time needed to change the flightpath angle ($\Delta\theta = \Delta\vartheta - \Delta\alpha$), will be increased significantly. This drawback can be eliminated by inserting a high-frequency filter in the control signal circuit for the flap robot because the low-frequency components of the acceleration can be eliminated by the natural reaction of an airplane with an autopilot. In this case too, the slow changes in the acceleration that take place when the airplane is maneuvering will for all practical purposes not be transmitted to the flap robot.

Let us, in concluding this section, consider several oscillograms illustrating the longitudinal motion of Airplane No. 4 flying in turbulent air.

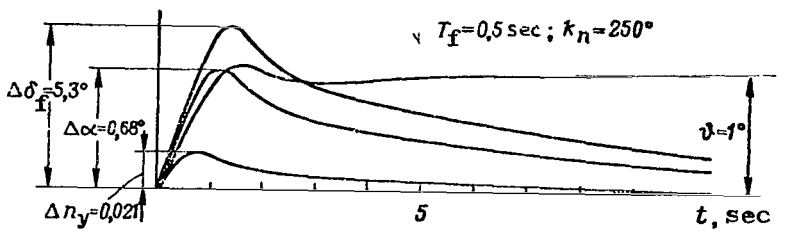

Figure 5.21. Transients for Airplane No. 4 with flap robot reacting to acceleration in the case of a step pitch control signal.

/190

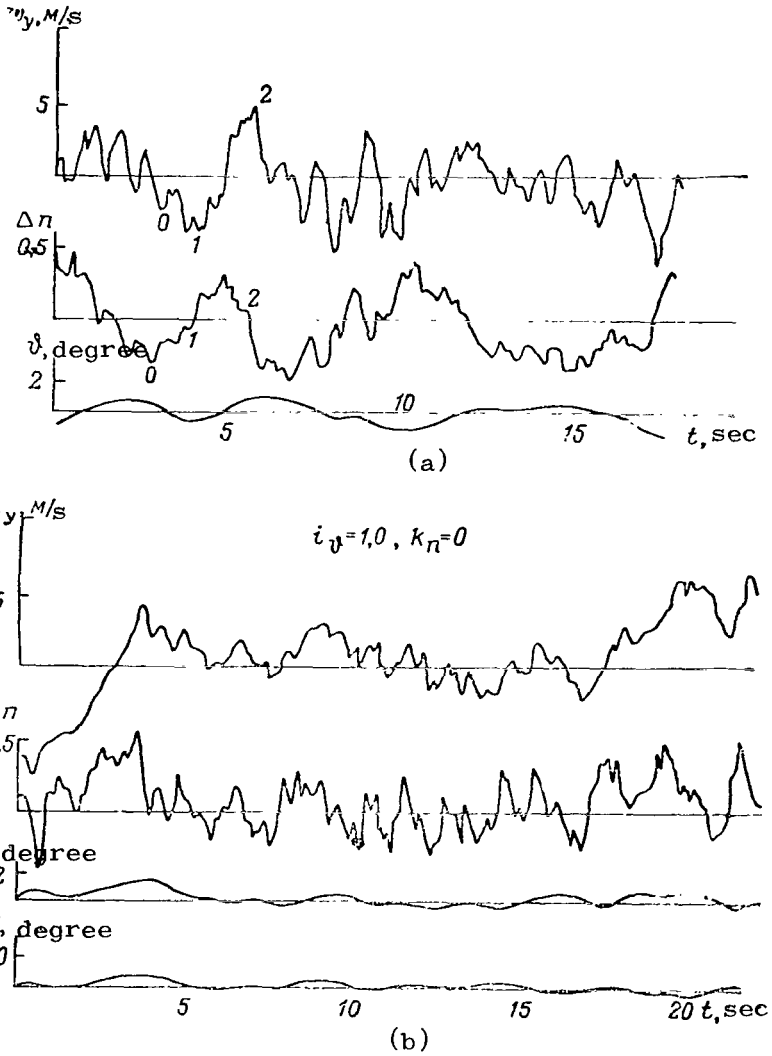

Figure 5.22. Oscillograms of the parameters of the longitudinal motion of Airplane No. 4 in turbulent air.

a - with fixed controls; b - with a conventional autopilot.

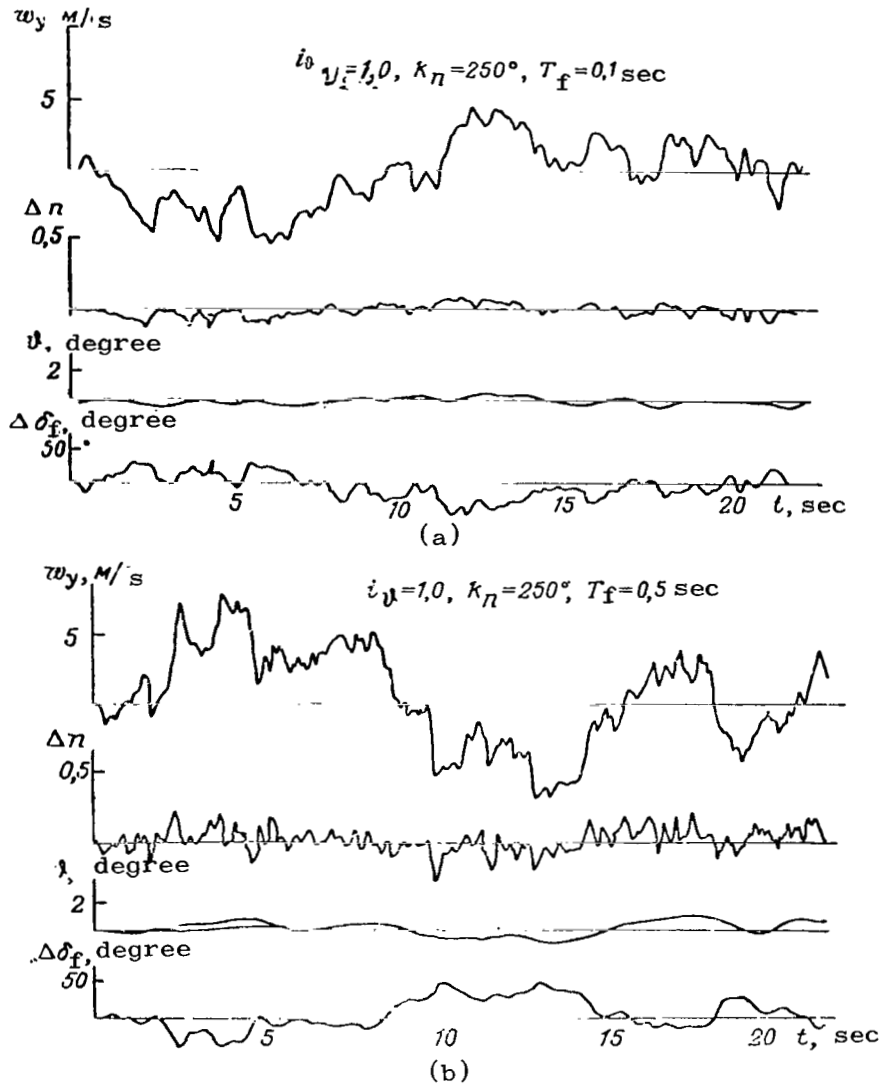

Figure 5.23. Oscillograms of the parameters of the longitudinal motion of Airplane No. 4 with flap robot reacting to acceleration and autopilot in turbulent air (for various values of the flap robot parameters).

These oscillograms were obtained by modeling airplane equations and control systems on an analog computer. The disturbance used was a random wind with characteristics corresponding to those obtained in the real atmosphere. Reference [44] presents the methodology for obtaining random signals with specified characteristics. /192

Figures 5.22 and 5.23 present the oscillograms for vertical wind w_y, acceleration Δn_y, angle of pitch $\Delta\vartheta$, and angles of elevator $\Delta\vartheta_e$, and flap, $\Delta\vartheta_f$, deflections.

Figure 5.22 shows the oscillograms for the airplane without autopilot and robot, while Figure 5.22b is that with autopilot, but without robot. A comparison of these oscillograms will show that the airplane with the autopilot develops rather significant angle of pitch oscillations, with the result that the acceleration curve differs greatly from the wind curve. The autopilot reduces angle of pitch oscillations.

Figure 5.23 presents the same data, but for an airplane with an autopilot and the robot of the third arrangement with large k_n and two T_f magnitudes.

The oscillograms shown in Figure 5.23 point out that a control system with a flap robot will substantially reduce the accelerations acting on the airplane.

The realization of the system described for opposing wind accelerations is quite difficult because of the need to build very high-powered high-speed drives for controlling the flaps.

5.5. Evaluation of the Probability of Achieving Permissible In-flight Accelerations

Let us assume the value of the acceleration permissible for the specified condition has been established by some method or other. As has been pointed out in section 5.2, this increase for one condition can be established by strength factors, and then will be the same of all such conditions. So far as other conditions are concerned, the permissible increase in the acceleration is associated with the airplane's attaining the lift coefficient value $C_{y\ per.}$ Each of these conditions has its own value, $\Delta n_{y\ per}$ (see Figure 5.4). At the same time, as in section 5.2, we will assume that C_y^{α} = constant to the value

$C_{y\ per}$. Given this assumption, one can use the linear equations associated with flight safety.

Let $\Delta n_y(t)$ be the increase in the vertical acceleration in homogeneous turbulence. It has been established experimentally [45] that the distribution of the instantaneous values of the acceleration in practically homogeneous turbulence are subordinate to a normal (Gaussian) law with a high degree of certainty. In this case Rice's formula [15, 46] can be used to establish the mathematical expectation of the number of excesses in one second with an increase in the acceleration $\Delta n_y(t)$ for some specified value ζ of this increase.[2] We will assume the specified value of the increase in the acceleration equal to the permissible value, that is, $\zeta = \Delta n_{y\ per}$. Rice's formula can be written in the form

/193

$$N(\zeta)=N_e e^{-\frac{1}{2}\left(\frac{\zeta}{\sigma_{n_y}}\right)^2}, \tag{5.16}$$

where

σ_{n_y} is the root-mean-square of the increase in the vertical acceleration for the realization of $\Delta n_y(t)$;

N_e is the mathematical expectation of the number of intersections in one second (with positive tilt) for the realization of the zero level.

What follows from the establishment of N_e is that this magnitude has the dimensionality of frequency. The value of N_e can be found through the formula

$$N_e=\frac{1}{2\pi}\frac{\sigma'_{n_y}}{\sigma_{n_y}}, \tag{5.17}$$

where

σ'_{n_y} is the root-mean-square of the derivative of the realization $\Delta n_y(t)$.

Let us point out that $N(\zeta)$, and N_e both yield the number of excesses per second only for a positive (or a negative) value of $\Delta n_y(t)$. The values of $N(\zeta)$ and N_e must be doubled in order to obtain the total number of excesses

---

2. The number of excesses is taken equal to the number of intersections with positive tilt for the realization of $\Delta n_y(t)$ for a specified value of increase in acceleration ζ.

including the positive and negative values of $\Delta n_y(t)$.

Equations (2.46) and (2.47) yield an expression for the root-mean-square of the increase in the vertical acceleration in terms of the amplitude of the characteristic curve for the airplane and the spectral density of the vertical wind gusts

$$\sigma_{n_y} = \sigma_w \sqrt{\int_0^\infty |W_{n_y w_y}(j\omega)|^2 s_w(\omega)\, d\omega}, \tag{5.18}$$

where

$s_w(\omega)$ is the normalized spectral density of the wind.

For the flight condition specified, wherein turbulence is stationary, the radicand is a constant, so that from Equation (5.18)

$$\sigma_{n_y} = \sigma_w A, \tag{5.19}$$

where

$$A = \sqrt{\int_0^\infty |W_{n_y w_y}(j\omega)|^2 s_w(\omega)\, d\omega}. \tag{5.20}$$

If the spectral density of some random stationary function x(t) is $S_x(t)$, /194 the spectral density of the derivative of that function will equal $\omega^2 S_x(t)$. Then, with Equation (5.18) taken into consideration, we obtain the expression for the root-mean-square of the derivative of the increase in the vertical acceleration as

$$\sigma_{n_y'} = \sigma_w \sqrt{\int_0^\infty \omega^2 |W_{n_y w_y}(j\omega)|^2 s_w(\omega)\, d\omega} = \sigma_w B, \tag{5.21}$$

where

B is for flight under stationary turbulence conditions is also a constant.

It should be pointed out that the B computation is definitely difficult, whereas the A computation can be made on analog computers using the methodology discussed in section 2.5. The B computation is difficult because when simplified Equation (1.33) is used for the spectral density of the vertical wind the integral under the radical in Equation (5.21) is divergent. There are several ways to do away with this difficulty. First, we need not take infinity as the upper limit for the integral, but instead the highest known value for the airplane's frequency, that is, practically several tens of oscillations per second. Second, the nonstationary nature of the flow over

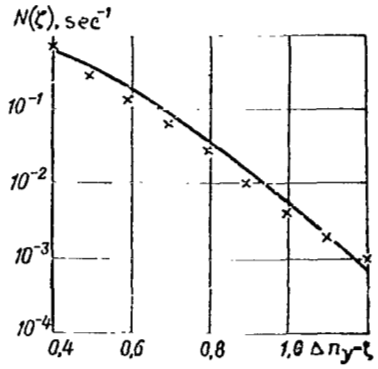

Figure 5.24. Comparison of experimental and computed results of the determination of the frequency of the excess in fixed values of the increase in the acceleration when flying in turbulent air.

the airplane can be considered by using Equation (3.40) for the square of the modulus of the Sears function. Use of the methodology for modeling airplane motion in turbulent air presented in this book for these computations requires the approximation of an expression containing the square of the angular frequency, ω, within the range of existing frequencyes for Equation (3.40) for a concrete problem. Third, and finally, the averaged spanwise vertical gusts can be taken into consideration and Equation (3.62) used for the spectral density of the vertical gusts.

Equations (5.19) and (5.21) result in Equation (5.16) yielding a final expression for the frequency of the excess in the increase of the acceleration of a specified value

$$N(\zeta)=\frac{1}{2\pi}\frac{B}{A}e^{-\frac{1}{2\sigma_w^2}\left(\frac{\zeta}{A}\right)^2} \tag{5.22}$$

Reference [46] contains the results of a comparison made of the experimental determination of the values of $N(\zeta)$ for various ζ with the computed values obtained using Equation (5.22), and with the characteristics of the airplane and the turbulence conditions that had prevailed during the experiment. Figure 5.24 shows these data. The concordance between the experimental results (crosses) and the computed results (the solid curve) is extremely good. This points to the possibility of using Rice's Equation (5.16) to determine the motion characteristics of an airplane in turbulent air. /195

If we are to make a quantitative assessment of the various methods and systems used to control an airplane under the conditions that prevail in gusts, we must assign permissible values for the increase in the acceleration, ζ, determine $N(\zeta)$ for these control methods, and compare the values of frequencies for the specified acceleration. Obviously, the best method will be that in which $N(\zeta)$ is least. However, the $N(\zeta)$ number means little, in and of itself, so the procedure indicated for comparing the different methods

used to control the airplane can be simplified if the relationship of the $N(\zeta)$ numbers for these methods is looked at at once. Let us write Equation (5.22) for two different control methods in the form

$$N_1(\zeta)=\frac{1}{2\pi}\frac{B_1}{A_1}e^{-\frac{1}{2\sigma_w^2}\left(\frac{\zeta}{A_1}\right)^2} \tag{5.23}$$

$$N_2(\zeta)=\frac{1}{2\pi}\frac{B_2}{A_2}e^{-\frac{1}{2\sigma_w^2}\left(\frac{\zeta}{A_2}\right)^2} \tag{5.24}$$

The relationship between $N_1(\zeta)$ and $N_2(\zeta)$ will show the number of times the probability of the airplane reaching the specified value of the increase in the acceleration, ζ will change with transition from the first airplane equation to the second. Let us call this relationship, or ratio, the gain if it is greater than unity, or the loss, if less than unity

$$K=\frac{N_1(\zeta)}{N_2(\zeta)}=\frac{A_2B_1}{A_1B_2}e^{\frac{\zeta^2}{2\sigma_w^2}\frac{A_1^2-A_2^2}{A_1^2A_2^2}} \tag{5.25}$$

That control method for which the root-mean-square of the increase in the acceleration is the greater, that is $A_1 > A_2$, can always be selected first. Then the gain, K, will be greater than unity.

The magnitudes A_1, A_2, B_1 and B_2 are constants for a specific airplane and a predetermined flight condition. What follows from Equation (5.25) is that /196 then the gain will increase with increase in the permissible acceleration, and will decrease with increase in the root-mean-square of the wind velocity, σ_w. The explanation is a simple one. The probability of reaching the permissible acceleration, ζ, decreases with increase in the permissible acceleration, and a small reduction in the acceleration will prove to have a much greater effect than would small ζ. K will equal unity for all σ_w values when $\zeta = 0$. Similar considerations explain the effect of σ_w. K equals infinity in the limit case of $\sigma_w = 0$.

Let us take an example of the use of Equation (5.25) to compare two methods of controlling Airplane No. 1 in turbulent air (all computations for a rigid airplane). The first method is that of the pilot controlling the

airplane, the second control by an autopilot. Based on the data in section 3.9, we can say that the root-mean-square of the acceleration will increase 34% in the first method.

Because Airplane No. 1 is a heavy transport airplane, the permissible increase in the acceleration for it in the cruising condition is selected on the basis of the structural strength of the airframe. The permissible increase is $\zeta = \Delta n_{y\ per} = 1.4$.

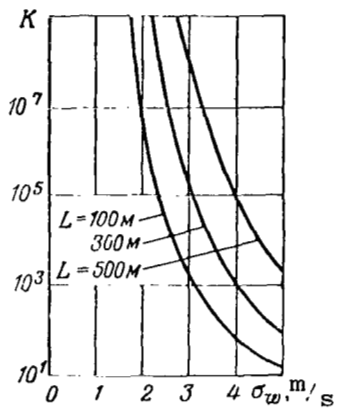

Figure 5.25. The gain factor as a function of the root-mean-square for the wind during the transition from pilot control to autopilot control.

The results of the gain computation for this case in terms of the root-mean-square of the vertical wind component are shown in Figure 5.25. The K values show the number of times the probability of the airplane reaching $C_{y\ per}$ is reduced during the transition from pilot control to autopilot control.

The very high gain (see Figure 5.25) is convincing proof of the desirability of using an autopilot when flying in turbulence. This recommendation is without adequate foundation only in very heavy turbulence, when airplane motion cannot be described by linear equations. There are two reasons why the airplane-autopilot system can become significantly nonlinear in severe turbulence, as would be the case, for example, when flying in a cumulous cloud zone, or in a storm zone. First, because of the high velocity of the vertical gusts, the increase in the lift /197 coefficient goes beyond the limit of the linear section of the $C_y = f(\alpha)$ curve. Second, control deflections cease being proportional to the control signal because of the limitation imposed by the magnitude of the hinge moment. The autopilot, therefore, is unable to oppose the action of high intensity gusts and provide reliable stabilization for the airplane. It is these limitations in modern autopilots that make it necessary to disengage them and shift to pilot control in very severe turbulence.

In the example considered, the computation for K as a function of the root-mean-square of the vertical gust velocity used data for a non-maneuvering airplane, one for which the limiting factor is the maximum permissible opera-

tional acceleration, established from the strength condition. In the case of maneuvering airplanes (fighters, for example), the maximum permissible operational acceleration is high, and can be realized only when maneuvering at high speeds and low altitudes. The acceleration attributable to vertical wind gusts is several times less than when maneuvering. Hence, the value of the acceleration determined with the strength condition in mind cannot be used in Equation (5.25) for ζ. For these airplanes we must use data similar to those in Figure 5.4, and then use these data to construct the graphics for K in terms of the M number for various values of σ_w and altitude.

CHAPTER VI

AIRPLANE TAKEOFF AND LANDING IN MOVING AIR

6.1. General Information

The takeoff and landing characteristics of an airplane, that is, the /198
lift-off and landing speeds, lengths of takeoff runs and roll-outs, depend on a great many factors. Included are aircraft and airfield parameters, such as weight, condition of the braking system and tires, and quality and condition of the runway, as well as meteorological conditions, such as wind velocity and direction, air temperature and density. The possibility of taking off and landing at a particular field in bad weather depends on how well equipped the field is with ground landing equipment, and on so-called "minimums" for the particular type of airplane. "Minimums" for an airplane and for fixed ground landing equipment refer to the set of minimum values of altitude of the lowest edge of the cloud cover and the slant range of the visibility at which it is safe to takeoff and land the airplane. However, wind characteristics around the field greatly influence the decision to takeoff, or land, and these are in addition to the "minimums." A wind component coinciding with the runway heading will change the length of the takeoff run and the roll out after landing in terms of the length of each needed for takeoff and landing in still air. The wind component perpendicular to the runway heading greatly complicates the takeoff and landing process, and when a crosswind increases to above a predetermined limit, taking off from and landing on that particular runway is curtailed. Large aerodromes have several runways, laid out on different headings, to ensure that airplanes will be able to takeoff and land in a strong wind.

This chapter will review the effect of the constant wind component on the takeoff and landing process for an airplane. Wind gusts will not be considered for two reasons. First, the statistical characteristics of wind gusts within the needed range of altitudes are still not adequate. The hypothesis with respect to the isotropic nature of turbulence used to obtain ana- /199
lytical characteristics of the wind velocity field in Chapter 1 is not valid

for low altitudes. Second, there are certain stages during the takeoff and landing when flight dynamics can, in principle, be described by nonlinear equations requiring special methods for their solution not taken up in this book. When the problem can be reduced to a linear and stationary one, the methods described in chapters 2-4 can be used to take the effect of wind gusts on takeoff and landing into consideration.

6.2. Takeoff in Moving Air

Takeoff is the airplane's motion process from the moment it starts to move to the moment it reaches some minimum altitude and flight speed. Figure 6.1 is a diagram of a takeoff. The "standard obstacle" along the axis of the runway, shown in Figure 6.1, is taken as 25 meters high, for takeoff and for landing. Let us take up in more detail the first of the two main stages of the takeoff, the takeoff run stage. The airplane's motion on the runway, when compared with its motion in the air, has a number of special features, the bases of which are the influence of the reactions from the supports (the wheels) and the change in the aerodynamic forces as a result of the proximity to the ground.

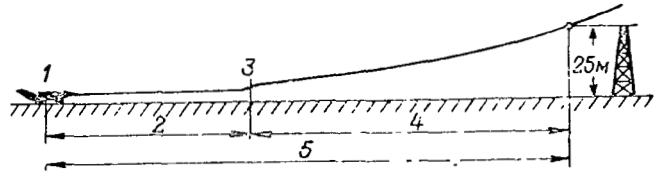

Figure 6.1. Takeoff Diagram:

1 - starting point; 2 - takeoff run; 3 - lift-off;
4 - acceleration with lift; 5 - takeoff distance.

The length of the takeoff run is a very important characteristic of the airplane. It depends on many factors, and some of them are not subject to precise consideration. First among these factors is the coefficient of friction of the wheels with respect to the runway, something that very much depends on the weather (precipitation) and on the condition of the tires, as well as on the aerodynamic forces, the magnitude of which depends on the pilot's actions, to some extent. Hence, the length of the takeoff is finally determined during the flight testing of the airplane. Wind has a very sub-

stantial effect on the length of the takeoff run required by the airplane. For example, the length of the takeoff run into a wind blowing at 10 m/s for the Il-28 is 1,060 meters, but the same airplane requires 1,900 meters when a tail wind is blowing at the same velocity [47]. However, because the takeoff is always into the wind, the shortening of the takeoff run attributable to the wind provides a safety factor on takeoff. Approximate formulas, obtained assuming constancy of acceleration of the airplane during the take- /200
off run,[1] can be used to evaluate the effect the wind has on the time and length of the take-off run

$$t_{tw}=t_t\left(1\pm\frac{W_x}{V_{1o}}\right), \tag{6.1}$$

$$D_{tw}=D_w\left(1\pm\frac{W_x}{V_{1o}}\right)^2, \tag{6.2}$$

where

$t_{t\,w}$ and t_t are takeoff time with, and without, a wind, respectively;

$D_{t\,w}$ and D_t are takeoff distance with, and without, a wind, respectively;

W_x is the steady wind component coinciding with the runway heading;

V_{1o} is the speed at which the airplane lifts off the runway.

A plus sign inside the parentheses in Equations (6.1) and (6.2) means a tail wind, a minus sign a head wind. Flight tests are the basis for obtaining data on takeoff and landing parameters when there is no wind, that is, under calm conditions.

The cross-wind component is much more important so far as influence on takeoff is concerned. To date the number of cases of failure to meet scheduled airplane movements because the crosswind is stronger than that set for the particular type of airplane is quite high.

Let us consider equations describing airplane motion during the takeoff run process in a crosswind. For purposes of simplification we will not consider the deformation of the wheel pneumatic devices and landing strut shock

---

1. The assumption for constancy of acceleration is very close to the actual acceleration in the case of modern jet airplanes with big power plants.

absorbers. Given these assumptions, airplane motion during the takeoff run will occur in one plane (that of the runway) and, as a result, will be described by two equations for the projections of the forces and by one equation for moments relative to the vertical axis. We will use geographic (x_g, y_g, z_g) and airplane body (x, y, z) coordinate systems to analyze these equations. Figure 6.2 is a diagram of the forces acting on an airplane during the takeoff run, as well as of the positions of the coordinate axes. Designations in this figure are:

x_g, y_g, z_g - geographic axis;

x, y, z - airplane body axes;

X - drag;

Y - lift;

Z - cross-wind force;

G - weight;

P - thrust produced by both engines; /201

M_y, M_z - moments about the y and z axes;

X_n, X_m - frictional forces created by the swaying nose and main wheels;

Y_n, Y_m - reactions of nose and main wheels;

Z_n, Z_m - lateral forces on the nose and main wheels the result of the angle of sideslip for the ground speed;

Z_{is}, Z_{ip} - lateral forces at the entrance to the right and left air intakes, the result of the angle of sideslip for the air speed;

ψ - angle of yaw;

β - angle of sideslip relative to the airspeed vector, V;

β_g - angle of sideslip relative to the ground speed vector, V_g;

β_w - angle of sideslip created by the wind.

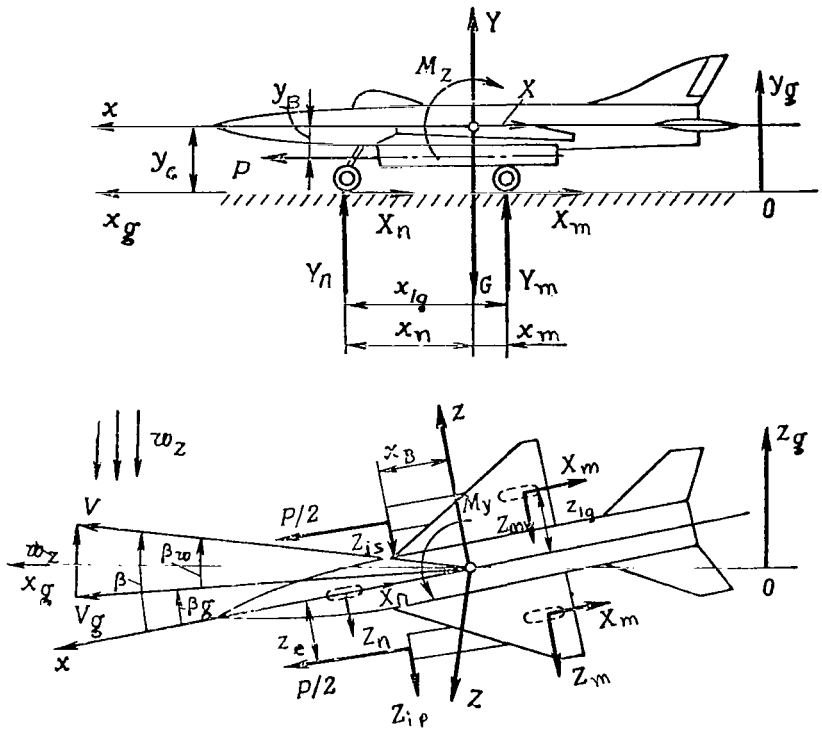

Figure 6.2. Forces and moments applied to an airplane during the take-off run by a crosswind.

The designations that pertain to linear dimensions are clear from the drawings in Figure 6.2. /202

Airplane motion in the $x_g Oz_g$ plane can be described by the equations (in body axes)

$$\left.\begin{aligned} m\frac{dV_{gx}}{dt} &= \Sigma X,\\ m\frac{dV_{gy}}{dt} &= \Sigma Y,\\ I_y\frac{d^2\psi}{dt^2} &= \Sigma M_y. \end{aligned}\right\} \qquad (6.3)$$

The following obvious relationships, stemming from the assumptions with respect to airplane motion in the plane of the runway, should be used to determine wheel reaction, and are in addition to Equation (6.3) describing airplane motion

$$\left.\begin{aligned}\Sigma Y&=0,\\ \Sigma M_x&=0,\\ \Sigma M_z&=0.\end{aligned}\right\} \tag{6.4}$$

Let us now proceed to a consideration of the right sides of Equation (6.3). The force diagram in Figure 6.2 tells us that

$$\Sigma X = P - X\cos\beta - X_f \tag{6.5}$$

where

X_f is the total frictional force applied to the wheels.

The frictional force can be determined through the relationship

$$X_f = \mu(Y_n + Y_m), \tag{6.6}$$

where

μ is the coefficient of friction of the sway; this coefficient varies between 0.03 and 0.05 for concrete runways.

The first formula in Equation (6.4) will be used to determine the forces of the reactions by the noise and main wheels of the landing gear ($Y_n + Y_m$)

$$Y_n + Y_m = G - Y. \tag{6.7}$$

Taking $\cos\beta \cong 1$ as approximate, and with Equation (6.7) in mind, Equation (6.5) finally yields

$$\Sigma X = P + (\mu C_y - C_x) S\frac{\rho V^2}{2} - \mu G. \tag{6.8}$$

Let us now move on to an analysis of the lateral forces acting on an airplane during the takeoff run. We will assume that the equations that follow will be used only for analyzing the motion of an airplane that has already gathered considerable speed. Actually, no particular difficulties arise in controlling airplane motion at slow speeds in a wind because the forces attributable to the wind are slight, whereas the frictional forces of the wheels on the runway are substantial. The action of the lateral wind is readily opposed /203 by turning the nose wheel, or by individual braking of the main wheels. Increase in takeoff run speed results in increase in lift, and reduction of the frictional force of the wheels on the runway. The nose wheel then lifts off the runway, and the end of the takeoff run is made on the main wheels (Figure 6.3).

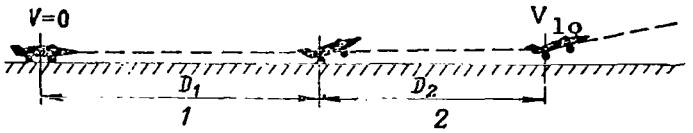

Figure 6.3. Two sections of the take-off run.
D_1 - on three wheels; D_2 - with nose wheel up.

The speed at which the airplane is moving is such that the following approximate kinematic relationships can be used

$$\beta_g \cong V_{gz}/V \quad \text{and} \quad \beta_w \cong w_z/V.$$

Let us consider the sum of the projections of the forces on the z axis

$$\Sigma Z = Z + Z_i + Z_n + Z_m \tag{6.9}$$

where

Z is the lateral aerodynamic force the result of the nonsymmetrical airplane blowing;

$Z_i = Z_{is} + Z_{ip}$ are the lateral forces at the engine intake inlet mouth;

Z_n and Z_m are the lateral forces acting on the nose and main wheels when sideslip occurs.

Let us suppose the rudder and the nose wheel are used during the take-off run to control the angle of yaw. Let us proceed to linearize the expressions for just the lateral forces attributable to the angle of sideslip and to the angles of nose wheel and rudder deflections, selecting for the initial undisturbed condition the straight-line movement of the airplane. Based on these assumptions, we obtain the following expressions for lateral forces.

The lateral aerodynamic force, Z, depends on the total angle of sideslip, β, relative to the air speed vector and on the rudder angle, δ_r

$$Z = C_z^{\beta} S \frac{\rho V^2}{2} \beta_g - C_z^{\bar{\omega}_z} S \frac{\rho V}{2} w_z + C_z^{\delta_r} S \frac{\rho V^2}{2} \delta_r \tag{6.10}$$

The lateral force acting at the air intake inlet mouths in the case of a nonsymmetrical flow over the airplane equals

$$Z_i = -kP\beta = -kP\beta_g + kPw_z/V, \tag{6.11}$$

where

$k = W_{in}/(W_{out} - W_{in})$;

W_{in} and W_{out} are the airstream velocities at the engine intake and outlet, respectively. /204

$Z_i \ll Z$, and Z_i, are usually disregarded when the airplane is flying. The role of Z_i can be substantial during the take-off run, and particularly over the initial section.

The lateral forces Z_n and Z_m depend on the angle of sideslip, β, relative to the ground speed vector, or on the angle by which the nose wheel is turned relative to the ground speed vector.

Accordingly,

$$Z_n + Z_m = Z_n^{\beta}\beta_g + Z_n^{\delta_n}\delta_n + Z_m^{\beta}\beta_g = Z_w^{\beta}\beta_g + Z_n^{\delta_n}\delta_n, \tag{6.12}$$

where

$$Z_w = C_{z\,w}(Y_n + Y_m) = C_{z\,w}(G - Y).$$

Thus,

$$Z_n + Z_m = C_{z\,w}^{\beta}(G - Y)\beta_g + C_{zw}^{\delta_n}Y_n\delta_n. \tag{6.13}$$

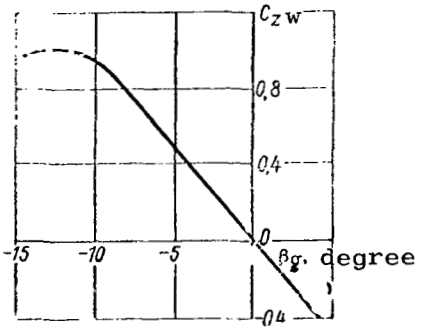

Figure 6.4. Coefficient of lateral force of wheels in terms of the angle of sideslip.

Figure 6.4 shows the graphic of $C_{z\,w} = f(\beta_g)$, determined experimentally. It is apparent that the coefficient $C_{z\,w}$ is equal to the ratio of the lateral force of the wheel to the normal reaction. What follows from the graphic in Figure 6.4 is that this ratio is near unity when angle β_g is about 10°. Beginning with some angle β_g, its further increase will result in a reduction of the lateral force of the wheel. The maximum value of $C_{z\,w}$ is equal to the coefficient of friction of the sideslip for the wheels moving over the runway.

Equations (6.10), (6.11), and (6.13) yield the expression for the sum of the projections of the forces on the z axis as

$$\Sigma Z=\left[C_z^{\beta}S\frac{\rho V^2}{2}+C_{z_w}^{\beta}\left(G-C_yS\frac{\rho V^2}{2}-kP\right)\right]\beta_g+$$
$$+C_z^{\delta_r}S\frac{\rho V^2}{2}\delta_r+C_{z_w}^{\delta_n}Y_n\delta_n-\left(C_z^{\beta}S\frac{\rho V}{2}-kP/V\right)w_z. \tag{6.14}$$

Finally, let us consider the moments about the y axis acting on the airplane during the takeoff run

$$\Sigma M_y=M_{yz}+M_{y\omega_y}+M_{yP}+M_{y\,b}+M_{yx}, \tag{6.15}$$

where

M_{yz} is the moment created by the lateral forces; /205

$M_{y\omega_y}$ is the moment attributable to the angular velocity ω_{y_1};

M_{yP} is the moment from the non-symmetrical thrust of the engines;

$M_{y\,b}$ is the moment from the non-symmetrical braking of the main wheels;

M_{yx} is the moment about the y axis attributable to the moment about the x axis.

On the basis of Figure 6.2, the moment about the z axis created by the lateral forces can be determined through the expression

$$M_{yz}=m_y^{\beta}lS\frac{\rho V^2}{2}\beta_g-m_y^{\dot{\beta}}lS\frac{\rho V}{2}w_z+kPx_1\beta_g-\frac{kPx_1}{V}w_z-$$
$$-C_{z_w}^{\beta}Y_nx_n\beta_g+C_{z_w}^{\beta}Y_mx_m\beta_g+m_y^{\delta_r}lS\frac{\rho V^2}{2}\delta_r-C_{z_w}^{\delta_n}Y_nx_n\delta_n. \tag{6.16}$$

The angular velocity, ω_y, causes the appearance of an aerodynamic damping moment and of an additional moment attributable to the changes in the lateral forces of all wheels because of the change in the angles of sideslip as a result of

$$M_{y\omega_y}=M_y^{\omega_y\omega_y}+M_{y_w}^{\omega_y}\omega_y=$$
$$=\left[m_y^{\omega_y}Sl\frac{\rho V^2}{2}+\frac{C_{z_w}^{\beta}}{V}(Y_nx_n^2+Y_mx_m^2)\right]\omega_y. \tag{6.17}$$

If the starboard engine has a thrust greater than that of the port engine of ΔP

$$M_{yP}=\Delta P_{z_e}, \tag{6.18}$$

where

z_e is the distance from the axis of the engine to the airplane's plane of symmetry.

The moment of non-symmetrical braking changes in the limits from zero to some maximum that depends on the difference in the forces applied to the right and left brake shoes. The maximum value for $M_{y\,b}$ is obtained when one wheel is completely braked, and the other is free. Then

$$M_{yb\max}=f\frac{Y_m}{4}z_{1g}. \tag{6.19}$$

where

f is the coefficient of friction of sideslip between the wheel and the runway surface.

The moment M_{yx} is set up with the appearance of the rolling moment. The rolling moment can appear during the takeoff run as a result of movement with sideslip, or with aileron deflection. That is,

$$M_x=M_x^{\beta}\beta_g-M_x^{\beta}w_z/V+M_x^{\delta_a}\delta_a. \tag{6.20}$$

A positive rolling moment increases the reaction of the right main wheel, /206 and decreases the reaction of the left. The difference in these reactions is

$$\Delta Y_m=M_x/z_{1g}. \tag{6.21}$$

The inequality in the reactions of the main wheels results in an inequality in the frictional forces, and a yawing moment occurs

$$M_{yx}=-\mu\Delta Y_m z_{1g}. \tag{6.22}$$

Substituting the value of ΔY_m and M_x from Equations (6.20) and (6.21) in Equation (6.22), we obtain

$$M_{yx}=-\mu\left(m_x^{\beta}lS\frac{\rho V^2}{2}\beta_g-m_x^{\dot{\beta}}lS\frac{\rho V}{2}w_z+m_x^{\delta_a}lS\frac{\rho V^2}{2}\delta_a\right). \tag{6.23}$$

These relationships now become the basis for finding expressions for the sum of the moments about the y axis

$$\Sigma M_y = \left(m_y^{\beta} lS \frac{\rho V^2}{2} + kP_{x\,i} - C_{zw}^{\beta} Y_n x_n + C_{zw}^{\beta} Y_m x_m - \mu m_x^{\beta} lS \frac{\rho V^2}{2}\right)\beta_g +$$

$$+\left[m_y^{\omega_y} lS \frac{\rho V^2}{2} + \frac{C_{zw}^{\beta}}{V}(Y_n x_n^2 + Y_m x_m^2)\right]\omega_y +$$

$$+ m_y^{\delta_r} lS \frac{\rho V^2}{2}\delta_r - C_{zw}^{\delta_n} Y_n x_n \delta_n - \mu m_x^{\delta_a} lS \frac{\rho V^2}{2}\delta_a + \Delta P z_e +$$

$$+ cf \frac{Y_m}{4} z_{1g} - \left(\frac{kP}{V} x_i + m_y^{\beta} lS \frac{\rho V}{2} + \mu m_x^{\beta} lS \frac{\rho V}{2}\right) w_z, \qquad (6.24)$$

where

c is a coefficient that changes from zero to one according to the degree of non-symmetry of wheel braking.

The expressions for the reactions of the nose and main wheels have not been expanded in Equations (6.14) and (6.24) to keep the notation short. Using the third of the expressions at Equation (6.4), and with Equation (6.7) and Figure 6.2 taken into consideration, we obtain

$$\left.\begin{aligned} Y_n &= (G - Y)\frac{x_m + \mu y_c}{x_{1g}} - \frac{M_z + P y_i}{x_{1g}}, \\ Y_m &= (G - Y)\frac{x_n - \mu y_c}{x_{1g}} + \frac{M_z + P y_i}{x_{1g}}. \end{aligned}\right\} \qquad (6.25)$$

Substituting the values for the right sides obtained from Equations (6.8), (6.14), and (6.24) in the original ones in Equation (6.3), and transposing the terms with unknown functions (airplane motion parameters) to the left sides of the equations, we obtain

/207

$$\left.\begin{aligned} & m\frac{dV_{gx}}{dt} + (C_x - \mu C_y) S \frac{\rho V^2}{2} = P - \mu G, \\ & mV\frac{d\beta_g}{dt} + \left[kP + (C_y C_{zw}^{\beta} - C_z^{\beta}) S \frac{\rho V^2}{2} - C_{zw}^{\beta} G\right]\beta_g = \\ & \quad = \left(\frac{kP}{V} - C_z^{\beta} S \frac{\rho V}{2}\right) w_z + C_z^{\delta_r} S \frac{\rho V^2}{2}\delta_r + C_{zw}^{\delta_n} Y_n \delta_n, \\ & I_y \frac{d^2\psi}{dt^2} - \left[m_y^{\omega_y} lS \frac{\rho V^2}{2} + \frac{C_{zw}^{\beta}}{V}(Y_n x_n^2 + Y_m x_m^2)\right]\frac{d\psi}{dt} + \\ & + \left[(\mu m_x^{\beta} - m_y^{\beta}) lS \frac{\rho V^2}{2} + C_{zw}^{\beta}(Y_n x_n - Y_m x_m) - kP x_i\right]\beta_g = \\ & \quad = -\left[(m_y^{\beta} + \mu m_x^{\beta}) lS \frac{\rho V}{2} + \frac{kP}{V}\right] w_z + m_z^{\delta_r} lS \frac{\rho V^2}{2} - \\ & \quad - C_{zw}^{\delta_n} Y_n x_n \delta_n - \mu m_x^{\delta_a} lS \frac{\rho V^2}{2}\delta_a + \Delta P z_e + cf \frac{Y_m}{4} z_{1g}. \end{aligned}\right\} \qquad (6.26)$$

Equation (6.26) must be supplemented by Equation (6.25) and the kinematic relationships

$$V \cong V_{gx} - w_x, \tag{6.27}$$

$$\frac{dz_y}{dt} \cong V_{gx}(\beta_g - \psi). \tag{6.28}$$

Let us once again emphasize the fact that Equations (6.26) and (6.28) cannot be used at the moment the airplane begins to roll, but only at the moment of attaining that speed at which the approximate relationships $\beta_w \cong w_z/V$ and $\beta_g \cong V_{gz}/V$ taken for the angle of sideslip can be satisfied with an acceptable degree of accuracy.

Equations (6.26) - (6.28) can be used, in principle, to determine five unknown parameters characterizing airplane motion during the takeoff run: V_{gx}, V, β_g, ψ and z_g. However, in order to obtain this solution, wind velocity ω_z must be specified as a function of time, and the connections with the many variables contained in the right sides of Equation (6.26) must be applied: P, ΔP, M_z, δ_r, δ_n, δ_a and C.

The most natural forms of these connections are the ratios used in the systems for controlling airplane takeoff automatically, since they link the variables indicated with the airplane motion parameters. However, they will not be taken up here because systems such as these have not yet been put to use.

Various assumptions, greatly simplifying the problem, are made when the pilot is flying the airplane and Equations (6.26) - (6.28) are used to analyze airplane motion. For example, the first expression in the Equation (6.26) /208 system can be used to make an analytical determination of the time and length of the take-off run if the take-off run stage is conventionally broken down into two stages, as in Figure 6.3. It can be supposed that a completely established angle of attack and, as a result, definite values of C_x and C_y, correspond to each of these stages. The transition from the first to the second stage is made after the airplane has reached a speed providing the elevator with sufficient power to control the angle of attack.

The lift-off speed for the airplane can be established through the

formula

$$V_{1o}=\sqrt{\frac{2G}{\rho S C_{y\ 1o}}}, \qquad (6.29)$$

where

$C_{y\ 1o}$ is selected somewhat less than $C_{y\ lim}$, and can be determined with control mechanization and effect of the proximity of the ground taken into consideration.

6.3. Landing in Moving Air.

Landing is the airplane motion process from the moment the airplane arrives in the airdrome area to the moment the airplane stops on the runway at the end of the roll-out run.

Wind in the airdrome area significantly complicates all stages of the landing, and its influence increases with approach of the airplane to the ground. The longitudinal wind component makes a considerable change in the length of the airplane's roll-out run, which is one of the most important characteristics. Because the length of the roll-out run upon landing usually is longer than the takeoff run, it is the roll-out run that determines runway length. Roll-out run is computed and determined experimentally for calm weather. When the wind component is along the runway the landing is made into the wind and the shortening of the length of the roll-out run increases landing safety. For this reason, and just as in the case of takeoff run consideration, we will limit ourselves to a very approximate evaluation of the influence of the longitudinal wind component on the time and length of the airplane's roll-out run. The formulas in what follow have been obtained by assuming constancy in the deceleration of the airplane during the roll-out run

$$t_{rw}=t_r\left(1\pm\frac{W_x}{V_1}\right), \qquad (6.30)$$

$$D_{r\,w}=D_r\left(1\pm\frac{W_x}{V_1}\right)^2, \qquad (6.31)$$

where

$t_{r\ w}$ and t_r are time of roll-out run in a wind and without wind, respectively;

$D_{r\ w}$ and D_r are the length of roll-out run in a wind and without

wind, respectively;

V_1 is landing speed.

A plus sign in Equations (6.30) and (6.31) is for a tail wind, W_x, and a minus sign for a head wind.

The equations obtained in the preceding section to describe the takeoff run can be used to describe the roll-out run, once certain corrections have been introduced. For this reason in what follows a specific stage of the landing will be considered, that of the landing approach from the moment of the beginning of the letdown to arrival at an altitude of 30 to 50 meters. /209

Crosswinds make the landing much more complicated.

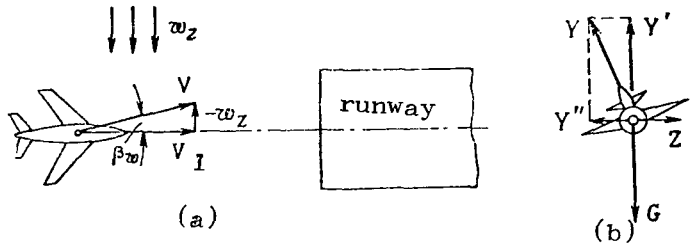

Figure 6.5. Landing with sideslip and roll.

a - plan view; b - view of the airplane from the tail.

It is desirable to analyze landing dynamics when there is a crosswind by assuming automatic control of the airplane because in such case the landing process lends itself to analytical description.

First, however, let us describe, briefly, the special features of landing in a crosswind when the airplane is being handled by the pilot. Crosswind complicates piloting an airplane. As was pointed out in Chapter 4, it causes the airplane to drift about the selected flight path (see Figure 4.1), which, in the case of a landing, coincides with the axis of the runway (in the horizontal plane). There are two ways in which the pilot can counteract drift after lining up along the runway axis:

(1) fly with sideslip and with roll;

(2) change course at which flying relative to the landing course. The landing course is taken as the course coinciding with the runway axis.

Let us consider the first of these. The pilot can use rudder and ailerons to sideslip and roll on the wing on the windward side (Figure 6.5 a and b).

An angle of sideslip

$$\beta=\beta_w=-w_z/V_1 \tag{6.32}$$

must be provided in order to fly along the runway axis without sideslip ($\beta_g = 0$), and this is in accordance with Equation (2.22) for the air speed, V, vector. The denominator of Equation (6.32) is the lowest landing speed at which the crosswind can be opposed solely by aerodynamic forces. The frictional forces of the wheels against the runway can also be used to oppose the crosswind after touchdown. /210

Taking it that in level flight the moments about the x and y axes should be zero, and moreover assuming that $dw_x/dz = dw_y/dz = 0$, from the second and third equations in the system of Equation (2.28) we obtain

$$\left.\begin{aligned}\frac{l_\beta}{V_1}w_z+l_a\delta_a=0,\\ \frac{n_\beta}{V_1}w_z+n_r\delta_r=0.\end{aligned}\right\} \tag{6.33}$$

Solving Equation (6.33) in terms of δ_a and δ_r, we find the angle the controls must be deflected to create sideslip β capable of opposing crosswind w_z

$$\left.\begin{aligned}\delta_a=-\frac{l_\beta}{l_aV_1},\\ \delta_r=-\frac{n_\beta}{n_rV_1}.\end{aligned}\right\} \tag{6.34}$$

If values from Table 2.2 are substituted for the coefficients of Equation (2.28), we obtain the following expressions for the angles δ_a and δ_r

$$\left.\begin{aligned}\delta_a=-\frac{1}{V_1}\frac{m_x^\beta}{m_x^{\delta a}}w_z,\\ \delta_r=-\frac{1}{V_1}\frac{m_y^\beta}{m_y^{\delta r}}w_z.\end{aligned}\right\} \tag{6.35}$$

Substituting the maximum values for δ_a and δ_r in Equation (6.35), we can find the limit for the crosswind velocity that can still be opposed by sideslip as

$$\left.\begin{aligned} w_{z1} &= -V_1 \frac{m_x^{\delta_a}}{m_x^{\beta}} \delta_{a_{max}}, \\ w_{z2} &= -V_1 \frac{m_y^{\delta_r}}{m_y^{\beta}} \delta_{r_{max}}. \end{aligned}\right\} \qquad (6.36)$$

Naturally, the lesser of the two limits for crosswind velocity provided by Equation (6.36) must be selected. Thus, the permissible crosswind value is limited by control power. The lesser value usually is obtained from the second expression in Equation (6.36). Let us demonstrate this by the following example. The landing regime for one of the airplanes can be characterized by the following data: V_1 = 70 m/s, m_x^{β} = -0.063, $m_x^{\delta_a}$ = -0.137, m_y^{β} = -0.069 /211
$m_y^{\delta_r}$ = -0.0458, $\delta_{r\ max}$ = 25° = 0.437 radian; $\delta_{a\ max}$ = 20^2 + 0.35 radian. Substituting these values in Equation (6.36) we obtain w_{z1} = 52 m/s, w_{z2} = 20 m/s.

It should be borne in mind that crosswind velocity permissible under real conditions should be somewhat less than the limit obtained through Equation (6.36). Some margin by which the controls can be moved must be retained in order to oppose wind gusts always accompanying the steady wind component.

Flying with sideslip causes a lateral aerodynamic force Z that attempts to curve the flight path. If the flight is to follow a straight line, roll must be created as shown in Figure 6.5b in order to counter force Z with the Y" component of the lift. The required angle of roll is obtained through the first equation of the system of Equation (2.28), with the expressions for k_{β} and k_{γ} listed in Table 2.2 taken into consideration

$$\gamma = \frac{C_z^{\beta}}{C_{ye} V_1} w_z. \qquad (6.37)$$

The roll must be taken off at the end of the hold prior to touchdown on the runway and the landing must be made on both wheels.

When the second method of countering wind action causing the airplane to drift off the runway axis is used the course is changed by an angle $\psi \cong w_z/V_1$ (Figure 6.6). In this method the longitudinal axis of the airplane does not coincide with the direction in which the center of gravity is moving, a movement taking place along the runway axis. The rudder must be used to

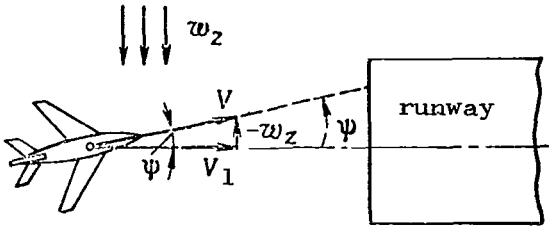

Figure 6.6. Landing with a course change in flight.

turn the airplane to line up its longitudinal axis with that of the runway just before landing. This is particularly important for airplanes with tail wheels, the main wheels of which, located in front of the center of gravity, create a destabilizing yawing moment upon touching down on the runway. In the case of airplanes with a nose wheel, the main wheels create a stabilizing yawing moment upon touching down on the runway, and this turns the airplane along the runway axis.

During the post-landing roll-out run the airplane, possessing yaw stability, will turn into the wind to eliminate sideslip. If the turning moment is /212 to be countered, use must be made of non-symmetrical braking of the main wheels, or the controlled nose wheel must be turned.

The analysis, and the formulas obtained for crosswind landing characteristics are for the steady-state condition. They do not indicate the process involved in making the transition to this condition. Moreover, the unfavorable nature of this transition, attributable to the unsatisfactory dynamic properties of the airplane, can make piloting during the landing extremely difficult.

Let us consider, briefly, what is involved in the landing approach when the airplane is controlled automatically.

Figure 6.7 is a diagram explaining the operation of a system used to make an automatic landing approach. The course (CIB) and glide path (GPB) beacons are used to form the glide path for the glide in the vertical plane passing through the runway axis, GO_1, and which has an angle of inclination $\theta_G = 2$ to

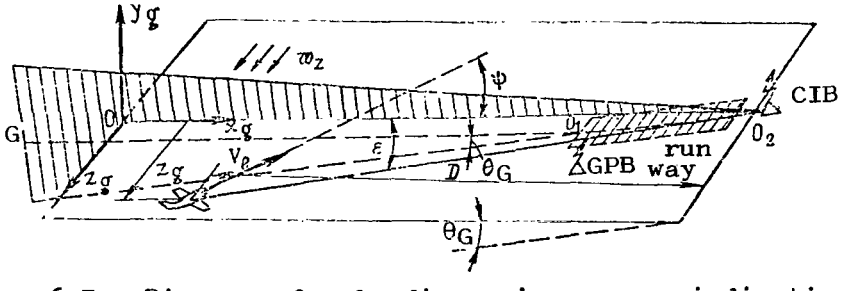

Figure 6.7. Diagram of a landing using course-indicating (CIB) and glide-path (GPB) beacons.

3° relative to the horizontal plane. The use of the instrumentation carried by the airplane to measure the normal and lateral deviations of the airplane from the glide path, and the introduction of the corresponding signals into the automatic control system can bring the airplane out at an altitude of 30 to 50 meters and 500 to 1,000 meters from the beginning of the runway. The pilot then takes over to make the landing.

The longitudinal motion of the airplane during the landing usually is considered within the vertical plane containing the glide path. Wind around the airdrome has its greatest effect on lateral motion. Let us analyze the lateral motion, which we will consider as taking place in the so-called lateral plane, that is, in an inclined plane perpendicular to the vertical plane passing through the course-indicating beacon. The angle of inclination of the lateral plane equals θ_G; that is, the intersection of the vertical and inclined (lateral) planes occurs along the line OO_2 parallel to the glide path GO_1. The line OO_2 in the lateral plane coincides with the runway axis and for purposes of brevity in what follows we will simply call it the runway axis. Let us note that in fact the lateral motion of the airplane does not /213 take place in the lateral plane, but in a plane parallel to it containing the glide path GO_1. However, in order to simplify the kinematic relationships, it is more convenient to consider the lateral motion of the airplane in the lateral plane.

Let us use a geographic system of coordinates to analyze the lateral motion. The x_g axis is along the line OO_2, the z_g axis is horizontal (see Figure 6.7). Thus, the lateral displacement of the airplane relative to the specified flightpath, for which the line OO_2, the runway axis, has been taken in lateral motion, equals z_g. The instrumentation aboard the airplane measures the angle ϵ, the angle between the runway axis and a line joining the airplane is to the right of the runway axis. Distance D is the projection of the airplane-course-indicating beacon line on the runway axis. Because of the smallness of angle ϵ, it can be considered that the distance coincides with the airplane-course-indicating beacon distance. Finally, the angle of yaw, ψ, determines the deviation of the airplane's longitudinal axis from the runway axis.

Let us consider the principal relationships that determine the movement of the airplane's center of gravity in the lateral plane. At the same time, for the sake of simplicity, we will ignore the transient times for airplane angular motions, taking it that they occur instantaneously. The problem is transformed from a dynamic to a kinematic one as a result of this assumption.

The last of the equations in the Equation (2.21) system yields

$$\frac{dz_g}{dt}=V_e(\beta_g-\psi_S). \tag{6.38}$$

Let us emphasize that angle β_g in Equation (6.38) is the angle of sideslip for the ground speed vector. Since the autopilot controls the angle of yaw, it can be assumed that the real angle of yaw, ψ, instantaneously acquires the value ψ_s, specified by the system of equations, and that in place of ψ in Equation (6.38) the angle ψ_s, which is equal to it, is introduced.

The angle of sideslip relative to the air, β, for the stable airplane will always equal zero, the result of ignoring the times of the angular motions. Therefore, and on the basis of the first equation in the Equation (2.22) system

$$\beta_g=-\beta_w=w_z/V_e.$$

Substituting this β_g value in Equation (6.38), we obtain

$$\frac{dz_g}{dt}=w_z-V_e\psi_S \tag{6.39}$$

Figure 6.7 is the basis for saying that

$$z_g=D\operatorname{tg}\varepsilon\cong D\varepsilon. \tag{6.40}$$

In the case of small ψ it can be taken that /214

$$D=D_0-V_et. \tag{6.41}$$

Combining Equations (6.38 - (6.41), we obtain

$$\frac{D}{V_e}\frac{d\varepsilon}{dt}-\varepsilon=\frac{w_z}{V_e}-\psi_S. \tag{6.42}$$

Some angle of yaw, ψ_s, control law must be specified in order to use Equation (6.42) for solving the problem of the movement of the airplane's center of

gravity. The simplest variant of such a law is

$$\psi_s = k_\varepsilon \varepsilon + \Delta, \tag{6.43}$$

where

Δ is the sum of the errors in the control system sensors.

Contained in Δ are the errors in measuring angles ψ and ε. And the error in the vertical-axis gyroscope when measuring the angle of roll, needed to provide the angular velocity $d\psi/dt$, too should be included. However, in the kinematic analysis it is assumed that the turn by angle ψ_s is made instantaneously, so the error in the vertical-axis gyroscope cannot be considered.

Substituting the ψ_s value from Equation (6.43) in Equation (6.42), we obtain

$$\frac{D}{V_e}\frac{d\varepsilon}{dt} + (k_\varepsilon - 1)\varepsilon = \frac{w_z}{V_e} - \Delta. \tag{6.44}$$

Introducing a new independent variable $D/V_e = t_o - t$, in place of t, from Equation (6.44) we have

$$(t_0 - t)\frac{d\varepsilon}{d(t_0 - t)} = (k_\varepsilon - 1)\varepsilon - \left(\frac{w_z}{V_e} - \Delta\right). \tag{6.45}$$

Integrating Equation (6.45), and with the relationship in Equation (6.40) taken into consideration, we obtain the solution ($w_z = W_z$ = constant)

$$\varepsilon = \varepsilon_0\left(\frac{t_0 - t}{t_0}\right)^{k_\varepsilon - 1} + \frac{W_z - V_e\Delta}{V_e(k_\varepsilon - 1)}\left[1 - \left(\frac{t_0 - t}{t_0}\right)^{k_\varepsilon - 1}\right], \tag{6.46}$$

$$z_g = z_{g0}\left(\frac{t_0 - t}{t_0}\right)^{k_\varepsilon} + (t_0 - t)\frac{W_z - V_e\Delta}{k_\varepsilon - 1}\left[1 - \left(\frac{t_0 - t}{t_0}\right)^{k_\varepsilon - 1}\right]. \tag{6.47}$$

Figure 6.8 presents the $z_g(t)$ graphics, constructed using Equation (6.47) and assuming wind W_z and the sum of the errors Δ are zero. The following initial conditions were selected for their construction: D_0 = 10,000 meters; t_0 = 180 seconds (V_e = 55.5 m/s); z_{g0} = 100 meters. The distance from the beginning of the runway to the course-indicating beacon site is 3,000 meters. The graphics in Figure 6.8 were constructed for various values of the coefficient k_ε, increase in which results in a reduction in the time required to bring the airplane into the runway axis.

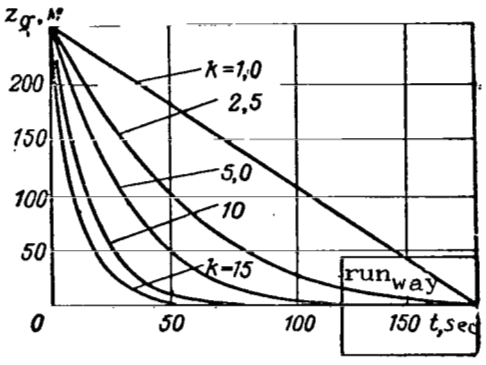

Figure 6.8. Nature of the liquidation of the lateral deviation of the airplane from the runway axis by the simplest automatic control system.

Comparison of the graphics will establish a value of k_ε = (7.5 - 10) as adequate for the problem under consideration. It must be remembered that the real airplane always rolls when making a turn, and that this roll is always limited. Increase in k_ε results in a reduction in the zone of linearity of the control system, to a sharp rolling of the airplane, and to high angular velocities $d\psi/dt$, all of which give passengers unpleasant sensations. /215

Let us evaluate the influence of the wind and of the errors in the control system on the accuracy with which the airplane is lined up with the runway axis, using the same numerical data used to construct the graphics in Figure 6.8 for the case of k_ε = 10. For our evaluation we will take the z_g value from the moment of approach of the airplane to the beginning of the runway, that is, when t = 126 seconds. Substituting this value in Equation (6.47), we obtain

$$\left.\begin{aligned} z_{gw} &\cong 6W_z, \\ z_{g\Delta} &= -333\Delta. \end{aligned}\right\} \qquad (6.48)$$

The relationships in Equation (6.48) show that with a crosswind W_z = 10 m/s, the lateral deviation is 60 meters, and for a total error Δ = 0.1 radian, the lateral deviation is 33.3 meters. These deviations can be summed, because of the random nature of both factors (W_z and Δ). Lateral deviations such as these are unacceptable when runway width is 60 meters.

The airplane control system considered will be called a static system in terms of the crosswind and measurement errors.

Let us, in order to eliminate the drawback noted for the static automatic control system, introduce in the Equation (6.43) angle of yaw control law the integral of the signal with respect to angle ε. The result will be for this law to acquire the form

$$\psi_s = k_\varepsilon \varepsilon + q_\varepsilon \int_0^t \varepsilon\, dt + k_\varepsilon \Delta\varepsilon + q_\varepsilon \int_0^t \Delta\varepsilon\, dt + k_\psi \Delta\psi. \tag{6.49}$$

The components of the errors in the control system, which we will consider to be random, but not dependent on the time of the magnitudes, have been expanded in Equation (6.49). Combining the Equation (6.49) control law with the kinematic equations in Equation (6.42), we obtain a general equation for the system considered for the case of integral control /216

$$\frac{D}{V_e}\frac{d^2\varepsilon}{dt^2} + (k_\varepsilon - 2)\frac{d\varepsilon}{dt} + q_\varepsilon \varepsilon = -q_\varepsilon \Delta\varepsilon. \tag{6.50}$$

The form of Equation (6.50) indicates that in the case of integral control the steady wind component, as well as the error in the course system, have no effect on the accuracy with which the airplane lines up along the runway axis; that is, a system with integral control is astatic with respect to the actions indicated. The error will result only from the error $\Delta\varepsilon$ when angle ε is measured. This error is very small, because practically speaking, Equation (6.50) can be considered homogeneous. This equation will be reduced to the following form by making the transition to a new independent variable $\mu = q_\varepsilon D/V_e = q_\varepsilon (t_0 - t)$

$$\mu \frac{d^2\varepsilon}{d\mu^2} + [1 - (k_\varepsilon - 1)]\frac{d\varepsilon}{d\mu} + \varepsilon = 0. \tag{6.51}$$

Finally, by substituting $\varepsilon = \mu^{\frac{\nu}{2}} x$, where $x = f(2\sqrt{\mu})$, Equation (6.51) will reduce to a Bessel equation of order ν;

$$\frac{d^2x}{d\tau^2} + \frac{1}{\tau}\frac{dx}{d\tau} + \left(1 - \frac{\nu^2}{\tau^2}\right)x = 0, \tag{6.52}$$

where

$$\tau = 2\sqrt{\mu} = 2\sqrt{q_\varepsilon (t_0 - t)}, \quad \nu = k_\varepsilon - 1.$$

The solution of Equation (6.52) for initial conditions

is in the form

$$\varepsilon = \varepsilon_0 \left(\frac{t_0 - t}{t_0}\right)^{\frac{k_\varepsilon - 1}{2}} [A_1 J_\nu(\tau) - A_2 Y_\nu(\tau)]. \tag{6.53}$$

Considering Equation (6.40), we obtain for the lateral deviation

$$z_g = z_{g0}\left(\frac{t_0 - t}{t_0}\right)^{\frac{k_\varepsilon - 1}{2}} [A_1 J_\nu(\tau) - A_2 Y_\nu(\tau)]. \tag{6.54}$$

J_ν and V_ν in Equations (6.53) and (6.54) are Bessel functions of the first and second kind of the order $\nu = k_\varepsilon - 1$ (ν is an integer). The constants A_1 and A_2 can be determined from

$$\left.\begin{aligned} A_1 &= \frac{Y'_\nu(\tau_0)}{J_\nu(\tau_0) Y'_\nu(\tau_0) - J'_\nu(\tau_0) Y_\nu(\tau_0)}, \\ A_2 &= \frac{J'_\nu(\tau_0)}{J_\nu(\tau_0) Y'_\nu(\tau_0) - J'_\nu(\tau_0) Y_\nu(\tau_0)}, \end{aligned}\right\} \tag{6.55}$$

/217

where

$$J'_\nu(\tau_0) = J_{\nu-1}(\tau_0) - \frac{1}{\tau_0} J_\nu(\tau_0),$$

$$Y'_\nu(\tau_0) = Y_{\nu-1}(\tau_0) - \frac{1}{\tau_0} Y_\nu(\tau_0),$$

$$\tau_0 = 2\sqrt{k_\varepsilon t_0} = 2\sqrt{k_\varepsilon D_0 / V_e}.$$

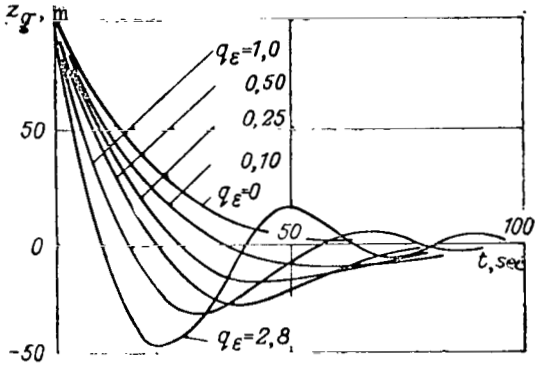

Figure 6.9. Nature of the elimination of the lateral deviation of the airplane from the runway axis by an automatic control system with an integral law.

Equation (6.54) was used to construct the graphics of $z_g = f(t)$, shown in Figure 6.9. The following were used for the initial conditions: D_0 = 8,900 meters; t_0 = 160 seconds (V_e = 55.5 m/s); z_{g0} = 100 meters. The value for the coefficient k_ε was that selected for the static system, that is, k_ε = 10 (see Figure 6.8). The values of the coefficient q_ε for each of the graphics are indicated in Figure 6.9. Comparing the curves, which are actually flight paths (because of the smallness of ψ, $x_g \cong V_c t$ is the abscissa), we can conclude that the smoothest flight path is obtained when

$q_\varepsilon = 0$, and that, as a result, the introduction of integral control results in a deterioration in the transients. This is in fact so because integral control was introduced in order to eliminate the errors arising as a result of the crosswind and measurement errors, these latter resulting in some drift rate for the airplane away from the runway axis. Therefore, in order to analyze the influence of the crosswind in the case of integral control, for example, we find the solution of Equation (6.50) for the following initial conditions: $\varepsilon(0)=0$, $\left(\frac{d\varepsilon}{dt}\right)_{t=0}=\left(\frac{W_z}{D_0}\right)$. What these initial conditions mean physically is that at time t = 0 the airplane encounters a crosswind gust of the unit function type. /218

The solution of Equation (6.50) for the initial conditions indicated is in the form

$$\varepsilon=-\frac{W_z}{V_e\sqrt{q_\varepsilon t_0}}\left(\frac{t_0-t}{t_0}\right)^{\frac{k_\varepsilon-1}{2}}[B_1J_\nu(\tau)-B_2Y_\nu(\tau)]. \tag{6.56}$$

For the lateral deviation we obtain

$$z_g=-\frac{W_z}{V_e}\sqrt{\frac{D_0V_e}{q_\varepsilon}}\left(\frac{t_0-t}{t_0}\right)^{\frac{k_\varepsilon+1}{2}}[B_1J_\nu(\tau)-B_2Y_\nu(\tau)], \tag{6.57}$$

where

$$\left.\begin{aligned}B_1&=\frac{Y_\nu(\tau_0)}{J_\nu(\tau_0)Y'_\nu(\tau_0)-J'_\nu(\tau_0)Y(\tau_0)},\\ B_2&=\frac{J_\nu(\tau_0)}{J_\nu(\tau_0)Y'_\nu(\tau_0)-J'_\nu(\tau_0)Y_\nu(\tau_0)}.\end{aligned}\right\} \tag{6.58}$$

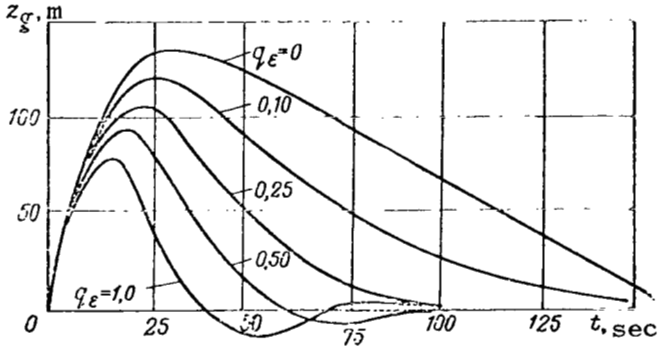

Figure 6.10. Nature of the motion of an airplane, the landing of which is controlled automatically, acted on by a step crosswind.

Figure 6.10 presents the flightpaths of an airplane which, at distance D = 8,900 meters from the course-indicating beacon and on the runway axis, encounters a wind gust W_z = 10 m/s (V_e = 55.5 m/s). k_ε = 10. Figure 6.10 shows the q_ε values for each flight path.

The curves in Figure 6.10 show that when $q_\varepsilon = 0$, the airplane approaches /219
the runway axis at high lateral speed at t = 160 seconds, and this is unacceptable. The maximum lateral deviations of the airplane from the runway axis are very great for small q_ε as well. Based on the graphics in Figure 6.10, it can be asserted that the most appropriate q_ε values are 0.5 to 1.0 for the example cited. At these values the lateral deviation from the runway axis and the time to line up on it are acceptable from the standpoint of landing safety.

Let us consider the complete equations of lateral airplane motion when the airplane is moving through the equisignal zone of the course-indicating-beacon, using the automatic control law for the airplane, selected on the basis of analysis of the simplified kinematic equations. To do so, let us combine the equations for the airplane with autopilot, Equation (2.30), the Equation (6.49) control law equation, and the kinematic relationships of Equations (6.40) and (6.41). The result is the following system of equations

$$\left.\begin{aligned}
&\frac{d\beta}{dt}+k_\beta\beta-k_\gamma\gamma-\frac{d\psi}{dt}=\frac{k_\beta}{V_e}w_z,\\
&l_\beta\beta+\frac{d^2\gamma}{dt^2}+(l_\gamma^{\cdot}+i_\gamma^{\cdot}l_a)\frac{d\gamma}{dt}+i_\gamma l_a\gamma+l_\psi^{\cdot}\frac{d\psi}{dt}-i_\psi l_a\psi=\\
&\qquad=\frac{l_\beta}{V_e}w_z-i_\psi l_a\psi_s,\\
&n_\beta\beta_g+n_\gamma^{\cdot}\frac{d\gamma}{dt}+f_\gamma n_r\gamma+\frac{d^2\psi}{dt^2}+(n_\psi^{\cdot}+f_\psi^{\cdot}n_r)\frac{d\psi}{dt}+\\
&\qquad+f_\psi n_r\psi=\frac{n_\beta}{V_e}w_z+f_\psi n_r\psi_s,\\
&\frac{dz_g}{dt}=V(\beta_g-\psi),\\
&\psi_s=k_\varepsilon\varepsilon+q_\varepsilon\int_0^t\varepsilon\,dt+k_\varepsilon\Delta\varepsilon+q^\varepsilon\int_0^t\Delta\varepsilon\,dt+k_\varepsilon\Delta\psi,\\
&z_g=D\varepsilon,\\
&D=D_0-V_et.
\end{aligned}\right\}\qquad(6.59)$$

As our concrete example, let us use the data for the airplane flying at a speed of V_e = 5.55 m/s used in the above examples to analyze the simplified lateral motion equations. Data on the coefficients of the Equation (6.59) system used to illustrate the movement of the airplane within the equisignal zone of the course-indicating beacon are listed in Table 6.1.

TABLE 6.1

/220

Commas represent decimal points.

k_β	k_γ	l_β	l_γ	l_ψ	l_a	n_β	n_γ	n_ψ
0,147	0,177	5,38	6,75	2,22	—13,7	1,45	—0,256	0,43
n_r	l_γ	i_γ	l_ψ	f_γ	f_ψ	f_ψ	k_ε	q_ε
—0,73	1,0	0	2,0	0,2	1,0	1,4	10	0,5

In this example we have not taken into consideration the errors in the sensors in the automatic control system; it is assumed that $\Delta\varepsilon$ and $\Delta\psi$ are zero.

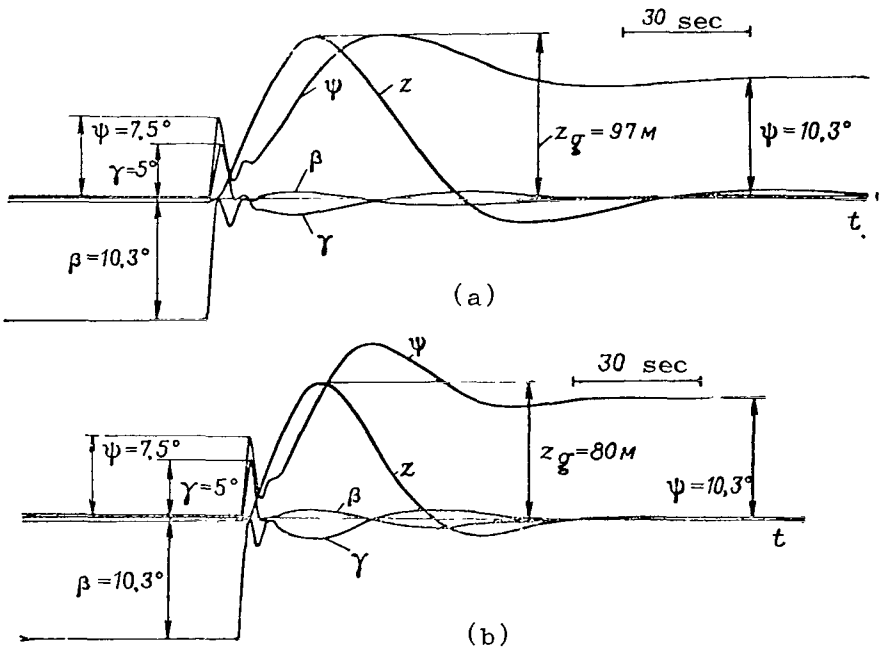

Figure 6.11. Airplane motion in the equisignal zone of the course-indicating beacon in a step crosswind.

a - change in distance from airplane to course-indicating beacon not taken into consideration;
b - effect of this change taken into consideration.

The Equation (6.59) system with coefficients those shown in Table 6.1 was integrated on an analog computer for zero initial conditions applicable to the case of the airplane entering a cross flow of air with a velocity of W_z = 10 m/s. Figures 6.11 and 6.12 show the results of this integration in /221 the form of oscillograms for the most important lateral motion parameters. Figure 6.11 shows airplane motion when a step crosswind with a velocity of W_z = 10 m/s is encountered 9,000 meters from the beginning of the runway. Figure 6.11a shows the oscillograms for the case when change in distance to the course-indicating beacon is not considered, while Figure 6.11b shows those when it is.

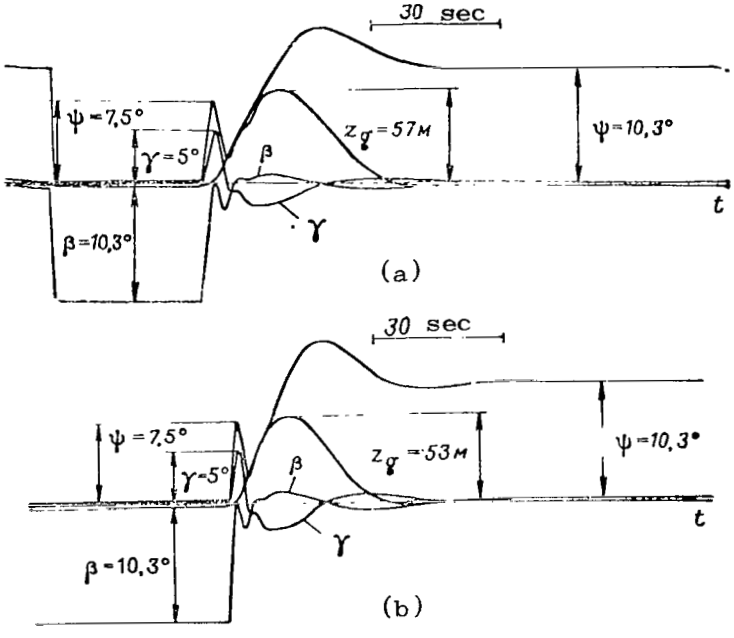

Figure 6.12. Airplane motion in the equisignal zone of the course-indicating beacon in the case of a step crosswind.

a - effect of change in distance from airplane to course-indicating beacon not considered;
b - effect of such change considered.

Figure 6.12 shows the oscillograms for the same flight condition, but for the case when the airplane encounters a step crosswind with a velocity of W_z = 10 m/s 6,000 meters from the course-indicating beacon, or 3,000 meters from the beginning of the runway. Figure 6.12a shows the oscillograms

characterizing the airplane motion when change in distance is not considered, while those in Figure 6.12b are for those when the change is considered.

The moment in time at which the airplane reaches the beginning of the runway in Figure 6.12 coincides with the dimensional arrow for z_g.

An analysis of the oscillograms shown in Figures 6.11 - 6.12 reveals that the automatic lateral motion control system used during the landing and described by Equation (6.59) with coefficients as listed in Table 6.1, practically ensures the elimination of the disturbance caused by a unit function type crosswind at distances less than 3,000 meters (Figure 6.12, z_g curves). In the first 5 seconds, approximately, the airplane with this system behaves as does the airplane with conventional autopilot stabilizing angles of roll and yaw (see Figure 4.4). During this time the airplane will be blown off the runway axis by the wind, the angle ε control signal will increase, and the system used to stabilize the airplane in the equisignal zone of the course-indicating beacon will begin to exert its influence. The wind will continue to blow the airplane off the runway, but at a decreasing rate, and within 15 to 20 seconds from the beginning of the process the airplane will begin to return to the runway axis. This process will be accompanied by smooth, small amplitude oscillations in angles of roll and sideslip. All lateral motion parameters for the airplane (roll, lateral deviation, sideslip) will be zero in the steady-state condition. The exception is the angle of yaw, because of which the initial sideslipping of the airplane caused by the crosswind is balanced. /222

In concluding this section, let us compare the processes involved in the motion when the airplane encounters a crosswind, obtained through the simplified Equation (6.50), and the more complete Equation (6.59). Figure 6.10 shows the solution of Equation (6.50) for the problem considered. A comparison of the graphics in this figure, which are for a system in which $q_\varepsilon = 0.5$, with the oscillogram for z_g in Figure 6.11 persuades us that the simplified Equation (6.50) for lateral deviation yields results that are extremely close to those obtained by analysis of airplane motion when its dynamic characteristics in terms of complete Equation (6.59) are taken into consideration.

Appendix A

A.1. General Airplane Data Used for the Computations in the Various Examples and Coefficients of Longitudinal Motion Equations

Data on five different types of airplanes were used for the computations. These data, and the results of the computations for the coefficients of the longitudinal motion equations, are given below.

Airplane No. 1. A straight-wing heavy transport airplane. Flight conditions: y_g = 8,000 meters; V_e = 650 km/h; M = 0.585; ρ_e = 0.05354 kg-sec^2-m^{-4}.

Airplane No. 2. A swept-wing fighter plane. Flight conditions: y_g = 10,000 meters; V_e = 860 km/h; M = 0.832, ρ_e = 0.04206 kg-sec^2-m^{-4}.

Airplane No. 3. A swept-wing heavy bomber. Flight conditions: y_g = 1,000 meters, V_e = 700 km/h; M = 0.578; ρ_e = 0.1134 kg-sec^2-m^{-4}.

Airplane No. 4. A straight-wing medium passenger airplane. Flight conditions: y_g = 1,000 meters; V_e = 288 km/h; M = 0.24; ρ_e = 0.1134 kg-sec^2-m^{-4}.

Airplane No. 5. A swept-wing heavy passenger airplane. Flight conditions: y_g = 2,900 meters; V_e = 700 km/h; M = 0.6; ρ_e = 0.09272 kg-sec^2-m^{-4}.

The coefficients of the longitudinal motion equations are listed in Table A.1.

TABLE A.1

/224

Coefficient	Airplane No. 1	Airplane No. 2	Airplane No. 3	Airplane No. 4	Airplane No. 5
a_ϑ	0,171	0,171	0,171	0,171	0,171
$a_{\dot{x}}$	0,00724	0,035	—	—	—
$a_{\dot{y}}$	0,0268	0,0197	—	—	—
a_y	—	—	—	—	—
a_δ	—	—	—	—	—
b_ϑ	0	0,056	0	0	0
$b_{\dot{x}}$	0,13	0,056	—	—	—
$b_{\dot{y}}$	0,731	1,13	1,39	1,61	1,15
b_y	—	—	—	—	—
b_δ	—	—	—	—	—
b_s	—	—	—	0,323	—
c_ϑ	0,676	1,28	1,14	1,65	0,94
$c_{\dot{x}}$	0,00567	—	—	—	—
$c_{\dot{y}}$	0,637	7,51	1,94	3,23	0,97
c_y	0,104	0,0556	0,13	0,427	0,12
c_δ	2,41	13,2	4,72	5,4	3,18
c_s	—	—	—	0,538	—

Commas represent decimal points.

Note. Table A.1 lists the values of the coefficients for which the angles in the motion equations are measured in degrees, and not in radians. The coefficient in the first term of the second equation of Equation (2.10), or the first equation of Equation (2.11), should therefore be written in the form $V_e/57.3$.

The information on autopilot gains is listed in Table A.2.

TABLE A.2

Gain	Airplane No. 1	Airplane No. 2	Airplane No. 3	Airplane No. 4	Airplane No. 5
l_ϑ	1,2	1,0	2,0	1,0	2,0
$l_{\dot{\vartheta}}$ sec	0,93	0,3	0,4	0	1,3
l_y °/m	0,07	0	0	0	0,08

Commas represent decimal points.

A.2. Expressions for the Coefficients of the Transfer Functions Establishing the Parameters of Longitudinal Motion as a Result of Wind Gust Activity. /225

In Equation (3.1)

$$\left.\begin{aligned} a_1 &= a_{\dot{x}} + b_{\dot{y}} + c_{\dot{\vartheta}} + c_{\ddot{y}} V_e, \\ a_2 &= a_{\dot{x}} b_{\dot{y}} + a_{\dot{y}} b_{\dot{x}} + c_{\dot{\vartheta}} (a_{\dot{x}} + b_{\dot{y}}) + V_e (a_x c_{\ddot{y}} + c_{\dot{y}}), \\ a_3 &= a_{\vartheta} (b_{\dot{x}} c_{\ddot{y}} - c_{\dot{x}}) + c_{\dot{\vartheta}} (a_{\dot{x}} b_{\dot{y}} + a_{\dot{y}} b_{\dot{x}}) + V_e (a_{\dot{x}} c_{\dot{y}} + a_{\dot{y}} c_{\dot{x}}), \\ a_4 &= a_{\vartheta} (b_{\dot{x}} c_{\dot{y}} - b_{\dot{y}} c_{\dot{x}}), \end{aligned}\right\} \quad (A.1)$$

$$\left.\begin{aligned} b_0 &= b_{\dot{x}} c_{\ddot{y}} - c_{\dot{x}}, \\ b_1 &= b_{\dot{x}} c_{\dot{y}} - b_{\dot{y}} c_{\dot{x}}. \end{aligned}\right\} \quad (A.2)$$

In Equation (3.2)

$$\left.\begin{aligned} c_0 &= a_{\dot{x}}, \\ c_1 &= a_{\dot{x}} b_{\dot{y}} + a_{\dot{y}} b_{\dot{x}} + a_{\dot{x}} (c_{\dot{\vartheta}} + c_{\ddot{y}} V_e), \\ c_2 &= a_{\vartheta} (b_{\dot{x}} c_{\ddot{y}} - c_{\dot{x}}) + c_{\dot{\vartheta}} (a_{\dot{x}} b_{\dot{y}} + a_{\dot{y}} b_{\dot{x}}) + V_e (a_{\dot{x}} c_{\dot{y}} + a_{\dot{y}} c_{\dot{x}}). \end{aligned}\right\} \quad (A.3)$$

In Equation (3.3)

$$\left.\begin{aligned} d_0 &= b_{\dot{x}}, \\ d_1 &= b_{\dot{x}} c_{\dot{\vartheta}} + c_{\dot{x}} V_e. \end{aligned}\right\} \quad (A.4)$$

In Equation (3.4)

$$\left.\begin{aligned} e_0 &= b_{\dot{x}}, \\ e_1 &= b_{\dot{x}} (c_{\dot{\vartheta}} + c_{\ddot{y}} V_e), \\ e_2 &= V_e (b_{\dot{x}} c_{\dot{y}} - b_{\dot{y}} c_{\dot{x}}). \end{aligned}\right\} \quad (A.5)$$

In Equation (3.7)

$$\left.\begin{aligned} f_0 &= c_{\dot{y}} - b_{\dot{y}} c_{\ddot{y}}, \\ f_1 &= a_{\dot{x}} c_{\dot{y}} - a_{\dot{y}} c_{\dot{x}} - c_{\ddot{y}} (a_{\dot{x}} b_{\dot{y}} + a_{\dot{y}} b_{\dot{x}}). \end{aligned}\right\} \quad (A.6)$$

In Equation (3.8)

$$\left.\begin{aligned} g_0 &= a_{\dot{y}}, \\ g_1 &= a_{\dot{y}} (c_{\dot{\vartheta}} + c_{\ddot{y}} V_e), \\ g_2 &= a_{\vartheta} (c_{\dot{y}} - b_{\dot{y}} c_{\ddot{y}}). \end{aligned}\right\} \quad (A.7)$$

In Equation (3.9) /226

$$\left.\begin{aligned} h_0 &= b_{\dot{y}}, \\ h_1 &= a_{\dot{x}} b_{\dot{y}} + a_{\dot{y}} b_{\dot{x}} + b_{\dot{y}} c_{\dot{\vartheta}} + c_{\dot{y}} V_e, \\ h_2 &= c_{\dot{\vartheta}} (a_{\dot{x}} b_{\dot{y}} + a_{\dot{y}} b_x) + V_e (a_{\dot{x}} c_{\dot{y}} + a_{\dot{y}} c_x). \end{aligned}\right\} \quad (A.8)$$

In Equation (3.10)

$$\left.\begin{aligned} i_0&=b_{\dot{y}},\\ i_1&=a_{\dot{x}}b_{\dot{y}}+a_{\dot{y}}b_{\dot{x}}+b_{\dot{y}}(c_{\dot{\vartheta}}+c_{\ddot{y}}V_e),\\ i_2&=(c_{\dot{\vartheta}}+c_{\ddot{y}}V_e)(a_{\dot{x}}b_{\dot{y}}+a_{\dot{y}}b_{\dot{x}}). \end{aligned}\right\} \qquad (A.9)$$

In Equation (3.13)

$$\left.\begin{aligned} a'_1&=b_{\dot{y}}+c_{\ddot{y}}V_e+c_{\dot{\vartheta}}),\\ a'_2&=b_{\dot{y}}c_{\dot{\vartheta}}+c_{\dot{y}}V_e, \end{aligned}\right\} \qquad (A.10)$$

$$\left.\begin{aligned} b'_0&=b_{\dot{x}}c_{\ddot{y}}-c_{\dot{x}},\\ b'_1&=b_{\dot{x}}c_{\dot{y}}-b_{\dot{y}}c_x. \end{aligned}\right\} \qquad (A.11)$$

In Equation (3.14)

$$\left.\begin{aligned} d'_0&=d_0=b_{\dot{x}},\\ d'_1&=d_1=b_{\dot{x}}c_{\dot{\vartheta}}+c_{\dot{x}}V_e. \end{aligned}\right\} \qquad (A.12)$$

In Equation (3.15)

$$\left.\begin{aligned} e'_0&=e_0=b_{\dot{x}},\\ e'_1&=e_1=b_{\dot{x}}(c_{\dot{\vartheta}}+c_{\ddot{y}}V_e),\\ e'_2&=e_2=V_e(b_{\dot{x}}c_{\dot{y}}-b_{\dot{y}}c_{\dot{x}}). \end{aligned}\right\} \qquad (A.13)$$

In Equation (3.17)

$$f'_0=f_0=c_{\dot{y}}-b_{\dot{y}}c_{\ddot{y}}. \qquad (A.14)$$

In Equation (3.18)

$$h'_0=h_0=b_{\dot{y}}. \qquad (A.15)$$

In Equation (3.19)

$$i'_0=i_0=b_{\dot{y}},\quad i'_1=b_{\dot{y}}(c_{\dot{\vartheta}}+c_{\ddot{y}}V_e) \qquad (A.16)$$

In Equation (3.22) /227

$$j_0=b_{\dot{x}}c_{\ddot{y}}-c_{\dot{x}},\quad j_1=c_{\dot{y}}b_{\dot{x}}-c_{\dot{x}}b_{\dot{y}},\quad j_2=-b_{\dot{x}}c_{\dot{v}}i_y; \qquad (A.17)$$

$$\left.\begin{aligned} k_1&=a_{\dot{x}}+b_{\dot{y}}+c_{\dot{\vartheta}}+c_{\ddot{y}}V_e+c_{\dot{v}}i_{\dot{\vartheta}},\\ k_2&=a_{\dot{x}}b_{\dot{y}}+a_{\dot{y}}b_{\dot{x}}+(a_{\dot{x}}+b_{\dot{y}})(c_{\dot{\vartheta}}+c_{\dot{v}}i_{\dot{\vartheta}})+a_{\dot{x}}c_{\ddot{y}}V_e+c_{\dot{y}}V_e,\\ k_3&=a_{\vartheta}(c_{\dot{x}}+b_{\dot{x}}c_{\ddot{y}})+(a_{\dot{x}}b_{\dot{y}}+a_{\dot{y}}b_{\dot{x}})(c_{\dot{\vartheta}}+c_{\dot{v}}i_{\dot{\vartheta}})+\\ &\quad+c_{\dot{v}}i_{\vartheta}(a_{\dot{x}}+b_{\dot{y}})+V_e(a_{\dot{x}}c_{\dot{y}}+a_{\dot{y}}c_{\dot{x}}),\\ k_4&=a_{\vartheta}(b_{\dot{x}}c_{\dot{y}}-b_{\dot{y}}c_{\dot{x}})+b_{\dot{y}}c_{\dot{v}}i_yV_e+c_{\dot{v}}i_{\vartheta}(a_{\dot{x}}b_{\dot{y}}+a_{\dot{y}}b_{\dot{x}}),\\ k_5&=c_{\dot{v}}i_yV_e(a_{\dot{x}}b_{\dot{y}}+a_{\dot{y}}b_{\dot{x}})-a_{\vartheta}b_{\dot{x}}c_{\dot{v}}i_y. \end{aligned}\right\} \qquad (A.18)$$

In Equation (3.23)

$$\left.\begin{aligned} l_0 &= a_{\dot{x}}, \\ l_1 &= a_{\dot{x}} b_{\dot{y}} + a_{\dot{y}} b_{\dot{x}} + a_{\dot{x}}(c_{\dot{\vartheta}} + c_{\ddot{y}} V_e + c_{\dot{\delta}} i_{\dot{\vartheta}}), \\ l_2 &= a_{\dot{\vartheta}}(b_{\dot{x}} c_{\ddot{y}} - c_{\dot{x}}) + (a_{\dot{x}} b_{\dot{y}} + a_{\dot{y}} b_{\dot{x}})(c_{\dot{\vartheta}} + c_{\dot{\delta}} i_{\dot{\vartheta}}) + \\ &\quad + a_{\dot{x}} c_{\dot{\delta}} i_{\dot{\vartheta}} + V_e(a_{\dot{x}} c_{\dot{y}} + a_{\dot{y}} c_{\dot{x}}), \\ l_3 &= a_{\dot{\vartheta}}(b_{\dot{x}} c_{\dot{y}} - b_{\dot{y}} c_{\dot{x}}) + c_{\dot{\delta}} i_{\dot{\vartheta}}(a_{\dot{x}} b_{\dot{y}} + a_{\dot{y}} b_{\dot{x}}). \end{aligned}\right\} \quad (A.19)$$

In Equation (3.24)

$$\left.\begin{aligned} m_0 &= b_{\dot{x}}, \\ m_1 &= b_{\dot{x}}(c_{\dot{\vartheta}} + c_{\dot{\delta}} i_{\dot{\vartheta}} + c_{\ddot{y}} V_e), \\ m_2 &= b_{\dot{x}} c_{\dot{\delta}} i_{\dot{\vartheta}} + V_e(b_{\dot{x}} c_{\dot{y}} - b_{\dot{y}} c_{\dot{x}}). \end{aligned}\right\} \quad (A.20)$$

In Equation (3.25)

$$\left.\begin{aligned} n_0 &= c_{\dot{y}} - b_{\dot{y}} c_{\ddot{y}}, \\ n_1 &= a_{\dot{x}} c_{\dot{y}} + a_{\dot{y}} c_{\dot{x}} - c_{\ddot{y}}(a_{\dot{x}} b_{\dot{y}} + a_{\dot{y}} b_{\dot{x}}), \\ n_2 &= b_{\dot{y}} c_{\dot{\delta}} i_y, \\ n_3 &= c_{\dot{\delta}} i_y (a_{\dot{x}} b_{\dot{y}} + a_{\dot{y}} b_{\dot{x}}). \end{aligned}\right\} \quad (A.21)$$

In Equation (3.26)

$$\left.\begin{aligned} q_0 &= a_{\dot{y}}, \\ q_1 &= a_{\dot{y}}(c_{\dot{\vartheta}} + c_{\ddot{y}} V_e + c_{\dot{\delta}} i_{\dot{\vartheta}}), \\ q_2 &= a_{\dot{\vartheta}}(c_{\dot{y}} - b_{\dot{y}} c_{\ddot{y}}) + a_{\dot{y}} c_{\dot{\delta}} i_{\dot{\vartheta}}, \\ q_3 &= a_{\dot{\vartheta}} b_{\dot{y}} c_{\dot{\delta}} i_{\nu}. \end{aligned}\right\} \quad (A.22)$$

In Equation (3.27) /228

$$\left.\begin{aligned} r_0 &= b_{\dot{y}}, \\ r_1 &= a_{\dot{x}} b_{\dot{y}} + a_{\dot{y}} b_{\dot{x}} + b_{\dot{y}}(c_{\dot{\vartheta}} + c_{\ddot{y}} V_e + c_{\dot{\delta}} i_{\dot{\vartheta}}), \\ r_2 &= (a_{\dot{x}} b_{\dot{y}} + a_{\dot{y}} b_{\dot{x}})(c_{\dot{\vartheta}} + c_{\ddot{y}} V_e + c_{\dot{\delta}} i_{\dot{\vartheta}}) + b_{\dot{y}} c_{\dot{\delta}} i_{\dot{\vartheta}}, \\ r_3 &= a_{\dot{\vartheta}}(b_{\dot{x}} c_{\dot{y}} - b_{\dot{y}} c_{\dot{x}}) + c_{\dot{\delta}}(i_{\dot{\vartheta}} + i_y V_e)(a_{\dot{x}} b_{\dot{y}} + a_{\dot{y}} b_{\dot{x}}). \end{aligned}\right\} \quad (A.23)$$

In Equation (3.28)

$$\left.\begin{aligned} s_0 &= b_{\dot{x}} c_{\ddot{y}} - c_{\dot{x}}, \\ s_1 &= c_{\dot{y}} b_{\dot{x}} - c_{\dot{x}} b_{\dot{y}}. \end{aligned}\right\} \quad (A.24)$$

In Equation (3.29)

$$\left.\begin{aligned} u_0 &= a_{\dot{x}}, \\ u_1 &= a_{\dot{x}} b_{\dot{y}} + a_{\dot{y}} b_{\dot{x}} + a_{\dot{x}}(c_{\dot{\vartheta}} + c_{\ddot{y}} V_e + c_{\dot{\delta}} i_{\dot{\vartheta}}), \\ u_2 &= (a_{\dot{x}} b_{\dot{y}} + a_{\dot{y}} b_{\dot{x}})(c_{\dot{\vartheta}} + c_{\dot{\delta}} i_{\dot{\vartheta}}) + a_{\dot{\vartheta}}(b_{\dot{x}} c_{\ddot{y}} - \\ &\quad - c_{\dot{x}}) + V_e(a_{\dot{x}} c_{\dot{y}} + a_{\dot{y}} c_{\dot{x}}) + a_{\dot{x}} c_{\dot{\delta}} i_{\dot{\vartheta}}, \\ u_3 &= a_{\dot{\vartheta}}(b_{\dot{x}} c_{\dot{y}} - b_{\dot{y}} c_{\dot{x}}) + c_{\dot{\delta}} i_{\dot{\vartheta}}(a_{\dot{x}} b_{\dot{y}} + a_{\dot{y}} b_{\dot{x}}). \end{aligned}\right\} \quad (A.25)$$

In Equation (3.30)

$$\left.\begin{aligned} v_0 &= b_{\dot{y}} \\ v_1 &= b_{\dot{x}}\,(c_{\dot{\vartheta}} + c_{\dot{y}}\ddot{V}_e + c_{\dot{\delta}} i_{\dot{\vartheta}}), \\ v_2 &= b_{\dot{x}}\, c_{\dot{\delta}} i_{\dot{\vartheta}} + V_e(b_{\dot{x}}\, c_{\dot{y}} - c_{\dot{x}}\, b_{\dot{y}}). \end{aligned}\right\} \qquad (A.26)$$

In Equation (3.31)

$$\left.\begin{aligned} w_0 &= c_{\dot{y}} - b_{\dot{x}}\, c_{\ddot{y}}, \\ w_1 &= a_{\dot{x}}\, c_{\dot{y}} + a_{\dot{y}}\, c_{\dot{x}} - c_{\ddot{y}}(a_{\dot{x}}\, b_{\dot{y}} + a_{\dot{y}}\, b_{\dot{x}}). \end{aligned}\right\} \qquad (A.27)$$

In Equation (3.32)

$$\left.\begin{aligned} x_0 &= a_{\dot{y}}, \\ x_1 &= a_{\dot{y}}\,(c_{\dot{\vartheta}} + c_{\dot{y}}\ddot{V}_e + c_{\dot{\delta}}\, i_{\dot{\vartheta}}), \\ x_2 &= a_{\dot{\vartheta}}(c_{\dot{y}} - b_{\dot{x}}\, c_{\ddot{y}}) + a_{\dot{y}}\, c_{\dot{\delta}}\, i_{\dot{\vartheta}}. \end{aligned}\right\} \qquad (A.28)$$

In Equation (3.33) /229

$$\left.\begin{aligned} y_0 &= b_{\dot{y}}, \\ y_1 &= a_{\dot{x}}\, b_{\dot{y}} + a_{\dot{y}}\, b_{\dot{x}} + b_{\dot{y}}\,(c_{\dot{\vartheta}} + c_{\ddot{y}}\ddot{V}_e + c_{\dot{\delta}}\, i_{\dot{\vartheta}}), \\ y_2 &= (a_{\dot{x}}\, b_{\dot{y}} + a_{\dot{y}}\, b_{\dot{x}})(c_{\dot{\vartheta}} + c_{\ddot{y}}\ddot{V}_e + c_{\dot{\delta}}\, i_{\dot{\vartheta}}) + b_{\dot{y}}\, c_{\dot{\delta}}\, i_{\dot{\vartheta}}, \\ y_3 &= a_{\dot{\vartheta}}(b_{\dot{x}}\, c_{\dot{y}} - b_{\dot{y}}\, c_{\dot{x}}) + c_{\dot{\delta}} i_{\dot{\vartheta}}(a_{\dot{x}}\, b_{\dot{y}} + a_{\dot{y}}\, b_{\dot{x}}). \end{aligned}\right\} \qquad (A.29)$$

In Equation (3.34)

(3.34):

$$\left.\begin{aligned} z_0 &= b_{\dot{y}}, \\ z_1 &= b_{\dot{y}}\,(c_{\dot{\vartheta}} + c_{\ddot{y}}\ddot{V}_e + c_{\dot{\delta}}\, i_{\dot{\vartheta}}), \\ z_2 &= b_{\dot{y}}\, c_{\dot{\delta}}\, i_{\dot{\vartheta}}, \\ z_3 &= b_{\dot{y}}\, c_{\dot{\delta}} i_q; \end{aligned}\right\} \qquad (A.30)$$

$$\left.\begin{aligned} \varphi_1 &= b_{\dot{y}} + c_{\dot{\vartheta}} + c_{\ddot{y}}\ddot{V}_e + c_{\dot{\delta}}\, i_{\dot{\vartheta}}, \\ \varphi_2 &= b_{\dot{y}}\,(c_{\dot{\vartheta}} + c_{\dot{\delta}}\, i_{\dot{\vartheta}}) + c_{\dot{y}} V_e + c_{\dot{\delta}}\, i_{\dot{\vartheta}}, \\ \varphi_3 &= c_{\dot{\delta}}(b_{\dot{y}}\, i_{\dot{\vartheta}} + i_q), \\ \varphi_4 &= b_{\dot{y}}\, c_{\dot{\delta}} i_q. \end{aligned}\right\} \qquad (A.31)$$

Appendix B

B.1. Computation of Inertial Coefficients and of the First Form of Oscillatory Wing and Flexure.

General Equation (3.91) provides the following expressions for the inertial coefficients in Equation (3.101):

$M_{11} = m$ airplane mass;

$M_{12} = M_{21} = 0$ the result of the orthogonal nature of the first and second generalized coordinates;

$$M_{13}=M_{31}=2\int_0^{l_1/2} m'(z_1)\xi(z_1)\,dz_1+2\sum_{w=1}^{m} m_w(z_{1w})\xi(z_{1w}),$$

where

z_1 is a coordinate of the given wing section along the axes associated with the axis of rigidity (Figures B.1 and B.2);

$l_1 = l/\cos\chi$ is the wing span with respect to the axis of rigidity;

χ is the sweepback angle with respect to the axis of rigidity;

$m'(z_1)$ is the wing mass per unit length with respect to the axis of rigidity;

$\xi(z_1)$ is the first normal form of oscillatory wing flexure equated to the vertical displacement of the wing tip;

$m_w(z_{1w})$ is the load mass on the wing, concentrated at a point with coordinate z_{1w} (engine, landing gear); /230

$M_{22} = I_z$ is the moment of inertia of the airplane about the z axis;

$$M_{23}=M_{32}=-2\int_0^{l_1/2}(x_{ar}+z_{1cg}\sin\chi+x_{1cg}\cos\chi)\xi(z_1)m'(z_1)\,dz_1-$$

$$-2\sum_{k=1}^{m}(x_{ar}+z_{1w}\sin\chi+x_{1w}\cos\chi)m_w(z_{1w})\xi(z_{1w}),$$

where

x_{ar} is the distance between the center of gravity and the point of intersection of the axis of rigidity for the wing and the root chord (+ if the center of gravity is located in front of the elastic axis);

x_{1cg}, z_{1cg} are the coordinates of the center of gravity of the wing section in the x_1Oz_1 system;

x_{1w}, z_{1w} are the coordinates of the concentrated loads

$$M_{33}=2\int_0^{l_1/2} m'(z_1)\xi^2(z_1)\,dz_1+2\sum_{k=1}^{m} m_w(z_{1w})\xi^2(z_{1w}).$$

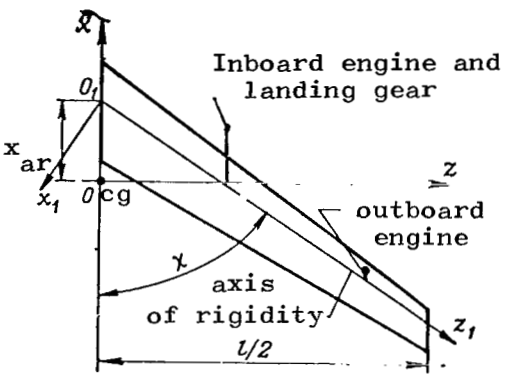

Figure B.1. Geometric relationships for a swept wing.

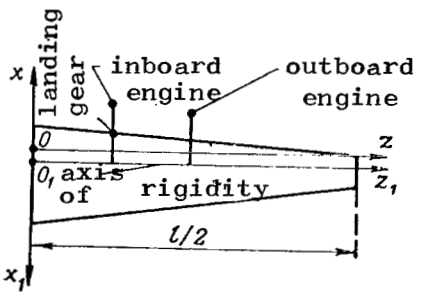

Figure B.2. Geometric relationships for a straight wing.

There are a great many approximate methods available for computing the normal forms and frequencies of the oscillations of an elastic wing, or of other airplane parts. In general, most of these methods are based on Equation (3.87), which can be written in the following form for such purposes

$$\frac{d}{dt}\frac{\partial T}{\partial \dot{q}_i}+\frac{\partial U}{\partial q_i}=0.$$

A detailed description of these methods can be found in [39], for example. /23

The following data are needed to compute the first normal form of just the flexural deformations of the wing, as well as to compute the inertial coefficients of the above-cited formulas:

(a) certain of the airplane's characteristics;

(b) geometry of the wing, and the position of its axis of rigidity;

(c) rigidity of the wing to spanwise flexure;

(d) spanwise distribution of the mass;

(e) positions of the centers of gravity for each of the wing sections into which the wing has been divided for the computation;

(f) masses of concentrated loads on the wing and the coordinates of the points of load applications.

Some of the data for airplanes Nos. 1 and 3 were given in Appendix A. Additional data for (a), above, and for the other items are listed in what follows.

(a) Airplane characteristics.

Sweepback of the wing with respect to the axis of rigidity:

Airplane No. 1, $\chi = 0°$;

Airplane No. 3, $\chi = 30°$.

Distance between center of gravity and point of intersection of axis of rigidity of the wing and the root chord:

Airplane No. 1, $x_{ar} = 0.8$ m;

Airplane No. 3, $x_{ar} = 4.45$ m.

(b) The geometries of the wings of airplanes Nos. 1 and 3 are shown in Figures B.1 and B.2.

Date for (c), (d), and (e), above, are listed in Table B.1.

TABLE B.1

Commas represent decimal points.

$\frac{2z_1}{l_1}$	EI кг·м$^{-2}$		$m'(z_1)$ кг·сек^2·м$^{-1}$		x_{1cg}	
	№ 1	№ 3	№ 1	№ 3	№ 1	№ 3
0,0	$47,9\cdot10^6$	$38,1\cdot10^6$	29,2	68,0	0,049	—0,300
0,1	$42,6\cdot10^6$	$31,5\cdot10^6$	32,3	83,6	0,165	0,132
0,2	$32,6\cdot10^6$	$25,4\cdot10^6$	31,4	52,4	0,145	0,256
0,3	$23,4\cdot10^6$	$18,5\cdot10^6$	87,0	53,8	0,051	0,260
0,4	$16,0\cdot10^6$	$13,1\cdot10^6$	73,3	56,2	0,098	0,372
0,5	$10,8\cdot10^5$	$8,3\cdot10^6$	48,6	45,6	0,166	0,432
0,6	$6,05\cdot10^6$	$5,7\cdot10^6$	55,3	31,1	0,039	0,258
0,7	$4,0\cdot10^6$	$4,3\cdot10^6$	52,8	29,2	0,012	0,225
0,8	$2,4\cdot10^6$	$2,9\cdot10^6$	39,7	25,9	0,083	0,228
0,9	$1,3\cdot10^6$	$1,7\cdot10^6$	26,7	24,6	0,003	0,119
1,0	$0,5\cdot10^6$	$1,1\cdot10^6$	6,5	20,1	0,018	0,040

(f) Data on concentrated loads on the wing are listed in Table B.2. /232

TABLE B.2

Commas represent decimal points.

Parameter	Inboard Engine		Landing Gear		Outboard Engine	
	No. 1	No. 3	No. 1	No. 3	No. 1	No. 3
m_W kg× ×sec²·м⁻¹	265	345	93,5	For Airplane No. 3 the load created by the landing gear is combined with the load created by the inboard engine.	221	149
x_{1W} м	−3,49	−2,60	−1,94		−2,86	−0,59
z_{1W} м	4,5	5,14	4,5		9,1	13,8

These data were used to compute the first form of the oscillatory wing flexure for both airplanes. The results are contained in Table B. 3.

The values of the inertial coefficients and of the natural frequency of the first harmonic of the flexural oscillations, ω_1, are listed in Table B. 4.

B.2. Formulas for the Coefficients of Equation (3.102) and Their Values for the Airplanes Considered

Table B. 5 lists the formulas and the values of the coefficients of those terms in Equation (3.102) attributable to wing flexure. The values of the other coefficients are listed in Table A.1 of Appendix A.

The following shorthand was adopted for Table B. 5

$$I_1 = \int_0^{l/2} b(z)\xi(z_1)\,dz, \qquad I_2 = \int_0^{l/2} b(z)\frac{\partial \xi(z_1)}{\partial z_1}\,dz,$$

$$I_3 = \int_0^{l/2} b(z)\xi^2(z_1)\,dz, \qquad I_4 = \int_0^{l/2} b(z)\frac{\partial \xi(z_1)}{\partial z_1}\xi(z_1)\,dz,$$

where

$z_1 = z \cos \chi$;

x_w is the distance between the center of pressure for the wing and the center of gravity for the airplane:

TABLE B.3

$\frac{2z_1}{l_1}$		0,0	0,1	0,2	0,3	0,4	0,5	0,6	0,7	0,8	0,9	1,0
$\xi(z_1)$	№ 1	0	0,018	0,053	0,105	0,177	0,274	0,380	0,520	0,650	0,830	1,00
	№ 2	0	0,020	0,062	0,112	0,183	0,275	0,378	0,514	0,656	0,837	1,00

TABLE B.4

Airplane	$M_{11}=m$ kg-sec$^2\cdot м^{-1}$	$M_{13}=M_{31}$ kg-sec^2	$M_{11}=M_{31}$ kg-sec$^2\cdot м^{-1}$	$M_{22}=I_z$ kg-m-sec^2	$M_{23}=M_{32}$ kg-sec^2	M_{33} kg-sec$^2\cdot м^{-1}$	ω_w sec^{-1}
№ 1	5320	0	685,4	274 720	—61,4	285,6	9,4
№ 3	5380	0	490	173 000	—1450	244	7,07

Commas represent decimal points.

for Airplane No. 1, x_w = 0.16 m;

For Airplane No. 3, x_w = 0.08 m.

TABLE B.5

/234

Coefficient	Formula	Value for Airplane No. 1	Value for Airplane No. 3	Measurement
$b_{\dot{w}}$	M_{13}/m	0,129	0,0912	—
b_w	$\rho_e V_e C_y^\alpha I_1/m$	0,20	0,395	sec^{-1}
b_w	$\rho_e V_e^2 C_y^\alpha \sin\chi I_2'/m$	0	7,77	sec^{-1}
$c_{\dot{w}}$	M_{23}/I_3	−0,013	−0,48	$\mathcal{M}^{-1}$
c_w	$\rho_e V_e C_y^\alpha x_w I_1/I_z$	0	0,285	$\mathcal{M}^{-1}sec^{-2}$
c_w	$\rho_e V_e^2 C_y^\alpha \sin\chi\, x_w I_2/I_z$	0	5,5	$\mathcal{M}^{-1}\cdot sec^{-2}$
$e_{\dot{\vartheta}}$	M_{32}/M_{33}	−0,0046	−0,104	$\mathcal{M}$
e_ϑ	$V_e M_{31}/M_{33}$	7,5	6,8	$\mathcal{M}\cdot sec^{-1}$
$e_{\dot{y}}$	M_{31}/M_{33}	2,39	2,0	—
e_y	$\rho_e V_e C_y^\alpha I_1/M_{33}$	3,7	8,6	sec^{-1}
e_w	$\rho_e V_e C_y^\alpha I_3/M_{33}$	2,03	4,85	sec^{-1}
e_w	$\rho_e V_e^2 C_y^\alpha \sin\chi I_4/M_{33}$	0	76,3	sec^{-1}

Commas represent decimal points.

Appendix C

C.1. Data on the Airplanes used to Compute the Lateral Motion Coefficients, and Coefficients of Lateral Motion Equations.

The data on lateral motion characteristics for airplanes Nos. 1, 2 and 5 were used in the examples in Chapter 4.

The following flight conditions were selected in the investigation of the lateral motion of Airplane No. 1: y_g = 400 m; V_e = 360 km/h; ρ_e = 0.120 kg-m^{-4}-sec^2; C_{ye} = 0.62.

Flight conditions for airplanes Nos. 2 and 5 were those used in analyzing longitudinal motion (Appendix A). Information on autopilot gains are listed in Table C.1.

TABLE C.1

Airplane	l_γ	$l_\gamma^\cdot$ sec	l_ψ	f_γ	f_ψ	$f_{\dot\psi}$ sec
№ 1	0,4	0	0,9	0,2	0,6	0,9
№ 2	1,0	0,35	0	0	6,0	2,0

Table C.2 lists the coefficients of the lateral motion equations. /235

TABLE C.2

Coefficient	Airplane № 1	Airplane № 2	Airplane № 5	Coefficient	Airplane № 1	Airplane № 2	Airplane № 5
k_β	0,11	0,116	0,137	l_a	3,9	22,4	15,1
k_γ	0,098	0,0394	0,0506	n_β	1,16	17,3	3,78
l_β	0,775	31,8	3,4	$n_\gamma^\cdot$	—0,04	0,048	0,0053
$l_\gamma^\cdot$	1,9	2,5	4,23	$n_{\dot\psi}$	0,32	0,385	0,33
$l_{\dot\psi}^\cdot$	0,51	1,41	1,0	n_r	0,785	5,74	1,72

Commas represent decimal points.

C.2. Expressions for Coefficients of Transfer Functions Determining the Parameters of Lateral Motion as a Result of Wind Gusts.

In Equation (4.1)

$$\left.\begin{aligned} a_1 &= l_\gamma^\cdot + k_\beta + n_{\dot\psi}^\cdot, \\ a_2 &= l_\gamma^\cdot k_\beta + l_\gamma^\cdot n_{\dot\psi}^\cdot + l_{\dot\psi}^\cdot n_\gamma^\cdot + k_\beta n_{\dot\psi}^\cdot + n_\beta, \\ a_3 &= k_\beta l_\gamma^\cdot n_{\dot\psi}^\cdot + k_\gamma l_\beta - k_\beta l_{\dot\psi}^\cdot n_\gamma^\cdot - l_\beta n_\gamma^\cdot + l_\gamma^\cdot n_\beta, \\ a_4 &= k_\gamma (l_\beta n_{\dot\psi}^\cdot - l_{\dot\psi}^\cdot n_\beta); \end{aligned}\right\} \quad (C.1)$$

$$\left.\begin{aligned} b_1 &= k_\beta, \\ b_2 &= k_\beta (l_\gamma^\cdot + n_{\dot\psi}^\cdot), \\ b_3 &= k_\beta (l_\gamma^\cdot n_{\dot\psi}^\cdot - l_{\dot\psi}^\cdot n_\gamma^\cdot) + l_{\dot\psi}^\cdot n_\beta - l_\beta n_\gamma^\cdot. \end{aligned}\right\} \quad (C.2)$$

In Equation (4.3)

$$\left.\begin{aligned} c_0 &= l_\beta, \\ c_1 &= l_\beta n_{\dot\psi} - l_{\dot\psi} n_\beta. \end{aligned}\right\} \tag{C.3}$$

In Equation (4.4)

$$\left.\begin{aligned} d_0 &= n_\beta, \\ d_1 &= l_{\dot\gamma} n_\beta - l_\beta n_{\dot\gamma}. \end{aligned}\right\} \tag{C.4}$$

In Equation (4.6)

$$\left.\begin{aligned} e_0 &= k_\gamma - n_{\dot\gamma}, \\ e_1 &= k_\gamma n_{\dot\psi}. \end{aligned}\right\} \tag{C.5}$$

In Equation (4.7)

/236

$$\left.\begin{aligned} f_1 &= k_\beta + n_{\dot\psi}, \\ f_2 &= k_\beta n_{\dot\psi} + n_{\dot\beta}. \end{aligned}\right\} \tag{C.6}$$

In Equation (4.8)

$$\left.\begin{aligned} g_0 &= n_{\dot\psi}, \\ g_1 &= k_\beta n_{\dot\gamma}, \\ g_2 &= k_\gamma n_\beta. \end{aligned}\right\} \tag{C.7}$$

In Equation (4.10)

$$\left.\begin{aligned} a_1' &= a_1 + i_{\dot\gamma} l_\alpha + f_{\dot\psi} n_\rho, \\ a_2' &= a_2 + i_{\dot\gamma} l_\alpha f_{\dot\psi} n_\rho + i_{\dot\gamma} l_\alpha (k_\beta + n_{\dot\psi} + i_\gamma l_\alpha) + \\ &\quad + f_{\dot\psi} n_\rho (k_\beta + l_{\dot\gamma}) + f_\psi n_\rho, \\ a_3' &= a_3 + i_{\dot\gamma} l_\alpha f_{\dot\psi} n_\rho k_\beta + i_{\dot\gamma} l_\alpha k_\beta n_{\dot\psi} + i_{\dot\gamma} l_\alpha f_\psi n_\rho + \\ &\quad + i_\gamma l_\alpha (k_\beta + n_{\dot\psi}) + i_\gamma l_\alpha f_{\dot\psi} n_\rho + i_{\dot\gamma} l_\alpha n_\beta + i_\psi l_\alpha n_{\dot\gamma} + \\ &\quad + f_\psi n_\rho (k_\beta + l_{\dot\gamma}) + f_{\dot\psi} n_\rho k_\beta l_{\dot\gamma} - f_\gamma n_\rho l_{\dot\psi}, \\ a_4' &= a_4 + i_{\dot\gamma} l_\alpha f_\psi n_\rho k_\beta + i_\gamma l_\alpha f_{\dot\psi} n_\rho k_\beta + \\ &\quad + i_\gamma l_\alpha (k_\beta n_{\dot\psi} + f_\psi n_\rho + n_\beta) + i_\psi l_\alpha (k_\beta n_{\dot\gamma} + f_\gamma n_\rho) + \\ &\quad + f_\psi n_\rho k_\beta l_{\dot\gamma} + f_{\dot\psi} n_\rho k_\gamma l_\beta - f_\gamma n_\rho (l_\beta - k_\beta l_{\dot\psi}), \\ a_5' &= i_\psi l_\alpha (k_\gamma n_\beta + k_\beta f_\gamma n_\rho) + f_\psi n_\rho (k_\gamma l_\beta + i_\gamma l_\alpha k_\beta); \end{aligned}\right\} \tag{C.8}$$

$$\left.\begin{aligned} b_0' &= b_0 = k_\beta, \\ b_1' &= b_1 + k_\beta (i_{\dot\gamma} l_\alpha + f_{\dot\psi} n_\rho), \\ b_2' &= b_2 + i_{\dot\gamma} l_\alpha (f_\psi n_\rho k_\beta - k_\beta n_{\dot\psi} + n_\beta) + i_\gamma l_\alpha k_\beta + \\ &\quad + f_{\dot\psi} n_\rho k_\beta l_{\dot\gamma} + f_\psi n_\rho k_\beta, \\ b_3' &= i_{\dot\gamma} l_\alpha f_\psi n_\rho k_\beta + i_\gamma l_\alpha (f_{\dot\psi} n_\rho k_\beta + k_\beta n_{\dot\psi} + n_\beta) + \\ &+ f_{\dot\psi} n_\rho k_\gamma l_\beta + i_\psi l_\alpha k_\beta n_{\dot\gamma} - f_\gamma n_\rho (k_\beta l_{\dot\psi} + l_\beta) + f_\psi n_\rho k_\beta l_{\dot\gamma} \end{aligned}\right\} \tag{C.9}$$

In Equation (4.12)

$$\left.\begin{aligned} c_0' &= c_0 = l_\beta, \\ c_1' &= c_1 + f_\psi n_r l_\beta, \\ c_2' &= i_\psi l_\alpha n_\beta + f_\psi n_r l_\beta. \end{aligned}\right\} \qquad \text{(C.10)}$$

In Equation (4.13) /237

$$\left.\begin{aligned} d_0' &= d_0 = n_\beta, \\ d_1' &= d_1 + i_\gamma l_\alpha n_\beta, \\ d_2' &= i_\gamma l_\alpha n_\beta - f_\gamma n_r l_\beta. \end{aligned}\right\} \qquad \text{(C.11)}$$

In Equation (4.15)

$$\left.\begin{aligned} e_0' &= e_0 = k_\gamma - n_\gamma, \\ e_1' &= e_1 + f_\psi n_r k_\gamma - f_\gamma n_r \\ e_2' &= i_\psi n_r k_\gamma. \end{aligned}\right\} \qquad \text{(C.12)}$$

In Equation (4.16)

$$\left.\begin{aligned} f_1' &= f_1 + f_\psi n_r, \\ f_2' &= f_2 + f_\psi n_r k_\beta + f_\psi n_r \end{aligned}\right\} \qquad \text{(C.13)}$$

In Equation (4.17)

$$\left.\begin{aligned} g_0' &= g_0 = n_\psi, \\ g_1' &= g_1 + f_\gamma n_r \\ g_2' &= g_2 + f_\gamma n_r k_\beta. \end{aligned}\right\} \qquad \text{(C.14)}$$

C.3. Derivation of Equation (4.27)

Figure C.1 is a square, inside which Equation (4.25) should be integrated. The first integral is taken with respect to the variable $\bar{z}_1$, but such that the independent variable $\eta = \bar{z}_2 - \bar{z}_1$ remains constant. In this case the function $R_{wy}(V_e\tau, \eta)$ also must be considered a constant in computing the Equation (4.28) integral. Figure C.1 explains the limits of the integration of Equation (4.28). If the lower limit is $\bar{z}_1 = -1$, then when η = constant, the upper limit should be $1 - \eta$. The integration includes only the upper part of the square above the $\bar{z}_1 = \bar{z}_2$ diagonal for these limits in the case of positive η values. The integration for negative η values, that is, in the lower part of the square below the diagonal, yields the same result. Therefore, in the transition from Equation (4.25) to Equation (4.27), the constant factor in the denominator is halved.

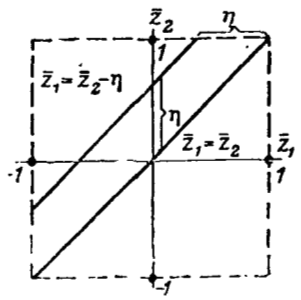

Figure C.1. Graphic explaining the integration of Equation (4.25).

Figure C.1 also explains the passage to the limits 0 and 2 in Equation (4.27) instead of the limits -1 and +1 in Equation (4.25). In the latter equation the integration should be with respect to $\bar{z}_2$, and in Equation (4.27) with respect to η. When $\bar{z}_1$ = constant, the variable η will change from 0 to 2 within the limits of the square when there is a change in $\bar{z}_2$ from -1 to +1. /238

C. 4. Determination of the Function $\varepsilon(\bar{z})$ for the Case of Uniform Spanwise Lift Distribution.

When $b_z = b_a$, Equation (4.24) yields

$$\varepsilon(\bar{z}) = \frac{C_y^{\alpha}\bar{z}}{-m_x^{\bar{\omega}x}}. \tag{C.15}$$

The rotary derivative $m_x^{\bar{\omega}x}$. must be found in order to find $\varepsilon(\bar{z})$. When a wing with angular velocity ω_x is rotated, wing element dz, moved out of the plane of symmetry a distance z, receives an increase in angle of attack $z\omega_x/V_e$. This increase in the angle of attack creates lift force

$$dY = C_y^{\alpha}\frac{z\omega_x}{V_e} b_a \frac{\rho_e V_e^2}{2} dz \tag{C.16}$$

and moment about the x axis

$$dM_x = -dYz = -C_y^{\alpha} z^2 \omega_x b_a \frac{\rho V_e}{2} dz. \tag{C.17}$$

The moment for the wing as a whole is obtained through Equation (C.17) as

$$M_x = -2\int_0^{l/2} dM_x = -\frac{C_y^{\alpha} l^3 \rho_e V_e}{24}\omega_x. \tag{C.18}$$

The dimensionless rotary derivative

$$m_x^{\bar{\omega}x} = -\frac{2V_e}{l} m_x^{\omega x} = -\frac{C_y^{\alpha}}{6}. \tag{C.19}$$

can be determined through Equation (C.18).

Substituting the value for $m\bar{\omega}_x$ from Equation (C.19) in Equation (C.15), finally

$$\varepsilon(\bar{z}) = 6\bar{z}. \qquad \text{(C.20)}$$

C.5. Transfer Functions for Forming Filters for Obtaining the Spectral Density of Motion Parameters the Result of the Spanwise Normal Wind Gradient. /239

(a) for Airplane No. 1:

$k=1$, $L=37{,}4$ м, $W_{x.x_1}(p)=\sigma_w 2{,}02\dfrac{0{,}72+0{,}0485p}{1+0{,}25p+0{,}01p^2}$,

$k=0{,}5$, $L=74{,}8$ м, $W_{x/x_1}(p)=\sigma_w 2{,}85\dfrac{0{,}48+0{,}0554p}{1+0{,}38p+0{,}025p^2}$,

$k=0{,}25$, $L=149{,}6$ м, $W_{x/x_1}(p)=\sigma_w 4{,}04\dfrac{0{,}3+0{,}0872p}{1+0{,}68p+0{,}0975p^2}$,

$k=0{,}125$, $L=299{,}2$ м, $W_{x/x_1}(p)=\sigma_w 5{,}7\dfrac{0{,}173+0{,}12p}{1+1{,}24p+0{,}237p^2}$,

$k=0{,}0625$, $L=598{,}4$ м, $W_{x/x_1}(p)=\sigma_w 8{,}08\dfrac{0{,}095+0{,}0357p}{1+0{,}963p+0{,}144p^2}$,

$k=0{,}03125$, $L=1194{,}8$ м, $W_{x/x_1}(p)=\sigma_w 11{,}4\dfrac{0{,}053+0{,}1p}{1+3{,}15p+0{,}742p^2}$,

(b) for Airplane No. 2:

$k=0{,}25$, $L=38{,}4$ м, $W_{x/x_1}(p)=\sigma_w 4{,}82\dfrac{0{,}3+0{,}009p}{1+0{,}07p+0{,}00103p^2}$,

$k=0{,}125$, $L=76{,}8$ м, $W_{x/x_1}(p)=\sigma_w 6{,}8\dfrac{0{,}173+0{,}0123p}{1+0{,}128p+0{,}00251p^2}$,

$k=0{,}0625$, $L=153{,}6$ м, $W_{x/x_1}(p)=\sigma_w 9{,}64\dfrac{0{,}095+0{,}00364p}{1+0{,}099p+0{,}00153p^2}$,

$k=0{,}03125$, $L=307{,}2$ м, $W_{x/x_1}(p)=\sigma_w 13{,}6\dfrac{0{,}053+0{,}0103p}{1+0{,}325p+0{,}00797p^2}$,

$k=0{,}015625$, $L=614{,}4$ м, $W_{x/x_1}(p)=\sigma_w 19{,}28\dfrac{0{,}0282+0{,}033p}{1+1{,}48p+0{,}064p^2}$.

C.6. Derivation of Equation (4.33).

Equation (4.33) can be obtained from Equation (4.31) after substitution of Equations (4.28) and (4.32) for uniform spanwise lift distribution. Then, from Equation (C.20) $\varepsilon(\bar{z}) = 6\bar{z}$, and it follows from Equation (4.28) that

$$\Gamma(\eta)=6(4-6\eta+\eta^3). \tag{C.21}$$

Let us analyze Equation (4.32). Applying the substitutions $V_e\tau = \xi$, $\omega/V_e = \lambda$, $b\eta/2 = \chi$, and using Equations (4.29) and (1.13), Equation (4.32) yields /240

$$P(\lambda, \chi)=\sigma_w^2 \int_{-\infty}^{\infty} e^{-i\lambda\xi}\left[1-\frac{1}{2L}\sqrt{\xi^2+\chi^2}\right] e^{-\frac{1}{L}\sqrt{\xi^2+\chi^2}}\, d\xi. \tag{C.22}$$

Let us introduce a new substitution, $\xi = \chi \operatorname{sh} t$, for purposes of reducing the Equation (C.22) integral to that tabulated. Then

$$d\xi=\chi \operatorname{ch} t\, dt, \quad \sqrt{\xi^2+\chi^2}=\chi \operatorname{ch} t.$$

With these relationships taken into consideration, Equation (C.22) yields

$$P(\lambda, \chi)=\sigma_w^2 \int_{-\infty}^{\infty} e^{-i\lambda\chi \operatorname{sh} t-\frac{1}{L}\chi \operatorname{ch} t}\left[1-\frac{\chi}{2L}\operatorname{ch} t\right]\operatorname{ch} t\, dt. \tag{C.23}$$

Let us designate $i\lambda\chi/A = \operatorname{sh}\alpha$, $\chi/AL = \operatorname{ch}\alpha$,

where

$$A=\frac{\chi}{L}\sqrt{1+\nu^2}=\frac{k\eta}{2}\sqrt{1+\nu^2}, \quad k=l/L.$$

With these designations taken into consideration, Equation (C.23) yields

$$P(\lambda, \chi)=\sigma_w^2\chi \int_{-\infty}^{\infty} e^{-A \operatorname{ch}(t+\alpha)} \operatorname{ch} t\, dt-\sigma_w^2 \frac{\chi^2}{2L}\int_{-\infty}^{\infty} e^{-A \operatorname{ch}(t+\alpha)} \operatorname{ch}^2 t\, dt. \tag{C.24}$$

Finally, the last substitution, $t + \alpha = u$ reduces Equation (C.24) to the form

$$P(\lambda, \chi)=\sigma_w^2\chi \int_{-\infty}^{\infty} e^{-A \operatorname{ch} u} \operatorname{ch}(u-\alpha)\, du -$$

$$-\sigma_w^2 \frac{\chi^2}{2L} \int_{-\infty}^{\infty} e^{-A \operatorname{ch} u} \operatorname{ch}^2(u-\alpha)\, du = \sigma_w^2 (I_1 - I_2), \tag{C.25}$$

$$I_1 = \chi \int_{-\infty}^{\infty} e^{-A \operatorname{ch} u} (\operatorname{ch} u \operatorname{ch} \alpha - \operatorname{sh} u \operatorname{sh} \alpha)\, du = \chi \operatorname{ch} \alpha \int_{-\infty}^{\infty} e^{-A \operatorname{ch} u} \operatorname{ch} u\, du =$$

$$= 2\chi \operatorname{ch} \alpha \int_{0}^{\infty} e^{-A \operatorname{ch} u} \operatorname{ch} u\, du = \frac{2\chi^2}{AL} K_1(A), \tag{C.26}$$

where /241

$K_1(A)$ is a modified first order Bessel function of the second kind.

$$I_2 = \frac{\chi^2}{4L} \int_{-\infty}^{\infty} e^{-A \operatorname{ch} u} [1 + \operatorname{ch} 2(u-\alpha)]\, du = \frac{\chi^2}{2L} \int_{0}^{\infty} e^{-A \operatorname{ch} u}\, du +$$

$$+ \frac{\chi^2}{2L} \operatorname{ch} 2\alpha \int_{0}^{\infty} e^{-A \operatorname{ch} u} \operatorname{ch} 2u\, du = \frac{\chi^2}{2L} [K_0(A) + \operatorname{ch} 2\alpha K_2(A)], \tag{C.27}$$

where

$K_0(A)$ and $K_2(A)$ are modified zero and second order Bessel functions of the second kind.

Using recurrence formulas for $K_2(A)$, we obtain

$$K_2(A) = \frac{2}{A} K_1(A) + K_0(A). \tag{C.28}$$

Substituting the values for I_1 and I_2 from Equations (C.26) and (C.27) in Equation (C.25) yields

$$P(\nu, \eta) = \sigma_w^2 L \left\{ -\frac{\left(\frac{k\eta}{2}\right)^2}{1+\nu^2} K_0\left[\frac{k\eta}{2}\sqrt{1+\nu^2}\right] + \frac{\frac{k\eta}{2}(1+3\nu^2)}{(1+\nu^2)^{3/2}} K_1\left[\frac{k\eta}{2}\sqrt{1+\nu^2}\right] \right. . \tag{C.29}$$

Substituting the values for (η) from Equation (C.21), and for P(v, η) from Equation (C.29) in Equation (4.31), we obtain

$$S_{m_x}(\omega) = -\frac{6\sigma_w^2 L \left(m_x^{\omega}\right)^2}{8\pi V_e^3} \int_0^2 (4 - 6\eta + \eta^3) \times$$

$$\times \left\{ -\frac{\left(\frac{k\eta}{2}\right)^2}{1+\nu^2} K_0\left[\frac{k\eta}{2}\sqrt{1+\nu^2}\right] + \frac{\frac{k\eta}{2}(1+3\nu^2)}{(1+\nu^2)^{3/2}} K_1\left[\frac{k\eta}{2}\sqrt{1+\nu^2}\right] \right\}. \tag{C.30}$$

The integration of Equation (C.30) will yield Equation (4.33) as well.

Appendix D

General Information on Probability Theory, the Methodology Used to Measure the Random Wind Velocity Component, and Processing Experimental Data.

Data from experiments show that in the majority of cases the distribution of the instantaneous values of wind velocity, or of any airplane motion parameters when flying in turbulent air, conforms to a normal law (Gauss law) with an accuracy sufficient for practical use. The frequency distribution /242 function in this case can be determined by

$$f(x)=\frac{1}{\sigma\sqrt{2\pi}}e^{-\frac{(x-m)^2}{2\sigma^2}}, \qquad (D.1)$$

where

x is a random magnitude;

m is the mathematical expectation of this magnitude;

σ is the root-mean-square of the random magnitude.

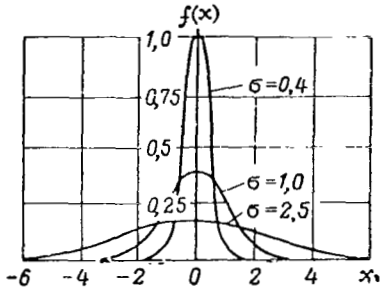

Figure D.1. Graphics of the frequency distribution function for a normal law of random magnitude distribution.

Figure D.1 is a graphic of the frequency distribution function for three different values of σ assuming m = 0. If m is different from zero, the corresponding curve is moved along the axis of abscissa by the magnitude m. Figure D.1 shows that the larger σ, the greater the probability the random magnitude will deviate significantly from its mathematical expectation.

In order to reduce the expression for the frequency distribution function for random magnitudes with different σ, and m, to a single formula, and then use that formula to compute a table, the following so-called normalization of the frequency distribution function can be used

$$f(t)=\frac{1}{\sqrt{2\pi}}e^{-\frac{t^2}{2}}, \qquad (D.2)$$

where

$t = x - m/\sigma$ is the argument of the tabled function.

The probability that the value of the random magnitude will be found in the interval $x_1 - x_2$ can be determined by the frequency distribution function integral, that is by the probability distribution function.

In the case of normalized distribution, this probability, for the interval $t_1 - t_2$, can be found from

$$\Phi(t_1, t_2) = \frac{1}{2\pi} \int_{t_1}^{t_2} e^{-\frac{t^2}{2}} dt, \qquad (D.3)$$

where

$$t_1 = \frac{x_1 - m}{\sigma} \text{ and } t_2' = \frac{x_2 - m}{\sigma}.$$

Equation (D.3) is called a Laplacian, or the probability integral. /243

Table 1 lists the values for the Equation (D.3) probability integral as a function of t_2 (assuming $t_1 = 0$).

TABLE D.1

Values of the probability integral $\frac{1}{2\pi} \int_0^{t_2} e^{-\frac{t^2}{2}} dt$

Commas represent decimal points.

t_2	$\Phi(t_2)$	t_2	$\Phi(t_2)$	t_2	$\Phi(t_2)$
0,00	0,0000	0,70	0,2580	1,50	0,4332
0,05	0,0199	0,75	0,2734	1,55	0,4394
0,10	0,0398	0,80	0,2881	1,60	0,4452
0,15	0,0596	0,85	0,3023	1,65	0,4505
0,20	0,0793	0,90	0,3159	1,70	0,4554
0,25	0,0987	0,95	0,3289	1,75	0,4599
0,30	0,1179	1,00	0,3413	1,80	0,4641
0,35	0,1368	1,05	0,3531	1,85	0,4678
0,40	0,1554	1,10	0,3643	1,90	0,4713
0,45	0,1736	1,15	0,3740	1,95	0,4744
0,50	0,1915	1,20	0,3849	2,00	0,4772
0,55	0,2088	1,25	0,3944	2,50	0,4938
0,60	0,2257	1,30	0,4032	3,00	0,49865
0,65	0,2422	1,35	0,4115	4,00	0,499968
0,67	0,2481	1,40	0,4192	4,50	0,499997
0,68	0,2517	1,45	0,4265	5,00	0,49999997

Table D.1 can be used to find the probability that the value of a random magnitude, the mathematical expectation, m, for which equals zero, will prove to be in some interval $\pm x_2$. Table D.1 was compiled for the interval $0\text{-}t_2$, so the following relationship must be used

$$\int_{-t_2}^{t_2} f(t)\,dt = 2\int_{0}^{t_2} f(t)\,dt,$$

that is, in computing the unknown probability, the $\Phi(t_2)$ value obtained from Table D.1 must be doubled.

The magnitude $[1 - 2\Phi(t_2)]$ yields the probability of the random magnitude being beyond the limits of the interval $\pm x_2$. The results of the computations are listed in Table D.2, where the intervals are expressed in σ values.

TABLE D.2

x_2	t_2	$2\Phi(t_2)$	$1-2\Phi(t_2)$	x_2	t_2	$2\Phi(t_2)$	$1-2\Phi(t_2)$
$\sigma/2$	1/2	0,3829	0,6171	2σ	2	0,9545	0,0455
$\sigma/3$	2/3	0,5000	0,5000	3σ	3	0,9973	0,0027
σ	1	0,6827	0,3173	4σ	4	0,999938	0,000062

Commas represent decimal points.

The data listed in Table D.2 show that about 32% of all random magnitude values will be in excess of $\pm\sigma$, that some 4.5% of the values will be in excess of $\pm 2\sigma$, and that only about 0.3% of the random magnitude values will be outside the limits $\pm 3\sigma$. Herein, therefore, the so-called "three sigma rule." This rule provides the method for making an approximate evaluation of the root-mean-square of the random magnitude. This value can be taken as equal to one-third of the largest of the known values. This is a very rough approximation, of course. /244

When an airplane is flying in moving air the disturbing action (the wind velocity) and the values of the parameters describing the airplane's motion, are random functions of time.

A function is called random when its realization, as a result of experience, is known to be random in nature; that is, it cannot be predicted in advance.

Let us consider just one class of random functions of greatest importance in the majority of problems dealing with flight dynamics in moving air, that of stationary random functions. A random function is said to be stationary if all its probability characteristics (determined below) are

independent of time. The mathematics of stationary functions is relatively simple, and computations can be made quite rapidly.

An additional limitation imposed on the stationary random functions considered in what follows is the assumption that these functions have an ergodic property. A random function has an ergodic property if the probability characteristics obtained by averaging one realization with respect to time (over a sufficiently long observation interval) are close to the characteristics obtained by averaging sets of realizations (for fixed time).

The fundamental probability characteristics of a stationary random function x(t) with an ergodic property can be determined through the following expressions.

The mathematical expectation, or arithmetical mean

$$\bar{x}(t) = \lim_{\text{when } T\to\infty} \frac{1}{2T} \int_{-T}^{T} x(t)\,dt. \tag{D.4}$$

The dispersion, or the mean-square of the function

$$\overline{x_0^2}(t) = \sigma_x^2 = \lim_{T\to\infty} \frac{1}{2T} \int_{-T}^{T} x_0^2(t)\,dt, \tag{D.5}$$

where

$x_0(t) = x(t) - \bar{x}(t)$ is the centered random function.

Only the centered random functions will be considered in what follows, /245
so for convenience the index in the notation of these functions will be omitted.

The correlation function characterizing the degree to which the values of the random function at times t and t + τ are associated is equal to

$$R_x(\tau) = \overline{x(t)\,x(t+\tau)} = \lim_{T\to\infty} \frac{1}{2T} \int_{-T}^{T} x(t)\,x(t+\tau)\,dt. \tag{D.6}$$

Comparing Equation (D.5) and Equation (D.6)

$$R_x(0) = \sigma_x^2. \tag{D.7}$$

A direct Fourier transform of the correlation function yields the spectral density of the random function [1]

$$S_x(\omega)=\frac{1}{\pi}\int_{-\infty}^{\infty}R_x(\tau)e^{-j\omega\tau}d\tau=\frac{2}{\pi}\int_{0}^{\infty}R_x(\tau)\cos\omega\tau\,d\tau. \qquad (D.8)$$

The spectral density characterizes the frequency distribution of the power of the random function x(t). Since the power cannot be negative, the spectral density is a positive function over the frequency range from 0 to $\pm\infty$. If the spectral density of the random function is known, and if an inverse Fourier transform is made, we obtain the correlation function

$$R_x(\tau)=\frac{1}{2}\int_{-\infty}^{\infty}S(\omega)e^{j\omega t}d\omega=\int_{0}^{\infty}S(\omega)\cos\omega\tau\,d\omega. \qquad (D.9)$$

It is possible to replace the lower limit of the integral with 0 (in place of $-\infty$) in Equations (D.8) and (D.9), so the correlation function and the spectral density are even numbers. Comparison of Equation (D.9) with Equation (D.7) results in the following relationship

$$\sigma_x^2=\int_{0}^{\infty}S(\omega)d\omega. \qquad (D.10)$$

Analytical expressions for correlation functions and spectral densities of random stationary processes can be quite diverse. Let us consider the characteristics of the random process known as "white noise," or as an "absolutely random process," for example. The spectral density of this process is constant over the entire frequency range; that is /246

$$S_a(\omega)=S_a(0)=\text{const.} \qquad (D.11)$$

Equation (D.11) explains the origin of the term "white noise." Actually, an approximate analog of this random process is "white light," the visible spectrum of which contains oscillations of different frequencies with identical amplitude.

---

1. It must be pointed out that other coefficients are often used before the integrals in Fourier transform formulas, and this must be taken into consideration in the computations.

The correlation function of "white noise" can be obtained in terms of its spectral density by using Equation (D.9), which yields

$$R_a(\tau)=\pi S_a(0)\,\delta(\tau). \tag{D.12}$$

Equation (D.12) explains the origin of the second designation in the process under consideration, that of an "absolutely random process." The correlation function of the δ-function type indicates the absence of a correlation between random function values, regardless of how close to each other they may be.

It must be emphasized that a random process of the "white noise" type is a mathematical idealization, because precise realization of such process is physically impossible. The dispersion in this process, as follows from Equation (D.10), will be infinitely large. Consequently, the power required to create the process too will be infinite. Nevertheless, "white noise" can replace the real spectrum successfully in those problems in which the spectrum of the random activity is much broader than the frequency bandpass for the system investigated.

Now let us proceed to a consideration of the methodology for measuring random wind velocity components at the airplane. The measurements and the processing of results are quite complex and time consuming.

The principal parameters subject to measurement in determining the vertical and lateral random components of the wind are the angles of attack and sideslip, respectively. The measurement of the pulsation of the total pressure at the air-pressure head inlet can be used to determine the longitudinal component. However, the angular and linear displacements of the airplane have a substantial effect on the results of these measurements.

Considering the kinematic relationships, we obtain the following formulas for determining each of the components of the true wind velocity when measured at the airplane:

for the longitudinal component

$$w_x(t)=(V-\overline{V})-g\int(n_x-\vartheta)\,dt, \tag{D.13}$$

for the vertical component

$$w_y(t)=V(\alpha_v-\vartheta)+g\int\Delta n_y dt+l_x\frac{d\vartheta}{dt}, \qquad \text{(D.14)}$$

/247

for the lateral component

$$w_z(t)=V(\psi-\beta_v)+g\int(n_z+\gamma)dt+l_y\frac{d\gamma}{dt}-l_x\frac{d\psi}{dt}. \qquad \text{(D.15)}$$

The following designations will be used in these formulas in addition to the already known ones:

α_v, β_v the angles of attack and sideslip, measured by a vane; these angles are considered positive if the vane is deflected clockwise relative to the z and y axes, respectively;

n_x, n_y, n_z the body axes acceleration components, measured by accelerometers considered as installed in the airplane's center of gravity;

Δn_y deviation of the normal acceleration from unity;

l_x, l_y distance from site where vane is installed to the airplane's center of gravity, read along the longitudinal, and normal axes;

V airplane's air speed, measured by the air-pressure head;

$\bar{V}$ the average air speed.

Equations (D.13) - (D.15) are valid for small deviations of the parameters from the initial condition of straight and level flight at constant speed.

The angles of attack and sideslip are measured by a vane, or by a special head that receives the difference in dynamic pressures resulting from noncoincidence between the longitudinal axis of the head and the direction of the flow of air incident to the airplane. The vane, or the head, is installed on a boom protruding from the nose of the fuselage. The boom should be at least 1.5 fuselage diameters in length to ensure that the distortion of the undisturbed flow at its end is slight [48]. Moreover, the boom should be quite rigid. The boom's natural angular frequency should be higher than frequency f_s[2], that is the highest frequency of the process under study that

2. Frequency f_s can be found through Equation (D.22), below.

is still of interest.

The realizations of the random wind velocity components, obtained from measurement data, and by computations using Equations (D.13) - (D.15), are subject to further processing in order to obtain correlation functions, or spectral densities, of these random processes.

A whole series of methodological errors occur when experimental data are used to determine the correlation functions and spectral densities for random stationary processes. There are two reasons why this is so: /248

(1) the realization is of limited duration;

(2) the continuous function n is replaced by discrete values.

It is necessary to evaluate these errors and to select that methodology for processing the experimental data yielding the least error. A method for solving this problem has been developed by Tukey [46]. The theoretical basis for the method can be found in [35].

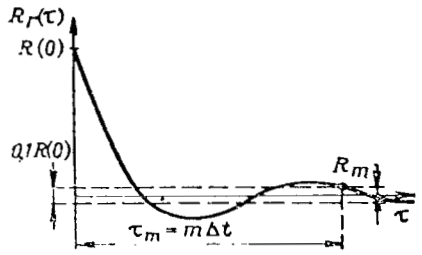

Figure D.2. Graphic explaining the determination of the time over which the correlation function decreases to 5% of its original value.

The processing of the realization of a random function results in the obtaining of n values of x_i, located at equal intervals, Δt. The m ordinate of the correlation function is determined through

$$R_r(\tau) = \frac{1}{n-r}\sum_{i=1}^{n-r} x_i x_{i+r}, \quad r = 0,\ 1,\ 2,\ldots,\ m \qquad \text{(D.16)}$$

and the value of m can be found through

$$m = \frac{\tau_{max}}{\Delta t}, \qquad \text{(D.17)}$$

where

τ_{max} is the time over which the correlation function will decrease to the value $|R_m| \leqslant 0{,}05R_z(0)$ (Figure D.2).

Then the preliminary values of the ordinates of the spectral density curve are determined through

$$L_r(\omega) = \frac{\Delta t}{\pi}\left[R_0 + 2\sum_{i=1}^{m-1} R_i \cos\frac{ir\pi}{m} + R_m \cos r\pi\right], \qquad \text{(D.18)}$$

where

$$\omega = r\pi/m\Delta t.$$

Finally, the refined (averaged) values of the ordinates of the spectral density curve are determined [46]

$$\left.\begin{aligned} S_0(\omega) &= 0{,}5L_0 + 0{,}5L_1, \\ S_r(\omega) &= 0{,}25L_{r-1} + 0{,}5L_r + 0{,}25L_{r+1}, \quad r = 1, 2, \ldots, m-1, \\ S_m(\omega) &= 0{,}5L_{m-1} + 0{,}5L_m. \end{aligned}\right\} \qquad (D.19)$$

What follows from these expressions is that the averaging band for each of the ordinates equals $2\Delta\omega$, where /249

$$\Delta\omega = \pi/m\Delta t. \qquad (D.20)$$

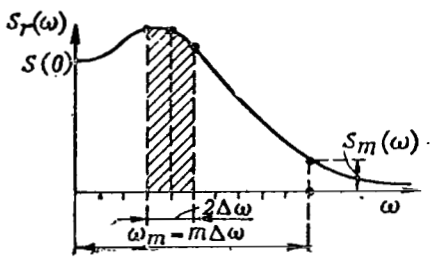

Figure D.3. Graphic of the refined spectral density.

The computation provides us with m + 1 values of the spectral density (Figure D.3), located in the interval $\Delta\omega$. This latter expression indicates that the larger m, the greater the frequency resolution in the computation made (the interval Δt is determined by the nature of the realization, and cannot change). But with decrease in $\Delta\omega$ comes a decrease in the averaging band, and this leads to a reduction in the statistical reliability of the value obtained.

Tukey established the fact that the statistical reliability, established by the confidence coefficient by using the relationship of the computed values of the ordinates of the spectral density, $S_r(\omega)$, obtained using the method indicated above, to the true values of these ordinates, $S(\omega)$, is subordinate to the χ^2-distribution law. The number of degrees of freedom is a parameter of this law

$$k = 1{,}6n/m. \qquad (D.21)$$

The graphic of the $S_r(\omega)/S(\omega)$ ratio as a function of the argument of k with a confidence coefficient of 0.9 (dashed) and 0.95 (solid line) is shown as Figure D.4.

This graphic shows that in order to obtain an $S_r(\omega)/S\omega$ ratio differing little from unity, the argument of k must be substantial, and this is possible

because of the decrease in m (for given n), or because of the increase in n (for given m).

In order to illustrate the basic provisions of this method, let us take as an example the graphics of spectral density computed using this method (Figure D.5). These graphics are for the acceleration spectral density measured at the airplane under very heavy turbulence conditions. The root-mean-square of the acceleration is $\sigma_{ny} = 0.49$. Since realization duration was short, it was possible to obtain a small number of discrete values for the acceleration (n = 200). Figure D.5 shows the graphics corresponding to the numbers m = 10, and m = 20. When m = 10, the curve obtained is smoother, but because of the low frequency resolution the individual features of the spectral density function disappear. When m = 20, the frequency resolution is greater, with a significant peak appearing at frequency $\omega = 1$, but smoothing and reliability of the graphic deteriorate substantially. /250

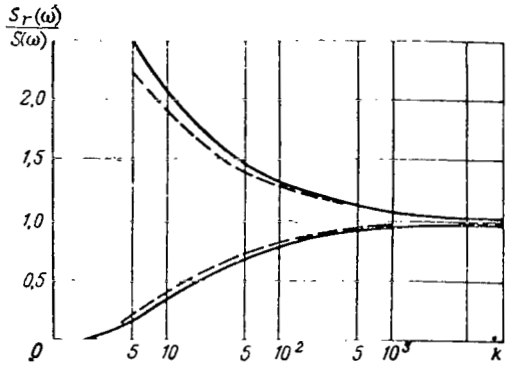

Figure D.4. Graphic of the $S_r(\omega)/S(\omega)$ ratio for determining the reliability of the computed values of the spectral density.

—— confidence coefficient 0.95;
---- confidence coefficient 0.9.

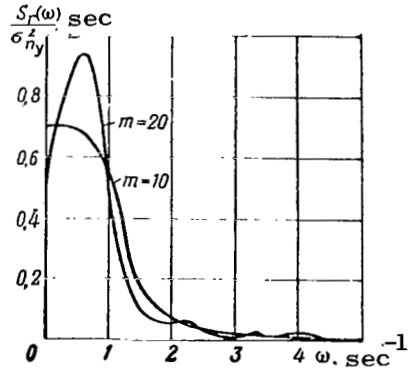

Figure D.5. Graphics of the normalized spectral density for two values of the m number.

The following sequence in processing the experimental data follows from Tukey's method in order to obtain the values of the spectral density with the required statistical reliability.

1. The nature of the realization is used to determine the highest significant frequency, f_s, such that that portion of the spectrum equating to the higher frequency contains a negligibly small part of the power of the process investigated. We associate this frequency with the spatial characteristics of the turbulence

$$f_s = \frac{\omega_s}{2\pi} = \frac{V_e \Omega_s}{2\pi}, \qquad \text{(D.22)}$$

where

V_e is the speed at which the airplane is flying;

Ω_s is the highest significant space frequency for which it is recommended that $\Omega \approx 0.1 \ \ m^{-1}$ [48].

Assuming that during the period corresponding to frequency f_s there should be at least two evaluations of the random function, from Equation (D.22) we find the time interval Δt over which we must obtain discrete values for this function

$$\Delta t = \frac{1}{2f_s} = \frac{\pi}{V_e \Omega_s} \approx \frac{\pi}{0,1 V_e}. \qquad \text{(D.23)}$$

2. Proceeding from the expected (on the basis of the type of realization) time, τ_m, over which the correlation function reaches the $0.05R_r(0)$ bands, m is determined through Equation (D.17).

3. The argument of k is determined from the graphics in Figure D.4 for the required reliability in the evaluations of the spectral density and confidence coefficient. /251

4. Equation (D.21) is used to find the number of points, n, required for the realization

$$n = 0.625 \text{ km}.$$

Then the total time required for the realization can be found from

$$t_r = n\Delta t.$$

If n is too large, Equation (D.21) allows us to select k and m values such that as a result of a reduction in resolution and reliability of the results, an acceptable n is obtained (proceeding from the capabilities of

digital computers used for the computations).

As soon as this methodology has provided all the data needed with respect to Δt, m, and n, the computations can be undertaken with Equations (D.16), (D.18), and (D.19). If, as a result of the computation, it develops that during the apriori determination of τ_m a significant error is assumed, a new τ_m value must be taken, obtained through Equation (D.16), and new m, n and t_r values determined.

For purposes of orientation, we mention the values of m and n recommended in [48] as providing good results

$$m = 40—60 \quad \text{and} \quad n = 1500—4000.$$

In conclusion, let us point out that the method described is not only useful for processing, but also for preparing and planning experiments for recording the realizations of random processes for purposes of a preliminary evaluation of the duration of a realization providing the required reliability of results.

REFERENCES /252

1. Zbrozek, J. K., "Atmospheric Gusts," J. Roy., Aeronaut. Soc., Vol. 69, No. 649, 1965.

2. Pinus, N. Z., Shmetter, S. M., Aerologiya, [Aerology], Gidrometeoizdat, 1965.

3. Selitskaya, V. I., Sutochnyy i godovoy khod meteorologicheskikh elementov v nizhnem sloye atmosfery 0.5 km nad pos. Voyeykovo, [Daily and Annual Course of Meteorological Elements in the Lower Layer of the Atmosphere 0.5 km Above the Village of Voyeykovo]," Trudy GGO, Issue 135, 1962.

4. Matveyev, L. T., Osnovy obshchey meteorologii, [Fundamentals of General Meteorology], Gidrometeoizdat, 1965.

5. Setton, O. G., Mikrometeorologiya, [Micrometeorology], Gidrometeoizdat, 1958.

6. Gandin, L. S., Problema vetrovykh nagruzok na stroitel'nyye sooruzheniya kak zadacha prikladnoy meteorologii, [The Problem of Wind Loads on Building Structures as One for Applied Meteorology], Trudy GGO, Issue 23, 1950.

7. Khintse, I. O., Turbulentnost', [Turbulence], Fizmatgiz, 1963.

8. Atmosfernaya turbulentnost' vyzyvayushchaya boltanku samoletov [Atmospheric Turbulence Causing Rough Air Conditions for Airplanes], Editor N. Z. Pinus, Gidrometeoizdat, 1962.

9. Ivanov, V. N., Volkovitskaya, Z. I., "Some Characteristics of the Boundary Layer of the Atmosphere," Sb. Pogranichnyy sloy atmosfery, [Collection The Boundary Layer of the Atmosphere], Proceedings of the Institute of Applied Geophysics, Issue 2, Gidrometeoizdat, 1965.

10. McCready, P. W., "The Structure of Atmospheric Turbulence," Journal of Meteorology, No. 6, 1953.

11. Betchelor, Dzh. [Batchlor, J], Teoriya odnorodnoy turbulentnosti, [Theory of Homogeneous Turbulence], IL, 1955.

12. Liepman, H. W., "On the Application of Statistical Concepts to the Buffeting Problem," JAS, No. 12, 1952.

13. Diederich, F. W., The Response of an Airplane to Random Atmospheric Disturbances, NACA report, 1345, 1958.

14. Kolmogorov, A. N., "The Local Structure of Turbulence in an Incompressible Fluid at Very Large Reynolds Numbers," DAN SSSR, Vol. 30, No. 4, 1941.

15. Press H., Meadows, M. T. and Hadlock I., A Reevaluation of Data on Atmospheric Turbulence and Airplane Gust Loads for Application in Spectral Calculations, NACA report, 1272, 1956.

16. Dobrolenskiy, Yu. P., Miloslavov, B. A. and Borisov, D. P., "Device for Measuring and Recording Wind Velocity Pulsations at the Altitude at Which the Airplane is Flying", Patent No. 134902, 1960.

17. Klinov, F. Ya., Andreyev, V. D., Poltavskiy, V. V. and Lobova, L. Ye., "Measurements of Two Components of Wind Direction on a Tall Meteorological Mast," Proceedings of the Institute of Applied Geophysics, Issue 2, 1965.

18. Zaborskiy, G. M., Zaytsev, V. A. and Ledokhovich, A. A., "Measurement of Temperature and of Vertical Wind Velocity Components at the Airplane," TsIP, Materials from the Scientific Conference on Aviation Meteorology, Gidrometeoizdat, 1963.

19. Pakhomov, L. A., Metod izmereniya trekh komponent vektora skorosti vetra v svobodnoy atmosfere na samolete, [A Method for Measuring the Three Components of the Wind Velocity Vector in Free Atmosphere at the Airplane], Dissertation in the competition for the science degree of Candidate of Technical Sciences, 1963. /253

20. Donely, P., Summary of Information Relating to Gust Loads on Airplanes, NACA report, 997, 1950.

21. Zbrozek, J. K., The Relationship Between the Discrete Gust and Power Spectra Presentations of Atmospheric Turbulence, with a Suggested Model of Low-altitude Turbulence, ARC RM, No. 3216, 1961.

22. Konstantinov, A. R., Issledovaniye turbulentnoy struktury vetra v prizemnom sloye atmosfery, [Investigation of the Turbulent Structure of the Wind in the Lowest Atmospheric Layer], Trudy GGO, Issue 16, 1949.

23. Charles, N. B. and Philiop, G. C., Requirements For the Flight Control System of a Supersonic Transport, SAE preprints, s. a. No. 679G.

24. Dobrolenskiy, Yu. P., "Turbulence of the Atmosphere as a Source of Disturbances in Systems for Automatic Control of Airplanes," Izv. AN SSSR, Energetika i avtomatika, [Power Engineering and Automation], No. 5, 1961.

25. Venttsel', Ye. S., Teoriya veroyatnostey, [Probability Theory], Fizmatgiz, 1962.

26. Ostoslavskiy, I. V. and Strazheva, I. V., Dinamika poleta, [Flight Dynamics], Mashinostroyeniye, 1965.

27. Etkin, B., Dinamika poleta, [Flight Dynamics], Mashinostroyeniye, 1964.

28. Dobrolenskiy, Yu. P., Ivanova, V. I. and Pospelov, G. S., Avtomatika upravlyaemykh snaryadov, [Automation of Guided Missiles], Oborongiz, 1963.

29. Bird, J. D., Fisher L. R. and Hubbard, S. M., Some Effects of Frequency of the Contribution of a Vertical Tail to the Free Aerodynamic Damping of a Model Oscillating in Yaw, NACA report, 1130, 1963.

30. Laning, J. H. and Bettin, R. G., Sluchaynyye protsessy v zadachakh avtomaticheskogo upravleniya, [Random Processes in Automatic Control Problems], IL, 1958.

31. Egglestone, J. M. and Phillips, W. H., The Lateral Response of Airplanes to Random Atmospheric Turbulence, NASA technical report, R-74, 1960.

32. Egglestone, J. M. and Diederiech, F. M., Theoretical Calculation of the Power Spectra of the Rolling and Yawing Moments on a Wing in Random Turbulence, NACA report, 1321, 1957.

33. Watson, G. N., Teoriya besselevykh funktsiy, [Theory of Bessel Functions], IL, 1949.

34. Loring, A. and Heffner, J., Metody obrabotki eksperimental'nykh dannykh, [Methods for Processing Experimental Data], IL, 1953.

35. Blackman, R. B. and Tukey, J. W., "The Measurement of Power Spectra From the Point of View of Communications Engineering," The Bell System Technical Journal, No. 3 - 4, 1958.

36. Kazakov, I. Ye. and Dostupov, B. G., Statisticheskaya dinamika nelineynykh avtomaticheskikh sistem, [Statistical Dynamics of Non-Linear Automatic Systems], Fizmatgiz, 1962.

37. Fung, Y. G., "Statistical Aspects of Dynamic Loads," JAS, No. 5, 1953.

38. Reissner, E. and Stevens, J., "Effect of Finite Span on the Airload Distributions for Oscillating Wings," NACA, T N 1195, 1947.

39. Bisplinghoff, R. L., Ashley, H. and Halfman, R. L., Aerouprugost', [Aeroelasticity], IL, 1958.

40. Bennet, F. V. and Pratt, K. G., Calculated Responses of a Large Sweptwing Airplane to Continuous Turbulence with Flight Test Comparisons, NASA technical report, R - 69, 1960.

41. Jones, T., The Unsteady Lift of a Wing of Finite Aspect Ratio, NACA report, 681, 1940.

42. Luthander, S. and Kaul, V., "A Possibility for Reducing the Dangerous Virbrations Experienced by Pilots in Heavy Turbulence," Proceeding of the Symposium on Civil Aviation Safety, Stockholm, 1966.

43. Shevelev, A. G., "Investigation of the Feasibility of Building Invariant Systems for Automatic Piloting," Sbornik nauchnykh trudov, [Collection of Scientific Papers], Kiev Institute GVF, Issue 2, 1962.

44. Bobnev, M. P., "Generation of Random Signals and Measurement of Their Parameters," Energiya, 1966.

45. Press, H. and Mazelsky, B., A Study of the Application of Power - Spectra Methods of Generalized Harmonic Analysis to Gust Loads on Airplanes, NACA report, 1172, 1954. /254

46. Press, H. and Houbolt, J. C., "Some Applications of Generalized Harmonic Analysis to Gust Loads on Airplanes, JAS, No. 1, 1955.

47. Baranov, A. M., Mazurin, N. I., Solonin, S. V., Yankovskiy, I. A., Aviatsionnaya meteorologiya, [Aviation Meteorology], Gidrometeoizdat, 1966.

48. Houbolt, J. C. Steiner, R. and Pratt, K. G., Dynamic Response of Airplanes to Atmospheric Turbulence Including Flight Data on Input and Response, NASA technical report, R - 199, 1964.

49. Atmospheric Turbulence and Its Relation to Aircraft, London, Her Majesty's Stationery Office, 1963.

50. Von Karman, Th., "Progress in the Statistical Theory of Turbulence," Turbulence - Classic Papers on Statistical Theory, S. K. Friedlander and L. Topper, eds., Interscience Publ., Inc., New York, 1961.

51. Belotserkovskiy, S. M., "A Method for Computing the Action of a Gust on an Arbitrary Thin Wing," Izv. AN SSSR, Mekhanika zhidkosti i gaza, No. 1, 1966.

52. Belotserkovskiy, S. M., "A Method for Computing the Coefficients of the Rotary Derivatives and of the Apparent Additional Masses for a Thin Wing of Arbitrary Shape in Plan," Sb. statey po aerogidrodinamike, [Collection of Articles on Aerohydrodynamics], Trudy TsAGI, Issue 940, 1964.

NASA-Langley, 1971 —— 1

NATIONAL AERONAUTICS AND SPACE ADMINISTRATION
WASHINGTON, D. C. 20546

OFFICIAL BUSINESS
PENALTY FOR PRIVATE USE $300

FIRST CLASS MAIL

POSTAGE AND FEES PAID
NATIONAL AERONAUTICS AN
SPACE ADMINISTRATION

12U 001 26 51 3DS 71166 00903
AIR FORCE WEAPONS LABORATORY /WLOL/
KIRTLAND AFB, NEW MEXICO 87117

ATT E. LOU BOWMAN, CHIEF, TECH. LIBRARY

POSTMASTER: If Undeliverable (Section 158 Postal Manual) Do Not Return

"The aeronautical and space activities of the United States shall be conducted so as to contribute . . . to the expansion of human knowledge of phenomena in the atmosphere and space. The Administration shall provide for the widest practicable and appropriate dissemination of information concerning its activities and the results thereof."

—NATIONAL AERONAUTICS AND SPACE ACT OF 1958

NASA SCIENTIFIC AND TECHNICAL PUBLICATIONS

TECHNICAL REPORTS: Scientific and technical information considered important, complete, and a lasting contribution to existing knowledge.

TECHNICAL NOTES: Information less broad in scope but nevertheless of importance as a contribution to existing knowledge.

TECHNICAL MEMORANDUMS: Information receiving limited distribution because of preliminary data, security classification, or other reasons.

CONTRACTOR REPORTS: Scientific and technical information generated under a NASA contract or grant and considered an important contribution to existing knowledge.

TECHNICAL TRANSLATIONS: Information published in a foreign language considered to merit NASA distribution in English.

SPECIAL PUBLICATIONS: Information derived from or of value to NASA activities. Publications include conference proceedings, monographs, data compilations, handbooks, sourcebooks, and special bibliographies.

TECHNOLOGY UTILIZATION PUBLICATIONS: Information on technology used by NASA that may be of particular interest in commercial and other non-aerospace applications. Publications include Tech Briefs, Technology Utilization Reports and Technology Surveys.

Details on the availability of these publications may be obtained from:

SCIENTIFIC AND TECHNICAL INFORMATION OFFICE

NATIONAL AERONAUTICS AND SPACE ADMINISTRATION

Washington, D.C. 20546